Non-Enzymatic Sensing of Creatinine for Early Detection of Chronic Kidney Disease

Sonal Bajpai

This dissertation is submitted for the degree of Doctor of Philosophy

July 2023

Department of Chemistry

Declaration

The work in this thesis has not been submitted for the award of a higher degree elsewhere. All the work done in this project is my own work, having had guidance from my supervisor, Professor Kathryn Toghill.

Part of the project *(Chapter 3 on bare GCE creatinine sensor)* has been filed as a patent.

Sonal Bajpai

Lancaster University, UK

Abstract

Chronic kidney disease (CKD) affects a 8-16 % of the global population. Creatinine is a useful biomarker for screening and detecting CKD. Creatinine concentrations in urine outside the normal clinical range (4.4-13.3 mM) gives an indication of kidney conditions including CKD, and requires further evaluation by the nephrologists in secondary care clinical settings. The fact that CKD is asymptomatic, it is critical to detect it at earlier stages and prevent its progression with medicines. Currently Jaffe reaction method of creatinine detection is the most widely used technique. Although, this significantly suffers from low specificity and high interferences from molecules including ascorbic acid. Enzymatic methods, although are highly specific, but have problems with high cost and low stability due to use of enzymes. Therefore, there is an urgent need to develop low cost and simple non-invasive creatinine detection methods, which is the focus of this *PhD project.*

We have developed a novel simple sensing mechanism based on bare glassy carbon electrode (GCE) which can detect creatinine electrochemically (LOD 60 µM and sensitivity 1.50 µA/mM) and colorimetrically (LOD 6.63 µM). An application for a patent has been made for this work. Additionally, nickel-based systems have also been studied to detect creatinine, although there is high interference to urea and requires further optimisation. SPE based creatinine sensing methods designed (LOD 60 µM) as part of a preliminary study in this project including surface modifications, aims to use creatinine sensing for POCT applications in future. Market testing of the concepts used in this project has informed us to evaluate albumin sensing.

Acknowledgements

I am firstly very grateful to have had an opportunity to work with Professor Kathryn Toghill on this project. I thank her for all her support and guidance during the entire course. This PhD journey has had a significant effect on my life and I feel very fortunate to have had worked on a project that not only trained me on electrochemical techniques and skills, but also contributing to the work that may bring an impact to solve real clinical challenges associated with chronic kidney disease. Kathryn has always guided me through the difficult times I have faced during this course, and I just am very grateful to have had a supervisor like her.

I would also like to thank Dr Geoffrey Akien, for his immense support with NMR studies. Thanks Geoff, for guiding me through techniques and the theory involved specifically related to creatinine work. Thanks for dedicating so much time. I am also very grateful to Professor Peter Fielden for guiding me through the thesis. I would also like to thank Dr John Hardy, for his help and support in the area of developing hydrogel work for SPE based sensing. Thanks John, for introducing me to the Chemistry Department at Lancaster University in 2016. I am very grateful.

I would not have been able to achieve this PhD without the help of the entire research team, Daniel, Luis, Hamza, Sam and Mark. I am again very fortunate for this and thank the Toghill Group for all their support. Thanks, Daniel, for all your support. Sam and Mark, thanks for always helping me with all the experimental work.

I would like to dedicate this thesis to my parents, without who I would not have been able to do this PhD. Their motivation and guidance has allowed me to reach this stage in my life.

Contents

Chapter 5 - Screen printed electrode (SPE) based Creatinine Sensing 130

List of Figures

List of Tables

List of Abbreviation

CKD   Chronic Kidney Disease

GCE   Glassy Carbon Electrode

eGFR   Estimated Glomerular Filtration Rate

MDRD   Modification of Diet in Renal Disease

ESKD   End Stage Kidney Disease

CVD   Cardiovascular Disease

POCT   Point of Care Testing

ATP   Adenosine Triphosphate

CE   Capillary Electrophoresis

GC-MS   Gas Chromatography Mass Spectrometry

LC-MS   Liquid Chromatography Mass Spectrometry

ISFET   Ion Selective Field Effect Transistors

CIH   Creatinine Iminohydrolase

CD   Creatinine Deiminase

ISE   Ion Selective Electrode

WE   Working Electrode

RE   Reference Electrode

LOD   Limit of Detection

PAA   Polyacrylic acid

PMB   Polymethylene Blue

CNF   Carbon Nanofiber

GQDs   Graphene Quantum Dots

rGO   Reduced Graphene Oxide

PDA	Polydopamine
NB	Nile Blue
SPCE	Screen Printed Carbon Electrode
PB	Phosphate Buffer
AA	Ascorbic Acid
UA	Uric Acid
PPy	Polypyrrole
PTA	Phosphotungstic Acid
PEI	Poly(ethyleneimine)
CNTs	Carbon Nanotubes
POMs	Polyoxometalates
GP	General Practice
CV	Cyclic Voltammetry
Glu	Glucose
CA	Chronoamperometry
HPLC	High-performance Liquid Chromatography
SHE	Standard Hydrogen Electrode
NHE	Normal Hydrogen Electrode
DPV	Differential Pulse Voltammetry
SCM	Super Conducting Magnet
HSQC	Heteronuclear Single Quantum Correlation
HMBC	Heteronuclear Multiple Bond Correlation
ESI	Electrospray Ionisation
ATR	Attenuated Total Reflectance
CE	Counter Electrode
LOQ	Limit of Quantification
AOAC	Association of Official Analytical Chemists
CB	Carbon Black

Nf   Nafion

MIPs   Molecularly Imprinted Polymers

AU   Artificial Urine

PVA   Polyvinylalcohol

Chapter 1 – Introduction

1.1 Chronic Kidney Disease and renal function

Kidney malfunctioning is one of the most severe chronic diseases that affects a large fraction of the global population[1]. The kidneys comprise about 1 million nephrons that allow excretion of waste products and also have homeostatic function[8]. Chronic kidney disease (CKD) occurs when the structure and function of the kidneys is affected [1]. In definition, if there is presence of kidney damage and decreased kidney function (based on glomerular filtration rate [GFR]) for 3 months or more, then the individual is considered to have CKD [1]. Glomeruli act as filters and filtration occurs at the glomerulus. A reduction in GFR occurs as a result of CKD. GFR reflects the number of functioning glomeruli and can give information on the extent of renal impairment. Estimated GFR (eGFR) based on creatinine concentrations considering factors including age, can be calculated using equations (e.g., Modification of Diet in Renal Disease (MDRD) equation). The current challenge is the fact that eGFR suffers from significant imprecision and inaccuracy [8].

CKD is diagnosed in around 8-16% of the population worldwide [9]. The main causes of CKD include diabetes and/or hypertension [10], the former being a condition that is steadily increasing in prevalence globally. Early stages of CKD (mild and moderate stage of CKD) are often asymptomatic but if detected on time can be reversible [1]. There is an urgent need to screen the disease in primary care (i.e. in general practice surgeries) (fig. 1.1) to prevent end stage kidney disease (ESKD) and cardiovascular disease, which is critical for patients in high risk groups such as diabetic and hypertensive[11-13]. The aim is to screen for CKD at early stages to reduce the risk and to further reduce the complications (fig. 1.1).
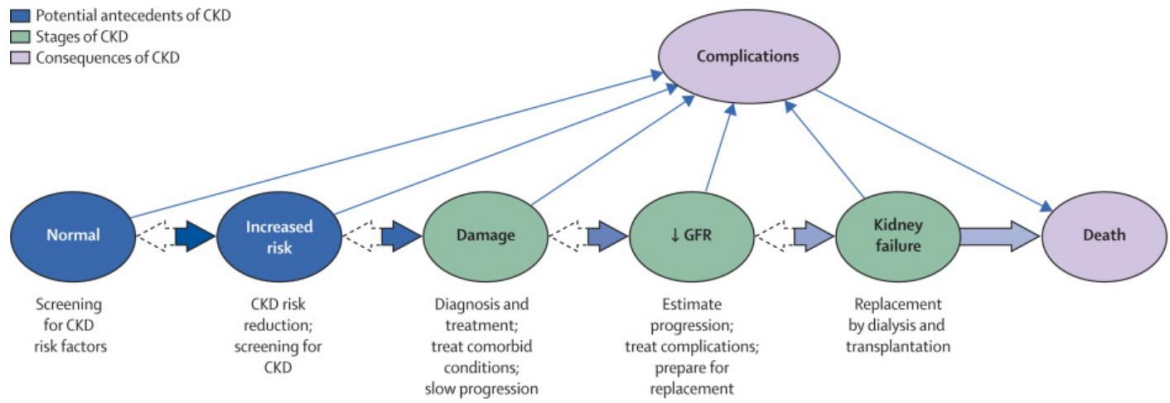
Figure 1.1: Conceptual model of CKD showing it is critical to detect it at an 'increased risk' stage[1].

Early detection of asymptomatic CKD is important such that the detection of the disease can occur in stages 1 and 2 (table 1.1), and further progression can be delayed using medicines [14]. In the later stages (symptomatic), the kidneys are significantly damaged and can also lead to cardiovascular disease (CVD) [2, 14].

According to the National Kidney Foundation, the stages of CKD are described as follows according to the Glomerular Filtration Rate (GFR), that defines the level of kidney function[15],

Table 1.1: Stages of CKD according to the National Kidney Foundation[15].

Stage	GFR (mL per minute per 1.73 m^2)
1	≥90 (normal or elevated GFR)
2	60 to 89 (mildly decreased GFR)
3	30 to 59 (moderately decreased GFR)
4	15 to 29 (Severely decreased GFR)
5	< 15 (Kidney Failure)

Over one million people worldwide are undergoing dialysis treatment, thus there is a critical need of a point-of-care testing (POCT) system to detect CKD at an earlier stage (i.e. before being symptomatic) and also to carry out frequent analysis for patients in later stages of CKD during dialysis treatment who require more than one test per day[2]. If early CKD screening was implemented, the POCT device could be useful in diabetic review clinics, GP practices,

pharmacies and for home-testing for diabetic and hypertensive patients, who are at high risk of developing CKD.

Various biomarkers have been considered for monitoring kidney function including creatinine, urine protein and cystatin C, but creatinine, due to its analytical simplicity, remains the most widely used biomarker [16]. Currently, renal function tests typically measure serum creatinine to determine eGFR levels[17]. A GFR of <60 ml/min per 1.73 m^2 [1] indicates presence of the disease[1]. For routine screening purposes determining urine creatinine could be more effective and less invasive, especially in conjunction with albumin, thus giving an albumin to creatinine ratio (ACR) which can be used as a highly accurate spot test for screening.

1.2 Creatine and Creatinine

Scientific studies on molecules including creatine and creatinine has been ongoing since 1847 [18]. Creatine is produced endogenously from L-arginine, L-methionine and glycine and is key for the production of adenosine triphosphate (ATP) [19-21]. In this process, creatine is converted into phosphocreatine involving an enzymatic reaction with creatine kinase [22]. Creatine is transported to tissues and organs, where it is metabolised to creatinine [2]. Creatinine exists as a breakdown product of phosphocreatine (fig. 1.2). It has no useful biological function and is removed from
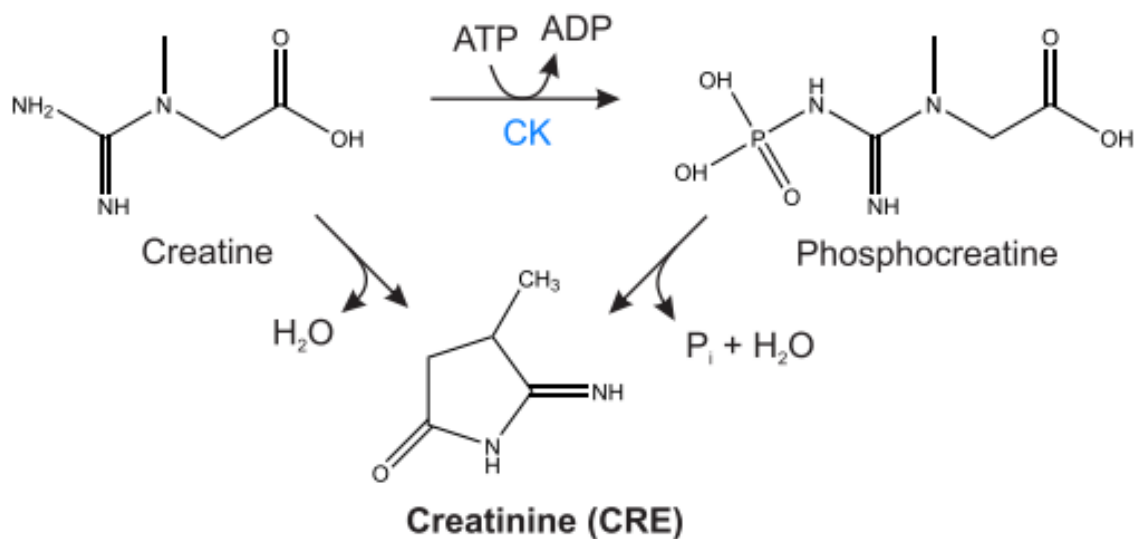
Figure 1.2: Metabolism of creatine to creatinine[2].

the body in urine via glomerular filtration in the kidneys [23]. It is to be noted that creatinine levels are fairly constant in the human body, though vary significantly from one person to the next based on muscle mass, size, weight, and gender[2]. Creatinine is the second most analysed

---

[1] The GFR results are reported normalised to 1.73 m^2 body surface area

biomolecule in the bioanalytical field after glucose for clinical applications [24]. Creatinine remains an important biomolecule as its concentration levels in biofluids (e.g., in blood serum[25]) indicates various clinical conditions of the kidneys. Health issues like CKD, cardiovascular problems and muscular disorders can be indicated if the creatinine levels in biofluids like blood, urine and saliva are out of the typical range, which is summarised in a review by Kumar et al. [2, 3] (table 1.2). It is to be noted there exists variation in these reported typical creatinine ranges according to each literature report as a result of analysis in different labs. For example, Bishop reports the normal range of creatinine in urine as 4.4-13.3 mM [26]. The normal range of creatinine in urine has been reported by Kumar et al. to be 4.4-18 mM[3] and creatinine levels outside this range can indicate various conditions including kidney disease, cardiovascular disease, muscular disorders and Parkinson's disease [3]. Although, major focus of this project remains on detection of creatinine for early detection of kidney conditions in particular chronic kidney disease, creatinine levels in biofluids can also indicate urine dilution[27] or thyroid dysfunction [28].

Table 1.2: Summary of healthy and harmful creatinine ranges in different biofluids as summarised by Kumar et al.[3]

Sample	Healthy creatinine levels	Harmful creatinine levels
Urine	4.4 - 18 mM	>20 and <3 mM
Blood	45-90 µM (Male) 60-110 µM (Female)	<40 and >150 µM
Saliva	4.4-17.7 µM	17.7 – 591 µM
Sweat	9.4-18 µM	60-200 µM

1.3. State-of-the-art creatinine sensing

Current medical diagnostic tests performed to detect CKD in laboratory or hospital settings are invasive, time consuming and high in cost. Many current creatinine detection methods are complex and have limitations towards miniaturisation for development of a POCT device. Electrochemical sensing offers advantages including low cost, high sensitivity, requirement of low sample volumes (few µl) and the fact that these sensors are easy to miniaturise [29]. Self-analysis of biofluids (e.g., urine) using a POCT medical device for diagnosis and management of several diseases including CKD would improve patient care significantly, in particular for patients at high risk of developing kidney conditions (patients with diabetes or hypertension). Currently,

plasma creatinine is used for assessment of renal function[30] although, this invasive test is not convenient for patients and research is focusing on development of non-invasive methods of assessment of renal function.

In a clinical setting the main approach to determining creatinine levels is a century old optical method of detection that relies on the Jaffe reaction (developed by Max Jaffe in 1886[31]). This involves the formation of a yellow chromogen through the reaction of creatinine and picric acid in alkaline conditions (fig. 1.3) [31]. Although, this method has low specificity due to interference with other chromogens, and also interference from high urine glucose and ascorbic acid [22, 32]. This technique is now outdated and not suitable for modern clinical analysis due to its low sensitivity and low specificity[33], and is also sensitive to pH. In comparison to other analytical techniques, the Jaffe reaction results for creatinine levels are about 15-25 % higher in value [34, 35].
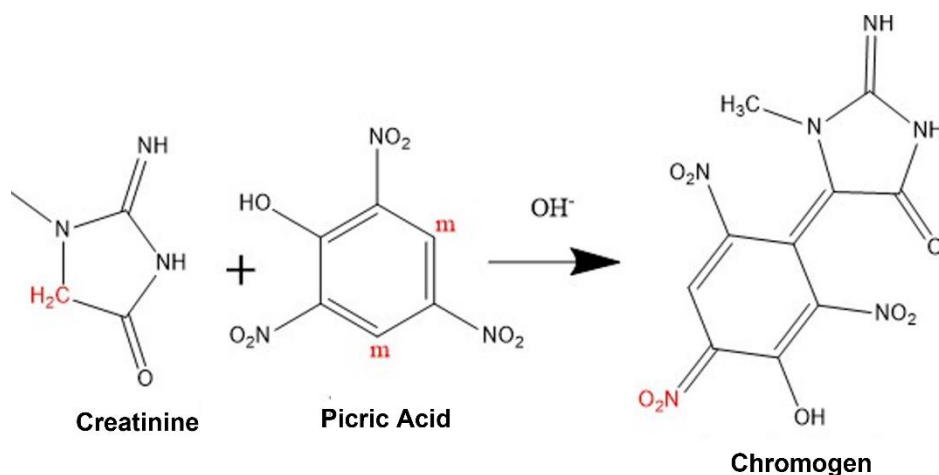
Figure 1.3: Widely used colorimetric Jaffe reaction for creatinine detection[3]

Various techniques have been investigated for creatinine detection including capillary electrophoresis (CE)[36], gas chromatography mass spectrometry (GC-MS)[37] and LC-MS[38], although these require high cost equipment, specially trained staff and involve highly complex techniques. They actively prevent systematic testing and spot screening in GP surgeries and on hospital wards. This means the Jaffe reaction is still the gold standard technique in clinical analysis due to its rapid analysis time (15 mins/sample) and low cost. However, research is now focusing on the development of electrochemical based sensors which rely on electron transfer for signal accession as they can be easily miniaturised, can be mass produced, have higher sensitivity and higher specificity and have low cost [30, 39].

1.3.1 Enzymatic creatinine biosensors

Enzymatic electrochemical sensing remains a widely used method due to its high selectivity, using either a one enzyme[40] or three-enzyme system. Enzyme-based creatinine biosensors have been developed in the past three decades due to their high selectivities [41] and are the only commercial electrochemical biosensors for creatinine to-date. These are based on either amperometry (mono-enzyme or tri-enzyme systems) and potentiometry involving ion sensitive or ion-selective field-effect transistors (ISFET) [42]. The potentiometric technique involves relating the analyte concentration to the potential when the electrochemical reaction is at equilibrium at zero current condition. Most potentiometric creatinine biosensors are based on hydrolysis of creatinine by creatinine iminohydrolase (CIH) or creatinine deiminase (CD), generating ammonia which is detected using ammonium ion-selective electrode (ISE) [41]. Meyerhoff and Rechnitz developed the first potentiometric creatinine biosensor in 1976 based on the ammonium ISE. The principle was based on the enzyme catalysed reaction of creatinine iminohydrolase and creatinine resulting in formation of N-methyl hydantoin and ammonia [43].

Although this biosensor has advantages including its simplicity, the drawbacks included poor storage stability, interference from endogenous NH_4^+, clinically irrelevant range of detection and a lifetime of 4 days [42].

Amperometric technique is based on heterogeneous electron transfer reaction involving electrochemical oxidation or reduction of the analyte. It involves applying a potential between the working electrode (WE) and the reference electrode (RE)[44]. The resulting current is related to the concentration of the analyte of interest[45]. These systems can reach very low detection limits, to even at 0.01 µM [46]. The majority of electrochemical amperometric biosensors rely on the three-enzyme system first introduced by Tsuchida and Yoda [47]. This method consists of a three-stage conversion process of creatinine to creatine, creatine to sarcosine and sarcosine to glycine. The last step produces electrochemically detectable oxygen or hydrogen peroxide. Detection of hydrogen peroxide is the preferred method due to interferences at oxygen electrodes that requires high potential for reduction process [41]. Recent techniques for designing these enzymatic biosensors also involve use of metal-based electrodes including cobalt based SPEs, where an electroactive complex of 1-methylhydantoin (an enzymatic reaction product with creatinine) with cobalt resulted in indirect measurement of creatinine concentrations [16].

Although these systems achieve great selectivities (the typical detection limits for creatinine enzymatic biosensors are 4.5 µM[48], 0.1 µM[49] and 0.01 µM[46]), the low stability of enzymes (as

they denature over time) and high cost adds to significant problems including low sensitivity and low reproducibility[44]. Thus, a large part of research is now directed towards development of non-enzymatic creatinine sensors which are low cost, highly stable as no enzymes are involved and have comparable selectivities. In summary, studies on non-enzymatic sensing of creatinine are showing promising results (in terms of high stability and repeatability) which can be applied to POC settings [30]. Currently there are no commercially available systems for non-invasive detection of creatinine e.g., in urine. The commercialised POCT hand-held devices are summarised in table 1.7 (Section 1.6.2).

1.3.2 Non-enzymatic creatinine biosensors

Typically, creatinine is not directly electroactive, and requires a secondary system to obtain a measureable electrochemical signal. Sensors are being developed with the aim to directly oxidise creatinine at the surface of bare or modified electrodes however. A study by Randviir & Banks, focused on developing a sensor platform for direct oxidation of creatinine at pH 9 in borate buffer solution at the surface of a bare gold electrode, but the system requires further optimisation in terms of detection of creatinine in blood serum at lower linear ranges (µM range instead of mM range) for its use in clinical analysis [22].

There exists a high affinity between the nitrogen of the aromatic ring in creatinine molecule and metal ions of silver, iron and copper [50]. In recent years, studies have significantly focused on developing sensing platforms for creatinine based on various metallic centres. Typically, the mechanism involves physical adsorption of creatinine at the metallic centre (forming a metal-creatinine complex), followed by a change in the amperometric signal [45]. In the non-enzymatic creatinine sensors reported in literature, there exists two different behaviours of the metal-creatinine complex: either there is a decrease in electroactive surface area as the complex agglomerates at the surface of the electrode (decreasing current signal) or there is desorption of a soluble reaction product (in the form of a soluble metal-creatinine complex), resulting in fresh layers of metallic centre at the electrode, therefore causing an increase in current signal [3]. It has been observed that the affinity of the metal-creatinine complex affects the current signal for creatinine detection. Most metal-based creatinine sensors work based on the formation of complex with the amino tautomer of creatinine (this form of creatinine exists at pH 7-8). Delocalisation of electrons around the three endocyclic N atoms in the amino tautomer of

creatinine (fig. 1.4), allows formation of the creatinine-complex with metals as they act as donors.
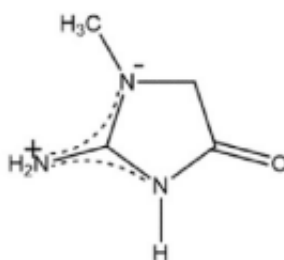
Figure 1.4: Amino tautomer of creatinine observed at pH 7-8[3].

Creatinine can bind with various transition metal ions such as Ag(I), Hg(II), Cd(II), Zn(II), Co(II), Ni(II), Cu(II), Pt(II) and Pd(II) to generate redox currents as it has several donor groups in its main tautomeric form. Based on this, research has been conducted to develop monometallic based sensors to detect creatinine [51]. Metal nanoparticles (NPs) have excellent electrocatalyst properties, along with providing enhanced electron transport and large effective surface area, which significantly has an effect on the electrochemical sensing process [52]. Various metal-based creatinine sensing systems in literature will be discussed in detail.

1.3.2.1 Copper based sensors

When using copper, the determination of creatinine in most studies is based on the chelation property of the analyte (and formation of a soluble copper-creatinine complex) rather than its redox behaviour[5, 7, 53]. However, some recent studies show that the redox behaviour of creatinine (electrooxidation) itself is possible[52, 54].

Comparison of different copper based electrochemical sensing methods for creatinine detection are summarised in table 1.3.

Table 1.3: Comparison of different copper based electrochemical sensing methods for creatinine detection.

Modification	Test solution	LOD (µM)	Detection Range (µM)	Sample	Reference
Cu/Pt	PBS	0.601	2.21-132.6	Urine	53

Cu/SPCE	PBS	0.0746	6-378	Serum	5
Cuprous nanoparticles encapsulated by polyacrylic acid (PAA) gel-Cu(II)	PBS	-	200-100 x 10^3	Urine	7
PMB (poly methylene blue)-Cu-CNF (Carbon nanofiber) nanocomposite	PBS	1768	4.42×10^{-3}-7.96	Serum, saliva, cerebral spinal fluid	54
Nafion-GQDs (Graphene Quantum Dots)-Cu	BR (Britton Robinson) buffer	-	1-450	Urine	55
Copper (with Nafion)	PBS	55.5	0-12300	Urine	56
CuNPs/PDA-rGO-NB/GC (PDA - polydopamine, rGO - reduced graphene oxide, NB - nile blue)	PBS	0.002	0.01-100	Urine, serum	51
Nafion/PAA gel-Cu2+ encapsulated Cu_2O NPs composite	PBS	0.3	1-2000	Saliva	57
PVA gel-Cu(II) PEDOT:PSS/cuprous oxide nanoparticles	PBS	0.06	0.4-960	Sweat	58

(CuO/IL/ERGO/SPCE) (copper oxide and ionic liquid composite onto an electrochemically reduced graphene modified screen-printed carbon electrode)	PBS	0.22	10-2000	Serum	59

Chen et al. developed a structural specific sensing scheme for creatinine detection in urine. An oxidative current (due to surface oxide regeneration) as a result is proportional to the concentration of creatinine. A surface oxide regeneration concept is investigated with respect to the catalytic activity of the copper electrode. Cuprous oxide is converted to a soluble copper-creatinine complex, and electrochemical oxidation of the exposed copper on the electrode surface occurs, regenerating the copper oxide. There exists no direct redox activity of creatinine in this process, and the method involves chelating ability between the copper layers and creatinine [53].

Copper electrodeposition has also been used for designing creatinine sensors. Raveendran et al. have developed a copper deposited non-enzymatic creatinine sensor where it is observed that upon application of a potential the copper undergoes electrochemical oxidation and cupric ions combine with creatinine in solution to form a soluble copper-creatinine complex. As a result, fresh copper surface is exposed and on an increase in concentration of creatinine, more copper undergoes electrochemical oxidation and the current signal increases as a result. The electrochemical sensing of creatinine using this method with cyclic voltammetry is shown in fig. 1.5 [5]. The study was performed in phosphate buffer (PB) of pH 7.4. Sato et al. have also shown cuprous oxide conversion to soluble copper-creatinine complex resulting in an increase in current signal using a copper electrodeposited gold electrode [56].
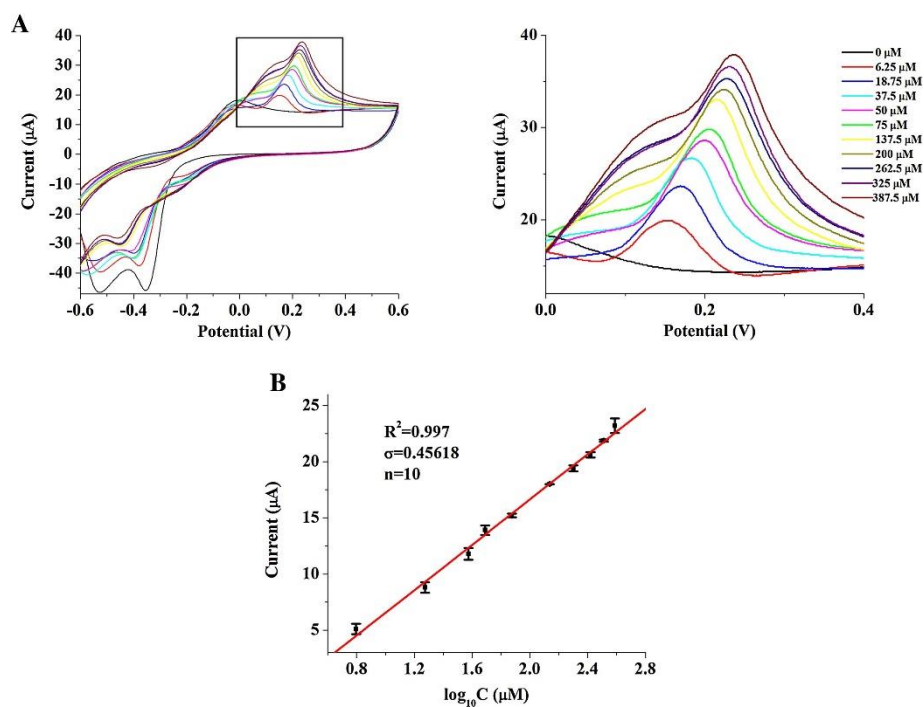
Figure 1.5: Electrochemical detection of creatinine with electrodeposited copper based screen-printed electrode[5].

A different mechanism of adsorption of creatinine with Cu(I) and Cu(II) ions on the electrode surface has been proposed by Kalasin et al. where the current signal *decreases* with the increase in concentration of creatinine[7]. It has been concluded that copper acts as a catalyst enhancing the oxidation of creatinine[54]. Cu(II) forms a complex with creatinine on the electrode surface when copper undergoes oxidation during the anodic scan. As a result the concentration of free Cu(II) decreases on increasing the concentration of creatinine and the oxidation current due to Cu/Cu(II) decreases [55].

Gao et al. investigated interaction of creatinine with Cu(II) ions on the surface of CuNPs and found adsorption led to reduced redox peak current intensities [51]. Copper(II) oxide has shown increased sensitivity towards detection of creatinine owing to its large surface area and electro-catalytic properties. The chelating ability of creatinine with CuO occurs through the formation of a soluble copper-creatinine complex [59]. Therefore, the interaction of Cu(II) with creatinine occurs in most cases through adsorption, causing a reduced current signal with increasing creatinine concentrations.

In some cases, interference removal from other molecules in the sample required additional steps. For example, uric acid interference (in a study by Raveendran et al.) required pre-treatment methods for eliminating its effect on creatinine response. The sensor showed no

11

interference with glucose, ascorbic acid, dopamine and urea. However, the samples were incubated with PbO_2 powder, in order to reduce the interference caused by uric acid [5].

In several studies, screen printed carbon electrode (SPCE) has been used as the substrate for development of the creatinine sensing platform. The fact the SPCE is a cost-effective and a disposable material, adds to its advantages, also allowing its potential use in POCT settings [5, 7, 57-59]. Non-enzymatic electrochemical creatinine sensing has been investigated using GC, Au and Pt electrode, finding Au giving the best performance in terms of redox signal with respect to copper [55, 56]. However, working with glassy carbon electrode (GCE) using electrodeposited NPs on the surface of the electrode gave significantly low LOD of 0.002 µM and relevant clinical range of detection (0.01-100 µM) in a study[51].

Polymer systems significantly enhance the sensitivity of creatinine detection platforms. Kalasin et al. combined cuprous nanoparticles with polyacrylic acid (PAA) gel for developing a platform to detect creatinine. The polymer gel allows reversible ionic cross-linking with the nanocomposites and also provides good mechanical properties[7, 58]. PAA gel-Cu(II) side chains were cross-linked with Cu_2O NPs (fig. 1.6) [7]. Creatinine forms a complex with Cu(II) as Cu(I) is oxidised to Cu(II), as a result giving increasing oxidation currents with increasing creatinine concentrations.
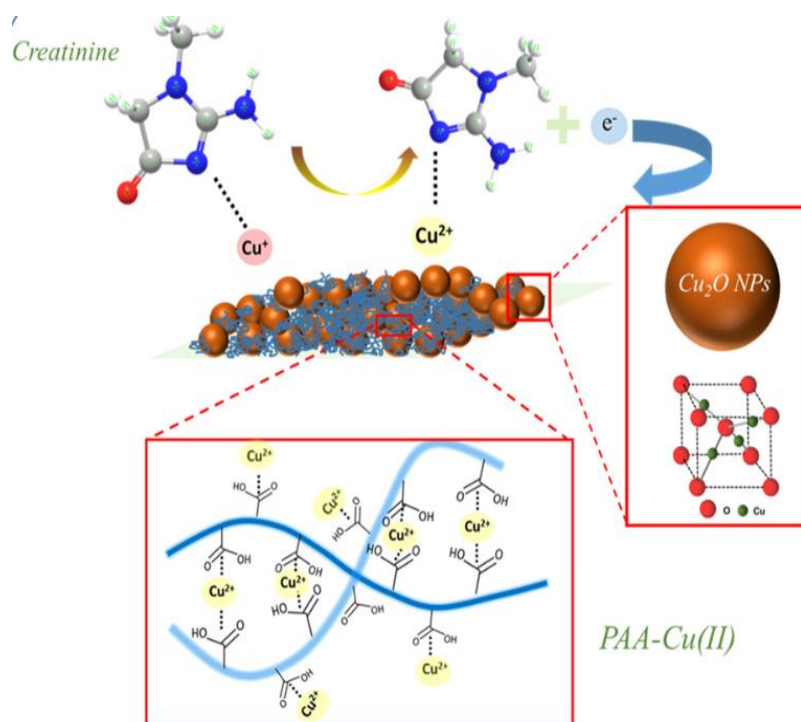
Figure 1.6: PAA-Cu(II) based creatinine electrochemical sensing [7].

Polymeric dye-based metal carbon nanofiber nanocomposites have also been used for detection of creatinine, where polymethylene blue (PMB) nanofibers were grown on the surface of copper doped carbon electrode. Creatinine was detected based on the recognition mechanism provided by PMB along with electrooxidation of creatinine which was catalysed by copper due to the formation of copper-creatinine complex. Carbon nanofiber based electrochemical sensors have shown to be of high mechanical strength and have high chemical stability in alkaline and acidic solutions. PMB increased the electrical conductivity and sensitivity of the analysis as a result of increased surface area of detection[54]. Graphene material additionally increases the electronic conductivity of the electrode, increasing the sensitivity of measurement[51, 55, 59]. Pedrozo et al. have improved the sensitivity of the sensor system by introducing graphene quantum dots (GQDs) mixed with Nafion polymer [55]. Nafion has also been used in other studies by Kalasin et al. and Sato et al. for potentially reducing the extent of interferences from negatively charged interferents including ascorbic acid (AA) and uric acid (UA) [57, 60].

Polydopamine (PDA) attached on reduced graphene oxide (rGO) loaded with nile blue (NB) has been drop coated onto the surface of GCE for developing a creatinine sensor. The use of PDA and rGO enhance the active sites and surface area for electron transfer [51]. Furthermore, a study has looked at developing a non-enzymatic creatinine sensor based on PVA-Cu(II)-PEDOT:PSS with cuprous and cuprite ions. The creatinine and cuprous ions were present at PEDOT sites [58].

Some limitations of the current copper sensors include requiring pre-treatment of samples (with PbO_2 powder) for interference removal including uric acid[5] and significantly complex procedures of sensor preparation.

1.3.2.2 Iron based sensors

Most iron-based creatinine sensors are designed based on the Fe(III) binding property to creatinine. Some studies are summarised in table 1.4.

Table 1.4: Comparison of different iron based electrochemical sensing methods for creatinine detection.

Modification	Test solution	LOD (μM)	Detection Range (μM)	Sample	Reference

Carbon black film in contact with paper-adsorbed iron (III) ions	NaCl	43	100-6500	Urine	61
FeCl$_3$ coated cotton fiber membranes	NaCl	-	884-21658.4	Urine	6
Fe$_2$O$_3$ integrated polyaniline (PANI) nanocomposite	PBS	0.144	1-13000	Serum	62
Fe^{3+} based µPAD (Paper-based analytical device)	NaCl	84	884-21.6 x 10^3	Urine	63

It has been observed in various studies that creatinine forms a complex with Fe(III) ions [6, 61, 63]. One possible mechanism involved the Fe(III)/Fe(II) redox pair where excess Fe(III) adsorbed onto the working electrode (WE) paper formed a complex with creatinine. The excess Fe(III) was measured and the concentration of creatinine was determined [6, 61, 63]. Kumar et al. also investigated formation of creatinine-Fe(III), where the redox current was dependent on the complex formation. As the creatinine concentration increased, Fe(III) formed a complex with creatinine and there was less available Fe(III) to form Fe(II) and as a result the Fe(III) reduction current decreased [6].
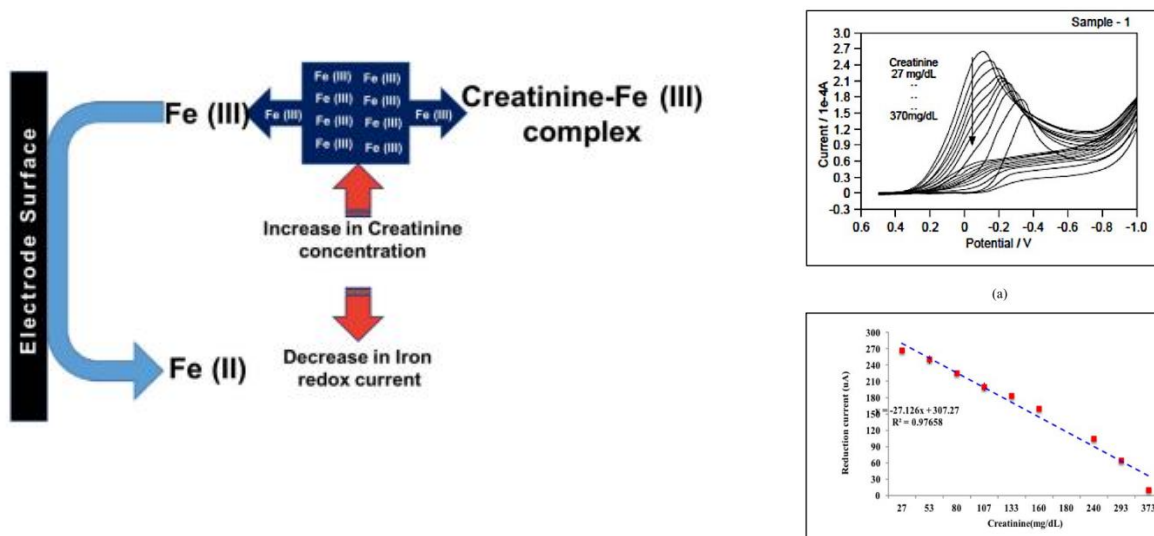
Figure 1.7: Fe(III) based detection of creatinine with reduced iron redox current on increasing creatinine concentrations[6].

A range of substrates have been used for iron-based creatinine sensing including GCE and SPEs. GCE based sensor has been used where Fe(III)-creatinine complex formation takes place. In this study, the conducting polymer PANI significantly enhances the surface area for interaction and allows faster charge transfer [62]. Alternatively, low cost carbon printed electrodes as disposable sensing platforms for creatinine detection have been used in a study by Kumar et al. based on $FeCl_3$ coated cotton fiber membranes[6]. Although, some of these studies add to advantages including low cost and use of no enzymes, overall, the preparation techniques are more complex than our sensing methods described *in this PhD* project for creatinine detection.

1.3.2.3 Other metal-based sensors

Binary nanoparticles (Fe-Cu), nickel foam iron doped materials and silver NPs are some of the other type of metal-based creatinine sensors developed with high sensor selectivities and sensitivities. The studies are summarised in table 1.5.

Table 1.5: Comparison of other metal based electrochemical sensing methods for creatinine detection.

Modification	Test solution	LOD (µM)	Detection Range (µM)	Sample	Reference

Fe-Cu-rGO (reduced graphene oxide) nanocomposite	PBS	0.01	0.01-1000	Whole blood	52
Keggin-type phosphomolybdate (PMo12)-doped polypyrrole (PPy) Film	H_2SO_4	0.005	1-100	-	64
Nickel foam iron doped	KOH	-	0.06-18 mM	1 M KOH	65
Reduced graphene oxide (RGO)/AgNPs film	PBS	0.743×10^{-6}	10×10^{-6}-120×10^{-6}	Urine	4
Silver nanoparticles (AgNPs)/multi walled carbon nanotube (CNT)/folic acid (FA)	BR buffer (CH_3COOH + H_3BO_3 + H_3PO_4)	0.008	0.01-200	Urine	66
MWCNT-inulin (a versatile carbohydrate polymer)-TiO2 bio-nanocomposite	PBS	0.06	0.2-1	Urine	67
Phosphotungstic acid/ poly(ethyleneimine) (PTA/PEI) multilayer	NH_4-HCl buffer	0.06	0.125-62.5	Urine	68

Various studies have shown the possibility of creatinine oxidation on different sensing platforms. Singh et al. observed creatinine oxidation to an oxime compound through the use of Fe_2O_3 (that bind to creatinine) and CuNPs (that act as an electrocatalyst in the reaction). Synergistic effect of binary copper-iron oxide significantly enhances the overall performance of this sensing system. Fe_2O_3 effectively captures creatinine through the secondary amine and allows formation of a complex with creatinine through the Fe(III) interaction, allowing creatinine oxidation. This sensor based on reduced graphene oxide (rGO) stabilised binary copper-iron oxide nanocomposite on 3D printed Ag-electrode gave a detection range between 0.01 to 1000 µM and LOD of 10 nM. The sensor responded in less than a minute and showed no interference in presence of uric acid, urea, dopamine and glutathione[52]. Direct oxidation of creatinine has also been investigated with nickel based electrochemical systems, where simultaneous urea and creatinine detection was investigated – nickel foam based electrocatalysts have been used for creatinine oxidation in a study by Carpenter & Stuve [65]. The studies were performed at pH 14 in 1 M KOH solutions. Reduced current densities are observed on nickel electrodes when creatinine is added to the system in presence of urea, due to possible site blocking due to stronger adsorption by creatinine on the electrode surface. Nickel hydroxy foam (NHF) and Fe-NHF were also used in this study for creatinine detection, where Fe-NHF gave the highest current densities for the electrochemical system. The overall current response in the CV and chronoamperometry study was significantly high (mA range) as a result of the use of high surface area metal based foams that provide increased number of active sites for the reaction. These reaction conditions were also used in our study with nickel electrodeposited GCE, as discussed in *Chapter 4*.

Other metal-based NPs, e.g., AgNPs have also been investigated for creatinine detection[4] (fig. 1.8), where creatinine adsorption on the metal active sites and direct creatinine oxidation are the mechanisms involved. Adsorption of creatinine at the WE, decreases the peak anodic current with increasing creatinine concentrations and allows effective detection of creatinine. Viswanath et al. developed the sensing technique using this method based on AgNPs and rGO, where the LOD was 0.743 pM with a linear range between 10 pM to 120 pM[4]. Although, Fekry et al. have used AgNPs to develop a method to oxidise creatinine directly on the surface of the WE, understanding the fact that AgNPs act as conduction centers enhancing the electron transfer from creatinine nitrogen centres. Sensor surface area is further increased due to use of folic acid and porous carbon nanotubes (CNTs), giving a significantly low LOD of 0.008 µM[66].

Creatinine can also form complexes with polyoxometalates (POMs) that are excellent redox catalysts. Guo et al. have studied a creatinine complex forming mechanism with Keggin-type phosphomolybdate (PMo$_{12}$) entrapped into a conducting polymer film of polypyrrole (PPy) [64]. PPy film enhances the conductivity of the system and improves the sensor sensitivity [64]. This indirect electrochemical sensing process involved complex formation between creatinine and PMo$_{12}$ (in presence of 0.50 M H$_2$SO$_4$), where creatinine replaces H$^+$ captured in the PMo$_{12}$ cavity, causing reduced peak currents with cyclic voltammetry due to less availability of H$^+$.
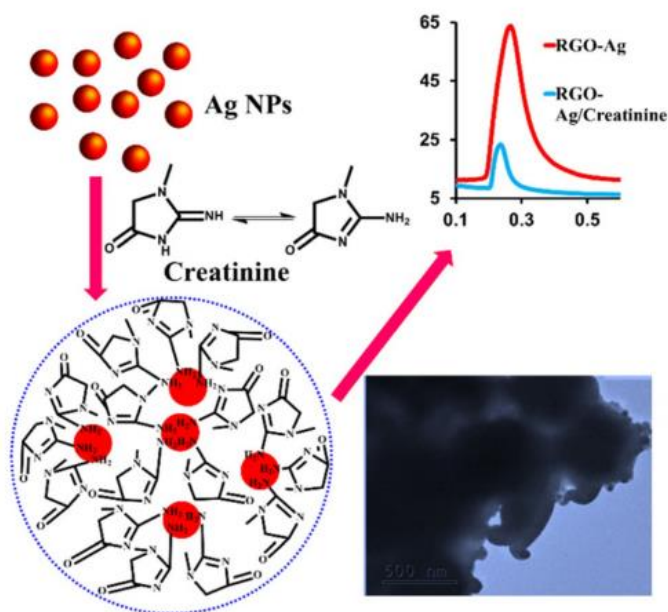
Figure 1.8: Electrochemical detection of creatinine based on AgNPs[4].

Although, the existing non-enzymatic creatinine sensing offers high sensor stability and short diagnostic times, there is still the need to develop simple, portable and low-cost alternatives for creatinine sensing. With the current non-enzymatic creatinine sensing techniques, there are limitations due to high cost, complex electrode preparation techniques and effect of interferences. As part of this PhD project, we have designed non-enzymatic creatinine sensors working based on unmodified electrode system (bare GCE and bare SPE) and based on a nanoparticle based system (Nickel-GCE). Few concepts of nanomaterial based sensing will be discussed below.

1.4 Nanomaterials and creatinine sensing

In the last few years, there has been significant research in the area of development of metal nanoparticles (particles with a mean diameter lower than 100 nm) based electroanalytical sensors. These materials show excellent physical and catalytic properties [69]. A faster electron transfer can be achieved through use of nanomaterial-based electrochemical sensors with high surface area and high conductivity. This enhances the sensitivity and selectivity of the electrochemical sensor. As a result of high surface area to volume ratio of nanomaterials, a higher number of active sites for redox reaction is available. The properties of nanoparticles are dependent on their shape and size and therefore, the morphology is critical [70]. Research is ongoing to incorporate nanomaterials for current and future sensing applications, including nanomaterials previously mentioned e.g., Ag NPs and Cu NPs.

Nickel based sensors have been explored and widely used seen in previous studies for glucose sensing[71, 72]. The fact that nickel catalyses the oxidation of glucose and other organic molecules in alkaline solution (through formation of Ni(II)/Ni(III) redox species), it was considered to explore creatinine sensing using this method (fig. 1.9).
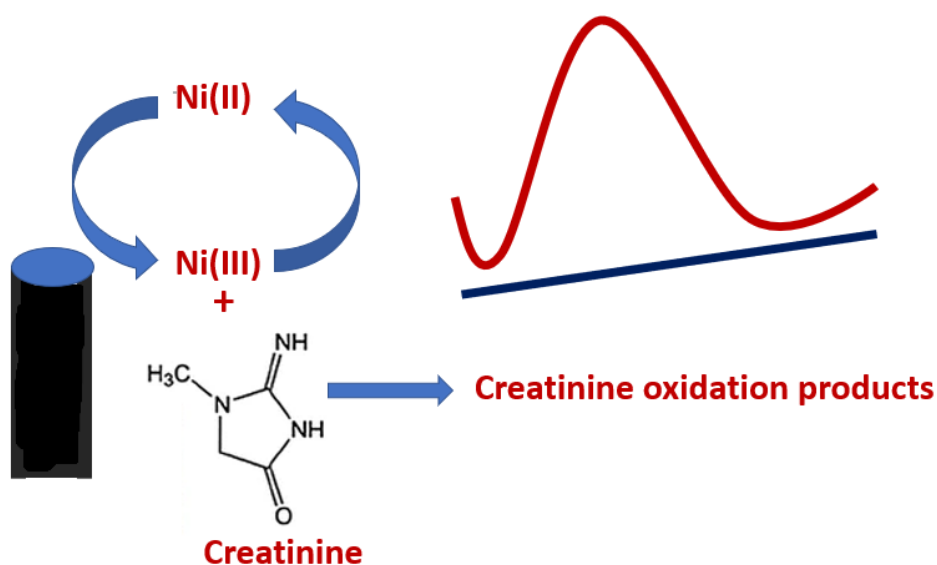
Figure 1.9: Schematic showing creatinine oxidation process on nickel nanoparticle based GCE.

1.5 Real sample analysis

As a result of multiple metabolic routes, creatinine is present in various biofluids. Physiological fluids like blood, urine, saliva and sweat have been analysed and investigated for development of creatinine sensor platforms. Research currently is shifting towards development of non-

invasive creatinine detection platforms in urine, saliva or sweat adding convenience for patients and possibility of measurements in real time.

1.5.1 Blood/plasma creatinine

Clinical analysis of creatinine in blood/plasma has been considered as the most widely used diagnostic fluid[3]. Detection of creatinine in blood or plasma is being considered a robust test for renal function assessment. Normal creatinine levels are found to be in the range of 40-150 µM. Creatinine levels higher than 500 µM indicate severe renal impairment where patients may require dialysis treatment or renal transplantation [30]. The conventional methods in labs require blood sampling in mL volumes [30]. Currently, research is now focusing on other non-invasive methods for clinical evaluation of kidney function through analysis in urine, sweat or saliva using POCT devices which would require microliters of volume of the sample making the tests more convenient. These biofluids could allow monitoring in real time and add to being user-friendly and convenient [30].

1.5.2 Saliva creatinine

Saliva creatinine can give information related to creatinine that observed in blood. Metabolic by-products of kidney failure can be monitored in saliva as the biofluid [73]. However, there exists low diagnostic accuracy and low specificity with this method of analysis, in comparison to traditional colorimetric creatinine detection methods including Jaffe reaction [74].

1.5.3 Sweat creatinine

Sweat creatinine measurement in wearable sensor devices is another alternative to creatinine analysis. Although, this technique is non-invasive but provides low sample volumes. Additionally, evaporation of sample causes overestimation of creatinine levels[75].

1.5.4 Urine creatinine

Urine has been used as a physiological fluid for many years to detect kidney diseases. Urea is the main component of urine and urea measurement gave information on the condition of the kidneys [30]. However, protein intake affects the urea levels in urine significantly and therefore is not a reliable biomarker for understanding renal function. Measurement of creatinine levels in urine is a more robust way to check kidney function. A more accurate way to analyse creatinine in urine is by performing 24h sample collection. A method for spot urine test, that is more convenient and beneficial requires calculation of albumin to creatinine ratio (*more discussion in Chapter 6 on Future Work).* This is a more robust clinical index for early screening of kidney disease. Normal creatinine levels in urine are between 4.4 – 13.3 mM[26]. Although, this clinical reference range may vary based on results from different labs.

Due to the advantages of measuring creatinine in urine non-invasively, this PhD project has considered developing a creatinine sensing platform for detection in urine.

1.6 Point-of-care testing (POCT)

Later chapters (*Chapter 5*) of the PhD project focus on development of a SPE system for creatinine sensing. SPEs allow miniaturisation of the sensing platform, requiring only few microliters of the sample and can easily be used for POC settings. The aim is to further develop this system into a POCT technology, where a one-spot analysis can give results to clinicians regarding kidney function.

Laboratory testing remains the dominant model for analyte testing currently. Although, economic pressures and providing more patient-centred care, is becoming the focus of healthcare systems[76]. The aim is to reduce costs of expensive care in secondary care hospital settings, and allowing early screening, diagnosis, and monitoring of clinical conditions at the primary care settings (e.g., GP surgeries). This way of testing is more convenient for patients as it avoids multiple visits to hospitals, especially for those who require frequent tests.

POCT diagnostic medical devices allow testing at the point of patient care, usually at patient's bedside. Several healthcare settings where these devices are now used include hospital-based wards, emergency department, general practice (GP) and home care[77]. The time of result is key in case of POCT devices, although the accuracy of result is significantly important. The idea is to

have a low-cost, user-friendly creatinine medical device that can be used for early screening of chronic kidney disease (CKD). This PhD project can be developed in further stages of the research study as discussed in *Chapter 6 on future work*, where a POCT device that measures albumin to creatinine ratio (ACR) would provide a robust clinical index for early detection of CKD.
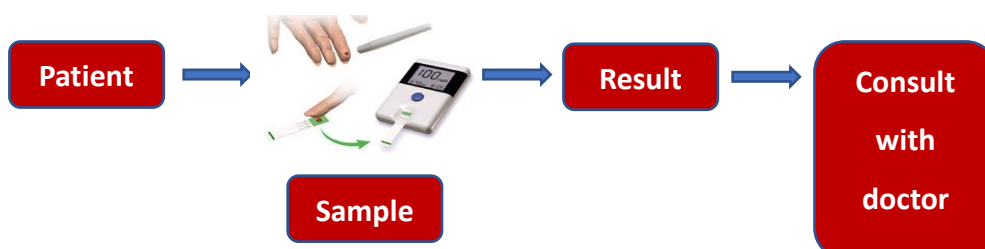
Figure 1.10: Pathway of POCT testing.

1.6.1 Laboratory automatic analysers and creatinine detection

A point-of-care (POC) screen printed electrode system would mean there is no need for samples to travel, no use of complex or expensive equipment and no requirement of skilled analytical personnel. There are already commercialised POC devices for creatinine detection including Nova Biomedical Stat Profile Critical Care Xpress (CCX), which allows multi-analyte detection of analytes along with creatinine. This technology although has a result time of 150 s has an error of approximately 11.4% and is used for blood samples [78].

Chemical and enzymatic methods based on benchtop automatic analyzers are currently used for creatinine detection in serum or urine [35]. The most common method is using Jaffe reaction where a creatinine-picrate complex forms in alkaline medium. The rate of increase in absorbance at 500 nm is directly proportional to the concentration of creatinine [35].

The other enzymatic method used in the current laboratory analyzers use the method where creatinine is hydrolyzed by creatininase to creatine. Creatinase converts creatine to urea and sarcosine. Sarcosine oxidase then converts sarcosine into glycine and formaldehyde along with the production of hydrogen peroxide. In presence of peroxidase, hydrogen peroxide reacts with 4-aminoantipyrine and N-ethyl-N-sulfopropyl-m-toluidine to yield a dye. The change in absorbance at 548 nm is directly proportional to the creatinine concentration [35]. However, the

use of enzymatic method is limited to point-of-care testing and dry chemistry because it is 10-folds more expensive than Jaffe method.

Through assessments, both Jaffe and enzymatic reaction methods have seen to meet the analytical performance requirements for routine use (table 1.6). Despite the fact that enzymatic method shows better performance at lower creatinine levels, Jaffe reaction still remains the best technique in use due to its cost (10 folds lower) in comparison to the enzymatic method.

Table 1.6: Method parameters applied on the lab analyzers using Jaffe or enzymatic method of detection[35].

Sample	Method	Detection range (mg/dL)	LOD (mg/dL)
Serum	Jaffe reaction	0.2-38.70	0.01
	Enzymatic reaction	0.25-40	0.01
Urine	Jaffe reaction	0.21-37.85	0.25
	Enzymatic reaction	0.1-40	0.07

1.6.2 POCT Creatinine Devices

At the point-of-care (POC) level, creatinine analysis must be according to the ASSURED guidelines: where the detection is Affordable, Sensitive, Specific, User-friendly, Rapid & Robust, Equipment-free and easily Delivered[76].

The idea of POC creatinine devices is to allow reliable creatinine testing at GP surgery or at patient's home. This has already been seen in case of glucose testing. There is a need to develop creatinine POC technologies that are more reliable, accurate, sensitive, low cost, and that provide rapid detection results, without the need of a trained personnel.

i-STAT and StatSensor are the most studied POC hand-held devices in literature [79]. All currently commercialised creatinine sensing POCT platforms are based on enzymes. The current commercialised creatinine POCT devices are summarised in table 1.7.
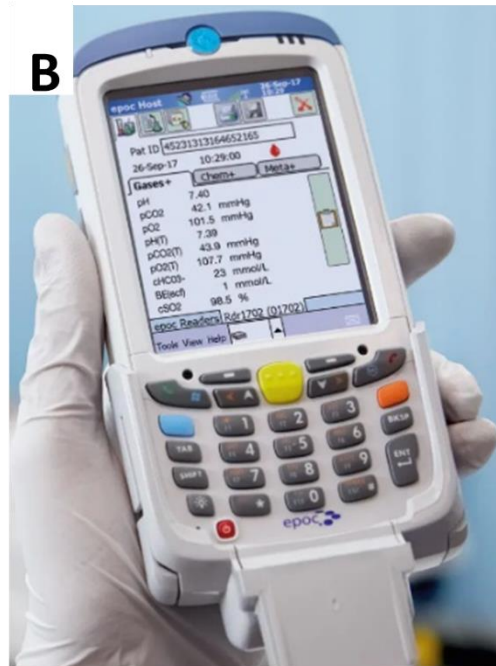
Figure 1.11: A) StatSensor (Nova Biomedical)[80] B) epoc® Blood Analysis System (Siemens Healthineers)[81]

Table 1.7: Summary of currently commercialised POCT hand-held devices for creatinine detection.

Device	Description	Limitations	Reference
epoc® Blood Analysis System (Siemens Healthineers)	Single test card technology Coefficient of variation for creatinine ≤ 15%	Largest bias in creatinine measurements in comparison to routine laboratory analyzers (Architect c8000 and Cobas c702 systems) 10 folds higher in cost than Jaffe method due to use of enzymes Less user-friendly device	82
i-STAT (Abbott)	Has acceptable error and showed least major errors for creatinine detection	Less user-friendly, high cost (£ 5,500)	79
StatSensor (Nova Biomedical)	Single use biosensor	Shows highest major error rate in a study [79] for creatinine detection High cost (in comparison to Jaffe method)	78

Such devices are already in use in hospitals today, but have disadvantages related to high cost. The fact that there is no POCT device commercialised that works non-invasively on biofluids including urine, sweat or saliva, therefore more research is required to develop these sensing devices.

1.7 Thesis outline and objectives

There has been significant research in the area of developing highly specific enzymatic creatinine biosensors, although they are high in cost and have less storage stability due to the presence of

enzymes. Therefore, research has recently shifted towards exploring non-enzymatic creatinine detection platforms that are low cost, simple and easy to fabricate platforms with high stability.

The aim of this PhD project is to contribute towards research in the area of development of non-enzymatic creatinine sensor platforms. We have developed sensor platforms using bare glassy carbon electrode (GCE), nickel based GCE and screen-printed electrodes (SPEs) using a technique where creatinine oxidation occurs due to presence of alkaline ferricyanide.

1.7.1 Chapters

1.7.1.1 Chapter 1

This chapter introduces the PhD research in the area of developing sensors for creatinine detection. A detailed literature review will describe the current techniques researched in the area of non-enzymatic creatinine sensing. Significance of nanomaterials in electrochemical sensing will be discussed, followed by a discussion on the significance of point-of-care testing platforms for creatinine detection.

1.7.1.2 Chapter 2

In this chapter, basics of electrochemical theory and methods will be introduced. The concepts of electrochemical cells, Faraday's Law and Nernst Equation will be discussed. Voltammetry techniques including cyclic voltammetry (CV) will be discussed in detail. Theory of spectroscopic methods including NMR will also be discussed, followed by a short discussion on electroanalytical systems and nanomaterial-based sensing.

1.7.1.3 Chapter 3

In experimental chapter 3, techniques developed for detection of creatinine using bare GCE in alkaline ferrocyanide solution is discussed. Characterisation methods including NMR and UV-vis techniques are used for analysis of the reaction mechanism and colorimetric creatinine detection, respectively. Electrochemical studies with cyclic voltammetry (CV) is used for analysing the electrochemical performance of the creatinine sensor in alkaline ferrocyanide solution. Selectivity studies are performed with artificial urine. Further sensor analysis is

performed with interferents including ascorbic acid (AA), uric acid (UA) and glucose (Glu). Electrochemical reaction mechanism is analysed in detail with NMR study.

1.7.1.4 Chapter 4

Chapter 4 introduces the use of a nickel based GCE for electrochemical detection of creatinine in alkaline ferrocyanide solution. SEM analysis is discussed where the surface of GCE is analysed in presence of nickel nanoparticles. Steps to prepare a nickel nanoparticle-based electrode by electrodeposition technique is also discussed. Electrochemical detection of creatinine by electrochemical techniques including cyclic voltammetry (CV) and chronoamperometry (CA) are mentioned. Optimisation studies were performed with different concentrations of KOH to evaluate the performance of creatinine sensing on the nickel based electrochemical platform. Studies with nickel foam as the electrode sensor for creatinine detection were also analysed. A short section also describes the limitations in terms of interference with urea, as urea is significantly electroactive on nickel-based electrodes.

1.7.1.5 Chapter 5

This chapter moves towards the miniaturisation of the creatinine sensors developed in chapter 3 using SPE based platforms, with the aim to develop this study such that these sensors can be used in a POCT setting. The bare GCE creatinine system with alkaline ferrocyanide is miniaturised onto an electrochemical cell with SPE system. Bare SPEs, nafion/SPEs and carbon black/nafion/SPEs are used in this study to understand and eliminate/reduce the extent of interferences with AA, UA and Glu. Selectivity studies are performed with artificial urine samples. PVA/KOH/ferrocyanide hydrogels were also investigated to evaluate the applicability of this sensor system towards POCT at later stages.

1.7.1.6 Chapter 6

This chapter presents the conclusions and future work of this PhD project. A summary of the experimental work for all chapters will be described. Research ideas are described for the next part of the research also related to the information understood through participation in the ICURe Discovery program. With various conversations with clinicians, we market tested the idea of the research involved in this PhD project and what future work could be done. A detailed discussion on albumin sensing and further miniaturisation of the sensor platform, along with other improvements to the technology is discussed.

1.8 References

1. A. S. Levey and J. Coresh, *The lancet*, 2012, **379**, 165-180.

2. R. Cánovas, M. Cuartero and G. A. Crespo, *Biosensors and Bioelectronics*, 2019, **130**, 110-124.

3. R. R. Kumar, M. O. Shaikh and C.-H. Chuang, *Analytica Chimica Acta*, 2021, **1183**, 338748.

4. K. B. Viswanath, R. Devasenathipathy, S. F. Wang and V. Vasantha, *Electroanalysis*, 2017, **29**, 559-565.

5. J. Raveendran, P. Resmi, T. Ramachandran, B. G. Nair and T. S. Babu, *Sensors and Actuators B: Chemical*, 2017, **243**, 589-595.

6. V. Kumar, S. Hebbar, R. Kalam, S. Panwar, S. Prasad, S. Srikanta, P. Krishnaswamy and N. Bhat, *IEEE Sensors Journal*, 2017, **18**, 830-836.

7. S. Kalasin, P. Sangnuang, P. Khownarumit, I. M. Tang and W. Surareungchai, *ACS Biomaterials Science & Engineering*, 2020, **6**, 1247-1258.

8. S. W. Walker, P. Rae, P. Ashby and G. Beckett, *Clinical Biochemistry*, John Wiley & Sons, 2013.

9. J. Coresh, E. Selvin, L. A. Stevens, J. Manzi, J. W. Kusek, P. Eggers, F. Van Lente and A. S. Levey, *Jama*, 2007, **298**, 2038-2047.

10. V. Jha, G. Garcia-Garcia, K. Iseki, Z. Li, S. Naicker, B. Plattner, R. Saran, A. Y.-M. Wang and C.-W. Yang, *The Lancet*, 2013, **382**, 260-272.

11. K. Matsushita, J. Coresh, Y. Sang, J. Chalmers, C. Fox, E. Guallar, T. Jafar, S. K. Jassal, G. W. Landman and P. Muntner, *The lancet Diabetes & endocrinology*, 2015, **3**, 514-525.

12. R. T. Gansevoort, K. Matsushita, M. Van Der Velde, B. C. Astor, M. Woodward, A. S. Levey, P. E. De Jong and J. Coresh, *Kidney international*, 2011, **80**, 93-104.

13. C. P. Kovesdy, *Kidney International Supplements*, 2022, **12**, 7-11.

14. P. Dasgupta, V. Kumar, P. Krishnaswamy and N. Bhat, *CSI Transactions on ICT*, 2018, **6**, 5-10.

15. A. S. Levey, J. Coresh, K. Bolton, B. Culleton, K. S. Harvey, T. A. Ikizler, C. A. Johnson, A. Kausz, P. L. Kimmel and J. Kusek, *American Journal of Kidney Diseases*, 2002, **39**, i-ii+ S1-S266.

16. P. Dasgupta, V. Kumar, P. R. Krishnaswamy and N. Bhat, *ACS omega*, 2020, **5**, 22459-22464.

17.   P. M. Hall, M. Schuman and D. G. Vidt, *CRC Critical Reviews in Clinical Laboratory Sciences*, 1976, **7**, 33-47.

18.   J. Liebig, *Justus Liebigs Annalen der Chemie*, 1847, **62**, 257-369.

19.   W. J. Visek, *The Journal of nutrition*, 1986, **116**, 36-46.

20.   S. Narayanan and H. Appleton, *Clinical chemistry*, 1980, **26**, 1119-1126.

21.   J. R. Knowles, *Annual review of biochemistry*, 1980, **49**, 877-919.

22.   E. P. Randviir and C. E. Banks, *Sensors and Actuators B: Chemical*, 2013, **183**, 239-252.

23.   N. V. Bhagavan, *Medical biochemistry*, Academic press, 2002.

24.   M. Joffe, C.-y. Hsu, H. I. Feldman, M. Weir, J. Landis and L. L. Hamm, *American journal of nephrology*, 2010, **31**, 426-434.

25.   H. Schiffl and S. M. Lang, *Molecular diagnosis & therapy*, 2012, **16**, 199-207.

26.   M. L. Bishop, *Clinical Chemistry: Principles, Techniques, and Correlations, Enhanced Edition: Principles, Techniques, and Correlations*, Jones & Bartlett Learning, 2020.

27.   S. Gamagedara, H. Shi and Y. Ma, *Analytical and bioanalytical chemistry*, 2012, **402**, 763-770.

28.   K. Spencer, *Annals of clinical biochemistry*, 1986, **23**, 1-25.

29.   M. Mascini and S. Tombelli, *Biomarkers*, 2008, **13**, 637-657.

30.   A. Tricoli and G. Neri, *Sensors*, 2018, **18**, 942.

31.   M. Jaffé, 1886.

32.   R. D. Perrone, N. E. Madias and A. S. Levey, *Clinical chemistry*, 1992, **38**, 1933-1953.

33.   I. Drion, C. Cobbaert, K. H. Groenier, C. Weykamp, H. J. Bilo, J. F. Wetzels and N. Kleefstra, *BMC nephrology*, 2012, **13**, 1-8.

34.   D. A. Walsh and E. Dempsey, *Analytica chimica acta*, 2002, **459**, 187-198.

35.   T. Küme, B. Sağlam, C. Ergon and A. R. Sisman, *Journal of clinical laboratory analysis*, 2018, **32**, e22168.

36.   H. Huang, Z. Chen and X. Yan, *Journal of separation science*, 2012, **35**, 436-444.

37.   S. M. Pedersen, C. Nebel, N. C. Nielsen, H. J. Andersen, J. Olsson, M. Simrén, L. Öhman, U. Svensson, H. C. Bertram and A. Malmendal, *European Food Research and Technology*, 2011, **233**, 1013-1021.

38.   Y. Jiang, X. Cheng, C. Wang and Y. Ma, *Analytical chemistry*, 2010, **82**, 9022-9027.

39.   M. Sreeramareddygari, S. Devaramani, R. Thippeswamy, S. Kempahanumakkagari and W. Surareungchai, 2021.

40.   J. M. Magalhães and A. A. Machado, *Analyst*, 2002, **127**, 1069-1075.

41.   C. Pundir, S. Yadav and A. Kumar, *TrAC Trends in Analytical Chemistry*, 2013, **50**, 42-52.

42.   A. J. Killard and M. R. Smyth, *Trends in biotechnology*, 2000, **18**, 433-437.

43. M. Meyerhoff and G. A. Rechnitz, *Analytica chimica acta*, 1976, **85**, 277-285.

44. C. L. Gonzalez-Gallardo, N. Arjona, L. Álvarez-Contreras and M. Guerra-Balcázar, *RSC advances*, 2022, **12**, 30785-30802.

45. R. R. Kumar, M. O. Shaikh and C.-H. Chuang, *Analytica Chimica Acta*, 2021, 338748.

46. P. Kumar, R. Jaiwal and C. Pundir, *Analytical biochemistry*, 2017, **537**, 41-49.

47. T. Tsuchida and K. Yoda, *Clinical Chemistry*, 1983, **29**, 51-55.

48. A. Soldatkin, J. Montoriol, W. Sant, C. Martelet and N. Jaffrezic-Renault, *Materials Science and Engineering: C*, 2002, **21**, 75-79.

49. H. Suzuki and Y. Matsugi, *Sensors and Actuators B: Chemical*, 2004, **98**, 101-111.

50. M. Mitewa, *Coordination chemistry reviews*, 1995, **140**, 1-25.

51. X. Gao, R. Gui, H. Guo, Z. Wang and Q. Liu, *Sensors and Actuators B: Chemical*, 2019, **285**, 201-208.

52. P. Singh, S. Mandal, D. Roy and N. Chanda, *ACS Biomaterials Science & Engineering*, 2021.

53. C.-H. Chen and M. S. Lin, *Biosensors and Bioelectronics*, 2012, **31**, 90-94.

54. I. Pandey, P. K. Bairagi and N. Verma, *Sensors and Actuators B: Chemical*, 2018, **277**, 562-570.

55. M. J. Pedrozo-Penafiel, T. Lopes, L. M. Gutierrez-Beleno, M. E. M. Da Costa, D. G. Larrude and R. Q. Aucelio, *Journal of Electroanalytical Chemistry*, 2020, **878**, 114561.

56. N. SATO, K. TAKEDA and N. NAKAMURA, *Electrochemistry*, 2021, 21-00016.

57. S. Kalasin, P. Sangnuang, P. Khownarumit, I. M. Tang and W. Surareungchai, *ACS Biomaterials Science & Engineering*, 2020, **6**, 5895-5910.

58. S. Kalasin, P. Sangnuang and W. Surareungchai, *ACS Biomaterials Science & Engineering*, 2020, **7**, 322-334.

59. S. Boobphahom, N. Ruecha, N. Rodthongkum, O. Chailapakul and V. T. Remcho, *Analytica Chimica Acta*, 2019, **1083**, 110-118.

60. N. SATO, K. TAKEDA and N. NAKAMURA, *Electrochemistry*, 2021, **89**, 313-316.

61. E. L. Fava, T. M. do Prado, A. Garcia-Filho, T. A. Silva, F. H. Cincotto, F. C. de Moraes, R. C. Faria and O. Fatibello-Filho, *Talanta*, 2020, **207**, 120277.

62. R. Sriramprabha, M. Sekar, R. Revathi, C. Viswanathan and J. Wilson, *Analytica Chimica Acta*, 2020, **1137**, 103-114.

63. E. L. Fava, T. Martimiano do Prado, T. Almeida Silva, F. Cruz de Moraes, R. Censi Faria and O. Fatibello-Filho, *Electroanalysis*, 2020, **32**, 1075-1083.

64. M. D. Guo and H. X. Guo, *Journal of Electroanalytical chemistry*, 2005, **585**, 28-34.

65. K. Carpenter and E. M. Stuve, *Journal of Applied Electrochemistry*, 2021, **51**, 945-957.

66. A. Fekry, S. Abdel-Gawad, R. Tammam and M. Zayed, *Measurement*, 2020, **163**, 107958.

67.	G. J. Kalaivani and S. Suja, *New Journal of Chemistry*, 2019, **43**, 5914-5924.

68.	P. Han, S. Xu, S. Feng, Y. Hao and J. Wang, *Talanta*, 2016, **151**, 114-118.

69.	D. Hernández-Santos, M. B. González-García and A. C. García, *Electroanalysis: An International Journal Devoted to Fundamental and Practical Aspects of Electroanalysis*, 2002, **14**, 1225-1235.

70.	D. Caschera, F. Federici, D. Zane, F. Focanti, A. Curulli and G. Padeletti, *Journal of Nanoparticle Research*, 2009, **11**, 1925.

71.	Y. Zhang, X. Xiao, Y. Sun, Y. Shi, H. Dai, P. Ni, J. Hu, Z. Li, Y. Song and L. Wang, *Electroanalysis*, 2013, **25**, 959-966.

72.	H. Nie, Z. Yao, X. Zhou, Z. Yang and S. Huang, *Biosensors and Bioelectronics*, 2011, **30**, 28-34.

73.	J. E. Lloyd, A. Broughton and C. Selby, *Annals of clinical biochemistry*, 1996, **33**, 428-431.

74.	T. J. Lasisi, Y. R. Raji and B. L. Salako, *BMC nephrology*, 2016, **17**, 1-6.

75.	Y. Y. Al-Tamer, E. A. Hadi and I. e. I. Al-Badrani, *Urological research*, 1997, **25**, 337-340.

76.	A. St John and C. P. Price, *The Clinical Biochemist Reviews*, 2014, **35**, 155.

77.	M. S. OAM, 2016.

78.	M. D. Shephard, *The Clinical Biochemist Reviews*, 2011, **32**, 109.

79.	C. van der Heijden, L. Roosens, H. Cluckers, A. H. Van Craenenbroeck and B. Peeters, *Clinica Chimica Acta*, 2019, **497**, 13-19.

80.	Nova Biomedical, https://novabiomedical.com/statstrip-creatinine/index.php, (accessed 31 May, 2023).

81.	Siemens Healthineers

https://www.siemens-healthineers.com/en-uk/blood-gas/blood-gas-systems/epoc-blood-analysis-system, (accessed 27 June, 2023).

82.	Z. Mohammed-Ali, S. Bagherpoor, P. Diker, T. Hoang, I. Vidovic, C. Cursio, F. Leung and D. Brinc, *Practical Laboratory Medicine*, 2020, **22**, e00190.

Chapter 2 – Electrochemical Theory and Methods

2.1 Electrochemical theory and methods

2.1.1 Electrochemistry and electroanalytical techniques

Electrochemistry involves charge separation at interfaces in electrochemical cells which can lead to charge transfer, either homogeneously in solution or heterogeneously on electrode surfaces [4, 11]. Orbital structures of molecules and band structures of metal electrodes are involved in electrochemical reactions at electrode surfaces [4].

Electrochemical methods are the most widely used methods for sensing analytes in a range of applications including biomedical and environmental [12]. These methods have advantages over other analytical techniques including spectrophotometry, HPLC (high-performance liquid chromatography) and colorimetry. Conventional analytical techniques are high in cost, complex and time-consuming [4]. Electrochemical methods are low cost, allow easy sample preparation and can perform multi-analyte detection along with high sensitivity and selectivity [12]. The solution-electrode interface (which forms the electrical double layer) is of interest in these methods of analysis [13].

2.1.1.1 Electrochemical cell reactions

The overall reaction in a two-electrode electrochemical cell involves two half-reactions – one taking place at the working electrode (WE) (of electroanalytical interest) and the other is at the reference electrode (RE), which standardizes the other half cell as a result of its constant composition phases. With a three-electrode cell, the counter electrode (CE) completes the circuit and allows charge to flow. The potential of a reference electrode is fixed. As a result, any changes in the electrochemical cell are due to the changes occurring at the working electrode, which in this case forms a key part of the sensor element. The energy of electrons in the WE can

be controlled (same as controlling potential of WE with respect to the RE). Faradaic and non-faradaic processes occur at electrodes in an electrochemical reaction process. Faradaic processes involve charge transfer at the electrode/solution interface, whereas in non-faradaic processes no charge transfer reaction occurs, although external currents may flow as a result of change in electrode-solution interface in terms of adsorption or desorption of molecules.

2.1.1.2 Electrochemical Cells

Electrochemical cells are a collection of interfaces with at least two electrodes and an electrolyte phase [4]. With a three-electrode cell (in voltammetry), working electrode (WE), counter electrode (CE) and reference electrode (RE) are used. Investigated processes occur at the WE. RE, which is at constant potential allows control of potential of the WE. Current flows between the WE and the CE.

Faradaic currents flow in electrochemical cells, which are of two types – galvanic and electrolytic. Spontaneous reactions occur in a galvanic cell, where there is conversion of chemical energy to electrical energy when the cell is connected externally by a conductor (fig. 2.1). An external voltage (greater than the open-circuit potential) is applied to an electrolytic cell, where chemical reactions occur as a result of input of electrical energy.
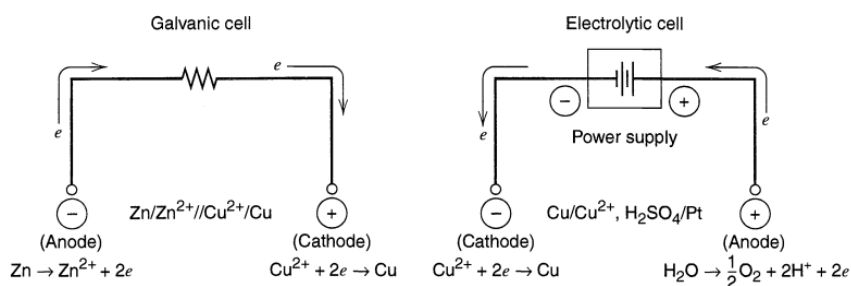
Figure 2.1: Galvanic and electrolytic cell referenced from[4]

2.1.1.3 Faraday's Law

The current in amperometric experiments can be integrated to get the charge that is transferred which relates to number of moles of analyte reduced or oxidised in the reaction, using Faraday's law (Equation 2.1).

$$Q = nFN \qquad \text{(Equation 2.1)}$$

where Q is charge transferred in Coulombs (C), N is number of moles of analyte converted in the reaction (oxidised or reduced) and n is number of moles of electrons transferred per mole of analyte[2].

2.1.1.4 Reference Electrode

A reference electrode (RE) has a stable equilibrium potential. A WE electrode potential is measured in relation to the RE potential.

By convention, the primary reference electrode chosen for electrochemical studies against which all the potentials are referenced is the SHE (Standard Hydrogen Electrode) or NHE (Normal Hydrogen Electrode) (Equation 2.2). It has a potential of 0 V at all temperatures [4].

$$Pt/H_2(a = 1)/H^+(a = 1) \qquad \text{(Equation 2.2)}$$

Another type of RE is the silver-silver chloride electrode,

$$Ag/AgCl/KCl \text{ (saturated in water)} \qquad \text{(Equation 2.3)}$$

with a potential of 0.197 V vs NHE[4].

The potential of a RE is fixed and any changes in the electrochemical cell are due to changes occurring at the WE surface[4]. These REs have a porous frit that separates the electrode from the solution[9]. For alkaline solutions, generally Hg/HgO RE is preferred to prevent the RE frit from dissolving in highly alkaline solutions.

2.1.1.5 Nernst equation

The redox reaction equilibrium is affected by the potential sweep at the working electrode surface. Equilibrium is established if the electron transfer rate is higher than the voltage scan

rate. Then, the equilibrium exists at faster rates at the WE surface with the potential scans. The applied potential (E) can be related to the equilibrium concentrations of the analyte in the forms of X and X^+, assuming reduction reaction occurs.

$$E = E^o - \frac{RT}{nF} ln \frac{X}{X^+}$$

(Equation 2.4)

where E^O is the standard reduction potential.

For reversible reactions (with fast electrode kinetics), the Nernst equilibrium is established at faster rates as the potential is scanned. For quasi-reversible and irreversible reactions (with slower electrode kinetics), the Nernst equilibrium may not be maintained [1].

2.1.1.6 Electrical double layer

Heterogeneous electrode reactions take place at the interfacial region between the electrode and solution which is also known as **double-layer capacitance** (fig. 2.3)[4]. This region is also termed as the 'Electrical Double Layer'. The structure of this region significantly affects the electrode process (in terms of electron transfer rate) and the electrochemical measurements [11]. This double layer can be viewed as a capacitor, which needs to be charged before obtaining a desired potential at the working electrode (WE). A capacitive current, also known as charging current (which is not due to oxidation or reduction of analyte in solution) as a result flows in the circuit, which may interfere with electrochemical measurements, and can be eliminated using techniques such as differential pulse voltammetry (DPV) [11, 14].

The electrical double layer is made of several layers on the solution side. The inner layer (also known as compact, Helmholtz or Stern layer) consists of mainly solvent molecules and also other specifically adsorbed molecules. The nature of the double layer can affect the rate of electrode processes in an electrochemical reaction. An analyte (electroactive molecule) which can approach only till the OHP, will experience a potential drop across the diffuse layer and therefore, the total potential it experiences will be less than the applied potential[5].
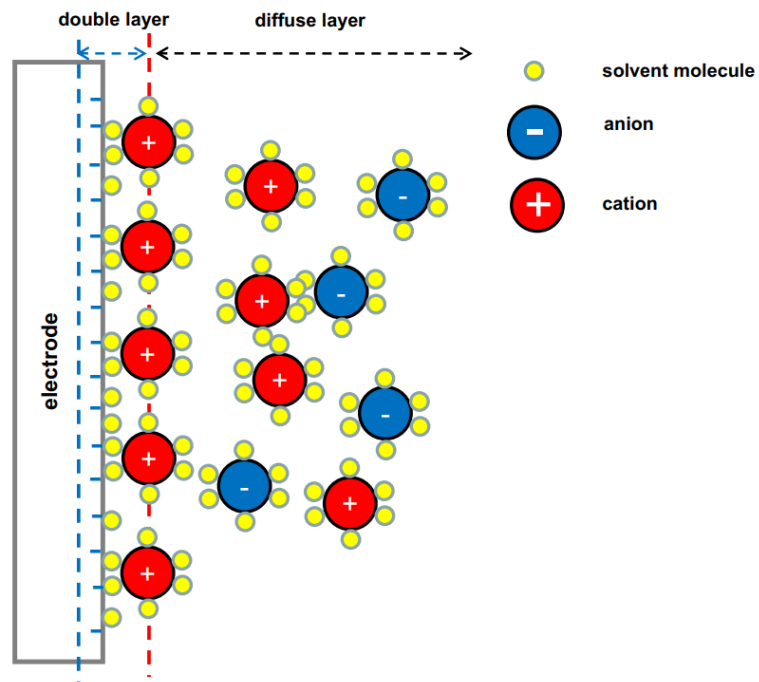
Figure 2.3: Electrical double layer at the electrode/electrolyte interface[5].

2.1.1.7 Controlled potential methods - Voltammetry

These amperometric methods involve applying a potential to an electrode (WE) surface, forcing an electrochemical reaction to occur. The system as a result moves away from its equilibrium state and the generated current is monitored. A typical three electrode electrochemical cell is shown (fig. 2.4)[2].
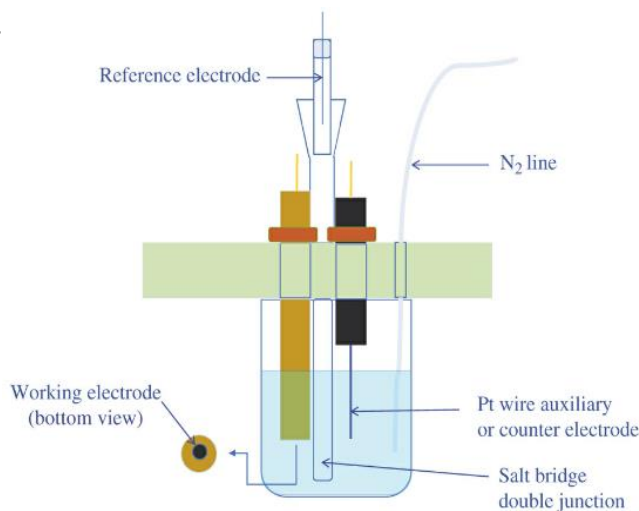
Figure 2.4: Three-electrode electrochemical cell[2].

Voltammetry is a common subset of controlled potential methods. Potential is scanned at a specified rate and current (a measure of rate of electrode surface reactions) is monitored using this technique (seen as a voltammogram in fig. 2.7). The current is a result of the redox reactions that occur at the electrode surface.

These methods of analysis measure faradaic current (which is a result of change in oxidation state of the analyte) which is directly proportional to the concentration of the analyte. In voltammetry, electrochemical potential is the independent variable that can be controlled, whereas current exists as a dependent variable, which is an outcome of an experiment [5].

These measurements provide information about processes at only the WE [5]. A typical electrochemical cell can be seen in fig. 2.5. Current flows between the WE and the CE. The RE is of a constant composition and maintains a fixed electrochemical potential that serves as a reference point relative to the WE potential, when using a potentiostat[5].
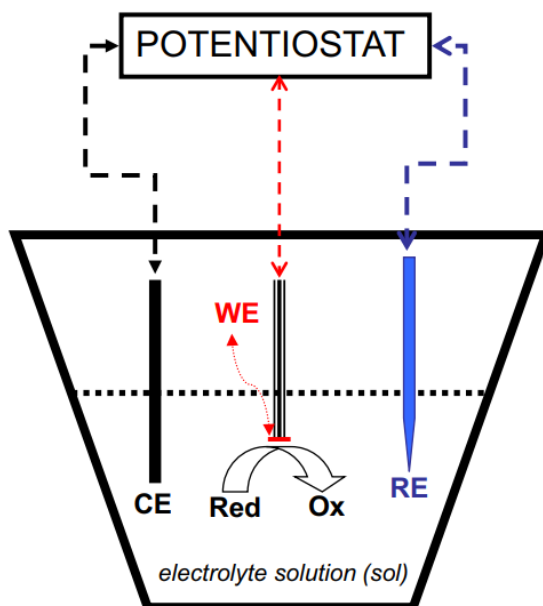
Figure 2.5: A typical three-electrode electrochemical cell with the WE, CE and the RE describing the oxidation of a dissolved analyte molecule[5].

2.1.1.7.1 Cyclic voltammetry

Cyclic voltammetry (CV) is the most widely used electrochemical technique which involves both electrode kinetics and diffusion. It is an extension of linear sweep voltammetry (LSV), where two linear sweeps, in opposing directions, are combined (fig. 2.6). During this experiment, a potential is applied to the working electrode and the current flow is recorded vs potential, in a 'cyclic voltammogram' [13]. The x-axis in a CV represents the applied voltage, while the y-axis represents the resulting current (fig. 2.7)[9].
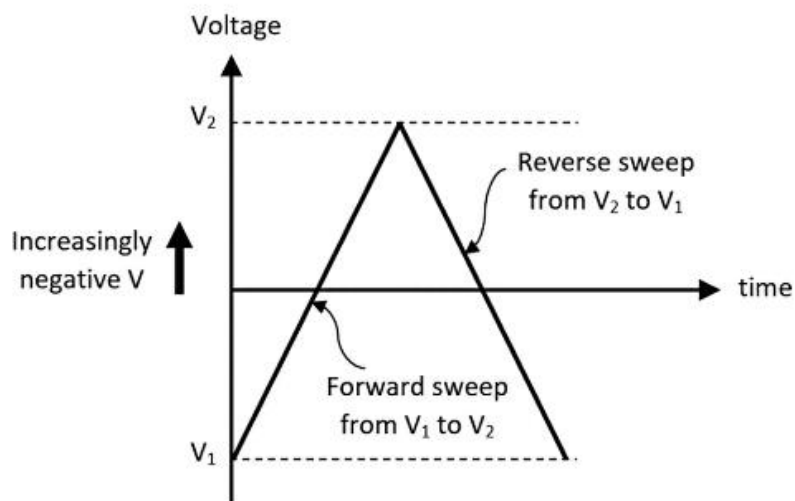
Figure 2.6: Detailed working of cyclic voltammetry[1].
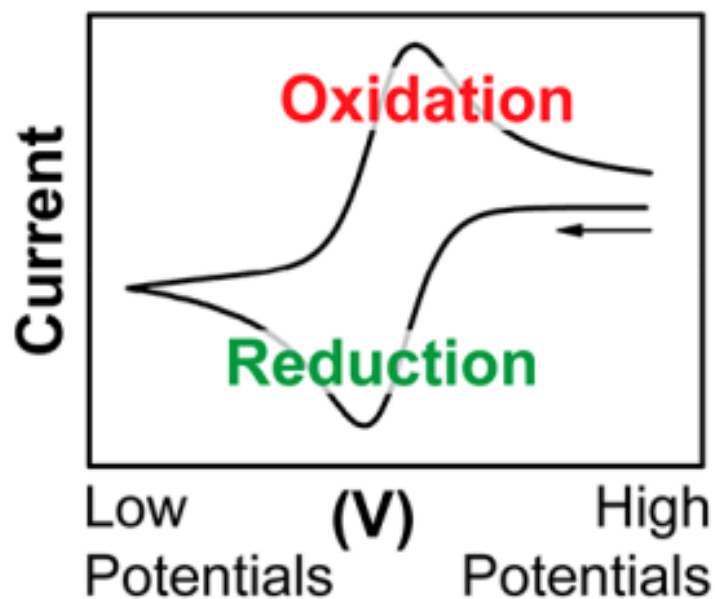
Figure 2.7: Cyclic voltammogram according to IUPAC convention [9, 10]

A variety of interfacial phenomena can be seen through the shape of a voltammogram. Both electrode kinetics and mass transport (diffusion, convection and migration) affect the overall current recorded. With an increase in potential at the W.E., moles of electrons transferred between the electrode and the analyte increases, causing an increase in current. As the potential sweep continues, the current then begins to decrease as a result of mass transport limitation, where a diffusion gradient forms near the surface of the electrode (diffusion boundary layer) and there is a difference between the analyte concentration at the surface (which is lower) and the bulk of the solution (which is higher). This diffusion of analyte over time decreases as the boundary layer grows in thickness, decreasing the overall current response as a result of lower concentrations of analyte at electrode surface for the redox reaction (fig. 2.8) [1].

Cathodic current

Current rises as more reduction occurs, more electrons transferred

Current declines even though voltage sweep continues

Forward sweep
$A + e^- \rightarrow A^-$

Voltage (more negative)
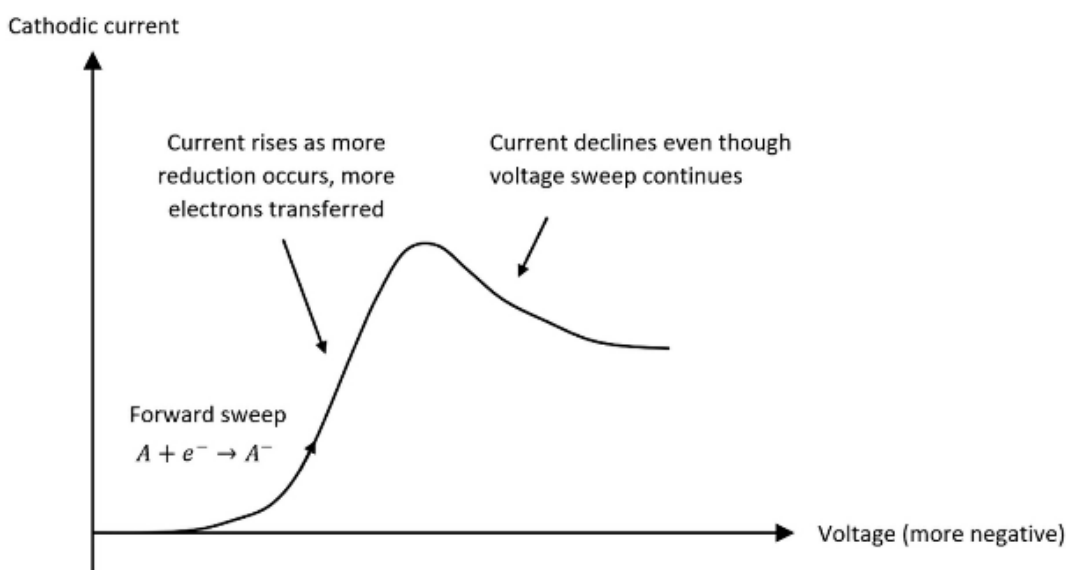
Figure 2.8: Voltammogram showing the effect of a negative-going potential sweep on current in the presence of a redox-active molecule[1].

These experiments are often performed with a static WE in unstirred solutions. Physicochemical processes including diffusion, convection and migration and chemical reactions are involved in this technique, such that migration and convection are minimised and only diffusion plays a part. It is to be noted that the heterogeneous redox reaction of interest takes place only at the electrode/electrolyte interface of the WE. There is exchange of electrons that occurs between the electrode and the redox active species in this electrode reaction. By controlling the applied potential at the WE, the redox equilibrium shifts to either oxidation or reduction. In experiments with creatinine as an analyte, it is understood that at the beginning, a bulk concentration of creatinine is present in the cell. When the potential of the WE is increasedin the positive direction, creatinine (CR) molecules close to the interface at the WE, begin to get oxidised to CR-O (according to Equation 2.5) and current flows in the circuit.

$$CR_{sol} \leftrightarrow CR - O_{sol} + ne^-$$ (Equation 2.5)

It can be understood that rate of diffusion is affected by the concentration gradient of the analyte. At the beginning of a voltammetry scan in unstirred solution, there exists a thin boundary layer (sometimes called the diffusion layer). The diffusional flux as a result is against a steep concentration gradient (fig. 2.9) and therefore more analyte diffuses through this layer towards the working electrode giving higher currents initially.

41

$[X^+] \cong [X^+]_{bulk}$ at a short distance from the electrode surface

Bulk concentration

Thin boundary layer, within which concentration gradient is steep (large)

Reactant concentration, $[X^+]$

$[X^+]_{surface} \cong 0$ as reduction reaction at surface is rapid, any X^+ is reacted (depleted) immediately

Distance from electrode
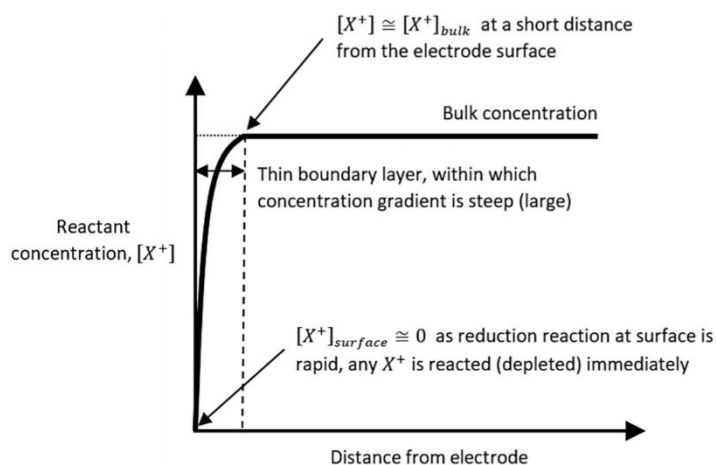
Figure 2.9: The concept of formation of thin layer boundary layer at the surface of the working electrode [1].

With time, this boundary layer grows in thickness (fig. 2.10) as the analyte depletes near the surface of the WE. Due to less availability of analyte and its mass transport limitation as diffusion rate slows down, the current decreases even though the potential sweeps to higher potentials.

Bulk concentration

Thicker boundary layer over time, concentration gradient decreases (less steep)

Reactant concentration, $[X^+]$

$[X^+]_{surface} \cong 0$

Distance from electrode
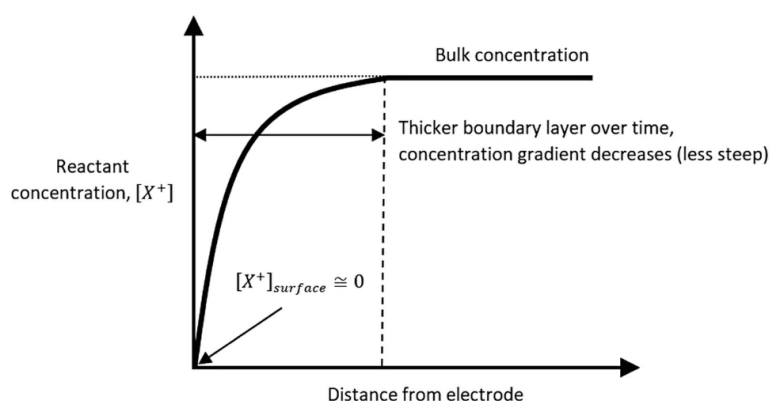
Figure 2.10: The concept of thick boundary layer forming at the surface of the working electrode [1].

Electrode kinetics significantly affects the current response in an electrochemical reaction. It can be reversible, quasi-reversible or irreversible.

2.1.1.7.2 Reversible Electron Kinetics

Reversible electron reactions are a result of rapid electron kinetics (fig. 2.11) where there is low barrier to electron transfer, and the rate constant is significantly higher than the mass transfer coefficient ($k^o \gg m_T$). The surface concentrations of the redox species is maintained at their

equilibrium values according to the Nernst equation. Therefore, reversibility depends on the value of the rate constant. The peak current observed in systems with reversible kinetics occurs before that observed in quasi-reversible and irreversible systems as a result of requiring higher potentials to raise current due to slower kinetics in comparison. Additionally, the peak current magnitude is much higher for reversible systems as a greater number of electrons are transferred per unit time at the WE surface due to faster electron kinetics[1].

In reversible systems, asscan rate is varied, the potential difference ΔEp between peak currents remains constant at a value of 59/n mV, where n is the number of moles of electrons transferred per reaction. The ratio of peak current magnitudes is 1 in case of reversible kinetics. The peak currents also increase with increasing scan rates. At higher scan rates, the diffusion boundary layer extending from the WE surface is thin, mass transport is not limiting the current, hence electron transfer occurs at higher rates, causing increased peak currents. At slower scan rates, a thicker diffusion boundary layer forms as the diffusive flux of reactant decreases with time and mass transport limitation takes effect with increasing time. Current decreases as a result with time (fig. 2.12).
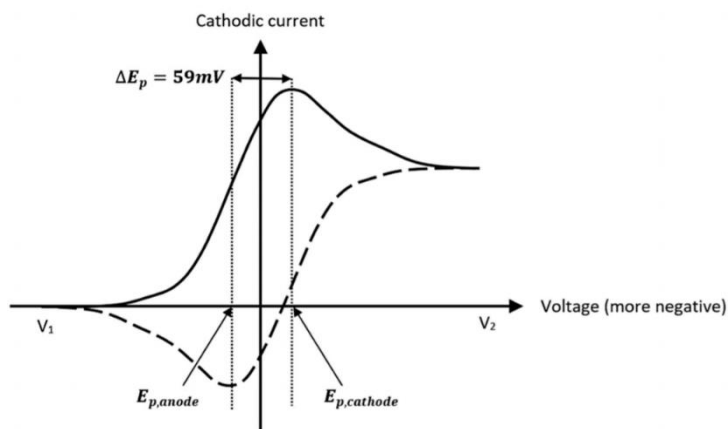
Figure 2.11: CV redox response in case of a reversible electrochemical system[1].
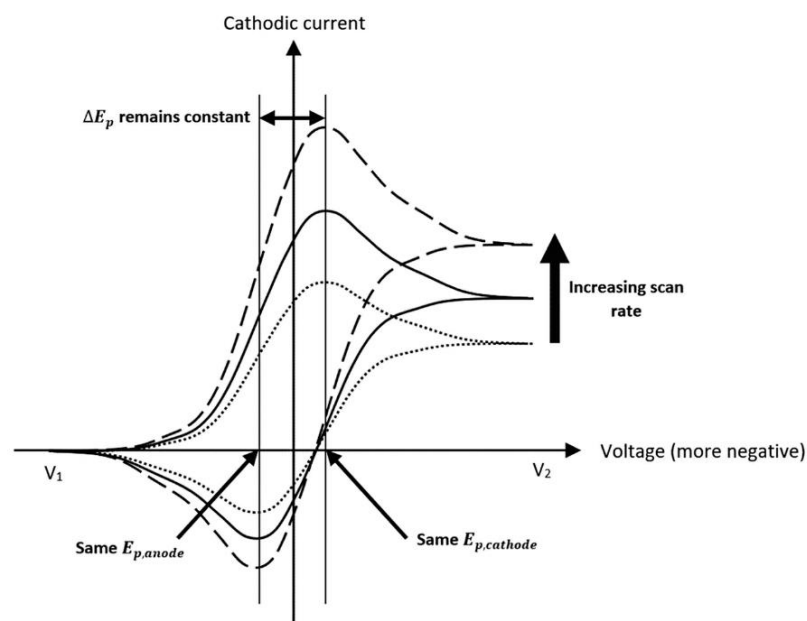
Figure 2.12: Effect of varying scan rates on redox response in case of reversible electron kinetics[1].

2.1.1.7.3 Non-reversible electron kinetics

The electron transfer rate constants for reversible reactions are much higher than that of quasi-reversible and irreversible electrochemical reactions. For non-reversible electron kinetics, there is high barrier to electron transfer resulting in more sluggish and slower electron kinetics.

2.1.1.7.4 Quasi-reversible Electron Kinetics

The quasi-reversible kinetics is intermediate between reversible and irreversible kinetics (fig. 2.13) where peak separation ΔEp is > than 59/n , meaning quasi-reversible processes occur at slower electron transfer rates than reversible processes and are also controlled by mass transport rates. Although for irreversible reactions, the reverse redox reaction in the reverse sweep doesn't exist. Only electron transfer rates control the current response in case of irreversible processes, and the Nernst equation is not applicable due to significantly slow kinetics. The Nernstian equilibrium at the electrode surface is not effectively maintained, as the reactions in the quasi-reversible case are not highly thermodynamically favourable. For quasi-reversible and irreversible reactions the forward peak current is always greater than the reverse

peak current as the reaction in the reverse scan doesn't occur at fast enough rates due to slower kinetics. With quasi-reversible kinetics, k^o (rate constant) ≈ m_T (mass transfer coefficient).

2.1.1.7.5 Irreversible Electron Kinetics

When the rate constants of electrochemical reactions are even lower in values and the reaction is significantly slow, then irreversible electron kinetics takes place. With irreversible kinetics, k^o (rate constant) << m_T (mass transfer coefficient). There exists no reverse peak in this case and ΔEp is not applicable (fig. 2.13).
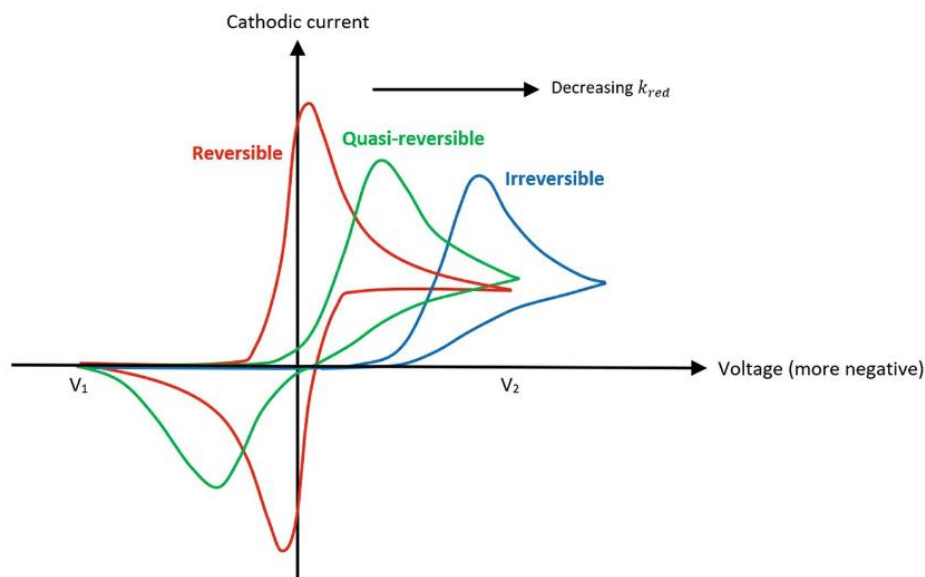
Figure 2.13: Comparison of CV redox response of electrochemical systems with different electrode kinetics[1].

2.1.1.8 Chronoamperometry

With this technique, a step potential is applied to allow reduction or oxidation reactions to occur at the surface of the WE. The step in potential allows a reaction to become thermodynamically favourable at those conditions. For example, applying a negative step potential allows reduction reaction to occur at the WE. There is a significant rapid increase in cathodic current (fig. 2.14), as a result of presence of bulk concentration of reactant X^+ at the electrode. With increasing time, a constant cathodic current response is observed as X^+ replenish at the WE surface due to stirring.
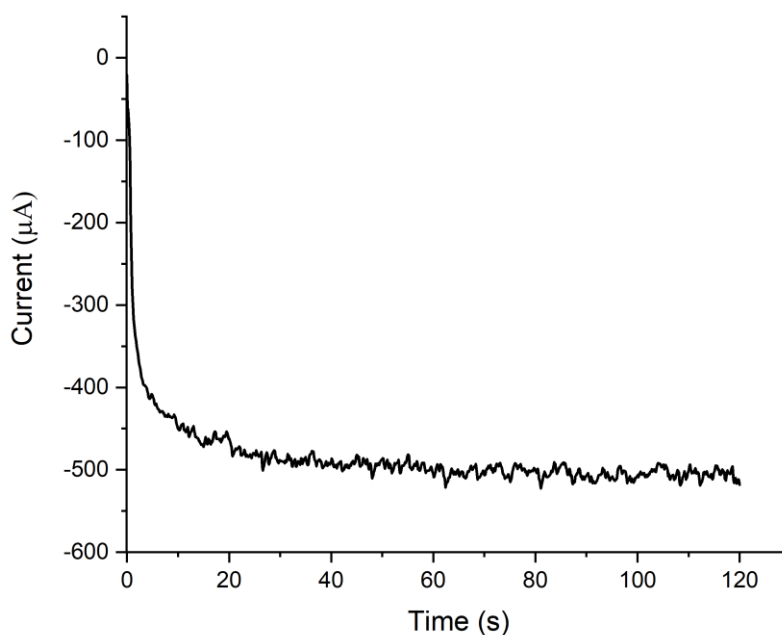
Figure 2.14: Chronoamperometry technique used at -1.3 V vs Ag/AgCl for electrodeposition of nickel from nickel nitrate solution.

2.1.2 Spectroscopic methods

2.1.2.1 UV-vis analysis

UV-visible spectroscopy measures the absorbance or transmittance of light and is a fast technique for analysis (fig. 2.15). Working wavelength between 200-1100 nm is present in most spectrophotometers. Transmittance represents the extent of light absorption at each wavelength and the wavelength of interest is the highest peak – λ_{max} [15].Electron transitions of organic compounds occurs while using this technique, where organic molecules absorb light and excite electrons from a lower energy orbital to a higher energy unoccupied orbital. According to the Beer-Lambert law (Equation 6),

$$A = log_{10} \frac{I_o}{I} = \varepsilon.b.C \qquad \text{(Equation 6)}$$

where A is light absorbance, b is the path length, C is the concentration and ε is the molar absorptivity[15].
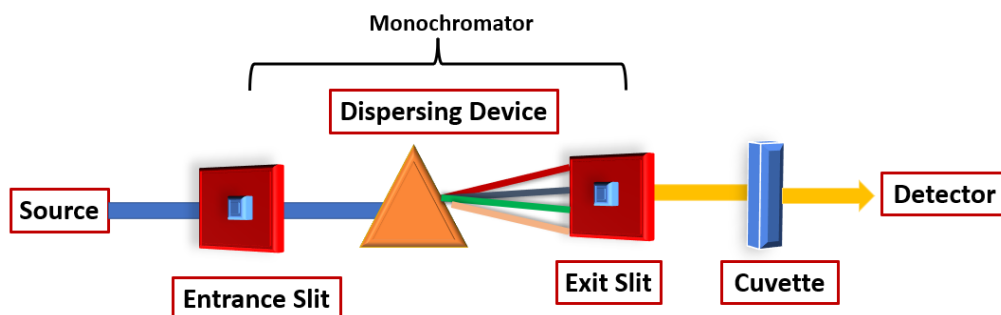
Figure 2.15: Schematic of UV-vis spectroscopy technique.

2.1.2.2 NMR analysis

NMR spectroscopy is a widely used analytical technique for characterisation of organic molecules since the 1950s. Information on local magnetic field around atomic nuclei can be observed using NMR. This technique can provide significant information on the structure of the molecule as a result of this magnetic field being influenced by features of the molecular structure including configuration, intermolecular interactions, conformation, etc,[16].

'Spin' is a quantum mechanical property of nuclei and results in a NMR signal[17]. Use of magnetic fields can give qualitative and quantitative information on gaseous, liquid or solid samples. Spinning nucleons (protons and neutrons) are characterised by a nuclear spin quantum number (m), which has a value of −1/2 or +1/2. Magnetic characteristics are described using nuclear spin (I), if with a value of 0, meaning the nuclei are magnetically inactive and therefore cannot be detected using NMR experiment [16].

The super conducting magnet (SCM) is the most important part of the NMR spectrometer. The signal to noise ratio and the resolution of the spectra are determined due to the strength of the magnetic field. Fourier Transform (FT) spectrometers are widely used currently to obtain NMR spectra. The NMR method involves applying a short pulse of radiofrequency radiation in the magnetic field to the sample, resulting in all nuclei excited at the same time, followed by detection of radiation by the FT spectrometer. This radiation is a result of nuclei going back to their lower energy state. Radiation with characteristic frequencies is given off by the nuclei in the sample[17].

Chemical shift occurs at the position of a signal along the x-axis of an NMR spectrum, which gives information on the structural environment of the nuclei producing the signal. Approximate proton chemical shifts in ^1H NMR is shown on fig. 2.16. Approximate carbon chemical shifts in ^{13}C NMR is shown in fig. 2.17.
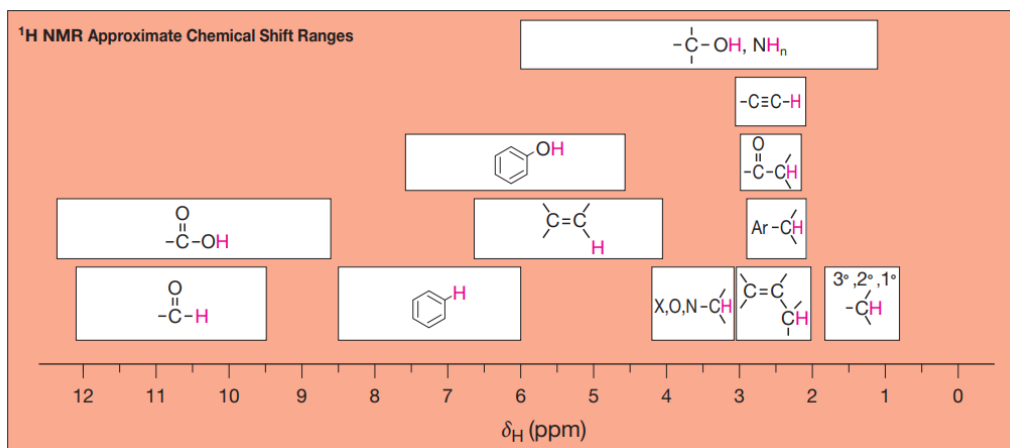
Figure 2.16: Approximate proton chemical shifts in ^1H NMR spectroscopy[3]
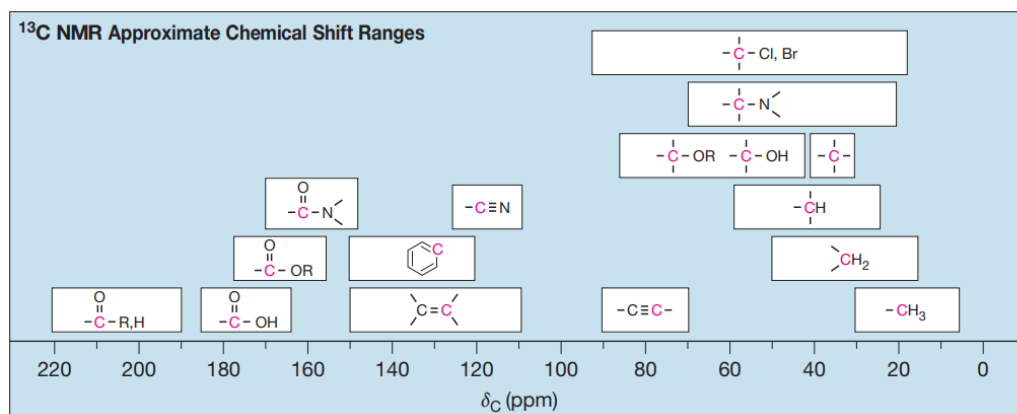
Figure 2.17: Approximate carbon chemical shifts in ^{13}C NMR spectroscopy[3]

2D NMR is a type of multidimensional NMR spectroscopy, including HSQC (Heteronuclear single quantum correlation) and HMBC (heteronuclear multiple bond correlation) techniques. When a more detailed additional structural information from ^1H and ^{13}C NMR spectra is required, 2D techniques are significantly useful and can provide precise information on which hydrogens and carbons are producing the respective peaks[3]. HSQC gives information on ^1H chemical shifts and X-nuclei directly bonded to the hydrogen atoms whereas, HMBC gives information over several bonds (generally 2-3)[18].

2.1.2.3 Mass spectrometry

Mass spectrometry is important for understanding structure of organic molecules. Mass of molecules can be measured using this technique to further characterise a particular molecule or in identifying an unknown. Overall, this technique can be used to analyse structure of a molecule. A mass spectrum is a plot of intensity against mass-to-charge ratio (m/z). The sample is first vaporized and then ionized, followed by sorting by mass-to-charge ratio before detection. Therefore, there are three processes involved in this process including ion generation, mass analysis and ion detection [19].

2.1.2.3.1 Electrospray Ionization (ESI)

This technique uses electrical energy to transfer ions from solution phase into the gas phase before mass spectrometric analysis takes place[8]. This has become a routine technique for

ionization of biomolecules. Ionization takes place in solution by protonation or deprotonation of the analyte[19]. The transfer of ions from sample solution into the gas phase done with ESI technique involves different stages: (1) dispersed fine spray of charge droplets are produced (2) Solvent evaporation then takes place followed by (3) ion ejection (seen in fig. 2.18)[8].
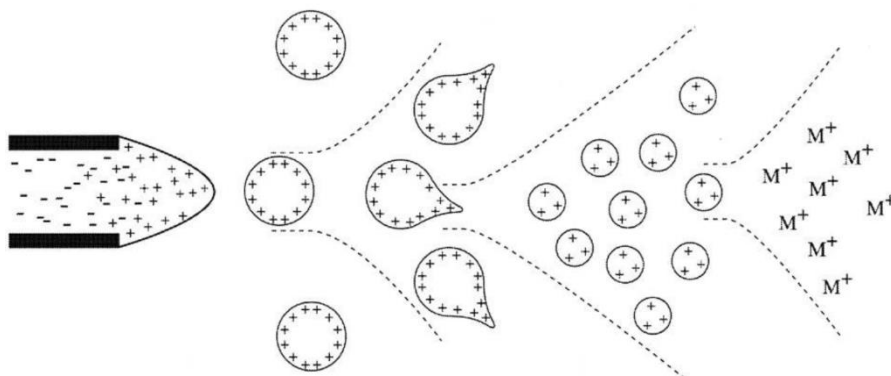
Figure 2.18: Schematic of ESI mass spectrometry technique[8].

In positive ion mode, molecular species [M+H]$^+$ is detected and in negative ion mode, molecular species [M+H]$^-$ is detected[19]. If the analyte can form complex or if it is in high concentrations, [2M+H]$^+$ or [2M-H]$^-$ ions could also be present[20].

2.1.2.4 Infrared Spectroscopy

This is one of the most common techniques used in organic chemistry. In summary, it is a technique where different IR frequencies are measured when a sample is positioned in the path of the IR beam. In this way, the chemical functional groups in the sample can be analysed. Gases, liquids and solids can be used for analysis with infrared spectroscopy[7].

All atoms at temperatures higher than absolute zero, are in continuous vibration with respect to each other. The organic molecule absorbs the radiation, when frequency of specific vibration of molecule equals the frequency of the IR radiation. Stretching and bending are the major types of molecular vibrations[7]. IR spectra is obtained by detection of transmittance (or absorption) intensity change as a function of frequency.

Attenuated total reflectance (ATR) is a type of IR technique where the infrared beam is directed towards a crystal at an angle which is less than the critical angle. Total internal reflection then occurs during this process (fig. 2.19). To ensure the critical angle is small, crystals of high

refractive index are selected. ATR crystals are often diamond, ZnSe, silicon and germanium. In terms of the ATR materials, diamond is considered an excellent material due to its robustness[7].
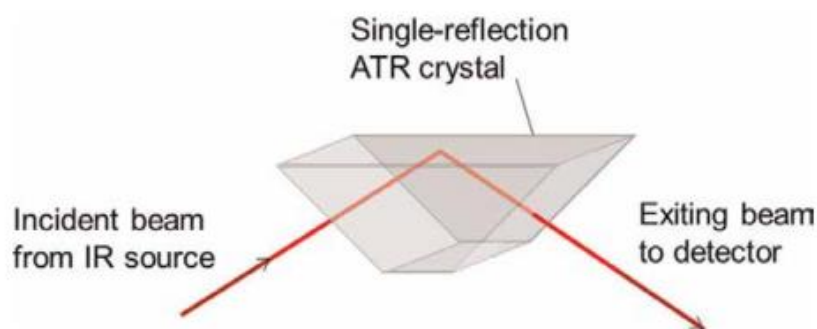
Figure 2.19: ATR technique of IR spectroscopy[7].

2.1.3 Electroanalytical systems

An electrochemical sensor is a device that can produce signals proportional to the concentration of analyte in the sample. Some advantages with electroanalytical systems include high sensitivity, low cost, simplicity and the fact that these systems are portable [2]. Electrochemical systems are easy to miniaturise (leading to better signal-to-noise ratio and requirement of low sample volumes)[21] and can be developed and effectively used in a POCT clinical setting. The fact that the sensing element of electrochemical sensors is small, the sample volumes required for analysis can be minimised and additionally, the selectivity and sensitivity of the sensor increases due to high surface to volume ratio and increased active sensing area. Due to the simplicity of electrochemical sensing techniques, these sensors are portable. Additionally, the low cost of sensor development allows mass production of these sensors, where they can then be used in POCT settings.

2.1.3.1 Sensor characteristics
The sensor must be able to detect the analyte in a wide linear range. The electrode response per analyte concentration (known as sensitivity) must be higher for a better function of the electrochemical sensor. Additionally, it is to be ensured that the sensor is highly selective for the analyte of interest and has minimised interferences from other molecules present in the sample. The response time of the sensor must be as low as possible to have a fast sensor output [6].

2.1.3.2 Electrodes in electroanalysis

Electroanalytical tools function with excellent performance for detection of analytes due to the electrodes used for analysis, where they act as source/sink for electrons as a result of applied potential.

2.1.3.2.1 Carbon based working electrodes

Carbon based working electrodes are widely used in electroanalysis due to their wide potential window, low cost, chemical inertness and minimal background current[22]. Glassy carbon electrodes (GCE) have been used in part of this project due to their favourable mechanical and electrical properties, and large working potential window in the solvents used [22]. Increased electron transport is observed when the GCE surface has been polished with alumina and diamond solution until it resembles a shiny mirror [23]. Carbon paste based SPEs (purchased from Metrohm DropSens) have also been used in part of this project. These materials mainly comprise of graphite powder and binders (organic solvents), and have minimal background current [22].

2.1.3.2.2 Screen-printed electrode technology

Miniaturisation of macroelectrodes (e.g., GCE) into a screen-printed electrode (SPE) platform has significant advantages including the possibility of development into a sensing device that is portable and can be used in POCT settings.

Screen-printed electrode (SPE) technology consists of WE, CE and RE (fig. 2.20) (prepared using various commercial inks) all on one single strip, allowing a large potential window [22]. Both chemical and biosensors have been fabricated using screen-printed electrode (SPE) technology [24-27]. This thick film technology has low unit costs and is widely used for mass production of disposable electrochemical sensors [27]. They are easier to miniaturise into devices that can be used for point-of-care (POC) applications as single-use disposable sensors that don't require electrode polishing before use, unlike GCEs. There is still an issue of reproducibility of hydrogel-based SPEs *(presented in Chapter 5),* for the fact that there may be less information on electrode composition and microscopic structures of each electrode on the SPE [27].
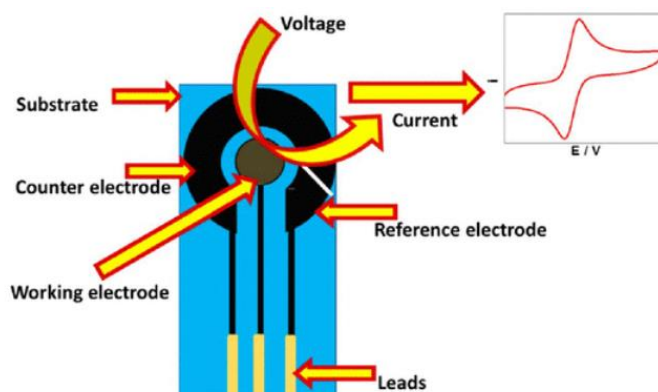
Figure 2.20: Schematic of a typical SPE[6].

2.1.4 Nanomaterials in electrochemical sensing

Nanotechnology recently has many applications in analytical chemistry. Nanoparticles (with sizes of 1-100 nm) have unique chemical, physical and electronic properties, and are effectively used for sensing applications.

Metal based nanomaterials (also known as 'electronic wires') have shown excellent electrocatalytic properties for electrochemical sensing applications recently (fig. 2.21). This leads to high sensitivities, wide linear ranges and lower LODs for sensors[21]. Using metal-based nanoparticles allow enhancement in catalysis and electron transfer.
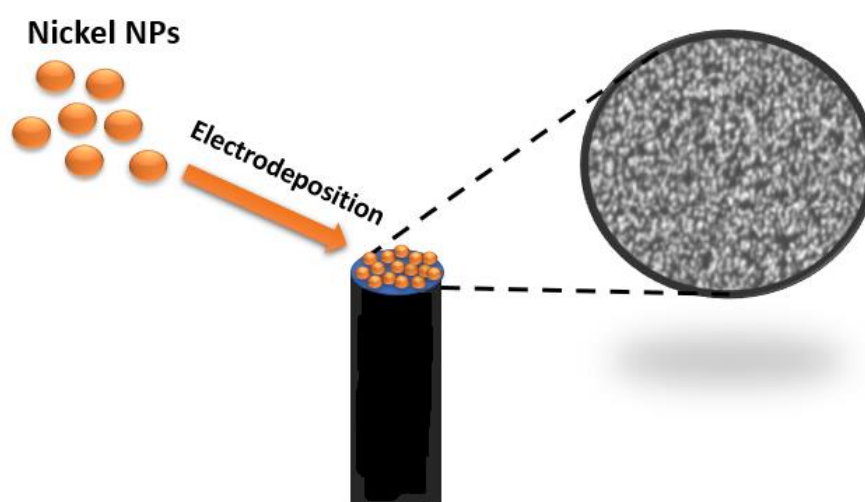
Figure 2.21: Schematic of nickel nanoparticles (NPs) based GCE sensor for electrochemical analysis.

Various nanoparticle-based sensors have been designed using Au, Pt, Pd and Cu for the electrochemical sensing of molecules e.g, glucose (table 2.1).

Table 2.1: Summary of metal NPs based glucose sensors.

Modification	LOD (µM)	Linear range	Sample	Reference
Au NP/Si substrate	0.14	0.5 µM – 12 mM	Serum	28
CuO/MWCNTs	0.2	0.10 - 1.2 mM	Serum	29
Pt/Pd nanoflakes/screen-printed gold film electrode (SPGFE)	20.6	1 – 16 mM	Blood	30

Some of the creatinine sensors developed based on metal nanoparticles are summarised in table 2.2.

Table 2.2: Summary of metal NPs based creatinine sensors.

Modification	LOD	Linear range	Sample	Reference
Polyacrylic acid gel/Cu(II)/SPE	6.5 µM	200 µM – 100 mM	Urine	31
Fe-Cu-rGO/Ag	10 nM	0.01-1000 µM	Whole blood	32
Carbon nanotubes/folic acid/AgNPs/carbon paste electrode	0.008 µM	1×10^{-8}- 2×10^{-4} M	Urine and Serum	33
AuNPs/colorimetric sensor	12.7 nM	-	Urine and bovine serum	34

In *Chapter 3*, a bare GCE system in alkaline ferrocyanide solution was investigated for creatinine detection. NMR studies were performed to understand the mechanism of the reaction, followed by colorimetric and electrochemical studies to develop the sensor.

2.2 References

1. X. W. Ng, *Concise Guide to Electrochemical Methods and Voltammetry*, Springer, 2022.

2. G. A. Mabbott, *Electroanalytical Chemistry: Principles, Best Practices, and Case Studies*, John Wiley & Sons, 2020.

3. T. G. Solomons, C. B. Fryhle and S. A. Snyder, *Organic chemistry*, John Wiley & Sons, 2023.

4. A. J. Bard, L. R. Faulkner and H. S. White, *Electrochemical methods: fundamentals and applications*, John Wiley & Sons, 2022.

5. V. Mirceski, S. Skrzypek and L. Stojanov, *ChemTexts*, 2018, **4**, 1-14.

6. A. Pandikumar and K. S. Devi, *Disposable Electrochemical Sensors for Healthcare Monitoring: Material Properties and Design*, Royal Society of Chemistry, 2021.

7. C.-P. S. Hsu, *Handbook of instrumental techniques for analytical chemistry*, 1997, **249**.

8. C. S. Ho, C. Lam, M. H. Chan, R. Cheung, L. Law, L. Lit, K. Ng, M. Suen and H. Tai, *The Clinical Biochemist Reviews*, 2003, **24**, 3.

9. N. Elgrishi, K. J. Rountree, B. D. McCarthy, E. S. Rountree, T. T. Eisenhart and J. L. Dempsey, *Journal of chemical education*, 2018, **95**, 197-206.

10. Nova Biomedical, https://novabiomedical.com/statstrip-creatinine/index.php, (accessed 31 May, 2023).

11. C. M. Brett, O. Brett and A. Electrochemistry, *Electrochemistry*, 1993, **67**, 444.

12. A. G.-M. Ferrari, S. J. Rowley-Neale and C. E. Banks, *Talanta Open*, 2021, **3**, 100032.

13. R. G. Compton and C. E. Banks, *Understanding voltammetry*, World Scientific, 2018.

14. F. Scholz, *Electroanalytical methods*, Springer, 2010.

15. F. S. Rocha, A. J. Gomes, C. N. Lunardi, S. Kaliaguine and G. S. Patience, *The Canadian Journal of Chemical Engineering*, 2018, **96**, 2512-2517.

16. A. Tampieri, M. Szabó, F. Medina and H. Gulyás, *Physical Sciences Reviews*, 2020, **6**, 20190086.

17. S. A. Richards and J. C. Hollerton, *Essential practical NMR for organic chemistry*, John Wiley & Sons, 2023.

18. T. Öman, M.-B. Tessem, T. F. Bathen, H. Bertilsson, A. Angelsen, M. Hedenström and T. Andreassen, *BMC bioinformatics*, 2014, **15**, 1-8.

19. R. J. Anderson, D. J. Bendell and P. W. Groundwater, *Organic spectroscopic analysis*, Royal Society of Chemistry, 2004.

20. A. Steckel and G. Schlosser, *Molecules*, 2019, **24**, 611.

21. G. Maruccio and J. Narang, *Electrochemical Sensors: From Working Electrodes to Functionalization and Miniaturized Devices*, Woodhead Publishing, 2022.

22. S. Manjushree and P. S. Adarakatti, *Recent Developments in Green Electrochemical Sensors: Design, Performance, and Applications*, 2023, 1-21.

23. V. Uskoković, *Carbon Trends*, 2021, **5**, 100116.

24. J. P. Hart and S. A. Wring, *TrAC Trends in Analytical Chemistry*, 1997, **16**, 89-103.

25. J. P. Hart and S. A. Wring, *Electroanalysis*, 1994, **6**, 617-624.

26. M. Albareda-Sirvent, A. Merkoci and S. Alegret, *Sensors and Actuators B: Chemical*, 2000, **69**, 153-163.

27. A. Morrin, A. J. Killard and M. R. Smyth, *Analytical letters*, 2003, **36**, 2021-2039.

28. N. Shen, H. Xu, W. Zhao, Y. Zhao and X. Zhang, *Sensors*, 2019, **19**, 1203.

29. L.-C. Jiang and W.-D. Zhang, *Biosensors and Bioelectronics*, 2010, **25**, 1402-1407.

30. X. Niu, M. Lan, C. Chen and H. Zhao, *Talanta*, 2012, **99**, 1062-1067.

31. S. Kalasin, P. Sangnuang, P. Khownarumit, I. M. Tang and W. Surareungchai, *ACS Biomaterials Science & Engineering*, 2020, **6**, 1247-1258.

32. P. Singh, S. Mandal, D. Roy and N. Chanda, *ACS Biomaterials Science & Engineering*, 2021, **7**, 3446-3458.

33. A. Fekry, S. Abdel-Gawad, R. Tammam and M. Zayed, *Measurement*, 2020, **163**, 107958.

34. H. Du, R. Chen, J. Du, J. Fan and X. Peng, *Industrial & Engineering Chemistry Research*, 2016, **55**, 12334-12340.

Chapter 3 - Bare GCE based Creatinine Detection

3.1 Introduction

Creatinine is a useful metabolite for the evaluation of chronic kidney disease (CKD). Creatinine concentrations in urine outside of the healthy range (4.4 to 13.3 mM) may indicate CKD and other kidney conditions. Early detection and monitoring can provide lifesaving intervention, and as such there is a need to develop rapid, low cost and highly selective electrochemical non-enzymatic creatinine sensors to overcome some of the limitations of state-of-the-art enzymatic creatinine biosensors or the long-established colorimetric Jaffe reaction method. A non-enzymatic creatinine sensing platform enabled by an electrocatalytic response of the metabolite to ferricyanide in alkaline conditions is presented (fig. 3.1). Using an unmodified glassy carbon electrode (GCE) and cyclic voltammetry a linear calibration plot was obtained giving a limit of detection of 60 μM with a standard deviation of 7%. The performance was evaluated in the presence of artificial urine and showed no interfering response to urea. Other variable, potentially interfering species commonly present in urine samples, such as ascorbate and glucose, were also tested. Finally, the sensing platform was translated to a screen-printed electrode modified with an alkaline hydrogel containing the iron couple, demonstrating the potential for a single use disposable sensor for a point of care device.
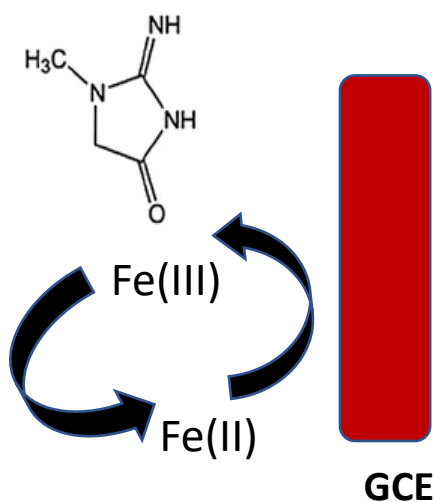
Figure 3.1: Mechanism of creatinine oxidation using alkaline ferricyanide electrochemical system.

Creatine is a naturally occurring nitrogenous organic acid which reacts with adenosine tri-phosphate (ATP) to form phosphocreatine in the process of cellular energy transfer. This is essential for many biological processes including muscle energetics and function.[2] The by-product of this reaction, creatinine (2-amino-1-methyl-5*H*-imidazole-4-one), has no useful biological function and is excreted via glomerular filtration into urine by the kidneys. Due to its reliable production in healthy adults, creatinine is the second most analysed molecule after glucose, as it is a biomarker to indicate whether a urine sample for drug testing has been tampered with. Creatinine levels in blood and urine can also be used to assess renal, muscular or thyroidal functioning [3][4]. Despite the importance of this biomarker in drug testing and disease monitoring, the main method to determine creatinine is the century old colorimetric Jaffe reaction, a dated, laborious and non-selective analytical technique [5]. Clinical laboratories use automated chemical or enzymatic methods mostly using the chemical Jaffe reaction method to detect creatinine [5]. Here a sample is reacted with picric acid to form a red-yellow complex which is detected using HPLC-UV/Vis [5]. The Jaffe method has low specificity and is affected by substances including glucose, bilirubin and protein. As a result, this procedure measures creatinine 15-25% higher than the actual value [6].

Table 3.1: Summary of current clinical methods of creatinine detection in urine using Abbott Architect lab analyzer [6].

Method	Linear Range (mM)	LOQ (µM)	LOD (µM)
Jaffe	0.11-14.4	110	13.9
Enzymatic	0.03-14.4	27.8	3.90

An alternative method to the Jaffe reaction, which is routinely used for clinical creatinine analysis is the enzymatic method with lab analyzers like the Abbott Architect analyzer [6]. Although, the performance of this technique is better than the Jaffe method in terms of specificity and LOD (table 3.1), its usage is limited to point-of-care testing as it is 10-fold more expensive [6].

Electrochemical sensor systems have various advantages over the currently used colorimetric Jaffe reaction including rapid detection, lower interference, simplicity and reduced cost of analysis [3]. Unfortunately, creatinine is not a directly electroactive molecule, therefore electrochemical sensing platforms commercialised to-date have enzymatic interfaces. Enzymes such as creatinine amidohydrolase (CA) and creatine amidinohydrolase (CI) demonstrate high selectivity and specificity, however, they have significant drawbacks including low storage stability and high cost [7].

Additionally, the fact that all these devices detect creatinine in whole blood, adds to the complexity of analysis due to influences arising from uraemia and treatment medications [8]. Therefore, research is now shifting towards development of non-enzymatic creatinine sensors that are easy to fabricate and have low cost of production yet overcome the inactivity of the molecule.

Many non-enzymatic creatinine sensors to-date have incorporated metal ions, both on the electrode surface [9, 10 11-24] and as a complexing agent in solution [25, 26]. Most studies have used copper as catalysing [10, 14, 15] or complexing agent [9, 12, 13, 16, 25, 26]. Studies have worked on electrocatalytic systems monitoring creatinine oxidation [10] or following an indirect mechanism by monitoring a suppression in signal [9, 11-16, 25, 26]. Chen et al. and Raveendran et al. have considered monitoring the oxidative current from the regeneration of the copper surface oxide layer which is proportional to the concentration of creatinine [25]. In a number of studies, the formation of a cupric-creatinine complex is exploited delivering very low detection limits in the nanomolar range [10, 13, 15, 25, 26]. Interferences from molecules like urea and glucose were also shown to be negligible [10-13, 15, 16, 26], but eliminating interference with uric acid in a study has shown to decrease the sensitivity of creatinine detection [25]. Recent work by Teekayupak et al. shows the use of copper based ionic liquid (to disperse CuO) [27]. CuO has previously been shown to chelate with creatinine as a soluble complex [25], causing generation of an oxidative current. Ionic liquid increased the electron transfer rate and the overall catalytic activity of the sensor system [27]. Although, sample preparation and dilution with phosphate buffer (PB) was required for real sample analysis using human urine, this system prepared a sensor with a linear range of 0.5 – 5 mM and a LOD of 37.3 µM [27].

Iron has also been studied as a metal modifier and complexing agent in a number of non-enzymatic creatinine sensor studies [18-21]. A microcell-based study by Fava et al. used a carbon black film working electrode and was based on the complexing of iron(III) ions with creatinine in a chemical step. [19] Kumar et al. also developed a non-enzymatic creatinine biosensor based on the Fe(III) binding property with creatinine. Disposable carbon printed electrodes were layered with $FeCl_3$ coated cotton fibre membranes to sense creatinine in urine samples. The low cost sensor did not require any sample preparation steps and gave results in less than a minute [20]. As with the copper complexes, the creatinine detection mechanism with iron has been indirect, focussing on the amount of unbound iron (III) in the solution that is reduced [19, 20]. Negligible interferences were also reported in iron based detection systems [19, 21].

While many of these non-enzymatic sensor systems are low cost and have shown a good response to creatinine with lower detection limits, there are limitations in terms of commercialisation due to either complexity of the processes and the electrode preparation techniques [9-11, 13-21, 23-26], difficulty in

removal of interferences (mainly uric acid) causing lower sensitivities of creatinine detection [25] , systems that are not easily miniaturised [10, 13, 25], limited linear range [12], requirement of sample preparation [11, 26] or high cost.

An alternative approach is to use an electrocatalytic redox mediator and directly monitor the enhanced current response of the mediator in the presence of a substrate. Commonly used in enzymatic systems, reversible redox species such as ferrocyanide or osmium complexes are shuttled between the electro-inactive enzyme and substrate and the electrode interface, the electroactivity of the redox mediator being measured as opposed to the substrate or enzyme. To-date such a mechanism has only been realised in one patent[28] and in a publication from 1956 by Kayser & Molitor, though the latter failed to prove it would work in blood or urine [29].

As well as a common redox mediator, ferricyanide is frequently used in organic synthesis as an oxidiser. Potassium ferricyanide is often referred to as an 'one electron abstracter' [30] and has been reported to extract an electron from an electron rich site in organic compounds [30-34]. Specifically, previous work has shown that ferricyanide acts as an oxidising agent in the oxidation of tertiary amines in the presence of hydroxide ions, suggesting that the hydroxide ions facilitate binding the alkali metal ions to the oxidant [35]. Anodic oxidation of tertiary amines in alkaline aqueous solution is a two-electron oxidation producing a secondary amine and an aldehyde as product [36].

$$R_2NCH_2R' + Fe(III)(CN)_6 + OH^- \rightarrow R_2NH + R'CHO + Fe(II)(CN)_6 \qquad \text{(Equation 3.1)}$$

This work reports on the oxidation of creatinine, a species containing tertiary, secondary and primary amine groups, in potassium hydroxide solutions by potassium ferricyanide. Potassium ferrocyanide (Fe(II)) is electrochemically oxidised to ferricyanide (Fe(III)) which catalytically oxidises creatinine to regenerate the ferrocyanide species. It is observed that an enhanced electrochemical response for the ferrocyanide occurs which can be correlated to creatinine concentrations to a low detection limit. We also study the reaction colorimetrically, thus reporting two low cost and high throughput routes to determining creatinine concentrations in biological fluids over a wide concentration range.

3.2 Experimental

3.2.1 Chemicals

Potassium hydroxide (Fisher Scientific), potassium ferricyanide, potassium ferrocyanide trihydrate, 99+%, for analysis (Acros Organics), creatinine anhydrous, ≥98% (Sigma-Aldrich), potassium chloride (Sigma-Aldrich), sodium chloride (Fisher Scientific), urea, 99.0-100.5% (Sigma-Aldrich), Bovine Serum Albumin, lyophilized powder, ≥96% (Sigma-Aldrich), sodium phosphate monobasic, ≥99% (Sigma-Aldrich) was purchased and used without further purification. Ultrapure water produced by a Milli-Q system of resistivity 18 MΩ cm was used throughout this work. L(+)-Ascorbic acid, 99% (Acros Organics), Glucose (Sigma-Aldrich) and uric acid, 99% (Thermo Scientific) were purchased.

3.2.2 Artificial urine sample analysis

Artificial urine was synthesised in accordance to procedures outlined in a study performed by Chang et al. [37]. A 100 ml solution of artificial urine was prepared using 1.82 g urea, 0.74 g sodium chloride, 0.44 g potassium chloride, 0.48 g sodium phosphate and 5 mg BSA. The artificial urine produced was a faintly yellow colour and transparent. It was kept in the refrigerator until required.

3.2.3 Measurement procedures

The electrochemical experiments were carried out in a three-compartment cell comprising the working electrode (WE), reference electrode (RE) and counter electrode (CE); all were supplied by IJ Cambria Scientific Ltd. The RE against which all the potentials were measured was a Ag/AgCl electrode immersed in 3 M NaCl. The CE was a graphite electrode and the WE a glassy carbon electrode (GCE – 3 mm diameter). An Ivium EmSTAT 3+ potentiostat was used in conjunction with the software (PSTrace) and a laptop computer to control the potentiostat. All measurements were made at room temperature (25°C). The electrocatalytic mechanism was investigated using cyclic voltammetry (CV).

Diamond (3F µm, Buehler) and alumina (0.05 µm, Buehler) solutions were used to polish the surface of the GCE between sets of experiments. Typical cyclic voltammetry experiments employed 10 ml of 1 mM potassium ferrocyanide in 1 M KOH in the electrochemical cell. Stock solutions of 20 mM and 200 mM creatinine in Millipore water were used to make standard creatinine additions to the

experimental cell. To account for the change in volume for some of the creatinine additions, a correction was made to the calibration plots and standard additions of the unknown.

3.2.4 Interference analysis

Interference study with ascorbic acid (AA), uric acid (UA) and glucose (Glu) were performed with and without creatinine, aiming to minimise the extent of interference in the creatinine sensing system.

3.2.5 Characterisation methods

A range of experimental techniques were used to understand the reaction mechanism of creatinine oxidation by ferricyanide.

3.2.5.1 NMR Analysis

All NMR experiments were carried out on a Bruker AVIII 400 equipped with a 5 mm broadband-observe (BBFO) probe. All NMR experiments were carried out in 1 M KOH solution i.e. a nominal pH of 14. The sample temperature was calibrated using MeOH-d_4 to be at 298.0 K.

3.2.5.2 UV-vis Analysis

UV-Vis analysis was carried out using an Agilent Technologies Cary 60 UV-vis. 0.05 mM creatinine additions (in artificial urine) were made to 4 ml solution of 1 mM ferricyanide and 1 M KOH and the results at 420 nm were analysed using the Scan application.

3.2.5.3 High performance liquid chromatography-tandem mass spectrometry (HPLC-ESI-MS)

High resolution mass assignment was performed using a Shimadzu LCMS-IT-TOF with electrospray ionisation (ESI). The ESI instrument parameters consisted of 1.5 L/min nebulising gas flow, 200°C CDL temperature, 200°C heating block temperature, and a detector voltage of 1.65 kV. Samples were introduced to the mass spectrometer as a bolus injection from a Shimadzu NexeraX2 UHPLC system consisting of two LC-30AD pumps, a SIL-30AC autosampler, and a CTO-20AC column oven. Injected samples were analysed in both positive and negative polarity scans with acquisition scan ranges of 150 – 1250 m/z and ion accumulation times of 5.0 msec. Mobile phase conditions were ultrapure water (18.2 M cm, TOC 2.0 ppb, Milli-Q Direct 16, Merck Millipore) and acetonitrile (HPLC Gradient Grade, Fisher Scientific) at a concentration of 50/50 v/v. Target peaks were picked, and formula identification was performed using LCMSsolutions software formula prediction function.

3.2.5.4 ATR-FTIR

Data were recorded with an Agilent Technologies Cary 630 FTIR with diamond ATR using MicroLab PC software. IR spectra were recorded at room temperature (25°C) between 4000 – 650 cm^{-1}. A total of 20 scans were performed at 4 cm^{-1} resolution which were averaged before Fourier transformation. All the absorbance spectra were recorded with air as the background on the clean prism surface and then compared. The diamond crystal was cleaned with propan-2-ol between each measurement.

3.2.6 Quantification calculations and analysis

The 3σ and 10σ methods were used to calculate the limit of detection (LOD) and limit of quantification (LOQ) respectively (Equation 3.2 and 3.3) from calibration plots [38].

LOD *= 3 x error of y-intercept/gradient of the line* (Equation 3.2)

LOQ *= 10 x error of y-intercept/gradient of the line* (Equation 3.3)

3.2.6.1 Errors in analytical measurements

% Recovery *= Detected concentration/spiked concentration x 100 (ref [39])* (Equation 3.4)

% Error *= (Measured value – actual value)/actual value x 100* (Equation 3.5)

3.3 Results and Discussion

3.3.1 The oxidation of creatinine by potassium ferricyanide

As previously stated, creatinine is not an electroactive molecule. Numerous studies have tried to activate creatinine and oxidise it directly at an electrode surface using various surface morphologies and electrocatalysts. However, it is frequently found that the creatinine response is poor and the response to other components in real samples is more pronounced.

As such, the most successful electrochemical approach towards creatinine biosensing has been to use enzymatic systems. It is typical in enzymatic biosensors for the reaction to be monitored electrochemically via a redox active mediating substance, such as the osmium complex in commercial glucose sensors.

A lesser studied metal modification for creatinine sensing is nickel. As discussed in Chapter 4, we began evaluating the electrocatalytic response of Ni-GCE to creatinine in KOH. However, in the course of our initial studies it was noted that on addition of creatinine to a yellow ferricyanide solution it

immediately became colourless, suggesting that the ferricyanide (Fe^{3+}) was reduced to ferrocyanide (Fe^{2+}). This prompted us to evaluate the reaction both colorimetrically and electrochemically on a simple, unmodified carbon electrode.

Creatinine is a cyclic compound comprising primary, secondary and tertiary amine groups. Reports in the literature indicate that alkaline ferricyanide is a known oxidant of tertiary amines and can be used in their selective oxidation [30, 31, 35]. It has been observed that oxidation of aliphatic tertiary amines with potassium ferricyanide in presence of hydroxide ions gives a secondary amine, aldehyde and potassium ferrocyanide as products (Equation 3.6).

$$R_2NCH_2R' + Fe(III)(CN)_6 + OH^- \rightarrow R_2NH + R'CHO + Fe(II)(CN)_6 \hspace{2cm} \text{(Equation 3.6)}$$

Given the distinct and instantaneous colour change, UV/vis experiments were made to characterise the response of ferricyanide to creatinine. The spectroscopy results are shown in fig. 3.2 and 3.3 alongside an average calibration plot (n=3) of the response with and without artificial urine. The absorbance at 420 nm was used to monitor the concentration of ferricyanide, as determined from a study in water. A series of 50 µM additions of creatinine in artificial urine were made to the 1 mM ferricyanide in 1 M KOH, giving a linear response over the range of 0.05 and 0.65 mM. The detection limit for creatinine was determined using 3σ IUPAC criteria[38] and was 38 µM (without artificial urine) and 6.63 µM (with artificial urine), respectively.
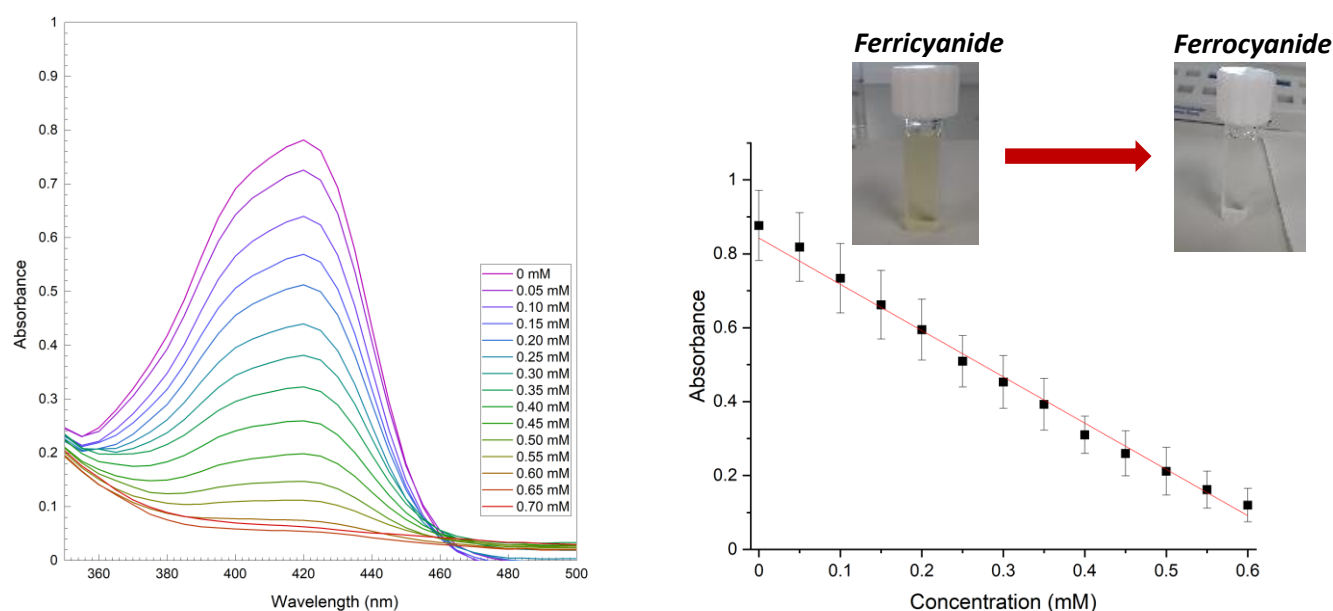
Figure 3.2: UV-vis analysis of ferricyanide based creatinine colorimetric sensor without artificial urine at 420 nm, LOD 38 µM, R-square 0.990.
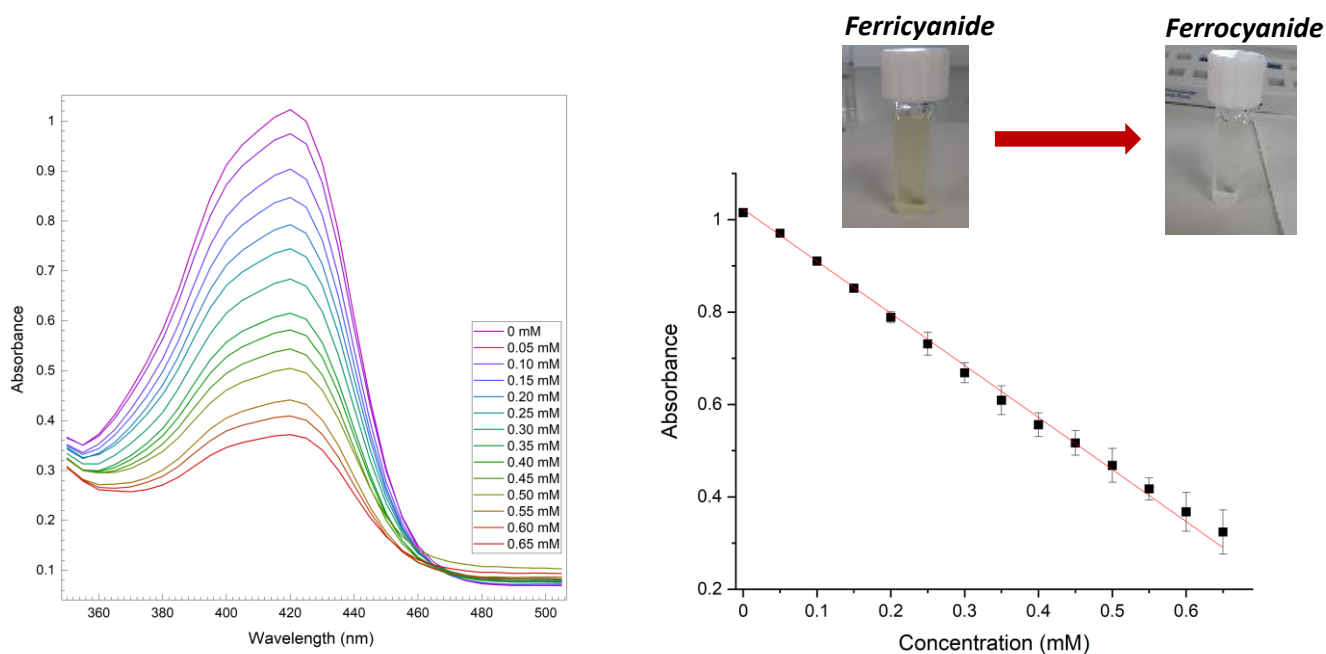
Figure 3.3: UV-vis analysis of ferricyanide based creatinine colorimetric sensor with artificial urine at 420 nm, LOD 6.63 µM, R-square 0.997

It is to be noted that the absolute error in the calibration graph (fig. 3.2 and 3.3) was calculated based on taking average of highest and lowest values in the three measurements. The LOD achieved with creatinine in artificial urine was lower, clearly indicating reduced interference with major components in artificial urine (including urea).

3.3.2 Evaluation of electroanalytical performance in alkaline potassium ferrocyanide

Prompted by the UV/vis studies and literature indicating that alkaline ferricyanide is an oxidant to tertiary amines, we sought to capture this response electrochemically. Creatinine is a complex amine, comprising primary, secondary and tertiary amine sites, therefore it was likely the ferricyanide was being reduced to ferrocyanide by the creatinine. As such it was hypothesised that an electrochemical response for ferrocyanide oxidation in the presence of creatinine should be enhanced in a manner characteristic of an electrochemically catalytic reaction (shorthand notation EC').

$$Fe^{2+} \rightarrow Fe^{3+} + e^-$$ (Equation 3.7)

$$Fe^{3+} + CR \rightarrow Fe^{2+} + CR - O$$
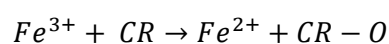
An initial study looked at a relatively high concentration of creatinine, to characterise the electrochemical response. Figure 3.4 shows the electrochemical response of 10 mM creatinine to a 1 mM ferrocyanide in 1 M KOH solution.
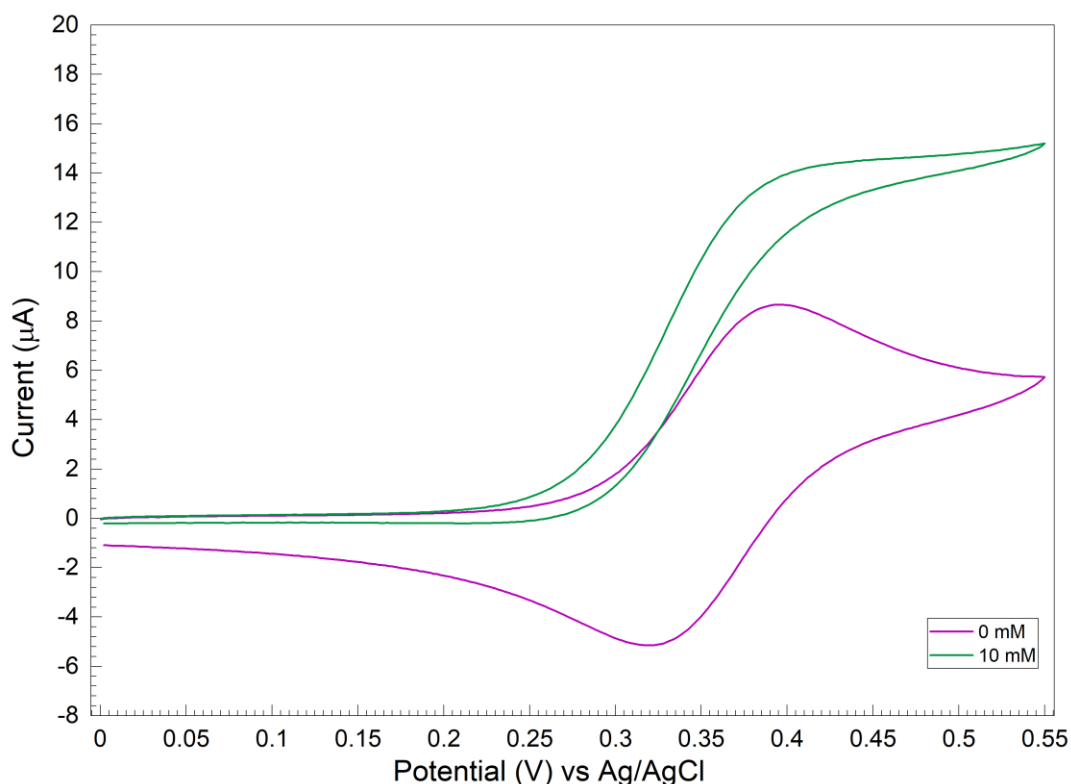
Figure 3.4: Electrochemical detection of creatinine with 10 mM addition to 1 mM ferrocyanide in 1 M KOH.

A typical electrocatalytic (EC') mechanism is evident in fig. 3.5 in which the electrochemical oxidation of ferrocyanide to ferricyanide prompts the chemical oxidation of creatinine by the ferricyanide, reforming the ferrocyanide. Correspondingly an enhanced anodic response is observed where the ferricyanide is reduced back to Fe(II) and re-oxidised by the electrode polarisation. This process is given in Equation 6, with ferro and ferricyanide depicted as Fe(II) and Fe(III) respectively, and creatinine and its oxidation product as CR and CR-O.

The magnitude of the catalytic current is dependent on the concentration of creatinine in solution. In the literature it has been suggested that the OH$^-$ ions act as a catalyst in the reaction of amines with ferricyanide [35], therefore the concentration of KOH used is apparently critical. Without the use of KOH in 1 mM potassium ferrocyanide an electrocatalytic behaviour was not observed. The response of

creatinine to potassium ferrocyanide was studied over a range of pHs from pH 7.2 (in PBS), 0.1 M KOH, to pH 14 in 1 M KOH. A minimum concentration of 0.6 M KOH was required for a colour change of 1 mM potassium ferricyanide to colourless (forming potassium ferrocyanide) as a result of creatinine oxidation, implicating the hydroxide ions in the chemical reaction. In pH 7.2 (neutral) solutions the ferricyanide gave no appreciable response to the creatinine. However, in the range pH 13 – 14 an electrocatalytic response to creatinine was observed when ferrocyanide was oxidised to ferricyanide (Fig. 5).

Electrochemically, the anodic response of the ferricyanide to creatinine additions was evaluated for 1 mM, and 20 mM ferrocyanide (fig. 3.5 and 3.6). Calibration plot shown inset, were derived from taking the current response at 0.40 V vs Ag/AgCl. The calibration plots in both instances are seen to plateau at higher concentrations of creatinine, corresponding to a reduction in current response. Higher concentrations of ferrocyanide (20 mM) caused plateauing of the calibration plot at lower creatinine concentrations in comparison to that seen with 1 mM. Therefore, so as to achieve a better LOD, 1 mM ferrocyanide and 1 M KOH were chosen as the optimised electrolyte composition for analysis.
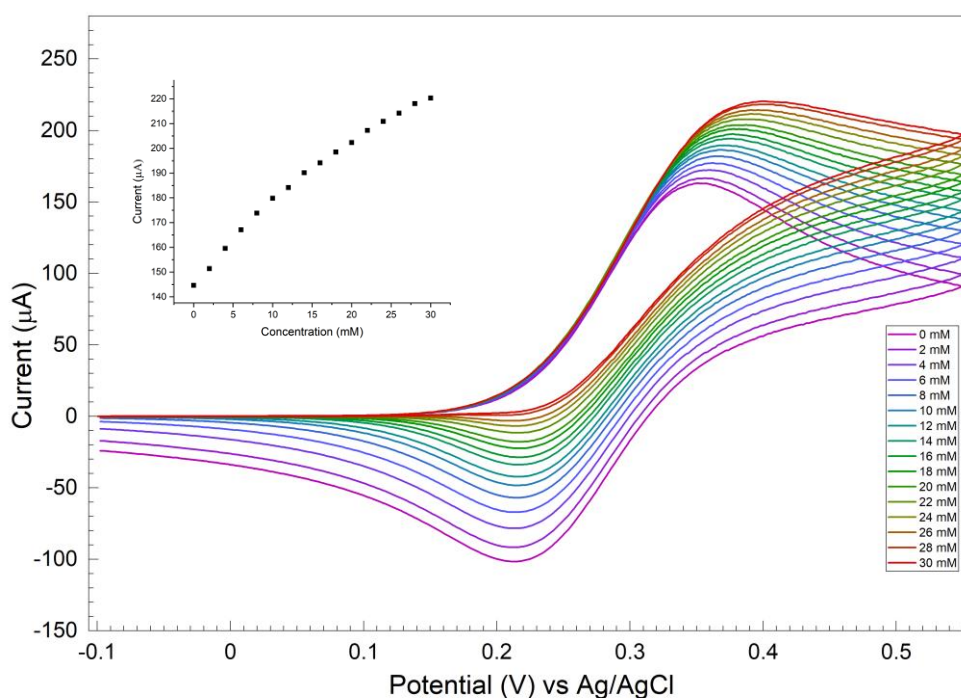
Figure 3.5: Detection of creatinine (with 2-30 mM creatinine additions) in 20 mM ferrocyanide and 1 M KOH with the calibration plot considering a fixed potential of 0.40 V (vs Ag/AgCl).

3.3.3 Evaluation of electroanalytical performance in alkaline ferrocyanide

An initial electrochemical study was done with 2 mM creatinine additions in the range 2-20 mM in a solution of 1 mM ferrocyanide and 1 M KOH (fig. 3.6). A clear electrocatalytic mechanism was observed for this reaction, where the anodic current increases with creatinine additions of higher concentrations according to explanation in section 3.3. The sensor response remains non-linear but was further investigated in the clinically relevant range (0-2.4 mM creatinine in the cell assuming dilution of a real sample for analysis using this sensor setup). According to equation below, 0-2.4 mM in a non-diluted real sample system translates to be,

C1 x V1 = C2 x V2

C1 x 1 ml = 2.14 mM x 11 ml

C1 = 23.54 mM

Therefore, the clinically relevant range analysed is between 0-23.5 mM. As reported before the range of creatinine concentration outside 4.4-13.3 mM may indicate kidney conditions including CKD [40].
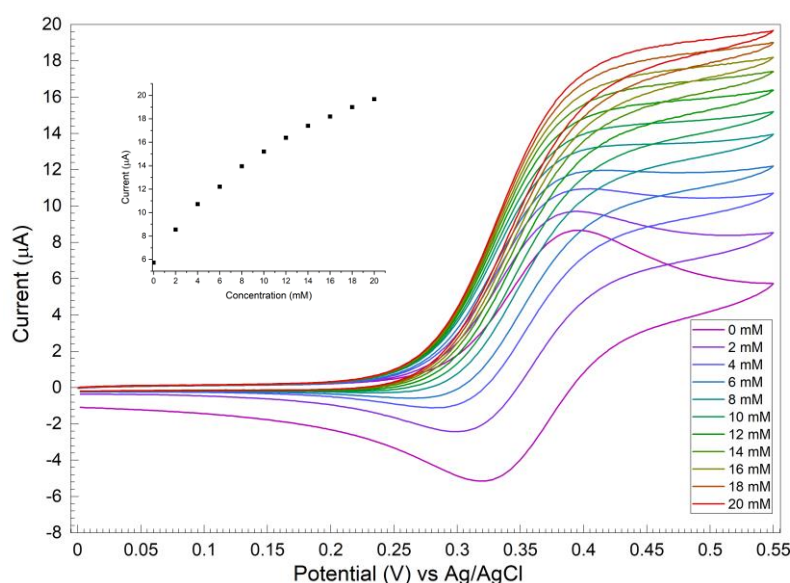
Figure 3.6: Detection of creatinine (with 2-20 mM creatinine additions) in 1 mM ferrocyanide and 1 M KOH considering a fixed potential of 0.55 V vs Ag/AgCl.

Fig. 3.7a shows the CVs obtained from making 0.2 mM additions of creatinine to a solution of 1 mM potassium ferrocyanide in 1 M KOH. For the calibration graph (inset) the concentration has been corrected to account for the volume of each addition (100 μL) thus giving the accurate creatinine range of 0 - 2.14 mM.
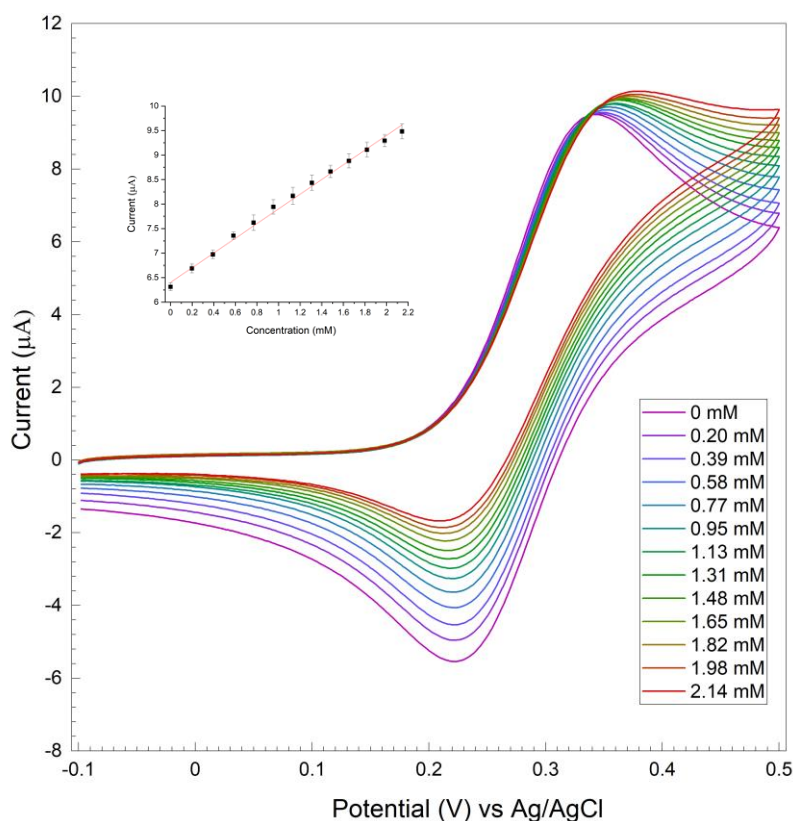
Figure 3.7 a) CVs for bare GCE in 1 mM potassium ferrocyanide and 1 M KOH with creatinine additions b) Adjusted calibration graph at 0.50 V (vs Ag/AgCl) in the range 0-2.14 mM, n=3, R-square 0.995 with LOD 60 μM and sensitivity 1.50 ± 0.03 μA/mM

Having obtained the calibration curve for creatinine detection for the clinically relevant range (fig. 3.7), a linear relationship (R^2=0.995) between current at 0.50 V and creatinine concentration was observed from 0.2 – 2.14 mM based on three repeat measurements. The sensitivity obtained was 1.50 ± 0.03 μA/mM. The 3σ and 10σ methods[38] were used to calculate the LOD and LOQ, respectively (see Methods). The average LOD and LOQ were 60 μM and 0.2 mM, respectively calculated based on the linear fit analysis.

3.3.4   Chronoamperometry studies

A fixed potential of 0.43 V was used for the chronoamperometry study. No step response was observed between 2 mM creatinine additions of 0-10 mM during stirring conditions. This concluded the fact that the system was not suitably sensitive to give higher current values in a step response.

3.3.5 Standard addition analysis

To evaluate the response of the alkaline ferrocyanide system as an analytical sensor for creatinine, a standard addition study was undertaken. Initially the standard addition work was in the optimal conditions given in Section 3.4, of 1 mM ferrocyanide in 1 M KOH. A scan without creatinine was taken to normalise the subsequent results. Following that, 1 ml of water/KOH containing physiological concentrations of creatinine (10, 17, 20 and 25 mM), was added to the cell for voltammetric analysis (the "unknown"). This corresponds to creatinine concentrations of 0.91, 1.54, 1.82 and 2.27 mM in the KOH. Three 0.4 mM additions of creatinine were then made using 22 µl of a 200 mM creatinine stock solution. The results for a 17 mM "unknown" addition from creatinine solution in water are presented in Figure 3.8. Concentrations 10 and 25 mM are given in Appendix A. The results are also summarised in Table 3.2.
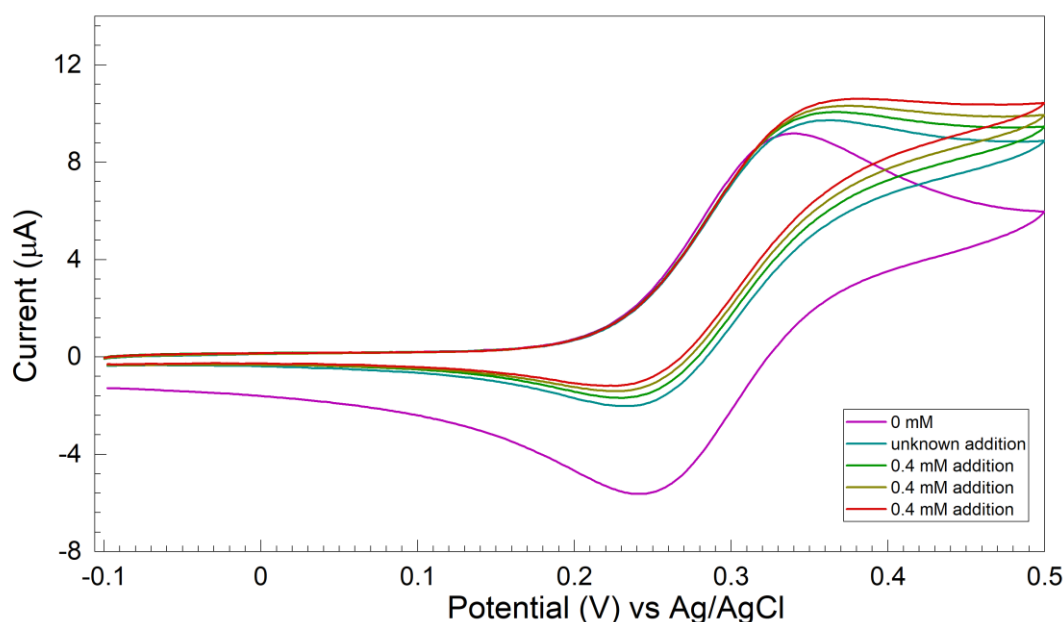
Figure 3.8: CV for 17 mM unknown addition from creatinine solution in water (with three known 0.4 mM creatinine additions from 200 mM stock)

Table 3.2: Creatinine standard addition analysis using creatinine stock in water on bare glassy carbon.

Creatinine stock concentration	Spiking (mM)	Detected (mM)	Recovery %
10	0.91	0.58±0.12	63.7
17	1.54	1.68±0.04	109.1

| 25 | 2.27 | 2.82±0.23 | 124.2 |

The calibration plot of current (at 0.50 V vs Ag/AgCl) vs creatinine concentration was generated from analysing the CV data (fig. 3.8) at 0.50 V vs Ag/AgCl. It is to be noted that each current value was adjusted based on the blank current (at 0 mM creatinine addition). The equation of the line obtained was rearranged to calculate the detected concentration of creatinine.

It is common for creatinine sensors and analytical methods for creatinine detection, such as the Jaffe reaction, to be negatively affected by the presence of other components in urine. As such, we tested our analytical system from a synthetic artificial urine sample. The CV measurements were again performed in an electrochemical cell containing 10 ml of 1 M KOH and 1 mM ferrocyanide. A scan without creatinine was taken such that the subsequent results could be normalised. Following that, 1 ml of artificial urine containing different physiological concentrations of creatinine (10, 17, 20 mM), was added to the cell for voltammetric analysis. The standard addition method ensures matrix effects are avoided in the analysis. Background current signal from the blank CV in presence of a real sample may be higher than that in a standard solution in water due to response to interfering species, therefore in a standard addition procedure, the standard and the unknown are combined to give an overall response. Table 3.3 presents the results of the standard additions made using artificial urine. Three repeats at each concentration were made. The results for a 17 mM unknown addition using CV study is shown in fig. 3.9.
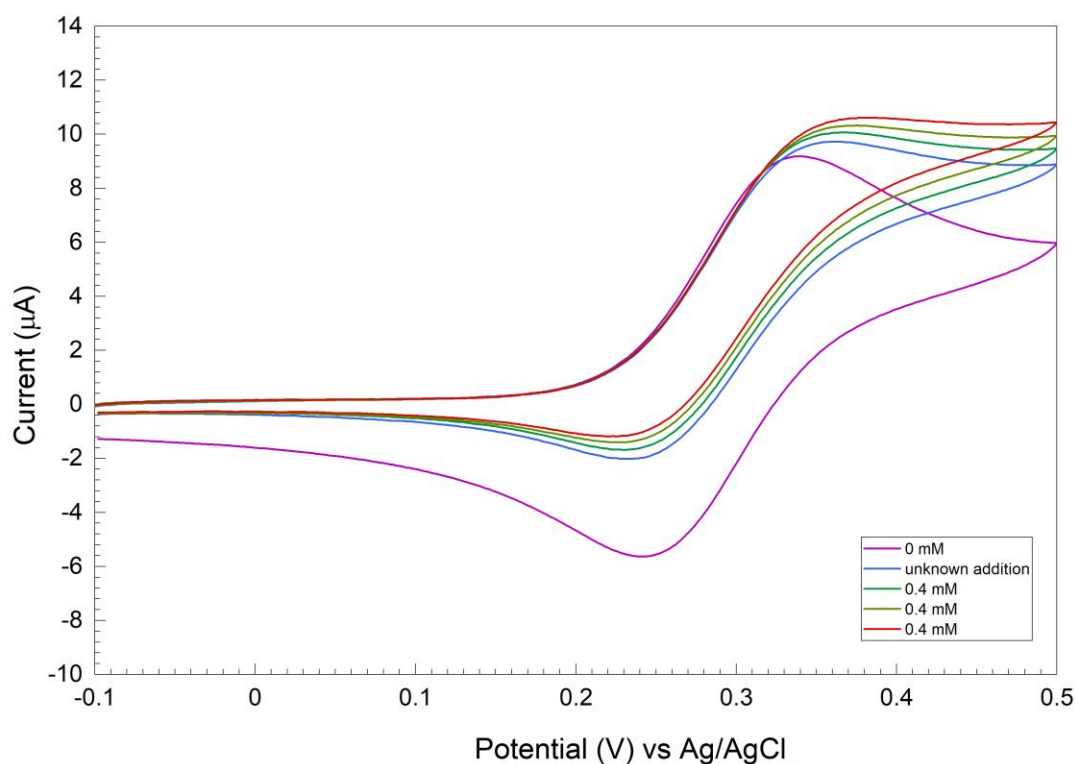
Figure 3.9: Standard addition study with a 17 mM CR in AU unknown addition followed by three known 0.4 mM CR additions from 200 mM CR stock in water.

Table 3.3: Creatinine standard addition analysis using artificial urine on bare glassy carbon.

Creatinine concentration in artificial urine (mM)	Spiking conc. (mM) in KOH	Detected (mM)	Recovery %
10	0.91	0.87 ±0.19	95.6
17	1.54	1.72 ±0.15	111.7
20	1.82	2.04 ±0.22	112.1
25	2.27	3.06±0.12	134.8

Recovery studies were done with three repeats in three artificial urine samples and results were in the range 95.6 – 134.8 %. According to the Association of Official Analytical Chemists (AOAC) standards (also followed in a glucose study [41]), the expected mean recovery for the analytes in this concentration range is between 95-105% [42]. It was observed that there was a deviation (higher than the expected

73

105%) of detected concentration result from the true value, in all cases except at 10 mM creatinine concentration in artificial urine. In comparison to literature, recovery % in most of the studies is in the expected range between 95-105%. A few studies in the literature are summarised in table 3.4 below.

Table 3.4: Summary of reported analytical analysis of previous non-enzymatic creatinine sensors for urine and serum samples.

Electrode Modification	Substrate	LOD (µM)	Sample	Recovery (%)	Reference
CdSe QD-HF/QD modified electrode (CdSe - Cadmium Selenide, QD - quantum dots, HF - hollow fiber)	Graphite Electrode	0.229	Serum	98.42 - 98.67	43
Copper	Screen-printed carbon electrode (SPCE)	0.0746	Serum	95.6 - 98	26
PMB (poly methylene blue)-Cu-CNF (Carbon nanofiber) nanocomposite	Activated carbon fiber	1768	Serum	97.8 – 98.2	10
Carbon black film in contact with paper-	Polyester	43	Urine	98 – 110	19

adsorbed iron (III) ions					
Fe3+ based µPAD (Paper-based analytical device)	Carbon Black	84	Urine	101.8 – 101.6	18
Reduced graphene oxide (RGO)/AgNPs film	Glassy Carbon Electrode	7.43×10^{-7}	Urine	99.89 – 102.24	23

While the results from the bare GCE in KOH to creatinine are not sensational, they show comparable results to the Jaffe reaction in terms of recovery yet without the cumbersome preparation and volatile compounds, or interference from the standard components of urine.

Literature studies summarised in Table 3.4, show use of various metal-based platforms for sensing creatinine including Cu, Fe and Ag. The substrate modifications include use of highly conductive materials including rGO, carbon black and QDs. This significantly enhances the sensitivity of the sensor due to high surface area of active sites at the WE. In a study by Fava et al., a microcell based SPE system was designed for creatinine detection. The mechanism involved complex formation between creatinine and Fe(III) ions, followed by electrochemical reduction of excess non-complexed Fe(III) ions. An increased analytical current signal was observed using carbon black as the substrate modification material[19]. Fava et al. also developed a multi-sensing device utilising this Fe(III) based detection mechanism for sensing of creatinine. The disposable paper-based device with multiplexed working electrodes detected glucose, creatinine and uric acid[18].

Further optimisation of the bare GCE/ferrocyanide-based creatinine sensor system is required to increase the accuracy and precision in the analysis. Based on the literature in Table 3.4, this could be achieved through increasing the sensitivity of the system using conductive materials to coat the GCE with carbon black (CB) or reduced graphene oxide (rGO).

3.3.6 Sensor analysis using other interferents

Patients may be prescribed ascorbic acid (AA) supplements for various reasons. The most common use reported is that for preventing and treating the common cold. Other uses include treatments for heart disease, cancer and asthma. AA in CKD patients is considered for improving outcome by decreasing oxidative stress. Oxidative stress and inflammation are common problems seen in CKD patients, which also causes increased risk of cardiovascular events [44]. Therefore, there could be presence of AA in urine of individuals being tested for CKD at early stages or when monitoring patients with a CKD diagnosis. It has been seen that the approximate non-metabolised concentration maximum limit of AA in urine is 1.1 mM and may be more in some cases (2 mM AA was tested in this work). There has been clear demonstration that AA interferes with urine and blood tests for molecules like glucose [45-49]. There are suggestions where it is considered to mention to patients not taking vitamin C supplements or eating fruits and vegetables before a test. A study on considering the effect of AA interference in urine test strips have used a method of calculating interference coefficients to account for sensitivity to ascorbate interference. The higher the interference coefficient, higher is the extent of AA interference [45]. Therefore, as a result only trained people would be able to use such sensing devices. Although, a simple analyte sensing method should be present to overcome these challenges. Chapter 4 (on optimisation techniques using screen-printed electrodes) addresses these issues and work has been done to reduce the extent of these interferences through modification of the surface of the working electrode with membranes like Nafion (Nf) and Carbon Black (CB).

Plasma uric acid (UA) levels in individuals with CKD rise due to lower glomerular filtration rate (GFR). The condition is known as hyperuricemia [50]. However, presence of normal levels of uric acid in healthy patients can affect their test results, when there is still a significant concentration of uric acid in urine. High levels of uric acid could also be present as a result of having a high purine diet with foods including fish and dried beans. Normal levels of UA in urine are between 1.5 − 4.5 mM [51]. Therefore, it is necessary to check the extent of the interference of uric acid in the creatinine sensing system.

Glycosuria is a condition where glucose is present in urine. It occurs as a result of more glomerular filtration through the kidneys, where the renal tubule can't absorb glucose. Glucose levels greater than 0.6 mM in urine occurs in glycosuria. Diabetic patients generally have glucose levels in urine between the range 3 - 16.7 mM [52]. Due to the fact that diabetic patients are at high risk of having CKD, it is essential that glucose interference in urine is considered during the application of the creatinine tests developed in this work, in a clinical setting.

Electrochemical sensing experiments were performed with using ascorbic acid (AA), uric acid (UA) and glucose as potential interferents which have seen to oxidise with ferricyanide according to previous

reports [53, 54]. The fact also has been that these interferents could oxidise on GCE in alkaline solutions specifically.

3.3.6.1 Ascorbic acid

As previously reported ascorbic acid (AA) can be oxidised using potassium ferricyanide in alkaline conditions [54]. It was also found that ascorbic acid could be electrochemically oxidised on electrochemically pre-treated screen-printed carbon electrodes which possessed excellent electrocatalytic activity towards the oxidation of ascorbic acid [55]. This is in accordance with this study with AA in 1 mM ferrocyanide and 1 M KOH using a bare GCE, where major electrochemical oxidation of AA is seen before formation of ferricyanide (through oxidation of ferrocyanide as the potential is scanned more positively in cyclic voltammetry (CV)) which reacts with creatinine to give the sensor response (fig. 3.10). Xiang et al. show typical CVs for AA oxidation at pH 7 (in 0.1 M phosphate buffer) in the presence of ferricyanide with electrochemical oxidation occuring at a potential of -0.1 V vs Ag/AgCl [55]. According to this study, in the potential window of -0.1 V to 0.50 V (vs Ag/AgCl), there is significant oxidation of AA nearing the starting potential of -0.1 V vs Ag/AgCl (fig. 3.10).
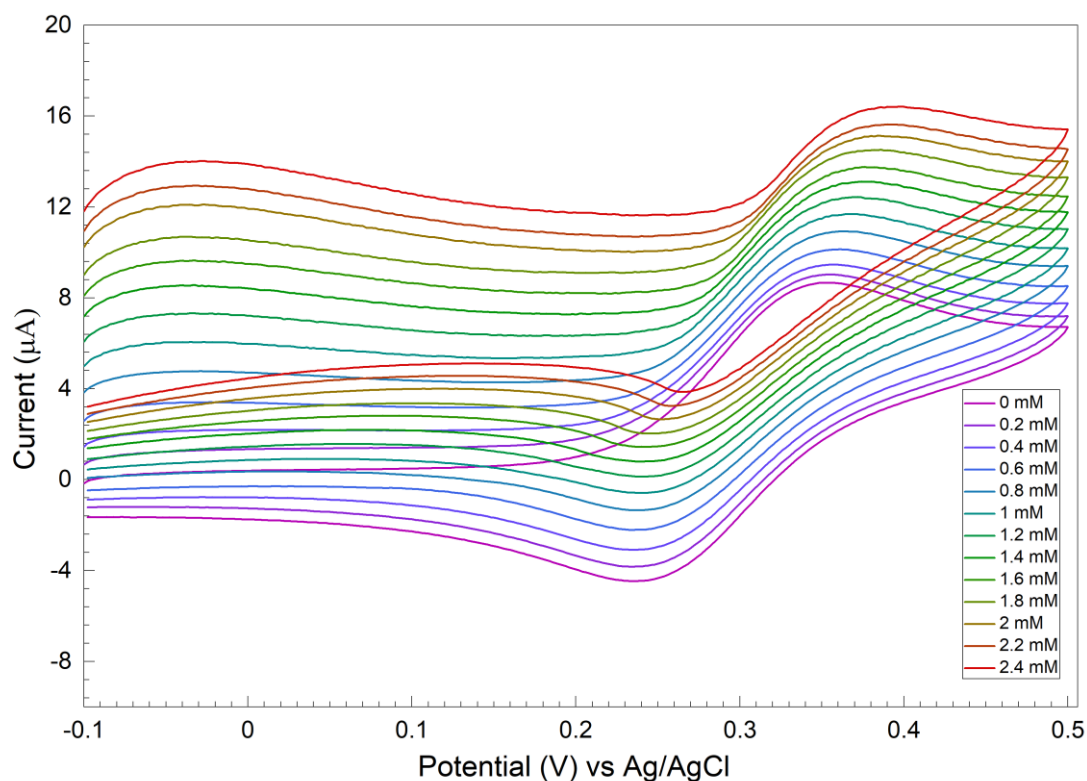
Figure 3.10: Electrochemical oxidation study with ascorbic acid (AA) in 1 mM ferrocyanide and 1 M KOH using a bare GCE system.

Fig. 3.11 clearly shows the result of oxidation of AA in presence of 1 mM ferrocyanide in 1 M KOH solution. It was observed that the oxidation of AA occurs at the surface of the bare GCE at the starting

potential giving a current response in both cases of testing AA addition in only KOH solution and then in alkaline ferrocyanide (fig. 3.11).
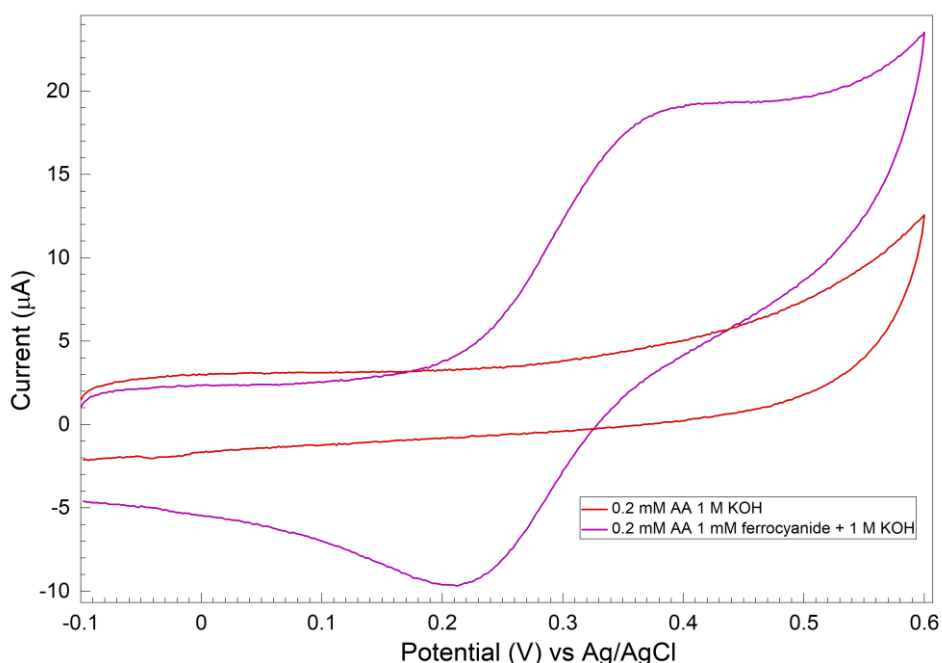
Figure 3.11: Oxidation of AA at 0.32 V vs Ag/AgCl on a bare GCE in different solutions of KOH and ferrocyanide.

It can be concluded that AA oxidises at -0.1 V vs Ag/AgCl well before the electrochemical oxidation step on the surface of the bare GCE (where creatinine oxidation would occur on its reaction with ferricyanide as it forms in the forward potential scan). Therefore, it is critical to prevent entry of AA to the surface through using charge-based membrane materials as AA exists in a negatively charged state. To test this hypothesis, a Nafion/carbon black coating was made on the GCE as the Nafion has a negative charge associated with it and would thus repel the AA ions. Nafion based creatinine sensors have been developed in previous studies to reduce/eliminate interferences with AA and UA [11, 14, 56]. It is evident in fig. 3.12, that the Nafion/CB based GCE system shows very little response to the AA suggesting it is indeed preventing AA from approaching the surface of the GCE. It is to be noted that carbon black (CB) was used specifically as a result of the fact that a higher Nafion concentration (which is required to significantly prevent entry of interferents to the surface of WE) increases resistance into the electrode/solution system and a conductive material in combination further improves the current response. In this case, a higher current response is obtained with CB, which could further give higher sensitivities and lower limits of detection. *The detailed Nafion based optimisation studies are discussed in Chapter 5 on SPE study.*
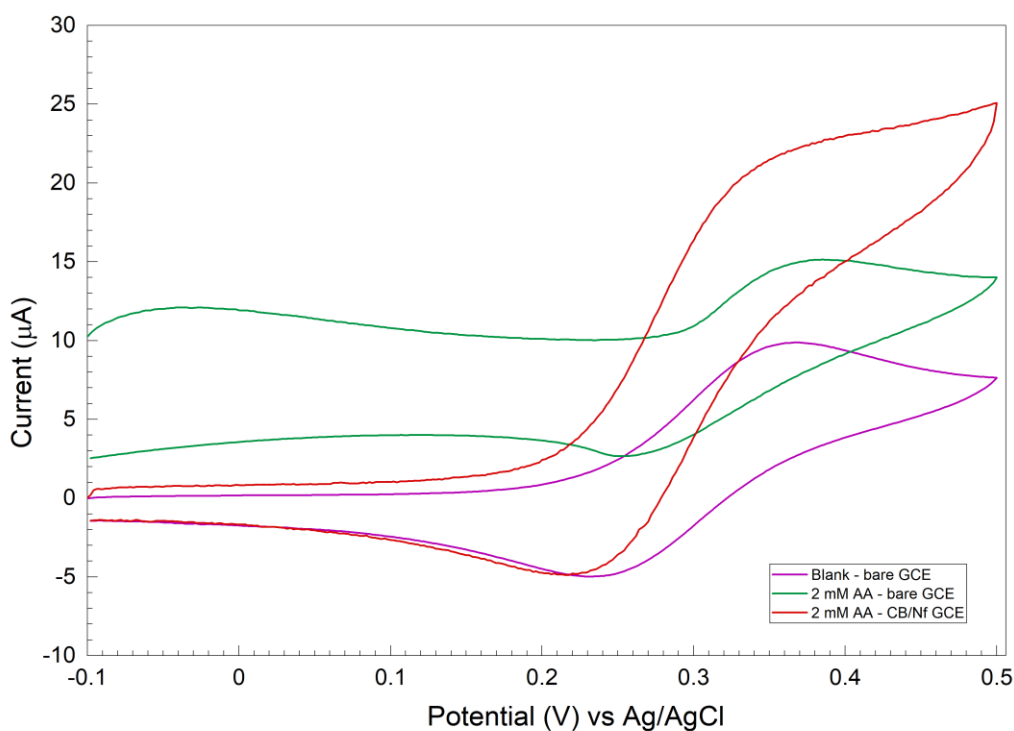
Figure 3.12: Comparison of current response of 2 mM AA addition to a bare GCE and a nafion (2 wt%) /CB (10 mg/ml) based GCE)

To conclude, the bare GCE/ferrocyanide system can be optimised to reduce/eliminate the extent of ascorbic acid interference and this work could potentially be extended to even eliminate uric acid interference as it is also negatively charged. *This has developed further using the CB/Nf/SPE based systems in Chapter 5.*

3.3.6.2 Uric acid

A previous report by Silverman & Gubernick has shown that uric acid can be oxidised using potassium ferricyanide and a colorimetric test can be performed based on this analysis[53]. The product observed in the reaction was reported to be potassium ferrocyanide [53]. In the experiment with bare GCE and alkaline ferrocyanide, uric acid additions between 0.2-1.2 mM shows similar oxidation behaviour as that of AA at -0.1 V vs Ag/AgCl where the onset of UA oxidation starts on the surface of the bare GCE (fig. 3.13). It could be understood that the entry of UA (also negatively charged similar to AA) could be prevented on the surface of bare GCE by using a Nf/CB based membrane system as that used for eliminating/reducing AA interference explained in section 3.3.6.1. *This is explored further in Chapter 5 with SPE based CB/Nf sensor system.*

It was not clear as to why the second anodic peak at 0.5 V vs Ag/AgCl decreased with increasing concentrations of UA. While AA raises the current response of the whole anodic sweep, in the UA study, ferricyanide formation is suppressed with increasing concentration of UA. This could therefore have a more detrimental effect on creatinine measurements, as while the baseline for the ferrocyanide oxidation shifts, the oxidation response is also clearly suppressed. Note that the concentrations shown here are very high with a physiological concentration of 1.5-4.5 mM expected in patients with conditions such as gout.
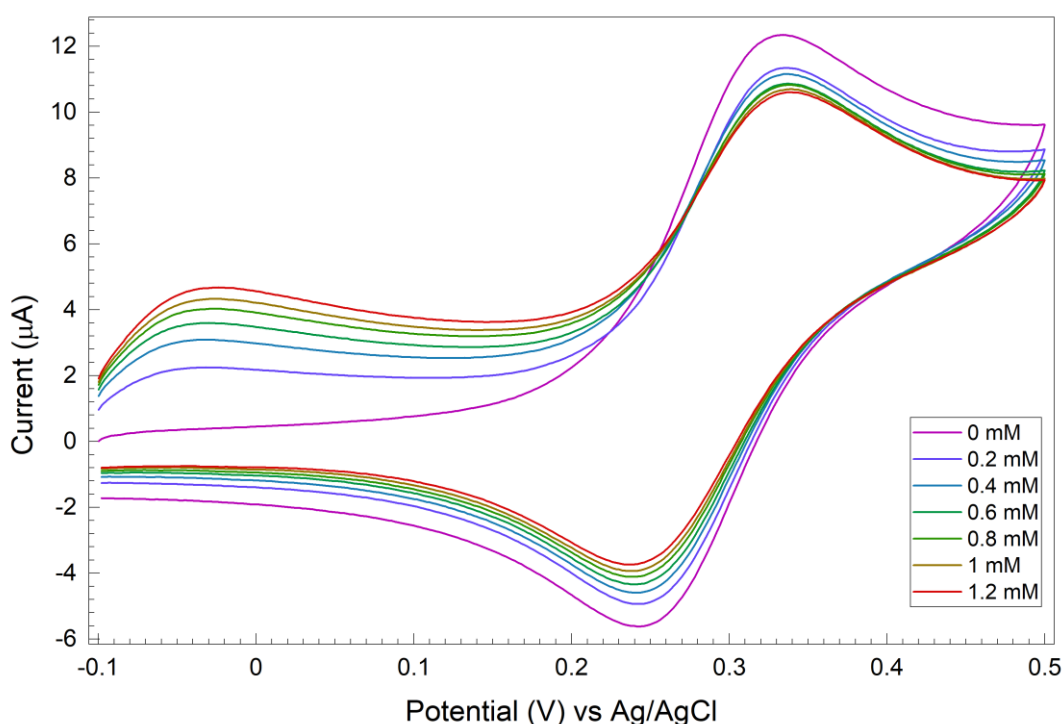
Figure 3.13: Electrochemical oxidation study with uric acid (UA) in 1 mM ferrocyanide and 1 M KOH using a bare GCE system.

3.3.6.3 Glucose

Diabetes is known to be prevalent in patients suffering chronic kidney conditions, and as such it is important to account for high concentrations of glucose in real samples. Figure 3.14 shows that the current at 0.50 V vs Ag/AgCl decreases as the glucose concentrations increase, with GCE system in alkaline ferrocyanide. Although, as seen in *Chapter 5*, glucose shows no interference with the SPE system observed in the CV study. It can be concluded that glucose may specifically be interacting with the GCE surface, causing interference in the system which is not seen in case of SPE. This is fortunate and is another advantage of the SPE system over the Jaffe reaction which is prone to false positives with glucose.
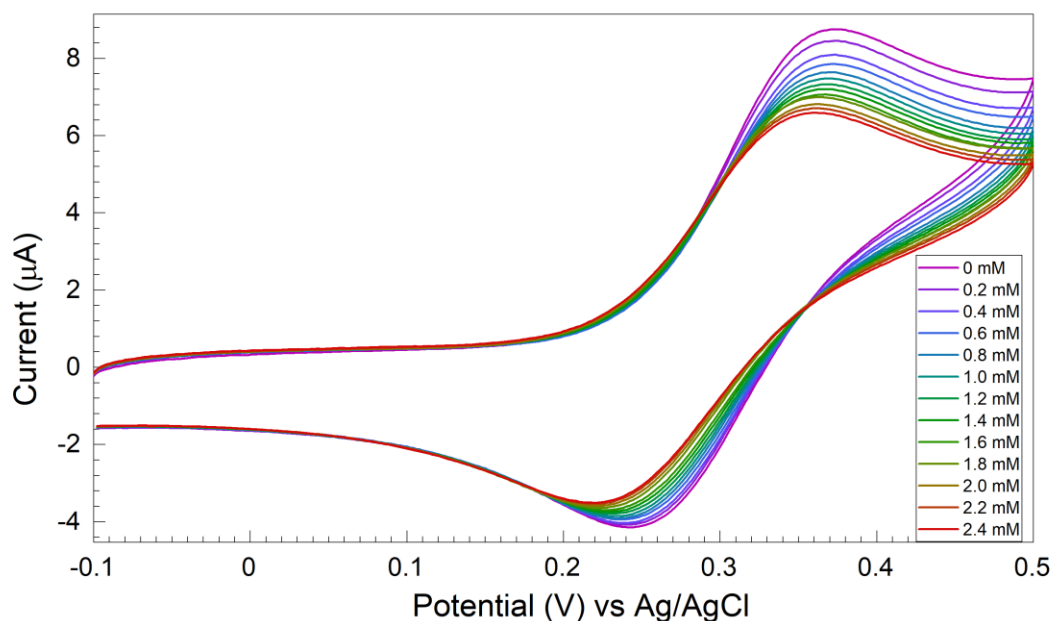
Figure 3.14: Glucose additions between 0.2-2.4 mM to alkaline ferrocyanide solution.

3.4 Mechanistic studies

An understanding of the reaction mechanism and the oxidation products of creatinine oxidation by ferricyanide was sought. A number of techniques were attempted, including mass spectrometry, infrared spectroscopy and nuclear magnetic resonance spectroscopy. The latter proved the most effective in revealing oxidation products and eluding to a mechanism of reaction.

3.4.1   NMR

The majority of NMR experiments have been performed using 1D ^{1}H NMR spectroscopy due to the high sensitivity of the ^{1}H nucleus which allows detailed structural information regarding the organic compounds to be given. The heteronuclear 2D NMR method allows additional structural information especially of new compounds, to be obtained. Heteronuclear single quantum correlation (HSQC) and heteronuclear multiple bond correlation (HMBC) are the two most commonly used 2D NMR techniques. HSQC gives information on 1H chemical shifts and X-nuclei directly bonded to the hydrogen atoms whereas, HMBC gives information over several bonds (generally 2-3) [57]. 1H-13C HSQC NMR experiments give highly sensitive information regarding the ^{1}H and ^{13}C carbon shifts which the ^{13}C NMR experiments on its own does not give. This greatly benefits compound identification through provision of more detailed biochemical fingerprint.

The issue of overlapping peaks of different components in solution can also be eliminated using the 2D 1H-13C HSQC technique [57]. This is particularly seen in this study later in the chapter where creatine and creatinine methyl peaks overlap in the 1H NMR spectra.

3.4.1.1 Creatinine-Creatine Equilibration Study

For initial analysis, the behaviour of creatinine in alkaline solution was studied to understand the degradation pathway of creatinine during oxidation to subsequent products. A ^{1}H NMR study was performed with 100 mM creatinine solution in KOH at different KOH concentrations with the range of 0.1, 1, 10, 100 and 1000 mM (fig. 3.18). It is to be noted that the experiment was initially performed with 100 mM creatinine as to understand the sensitivity of the NMR equipment for detecting the molecular structure. Once the signal-to-noise ratio was understood, further experiments were performed at a lower concentration of 10 mM. As can be observed from fig. 3.16, there exists an equilibrium between creatinine and creatine in the alkaline solution of KOH. As the pH increases, the concentration of creatine increases and that of creatinine decreases. Creatine is characterised by two singlets, one at 2.98 ppm corresponding to the methyl group which overlaps with methyl group of creatinine and the other at 3.97 ppm corresponding to the methylene group. At pH 14, (same as the electrochemical reaction condition), there is a significant concentration of creatine present, which is likely to be part of the mechanism as discussed later. Additionally, there is a small shift in ppm of the peak corresponding to the methyl and methylene groups of creatine and creatinine at pH 14. This occurs due to the formation of the deprotonated forms of creatinine and creatine (fig. 13.15B and 13.15C).
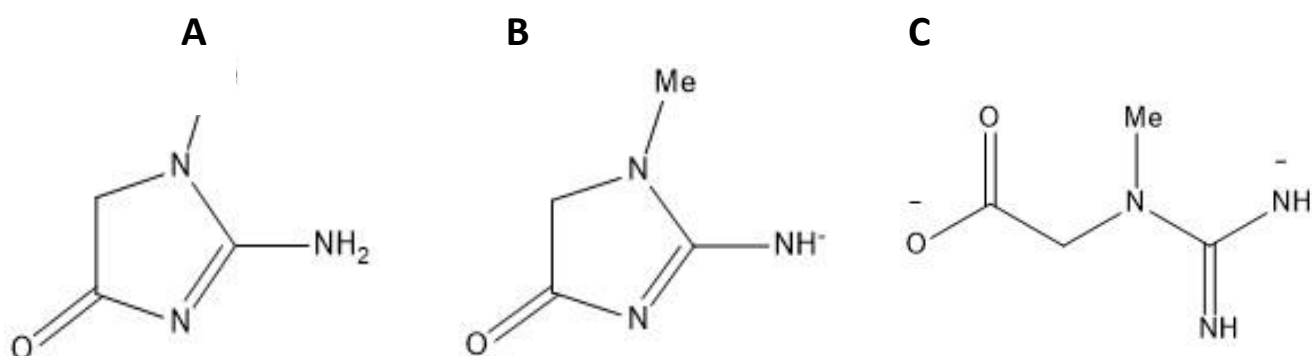
Figure 3.15: A) Creatinine   B) Deprotonated creatinine   C) Deprotonated creatine.
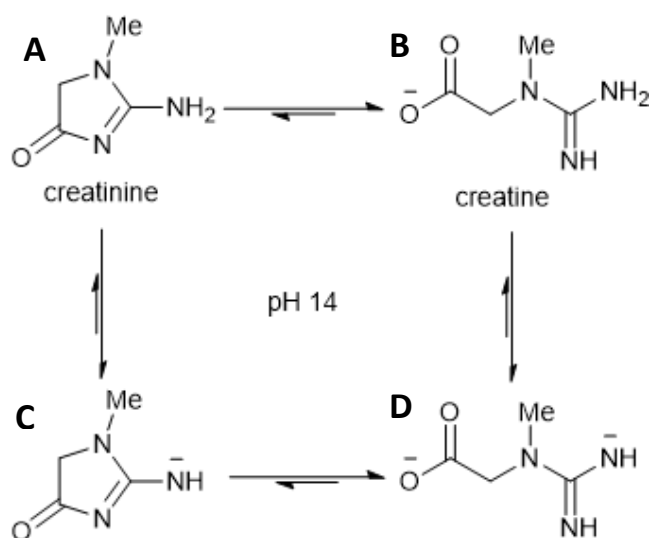
Figure 3.16: Equilibration between creatinine and creatine at pH 14 with A) creatinine B) creatine C) deprotonated creatinine D) deprotonated creatine.

A time dependent study (fig. 13.18) showed that total time for complete equilibration takes about 3 days, although certain concentration of creatine is present after 6 h showing that the mechanism might involve creatine as it is formed readily in alkaline solution in pH 14 as seen in fig. 3.17.
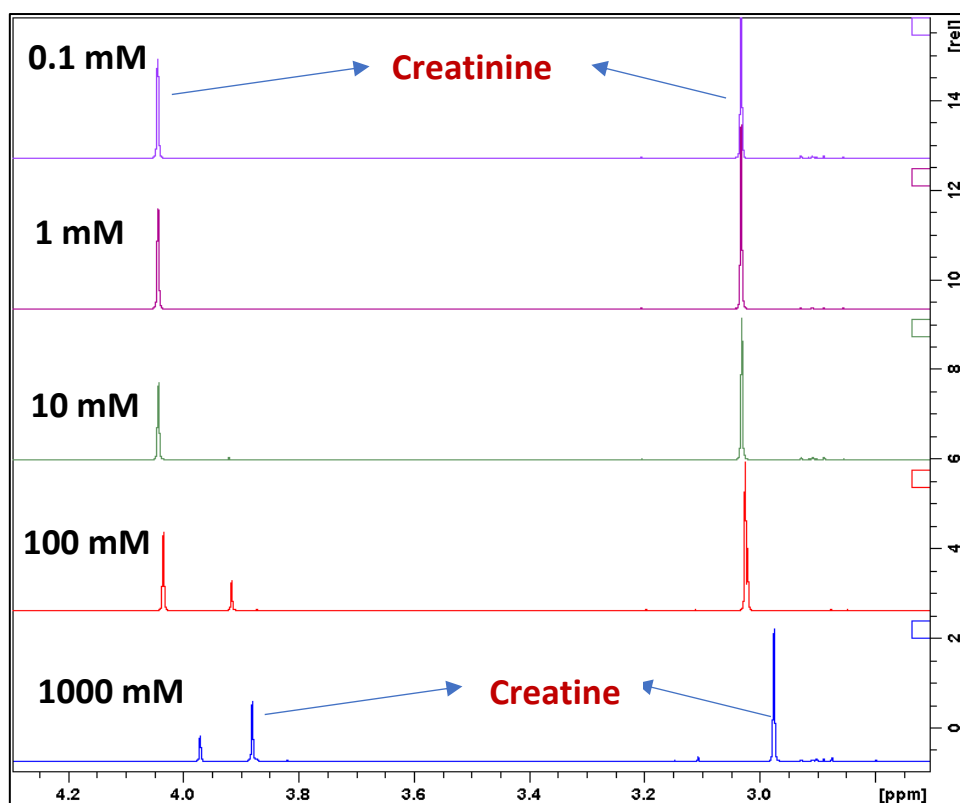
Figure 3.17: ^1H NMR study on creatinine-creatine in alkaline solution at different KOH concentrations after 6 h of preparation.

3.4.1.2 Creatinine-ferricyanide reaction study

Mechanism of reaction of creatinine with ferricyanide was investigated by comparing NMR data with 10 mM creatinine in 1 M KOH and 50 mM creatinine in 1 M KOH & 100 mM ferricyanide. Creatine and creatinine peaks were absent (fig. 3.19) meaning either creatinine was directly converted to another oxidation product either by degradation of creatinine to creatine which then converts into subsequent products or by degradation of creatinine to another product. It must also be noted that this could occur through dual mechanism pathways, either through creatinine or through creatine into oxidation products as both the initial molecules are present at pH 14 reaction conditions.
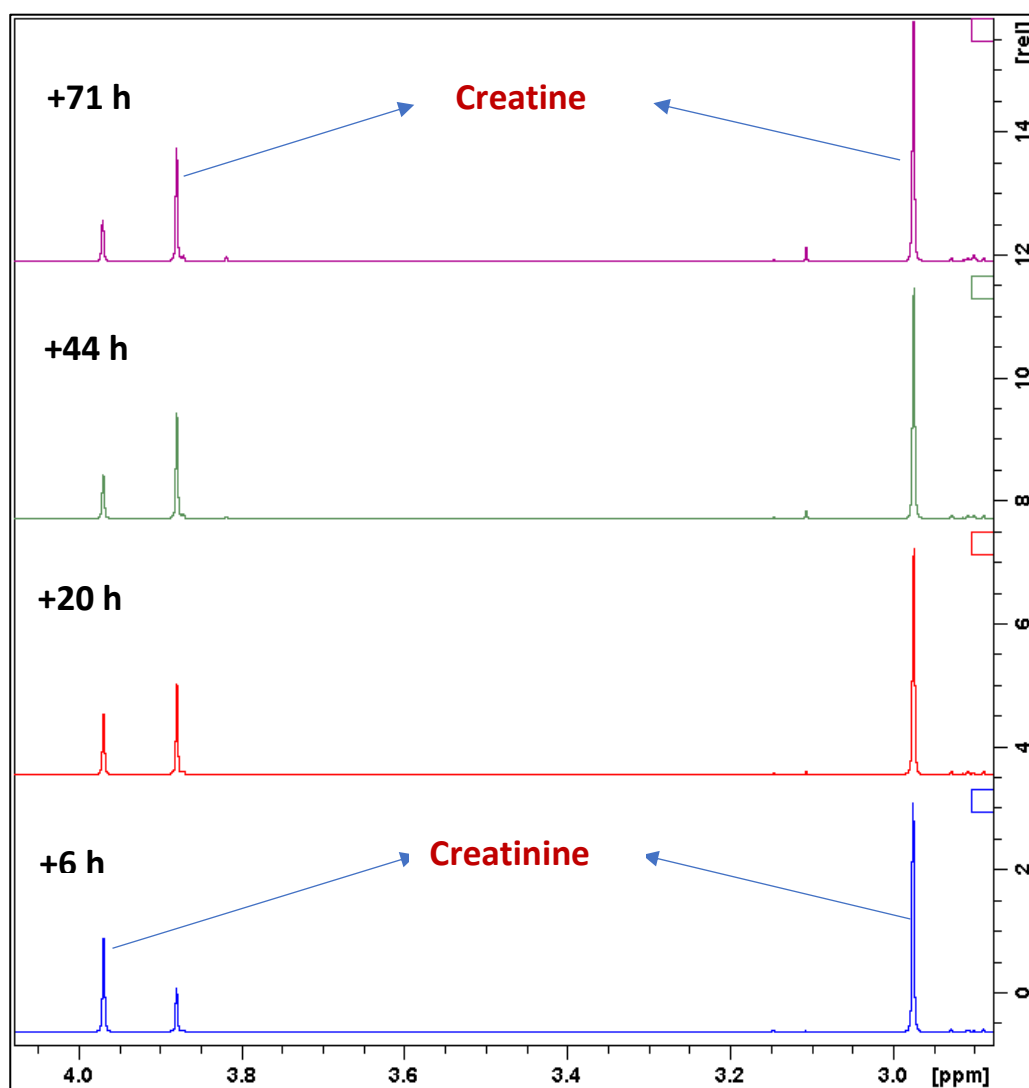
Figure 3.18: Time dependent ¹H NMR study on creatinine-creatine equilibration in alkaline solution at pH 14.
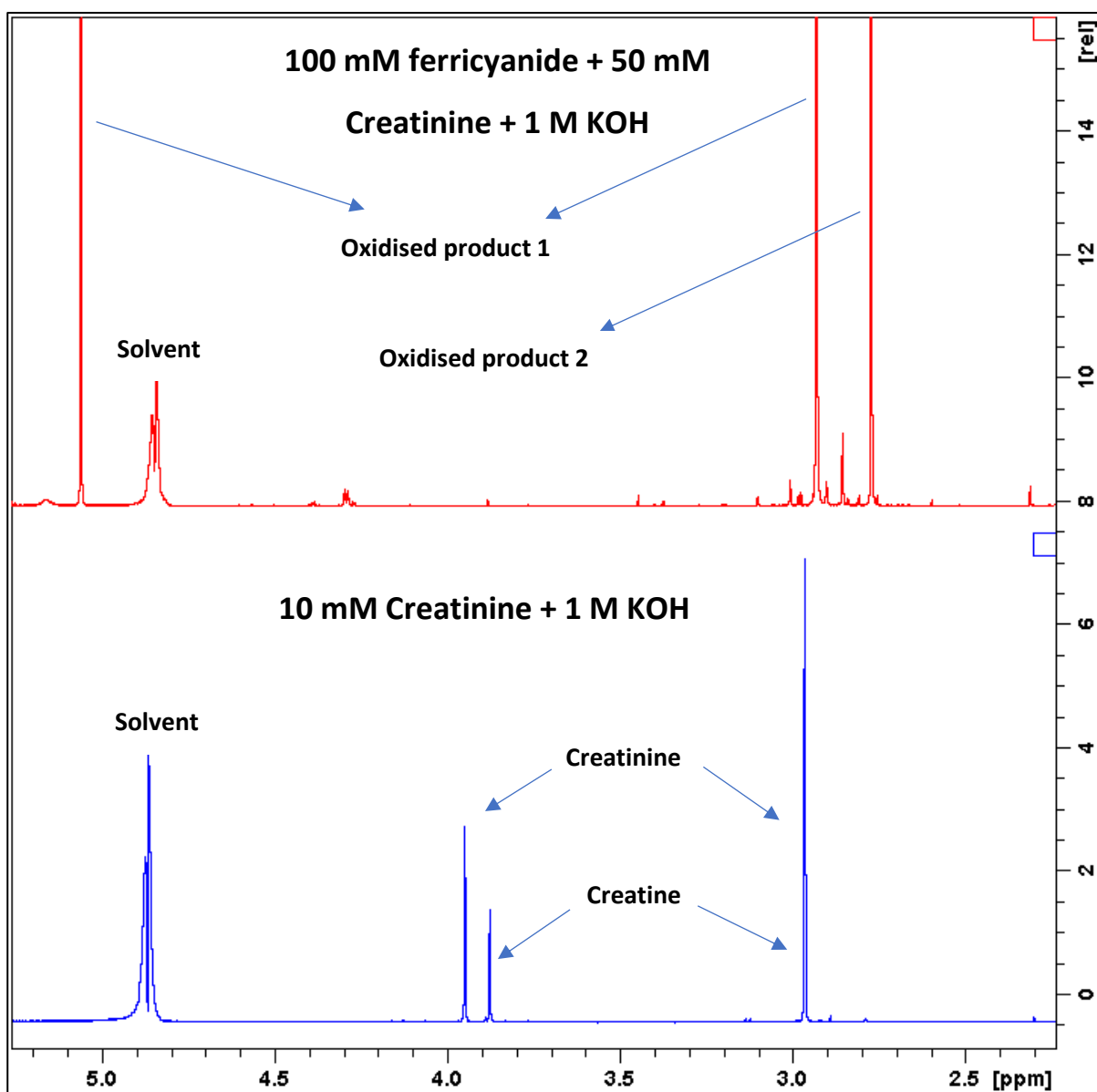
Figure 3.19: ^{1}H NMR study on the reaction of ferricyanide with creatinine.

3.4.1.3 Creatinine ferricyanide reaction products study

3.4.1.3.1 Mechanism study

At pH 14, it was confirmed using NMR that deprotonated creatinine and creatine (fig. 3.20B and 3.20C) are present in alkaline solution before ferricyanide is present.
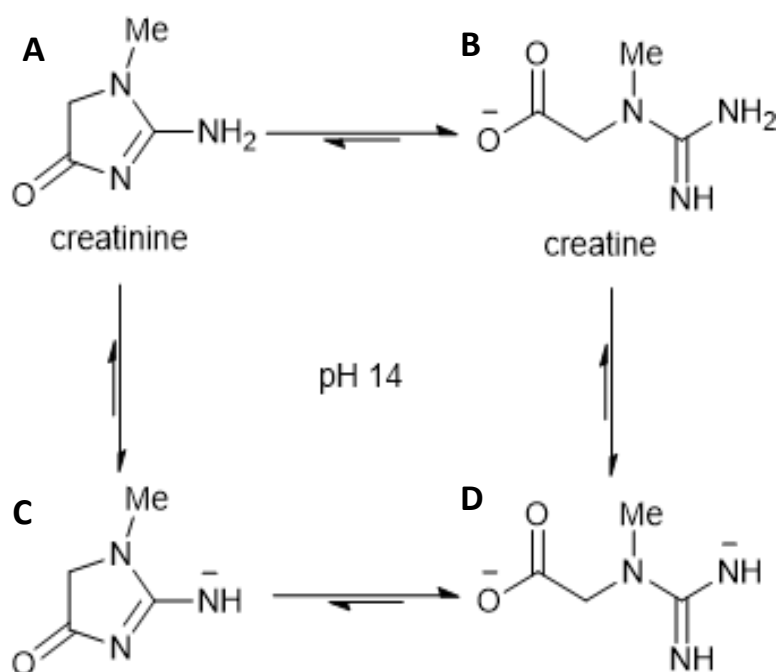
*Figure 3.20: Equilibration between creatinine and creatine at pH 14
with A) creatinine B) creatine C) deprotonated creatinine D)
deprotonated creatine.*

Various compounds including creatol, methylguanidine, 1-methylhydantoin, sodium oxalate, glyoxylic acid and methylglyoxal were studied using NMR since they were initially assumed to be possible reaction products of creatinine oxidation. 1-methylhydantoin and methylglyoxal pure compound NMR spectra didn't correlate with the NMR spectra of the reaction mixture with creatinine and ferricyanide and were seen not to be products of the reaction. 1-methylhydantoin was relatively stable at pH 14 and the peaks of the pure compound did not correlate. Similarly, for methylglyoxal which readily changed to lactic acid in its pure form at pH 14, there was no correlation with peaks of the NMR spectra of the reaction mixture with creatinine. As evident from fig. 3.19, no correlation with the reaction product NMR spectra is seen.

It has been discovered in experimental studies that creatol (5-hydroxycreatinine) is the key precursor in the synthesis of methylguanidine [58]. A previous study with activated carbon has shown the conversion of creatinine to methylguanidine via conversion to creatol [1]. Creatol is a direct product of the reaction of creatinine with the hydroxyl radical in vivo [1,58]. Under oxidative conditions, it has been

known that a group containing an oxygen atom [59], can substitute one of the protons at the C-5 of the imidazoline ring[1,]
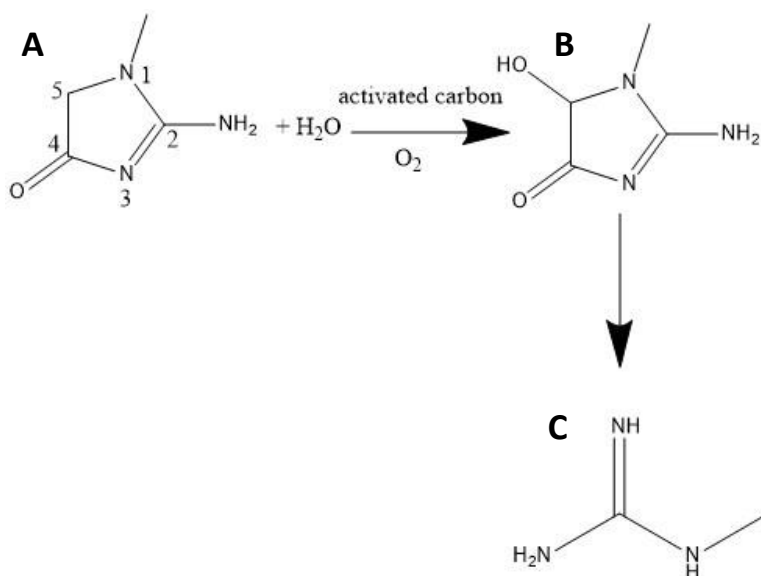
Figure 3.21: Conversion of A) Creatinine to B) Creatol and C) Methylguanidine [1].

In accordance to the mechanism suggested by Krawzyck et al. [1], the present NMR study identifies the presence of both creatol and methylguanidine in the solution after reaction with ferricyanide through analysis by ^1H NMR, ^{13}C NMR, HMBC (Heteronuclear Multiple Bond Correlation) and HSQC (Heteronuclear Single Quantum Correlation).

The deprotonated forms of creatine and creatinine are confirmed by the NMR results. It is assumed that the oxidation of creatinine occurs through conversion of creatinine to creatol and then conversion to methylguanidine and hydrate (formed from conversion of glyoxylic acid) (fig. 3.22).

In the initial study, the carbonyl peak of creatol was not identified with NMR as the difference between the preparation of solution (containing 50 mM creatinine, 100 mM ferricyanide and 1 M KOH) to the analysis was about 3-4 days. This delay could have resulted in degradation of the reaction product (creatol) at the analysis time. Therefore, the next set of experiments were analysed within a day of preparation of solutions and creatol was identified as one of the products (with detectable C=O group) along with methylguanidine and hydrate (formed from glyoxylic acid) (fig. 3.22 and table 3.5 & 3.6).
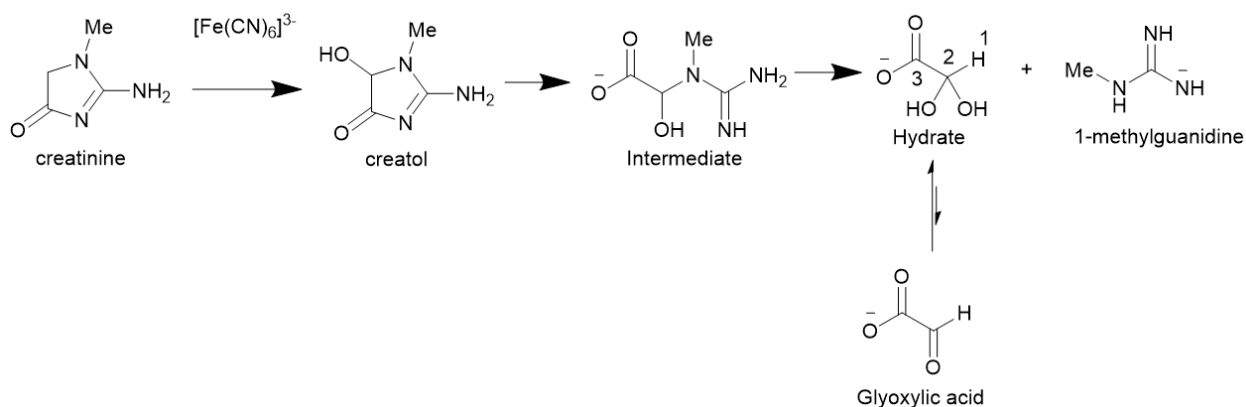
Figure 3.22: Proposed mechanism of creatinine oxidation with ferricyanide forming final detectable products of creatol and methylguanidine using NMR techniques.
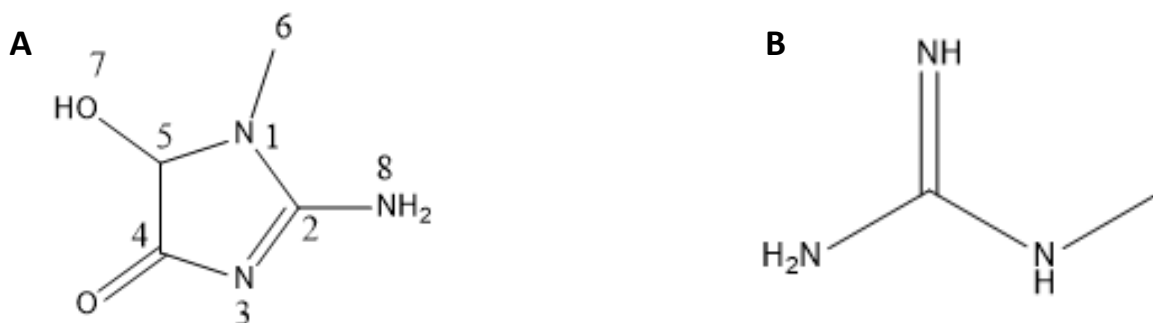
Figure 3.23: A) Creatol B) Methylguanidine

Table 3.5: [1]H and ^{13}C shifts of creatol (A) and methylguanidine (B) in 1 M KOH solution obtained from a combination of 1D ^{1}H and 2D ^{1}H-^{13}C HMBC & HSQC NMR techniques (refer to fig. x).

[1]H chemical shifts [ppm] of hydrogen number for Creatol (A) and Methylguanidine (B)			[13]C chemical shifts [ppm] of carbon number for Creatol (A) and Methylguanidine (B)					
Creatol (A)		**Methylguanidine (B)**	**Creatol (A)**				**Methylguanidine (B)**	
5	6	CH$_3$	2	4	5	6	CH$_3$	CN
5.09	2.93	2.76	167.8	193	88.7	27.8	27.9	159.8

Table 3.6: 1H and 13C shifts of hydrate (formed from glyoxylic acid) in 1 M KOH solution obtained from a combination of 1D 1H and 2D 1H-13C HMBC & HSQC NMR techniques (refer to fig. x).

¹H chemical shifts [ppm] of hydrogen number for Hydrate (formed from glyoxylic acid)	¹³C chemical shifts [ppm] of carbon number for Hydrate (formed from glyoxylic acid)	
1	C-H	C=O
5.16	92.8	181.5

3.4.2   HPLC-ESI-MS study

An ESI-MS study was performed to analyse the reaction products of creatinine oxidation using ferricyanide. Fig. 3.24 shows the ESI mass spectrum of creatinine in deionised (DI) water. It is evident from the mass spectrum that creatinine was successfully detected by the equipment, also seen in the predicted region for 114.0662 m/z according to [M+H]+ calculated for creatinine (fig. 3.25).
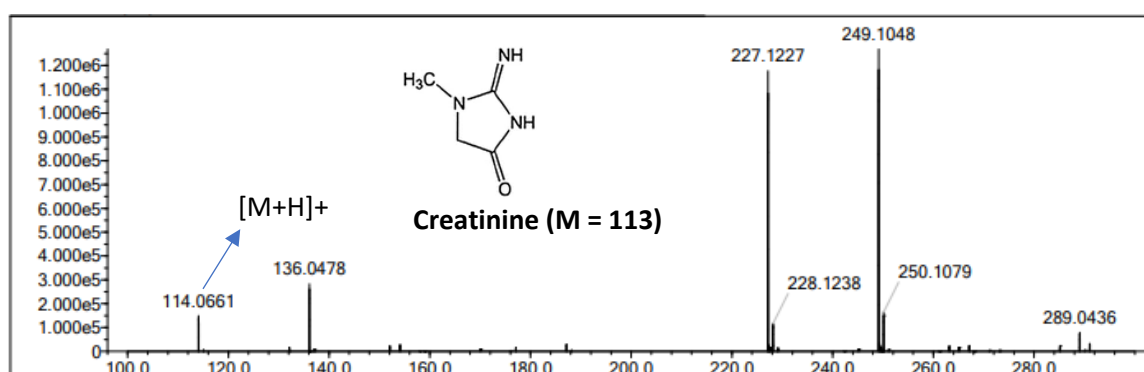
Figure 3.24: Mass spectra of creatinine (M/Z = 113).

C4 H7 N3 O [M+H]+ : Predicted region for 114.0662 m/z

114.0662

115.0683
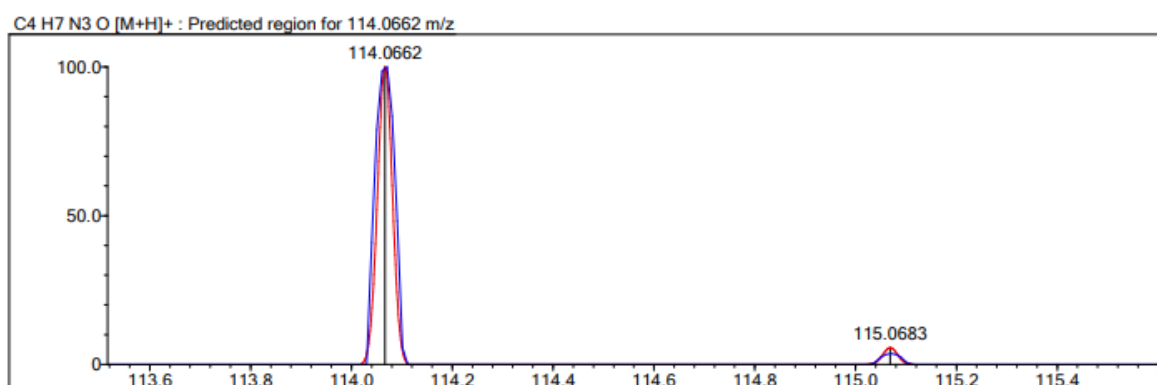
Figure 3.25: [M+H]+ predicted region for creatinine.

A solution comprising 5 mM creatinine, 10 mM ferricyanide and 600 mM KOH was analysed to determine the oxidation reaction products. The mass spectra in the positive and negative mode are shown in fig. 3.26 and 3.27.
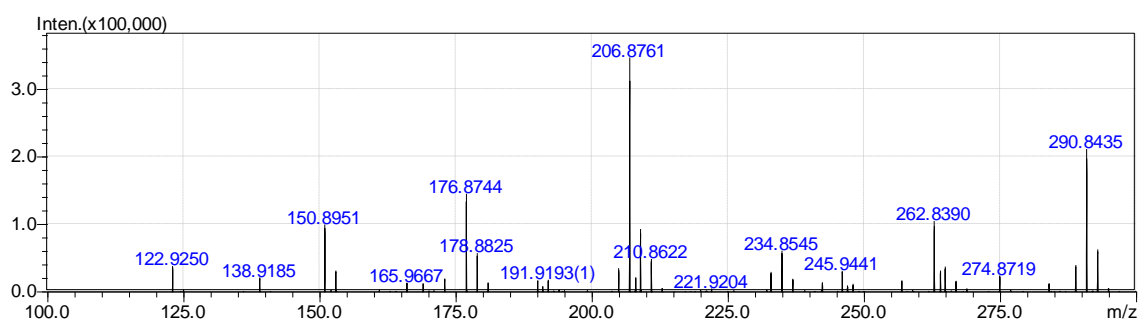
Figure 3.26: Mass spectra [of 5 mM creatinine + 10 mM ferricyanide + 600 mM KOH] with ESI+ (positive mode)
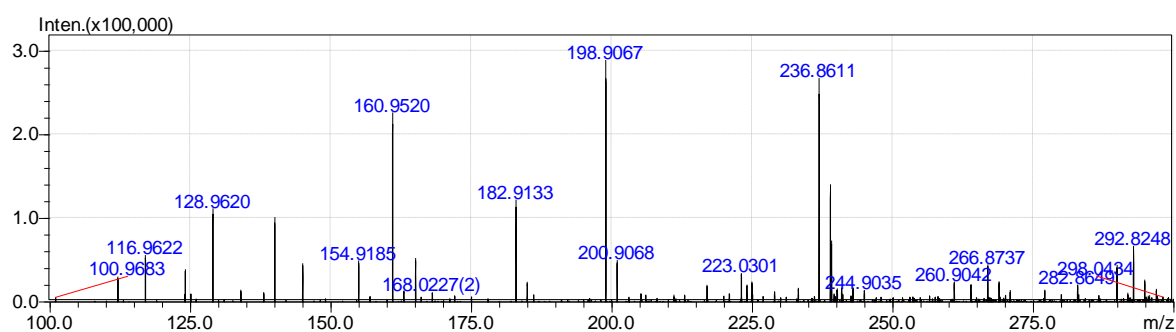
Figure 3.27: Mass spectra [of 5 mM creatinine + 10 mM ferricyanide + 600 mM KOH] with ESI- (negative mode).

Based on the NMR results, which identified methylguanidine and creatol as the reaction products, further analysis using the ESI-MS study didn't give any conclusive results in terms of confirming these reaction products as a result of possibly the molecules being too volatile or not ionising well with the

90

ESI technique. This resulted in low sensitivity of this technique. Different mass adducts (with accurate mass predictions) which should have been identified for creatol and methylguanidine are summarised in table 3.7. It is very clear these adduct fragments are not present in the mass spectra obtained (fig. 3.26 and fig. 3.27).

Table 3.7: Accurate mass predictions for different adducts of creatol and methylguanidine.

Ion (Methylguanidine)	m/z	Ion (Creatol)	m/z
[M+H]+	72.0318	M+	129.0533
[M+K]+	109.9877	[M+H]+	130.0611
[M+Na]+	94.0138	[M+Na]+	152.043
[M+NH4]+	89.0584	[M+K]+	168.017
M+	71.024	[M+NH4]+	147.0877
[M+CH3COO]-	130.0384	M-	129.0544
[M+Cl]-	105.9939	[M-H]-	128.0466
[M+HCOO]-	116.0227	[M+HCOO]-	174.052
[M-H]-	70.0173	[M+CH3COO]-	188.0677
M-	71.0251	[M+Cl]-	164.0232

Therefore, it was understood that ESI-MS was not a sensitive enough technique for determination of the reactions products of creatinine oxidation.

3.4.3 ATR-FTIR

FTIR studies were also performed to confirm the creatinine/ferricyanide reaction products. The cyanide peak (at 2115 cm^{-1}) seen in the solution of ferricyanide and KOH (without creatinine), is not present when creatinine is introduced with the same solution components. Additionally, a different peak at 2037 cm^{-1} is seen, which could be C=O, as the carbonyl functional group identification region in FTIR is between 2000-3000 cm^{-1} [60] (fig. 3.28). It is to be noted that this functional group is present in creatol (fig. 12) (one of the products identified by the NMR study).
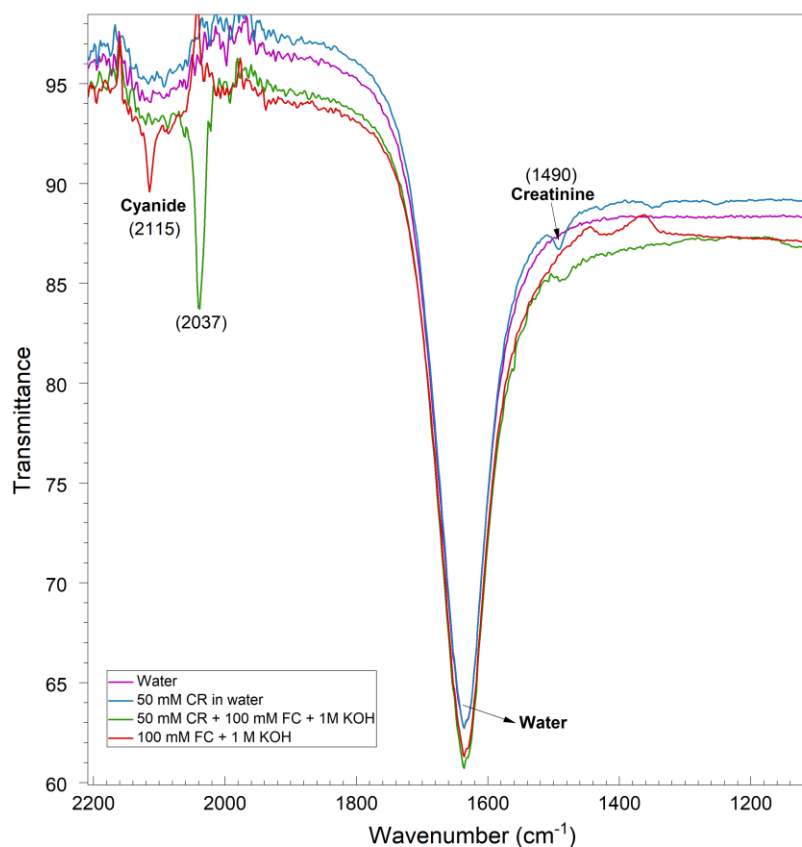
Figure 3.28: ATR-FTIR results for analysis of creatinine oxidation products (FC-ferricyanide, CR-creatinine).

Although, no additional data on functional group identification was seen using this technique, it was concluded that the technique was not sufficiently sensitive in terms of understanding the structures of the reaction products. However, it was evident and understood that ferricyanide participates in the reaction with creatinine in alkaline medium as the cyanide peak is not seen in the spectrum when the reaction solution with creatinine, KOH and ferricyanide was used.

3.5 Conclusions

The sensing ability of bare GCE in 1 mM potassium ferrocyanide and 1 M KOH was examined for non-enzymatic creatinine detection. The fact that a bare GCE could be used to sense creatinine, adds to its advantages of low cost in comparison to a method that would require chemical modification adding to production costs increasing final price of the sensor. It was concluded that creatinine, a complex amine can be oxidised in alkaline solution of 1 M KOH in presence of 1 mM potassium ferrocyanide. Further mechanistic studies are ongoing however, so far it can be understood that ferricyanide could abstract an electron from the nitrogen centres in creatinine molecule (oxidising it to other products)

as similar behaviour has been seen with other amines in the literature. The sensitivity and LOD of the sensor were obtained as 1.50 µA/mM & 60 µM, respectively. Studies with urea (major component of urine) showed no interference in this system. It is understood that this study can be further be optimised using artificial urine samples and could have high potential for incorporation in a sensing device due to its high selectivity, sensitivity, stability and low cost.

3.6 References

1.   H. Krawczyk, *Journal of pharmaceutical and biomedical analysis*, 2009, **49**, 945-949.

2.   R. Cánovas, M. Cuartero and G. A. Crespo, *Biosensors and Bioelectronics*, 2019, **130**, 110-124.

3.   A. J. Killard and M. R. Smyth, *Trends in biotechnology*, 2000, **18**, 433-437.

4.   R. D. Perrone, N. E. Madias and A. S. Levey, *Clinical chemistry*, 1992, **38**, 1933-1953.

5.   M. Jaffé, 1886.

6.   T. Küme, B. Sağlam, C. Ergon and A. R. Sisman, *Journal of clinical laboratory analysis*, 2018, **32**, e22168.

7.   R. R. Kumar, M. O. Shaikh and C.-H. Chuang, *Analytica Chimica Acta*, 2021, **1183**, 338748.

8.   K. L. Schnabl, S. Bagherpoor, P. Diker, C. Cursio, J. DuBois and P. M. Yip, *Clinical biochemistry*, 2010, **43**, 1026-1029.

9.   S. Kalasin, P. Sangnuang, P. Khownarumit, I. M. Tang and W. Surareungchai, *ACS Biomaterials Science & Engineering*, 2020, **6**, 1247-1258.

10.   I. Pandey, P. K. Bairagi and N. Verma, *Sensors and Actuators B: Chemical*, 2018, **277**, 562-570.

11.   M. J. Pedrozo-Penafiel, T. Lopes, L. M. Gutierrez-Beleno, M. E. M. Da Costa, D. G. Larrude and R. Q. Aucelio, *Journal of Electroanalytical Chemistry*, 2020, **878**, 114561.

12.   N. SATO, K. TAKEDA and N. NAKAMURA, *Electrochemistry*, 2021, 21-00016.

13.   X. Gao, R. Gui, H. Guo, Z. Wang and Q. Liu, *Sensors and Actuators B: Chemical*, 2019, **285**, 201-208.

14.   S. Kalasin, P. Sangnuang, P. Khownarumit, I. M. Tang and W. Surareungchai, *ACS Biomaterials Science & Engineering*, 2020, **6**, 5895-5910.

15.   S. Kalasin, P. Sangnuang and W. Surareungchai, *ACS Biomaterials Science & Engineering*, 2020, **7**, 322-334.

16.   S. Boobphahom, N. Ruecha, N. Rodthongkum, O. Chailapakul and V. T. Remcho, *Analytica Chimica Acta*, 2019, **1083**, 110-118.

17.   P. Singh, S. Mandal, D. Roy and N. Chanda, *ACS Biomaterials Science & Engineering*, 2021.

18.   E. L. Fava, T. Martimiano do Prado, T. Almeida Silva, F. Cruz de Moraes, R. Censi Faria and O. Fatibello-Filho, *Electroanalysis*, 2020, **32**, 1075-1083.

19.   E. L. Fava, T. M. do Prado, A. Garcia-Filho, T. A. Silva, F. H. Cincotto, F. C. de Moraes, R. C. Faria and O. Fatibello-Filho, *Talanta*, 2020, **207**, 120277.

20.   V. Kumar, S. Hebbar, R. Kalam, S. Panwar, S. Prasad, S. Srikanta, P. Krishnaswamy and N. Bhat, *IEEE Sensors Journal*, 2017, **18**, 830-836.

21.   R. Sriramprabha, M. Sekar, R. Revathi, C. Viswanathan and J. Wilson, *Analytica Chimica Acta*, 2020, **1137**, 103-114.

22.   K. Carpenter and E. M. Stuve, *Journal of Applied Electrochemistry*, 2021, **51**, 945-957.

23.   K. B. Viswanath, R. Devasenathipathy, S. F. Wang and V. Vasantha, *Electroanalysis*, 2017, **29**, 559-565.

24.   A. Fekry, S. Abdel-Gawad, R. Tammam and M. Zayed, *Measurement*, 2020, **163**, 107958.

25.   C.-H. Chen and M. S. Lin, *Biosensors and Bioelectronics*, 2012, **31**, 90-94.

26.   J. Raveendran, P. Resmi, T. Ramachandran, B. G. Nair and T. S. Babu, *Sensors and Actuators B: Chemical*, 2017, **243**, 589-595.

27.   K. Teekayupak, C. Aumnate, A. Lomae, P. Preechakasedkit, C. S. Henry, O. Chailapakul and N. Ruecha, *Talanta*, 2023, **254**, 124131.

28.   T. Nakaminami, K. Kashiwada and A. Fukunaga, *Journal*, 2010.

29.   F. KAYSER and A. MOLITOR, 1956.

30.   B. Thyagarajan, *Chemical Reviews*, 1958, **58**, 439-460.

31.   C. Audeh and J. L. Smith, *Journal of the Chemical Society B: Physical Organic*, 1970, 1280-1285.

32.   D. G. Lambert and M. M. Jones, *Journal of the American Chemical Society*, 1966, **88**, 4615-4618.

33.   J. R. L. Smith and D. Masheder, *Journal of the Chemical Society, Perkin Transactions 2*, 1976, 47-51.

34.   S. M. Zourab, E. M. Ezzo, H. J. El-Aila and J. K. Salem, *Journal of surfactants and detergents*, 2005, **8**, 83-89.

35.   K. Abbas and D. Marji, *Zeitschrift Für Naturforschung A*, 2005, **60**, 667-671.

36.   M. Masui, H. Sayo and Y. Tsuda, *Journal of the Chemical Society B: Physical Organic*, 1968, 973-976.

37.   Y.-C. Chang, Y.-H. Chu, C.-C. Wang, C.-H. Wang, Y.-L. Tain and H.-W. Yang, *Biosensors*, 2021, **11**, 339.

38.   C. Brett and A. M. O. Brett, *Electroanalysis*, Oxford University Press, 1998.

39.   P. Wilson, S. Sorto and A. K. Apawu, *Chemistry-Methods*, 2022, **2**, e202100049.

40.   M. L. Bishop, *Clinical Chemistry: Principles, Techniques, and Correlations, Enhanced Edition: Principles, Techniques, and Correlations*, Jones & Bartlett Learning, 2020.

41.   M. Artigues, J. Abellà and S. Colominas, *Sensors*, 2017, **17**, 2620.

42.   A. International, *Journal*, 2016.

43.   S. Hooshmand and Z. Es' haghi, *Analytica chimica acta*, 2017, **972**, 28-37.

44.   S. Karahan, B. Afsar and M. Kanbay, *Clinical kidney journal*, 2018, **11**, 530-531.

45. B. Berg, 1986.

46. L. Olansky and L. Kennedy, *Journal*, 2010, **33**, 948-949.

47. L. Heinemann, *Diabetes technology & therapeutics*, 2010, **12**, 847-857.

48. B. M. Katzman, B. R. Kelley, G. R. Deobald, N. K. Myhre, S. A. Agger and B. S. Karon, *Journal of Diabetes Science and Technology*, 2021, **15**, 897-900.

49. S. Vasudevan and I. B. Hirsch, *Diabetes care*, 2014, **37**, e93-e94.

50. A. Srivastava, A. D. Kaze, C. J. McMullan, T. Isakova and S. S. Waikar, *American Journal of Kidney Diseases*, 2018, **71**, 362-370.

51. NHS North Bristol NHS Trust, https://www.nbt.nhs.uk/severn-pathology/requesting/test-information/urate#:~:text=Reference%20range%3A%201.5%20%2D%204.5%20mmol%2F24hr., (accessed March 23 2023).

52. S. L. Cowart and M. E. Stachura, *Clinical Methods: The History, Physical, and Laboratory Examinations. 3rd edition*, 1990.

53. H. Silverman and I. Gubernick, *J. biol. Chem*, 1947, **167**, 363.

54. R. Duan, J. Jiang, S. Liu, J. Yang, J. Zhu, M. Qiao, J. Yan and X. Hu, *Instrumentation Science & Technology*, 2017, **45**, 312-323.

55. L. Xiang, H. Ping, L. Zhao, Z. Ma and L. Pan, 2010.

56. N. SATO, K. TAKEDA and N. NAKAMURA, *Electrochemistry*, 2021, **89**, 313-316.

57. T. Öman, M.-B. Tessem, T. F. Bathen, H. Bertilsson, A. Angelsen, M. Hedenström and T. Andreassen, *BMC bioinformatics*, 2014, **15**, 1-8.

58. S. Nagase, K. Aoyagi, M. Narita and S. Tojo, *Nephron*, 1986, **44**, 299-303.

59. H. Krawczyk, A. Pietras and A. Kraska, *Spectrochimica Acta Part A: Molecular and Biomolecular Spectroscopy*, 2007, **66**, 9-16.

60. I. Fleming and D. H. Williams, *Spectroscopic methods in organic chemistry*, Springer, 1966.

Chapter 4 - Creatinine detection on nickel-based electrodes

4.1 Introduction

Since the early works of Fleischmann et al. [1], electrocatalytic oxidation of small organic compounds at nickel electrodes has been explored in a number of studies [2-6]. It is well known that nickel shows excellent electrocatalytic activity in alkaline medium [7]. In aerated alkaline solution, a nickel hydroxide layer forms on the surface of the electrode as a result of the reaction with dissolved oxygen. It has been observed that this nickel hydroxide layer, reversibly oxidises to nickel oxyhydroxide (NiOOH) at potentials around 0.4 V vs Ag/AgCl [7]. The NiOOH is catalytically active and irreversibly oxidises small organic molecules seen in the technique of cyclic voltammetry (CV). This can be used as a quantitative system to determine concentration of analytes. Nowadays, various low-cost nickel-based electrodes have been explored for non-enzymatic sensing of small organic compounds including glucose [8-12], alcohols[13-15] and formaldehyde [16-19].

Despite the use of metal modified electrodes for creatinine analysis, there is only one report of a nickel-based electrode (nickel/iron foam sensor) for simultaneous detection of creatinine and urea in alkaline medium (pH 14). It was observed that creatinine and urea co-oxidise on the surface of the nickel/iron foam system, due to concurrent reactions of these analytes in alkaline solution. Creatinine effectively forms a strong inner sphere complex with nickel electrode at pH 14. Although, in presence of urea, creatinine binds preferentially to the WE and decreases the overall current density. However, using 1 mol% Fe based nickel foam electrodes allowed co-oxidation of creatinine and urea on WE. Increased currents upto 50 mA is observed in case of using the Fe-Ni foam electrodes [20]. It is understood that creatininase (the enzyme that catalyses the hydrolysis of creatinine) has two zinc(II) active sites and that the enzyme activity increases when the metal centers are replaced in the order Mn(II) > Co(II) > Mg(II) > Fe(II) > Ni(II) = Zn(II) [21]. There is a significant need for development of low cost and simple creatinine sensor platforms with improved performance.

This chapter investigates the nickel system with creatinine, based on the fact that creatinine (also a small organic molecule) could potentially be oxidised at the surface of a Ni-based glassy carbon electrode (Ni-GCE). This is the first report of using a nickel modified GCE for creatinine detection.

Techniques of voltammetry and chronoamperometry are used to develop the quantitative sensor system. Building on the work in the previous chapter the Ni-GCE is also studied in the presence of ferrocyanide, to understand if the product of creatinine oxidation by ferricyanide is electroactively oxidised by NiOOH (fig. 4.1). Furthermore, the chapter explores the interfering response of the nickel electrode to urea.
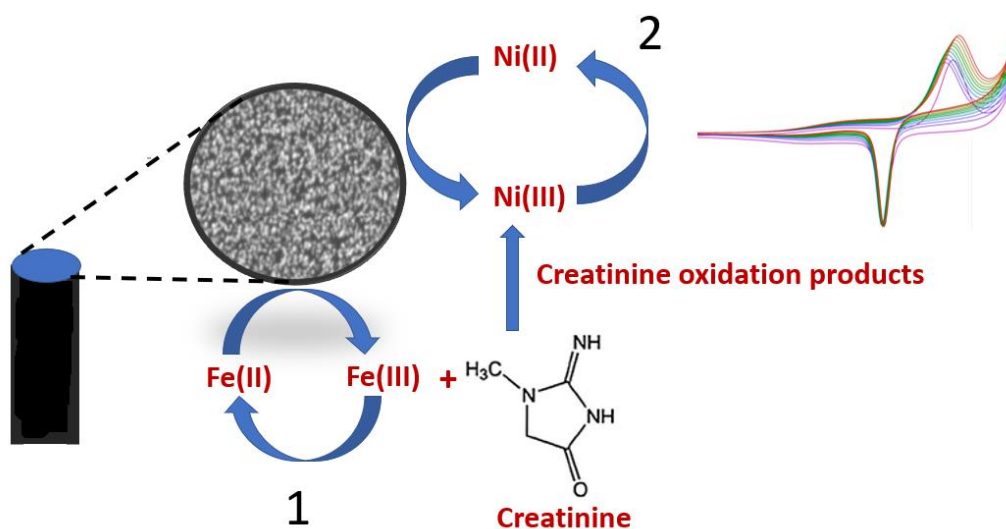
Figure 4.1: Electrochemical detection of creatinine using nickel based GCE system.

4.2 Experimental

4.2.1 Chemicals

Potassium hydroxide (Fisher Scientific), potassium ferricyanide, 99+%, potassium ferrocyanide trihydrate, 99+%, for analysis (Acros Organics), creatinine anhydrous, ≥98%, Poly(vinyl alcohol) Mw 89,000-98,000, 99+% hydrolyzed (Sigma-Aldrich) was purchased and used without further purification. Urea (99.0 – 100.5%) was purchased from Sigma Aldrich.

4.2.2 Apparatus

An Ivium EmSTAT 3+ was the potentiostat used in conjunction with the software (PSTrace) and a laptop computer to control the potentiostat. The CE was the carbon rod, RE was the Ag/AgCl in 3M NaCl and Hg/HgO in 1 M KOH, the WE was the glassy carbon electrode (GCE, diameter 3 mm, 0.07 cm^2); all supplied by IJ Cambria Scientific Ltd.

4.2.3 Morphology analysis

Scanning Electron Microscopy (SEM) were obtained on JEOL JSM-7800F SEM Microscope. Nickel deposited GCE was analysed by SEM using JEOL JSM-7800F SEM microscope. The conditions for surface analysis were 5 kV acceleration voltage, WD 10 mm and magnification of x 50,000.

4.2.4 Electrochemical cell setup

The electrochemical experiments were carried out in a three-compartment cell including the WE, RE and CE. The RE against which all the potentials were measured was a Ag/AgCl electrode immersed in 3 M NaCl. Some experiments were also performed with Hg/HgO RE immersed in 1 M KOH. The CE was a carbon electrode and WE a glassy carbon electrode (GCE). In some experiments potassium chloride was added to maintain constant ionic strength at varying pH of KOH solutions. All measurements were made at room temperature.

The electrocatalytic behaviour of creatinine oxidation on Ni electrode in alkaline medium was investigated using cyclic voltammetry (CV) and chronoamperometry. The creatinine oxidation current may show dependence on the concentration of creatinine and KOH. During voltammetry, for each experiment the working potential was chosen such that no electrolyte or solvent decomposition occurred.

4.2.5 Ni-GCE preparation

A GCE (3 mm diameter, 0.07 cm^2) was polished with diamond (3F μm, Buehler) and alumina (0.05 μm, Buehler) solutions, followed by cleaning in an ultrasonicator for 5 mins where the electrode was immersed in ethanol/water solution after which the electrode was rinsed thoroughly with deionised water.

Nickel was deposited on the GCE by cathodic reduction of a degassed 1 mM $Ni(NO_3)_2$ solution in 0.1M acetate buffer solution (pH 5) as was previously optimised in a study [22]. The GCE was held at -1.3 V vs Ag/AgCl for varying electrodeposition times (30s, 60s and 120s) under constant stirring.

4.2.6 Electrode conditioning

Following the electrodeposition, the modified electrode was transferred to a non-degassed potassium hydroxide solution in order to form the $Ni(OH)_2$ layer on GCE. CVs were performed in the potential window of 0.15 to 0.55 V vs Ag/AgCl, at 200 mV/s scan rate for 200 cycles, with a starting potential of 0.15 V vs Ag/AgCl.

4.2.7 Electrochemical detection of creatinine on Ni-GCE

Techniques used for electrochemical detection of creatinine were cyclic voltammetry (CV) and chronoamperometry (CA). 10 ml of 1 M KOH was transferred to the electrochemical cell and placed with Ni-GCE and the Ag/AgCl RE (or Hg/HgO RE) and the graphite CE, connected to the potentiostat. Blank and creatinine addition CV studies were done in a potential window of 0.15 to 0.55 V vs Ag/AgCl, at a scan rate of 50 mV/s and the first scan was considered for analysis, with a starting potential of 0.15 V vs Ag/AgCl.

The chronoamperometry study was performed by selecting a fixed potential (E_{dc}) based on the CV with creatinine additions. Creatinine additions was made to a stirred solution of potassium hydroxide or alkaline ferrocyanide at the specific linear range. A current vs time plot was generated.

4.3 Results and Discussion

4.3.1 Electrodeposition of Ni on GCE

Electrodeposition involves preferential nucleation and growth of the metal nanoparticles (NPs) on the surface of the electrode. It gives high purity of deposits and involves a simple procedure [23]. Potentiostatic deposition was used to prepare the metallic Ni deposited GCE. The electrodeposition of nickel onto the GCE was done using chronoamperometry at -1.3 V vs Ag/AgCl for 120s electrodeposition time (which was selected on optimisation seen later in the chapter).

Chronoamperometry involving instantaneous perturbation of the electrode potential is used in this study (fig. 4.2). The system is then monitored as it follows towards its new steady state. The solution was deoxygenated prior to chronoamperometry, so as to ensure there are no other competing electron transfer reactions at the surface (such as oxygen reduction). The solubility of oxygen in solutions which are open to the atmosphere is up to 10^{-4} M, therefore in order to reduce the oxygen partial pressure to a very low value, nitrogen is passed through the solution [24]. It was also necessary to avoid formation of bubbles near the GCE surface (due to water reduction) in order to obtain a smooth deposition of nickel on GCE.
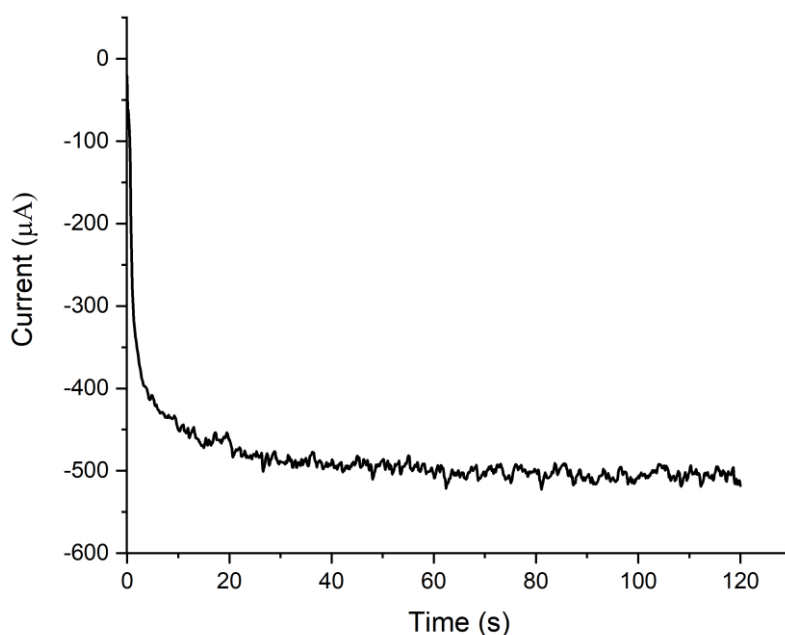
Figure 4.2: Electrodeposition of Ni on GCE using chronoamperometry fixed at -1.3 V vs Ag/AgCl for 120s.

This process involved formation of a new nickel metal phase on the surface of the GCE through reduction of Ni^{2+} ions from the 1 mM $Ni(NO_3)_2$ solution dissolved in sodium acetate buffer (pH 5) [22]. The formation of the metal layer involved several stages [25]:

1. Nucleation & growth of the isolated centres
2. Continuous layer formation by overlapping of these isolated centres
3. Thickening of the layer

The first step is the formation of nuclei of the nickel metal phase on the GCE causing a sudden increase of current after t=0 at constant potential after which it fluctuates between 25 to 120s. This requires a large cathodic overpotential (in this case -1.3 V vs Ag/AgCl). Once the nuclei centres formed are big enough and stable, they grow rapidly as a result of constant application of the overpotential. The nickel nuclei once formed grow readily on the surface of the GCE, as a result of overlapping of the formed nuclei as they grow. Once the continuous layer of nickel metal forms, the current is constant at constant potential as the current flowing reaches a mass transport limited plateau value with an increased magnitude as the solution is stirred.

The solution was constantly stirred. As a result of constant stirring, a thin diffusion layer where the concentration of Ni^{2+} is different from that in the bulk of the solution forms. It takes approximately 10 s for this boundary layer to form at the time at which there is a high increase in cathodic current before it reaches a steady state value. During the experiment, at t=0, the potential is stepped to -1.3V vs Ag/AgCl from a point when the surface concentration of Ni^{2+} changes instantaneously from the bulk concentration to zero. At -1.3 V vs Ag/AgCl, the reduction of Ni^{2+} ions occur in the system, allowing deposition of Ni metal on the surface of the GCE. Following this, the current reaches a steady state value when the concentration profile forms. As a result of forced convection (constant stirring), the concentration profile remains steep and the diffusion layer remains thin.

4.3.2 Ni(OH)$_2$ layer enrichment
It has been observed that when nickel is immersed in alkaline solutions, a Ni(OH)$_2$ film is formed after the spontaneous dissolution of the metal [26, 27].
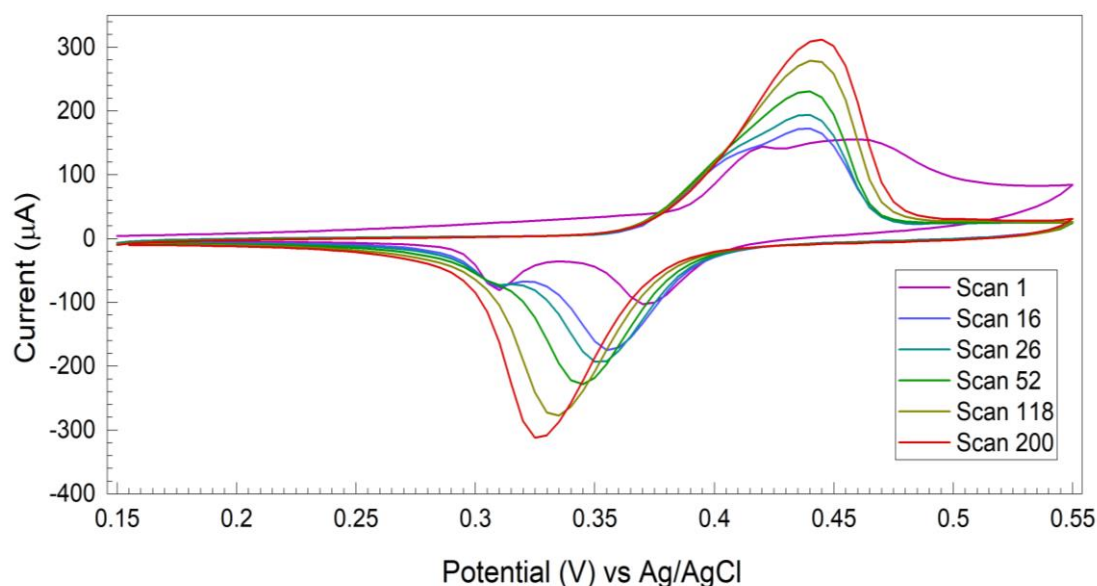
Figure 4.3: First CVs and last CV (scan 200) overlay for a 120s Ni-GCE in 1M KOH at a scan rate of 0.2V/s.

A typical cyclic voltammogram is seen when Ni-GCE is placed in KOH solution due to formation of Ni(OH)$_2$ species as shown by other studies (fig. 4.3) [1, 27, 28]. The first CV differs from the successive voltammetry scans. The current of the first cycle is related to the oxidation of Ni to Ni(II) followed by formation of α -Ni(OH)$_2$ which is converted to the more stable ß- Ni(OH)$_2$ [29] Two oxidation peaks seen in scan 1 in fig. 3 with the sample cell containing 1M KOH, correspond to the α -Ni(OH)$_2$ and ß- Ni(OH)$_2$, respectively oxidising to NiOOH [30, 31]. ß- Ni(OH)$_2$ (more stable form) is favoured in the voltammetry performed in 1M KOH [22]. Therefore, conditioning allows the crystalline phases of Ni(OH)$_2$ to settle to

aged ß-phase as the two oxidation peaks merge and there is a significant increase in the redox currents [15, 32].

Studies have shown that deposition from aqueous nickel nitrate solution, causes nickel hydroxide to precipitate along with the nickel on the surface of electrodes [33, 34]. The following Equations describe this:

$$NO_3^- + 7H_2O + 8e^- \rightarrow NH_4^+ + 10OH^- \qquad \text{(Equation 4.1)}$$

$$Ni^{2+} + 2OH^- \rightarrow Ni(OH)_2 \qquad \text{(Equation 4.2)}$$
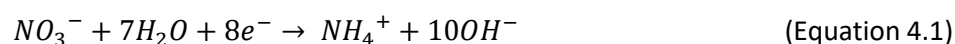
Electroreduction of NO_3^- causes the formation of $Ni(OH)_2$ (equation 1 & 2).

Two crystallographic species of Ni(OH)$_2$ (α & ß) are formed after electrodeposition from nickel nitrate solution and conditioning cycles in 1M KOH. α -Ni(OH)$_2$ is hydrated and ß- Ni(OH)$_2$ is anhydrous and more stable than the other form. As seen in scan 1 (fig. 4.3), Ni(OH)$_2$ is oxidised to NiOOH species upon application of the potential and the oxidation peak shoulder is due to the oxidation of α -Ni(OH)$_2$, while the main peak is a result of oxidation of ß- Ni(OH)$_2$. On the reduction in scan 1, 2 peaks are observed due to reduction of ɣ-NiOOH and ß-NiOOH [35]. On electrooxidation of each type of nickel hydroxide, ɣ-NiOOH and ß-NiOOH are formed, where the ɣ species is relatively unstable. Conditioning cycles on Ni-GCE in strong alkali solution allow ageing of the material. Eventually, the ß phase covers the surface of the GCE as the conditioning progresses as seen in scan 200 in fig. 4.3. The changes in peak position are likely to be due to changes in the crystal structures of nickel hydroxide and the nickel oxyhydroxide [36-38]. The oxygen evolution reaction (OER) occurs (not shown) after 0.55 V vs Ag/AgCl in the positive scan.

4.3.3 Electrochemical studies of creatinine detection

Creatinine additions were made in aerated 1 M KOH solution supporting a GCE working electrode. Nickel reacts with dissolved oxygen in aerated alkaline solution to form Ni(OH)$_2$ which is reversibly oxidised to NiOOH at low potentials of 400 mV vs Ag/AgCl [39]. The main idea with this electrochemistry involves maintaining nickel in the +3 state (NiOOH) on the surface of the electrode that could catalyse the irreversible oxidation of creatinine (seen similar to with other organic compounds like glucose[40-42]), producing an increased anodic current response resulting in a quantifiable system. The chosen potential (based on the linearity seen in the CV with increasing concentration additions) should have a strong catalytic effect on creatinine, minimising any effect on interfering species like urea. The anodic and the cathodic peak in the CV are due to the Ni(II)/Ni(III) redox couple following Equation 3:

$$Ni\,(OH)_2 + OH^- \leftrightarrow NiOOH + e^- \qquad\qquad \text{(Equation 4.3)}$$

In presence of creatinine, it is possible NiOOH compound is reduced and more $Ni\,(OH)_2$ is formed according the Equation 4.4:

$$NiOOH + creatinine \rightarrow\ Ni\,(OH)_2 + oxidation\ products\ of\ creatinine$$
(Equation 4.4)
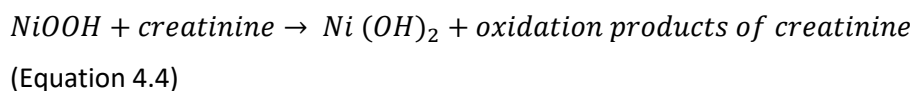
An initial study was done in the creatinine concentration range between 0-50 µM, which showed no significant increase in anodic current response at any positive potentials (fig. 4.4). This could be due to the limited sensitivity of the nickel detection system. Further studies were carried out with creatinine additions in the range 0-400 µM with 50 µM additions in 1M KOH (cycling between 0.15 to 0.55V vs Ag/AgCl) such that the detection is within the clinical range for detection (>150 µM creatinine concentration in blood indicates kidney damage) of chronic kidney disease (CKD) (fig. 4.5). The conditions of the electrolyte (1M KOH) used were similar to a study by Carpenter et al. [20]. The increase in Ni(II)/Ni(III) oxidation peak and its anodic shifting gives a clear indication of creatinine catalytic oxidation on the surface of GCE (fig. 4.5). Although there was anodic current response as a result of creatinine oxidation in the range 0-400 µM, a non-linear calibration was obtained at 0.47 V (fig. 4.6B). Optimisation (in terms of the sensor performance) in the mM range was carried out before the lower linear range could be investigated in further studies.
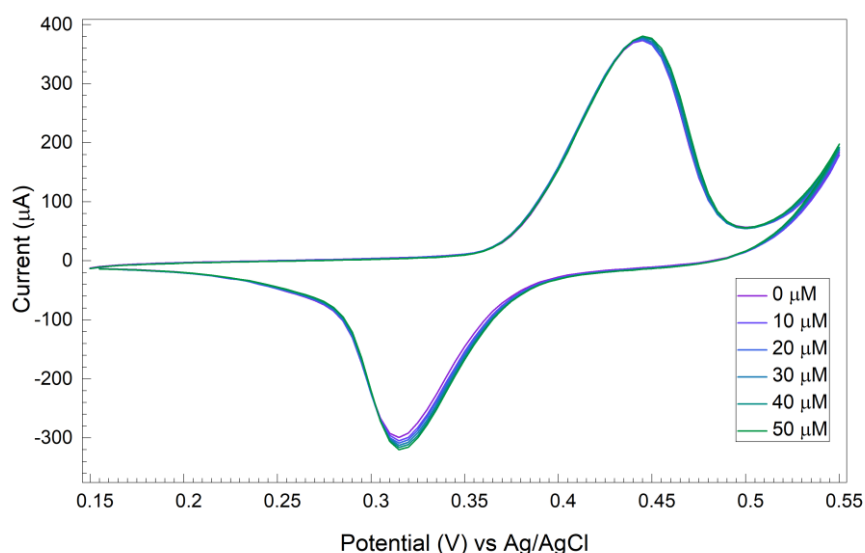
Figure 4.4: Detection of creatinine using Ni-GCE in the 0-50 µM range (cycling between 0.15 to 0.55V in 1M KOH)
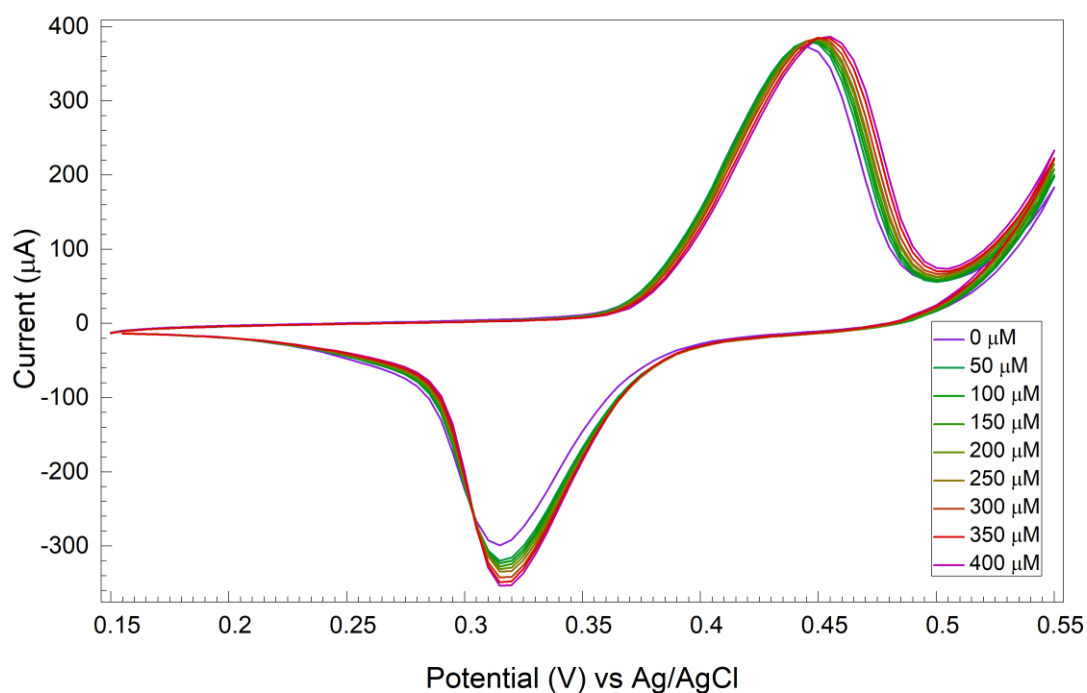
Figure 4.5: Detection of creatinine using Ni-GCE in the 0-400 µM range (cycling between 0.15 to 0.55V in 1M KOH)
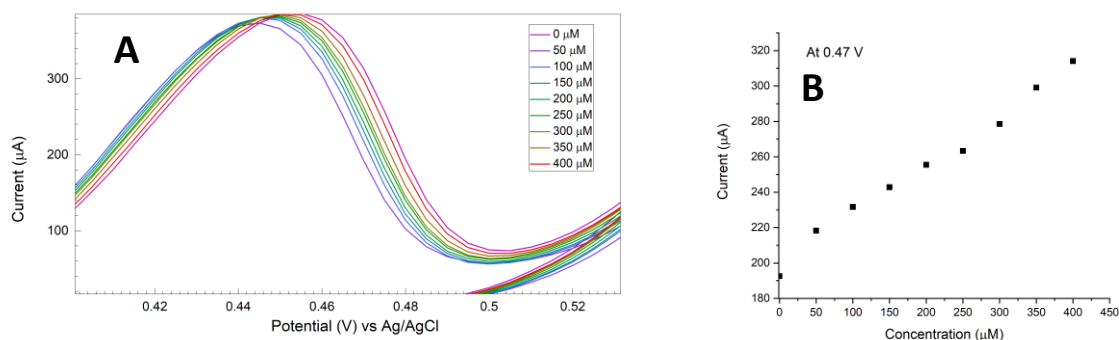
Figure 4.6: A) Inset to fig. 4.5 B) Calibration graph in the range 50 - 400 µM analysed at a fixed potential of 0.47 V vs Ag/AgCl.

4.3.4 Sensor optimisation at higher creatinine concentrations

Creatinine additions between 2-20 mM were done using a Ni-GCE in 1 M KOH solution with a potential for use as a sensor with urine samples (creatinine concentrations outside clinical range of 4.4-13.3 mM indicate kidney conditions as reported[43]). The potential chosen for the calibration graph was that post nickel oxidation (0.44 V vs Ag/AgCl) at which creatinine oxidation is observed with NiOOH on the surface of the GCE. It is understood that creatinine is oxidised on the surface of Ni-GCE and the conversion of NiOOH back to $Ni(OH)_2$ occurs after the oxidation process (fig. 4.7).

105

The peak current increase with concentration was also analysed in the form of a calibration graph (fig. 4.7). Both calibration data showed an increase in current with increasing concentration although the data were not linear.
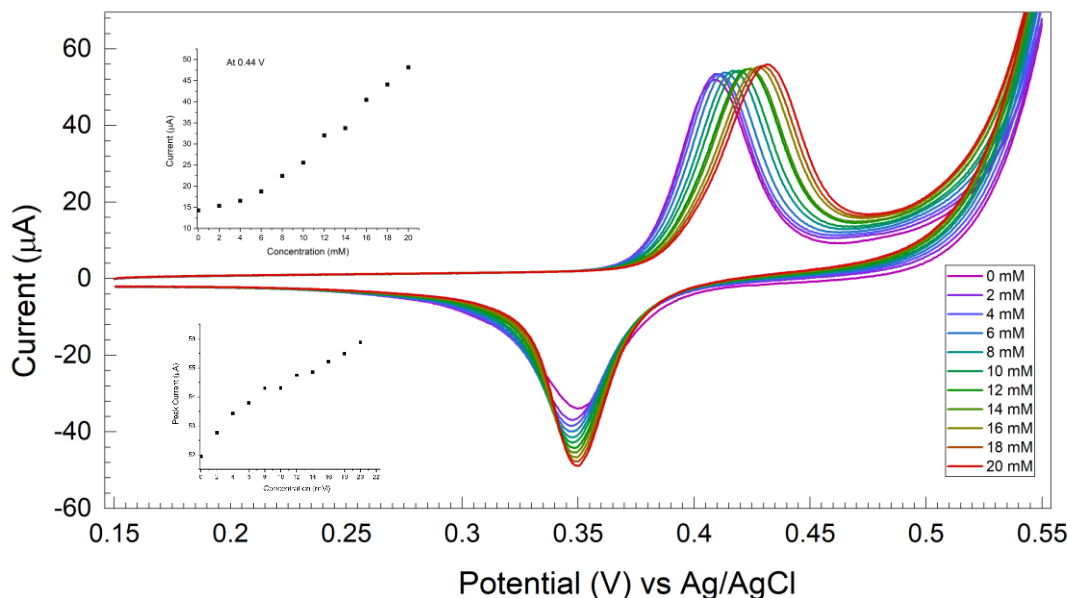
Figure 4.7: Creatinine detection with Ni-GCE in 1M KOH in the range 0-20 mM; scan rate - 50 mV/s

Electrocatalytic performance for achieving a linear sensor calibration with characteristics of high sensitivity and low limit of detection (LOD) is required for an efficient sensing platform. Further sensor optimisation to obtain better electrocatalytic performances of Ni-GCE creatinine sensor was done in terms of the working conditions (KOH concentration and nickel electrodeposition times) for creatinine additions between 2-20 mM.

4.3.4.1 Effect of KOH concentration

The CV studies were done in different KOH concentrations (1M, 0.1M and 0.01M) with creatinine additions in the 2-20 mM range. Conditioning (200 cycles) was performed in 1M KOH solution using cyclic voltammetry to convert the unstable α-Ni(OH)$_2$ (hydrous form) formed during the forward anodic scan from oxidation of Ni into more stable ß-phase (anhydrous) (fig. 4.8). At higher positive potentials, this ß-phase Ni(OH)$_2$ is converted into ß-NiOOH or partially converted into ϒ-NiOOH that accumulates on the surface of the GCE. In the anodic scan, Ni(II) oxidises into the Ni(III) form and in the cathodic scan, Ni(III) reduces back into the Ni(II) form. Studies have shown that this reaction is either quasi-reversible or irreversible on electrodes where nickel has been electro-deposited based

106

on the potential peak separation [4]. In this study, we can see that the redox couple Ni(II)/Ni(III) exhibits quasi-reversible behaviour with peak potential separation approximately 125 mV (for reversible systems it is 56.6/n mV) in scan 200. Additionally, the forward peak is larger than the reverse peak showing the quasi-reversible behaviour. It can also be observed from fig. 4.8 that the current at the anodic and cathodic peaks increases with each potential sweep cycle. During this process, OH^- enters into the $Ni(OH)_2$ layer, forming a thicker NiOOH layer each time during the Ni(II)/Ni(III) redox conversion. This phenomenon has also been observed in a similar study [4].
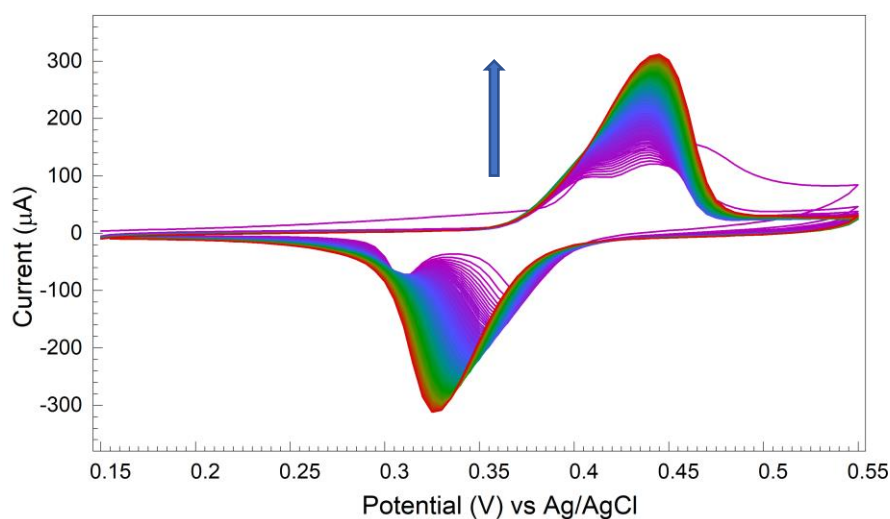
Figure 4.8: Conditioning cycles using cyclic voltammetry (200 cycles) in 1M KOH using Ni-GCE showing growth of $Ni(OH)_2$ layer with each CV scan.

Different concentrations of KOH solutions were prepared such that the ionic strength was maintained to 1 M by addition of KCl. The supporting electrolyte concentration is key in lowering the cell resistance and the ohmic potential drop (which gives potential-control error). In addition, it also decreases the electric field and minimises migration effect on the analyte. This is important as the equations used to determine limiting or peak currents are assumed to be based on the fact that mass transport is only by diffusion processes[44].
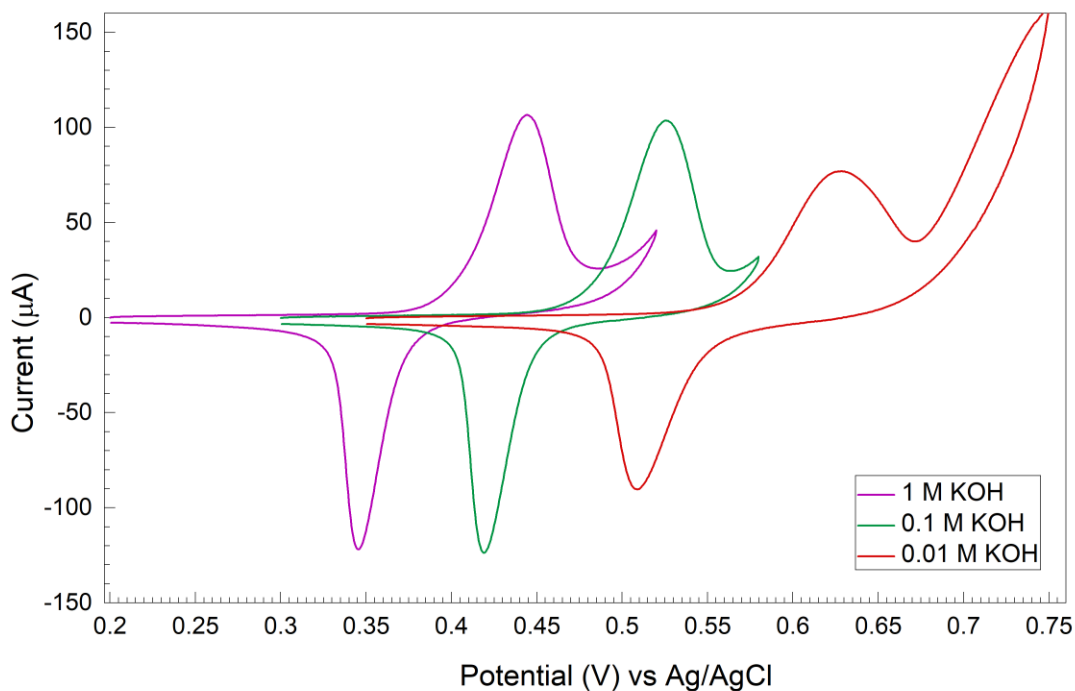
Figure 4.9: Overlay of CVs for 120s Ni deposition in 1 M, 0.1 M and 0.01 M KOH at 10 mM creatinine.

The effect of different KOH concentrations on creatinine oxidation at the Ni-GCE is presented (fig. 4.9). It has been seen previously that the OH^- ion in a nickel electrode system participates in the oxidation of molecules like methanol [45], meaning it enhances the analyte oxidation. A higher concentration of hydroxide ions in 1 M KOH, could further enhance the creatinine oxidation allowing oxidation at a lower onset potential in comparison to that seen at 0.1 M and 0.01 M KOH concentrations. The enhancement of the oxidation could be due to formation of a thicker NiOOH layer on the surface of the GCE, due to diffusion of higher concentration of OH- ions on the surface of $Ni(OH)_2$/GCE [4].

4.3.4.1.1 Studies using 1M KOH

Various repeat studies were performed using 1 M KOH as the base electrolyte. The pH of the solution was confirmed to be 14. The resulting CV in 1 M KOH for 2-20 mM creatinine additions is shown in fig. 4.10. At potentials higher than 0.52 V vs Ag/AgCl, oxygen evolution reaction is observed. The reverse scan involves conversion of NiOOH back to $Ni(OH)_2$, referred to as the Ni(III) reduction peak. This occurs after creatinine is oxidised with NiOOH on the surface of the nickel GCE.

The electrocatalytic response towards creatinine is evident in the forward scan with the shifting of the anodic peak and an increasing anodic current response. Due to the shifting peaks, a fixed potential of 0.46 V vs Ag/AgCl was chosen for chronoamperometry analysis based on procedures described in the literature [15, 18, 22].

Figure 4.10: 0-20 mM additions of creatinine to 1M KOH solution at a scan rate of 50 mV/s cycling between 0.15 and 0.55V vs Ag/AgCl.

Figure 4.11: A) Chronoamperometry at 0.46 V with 2 mM standard additions of creatinine under constant stirring in 1M KOH B) Corresponding calibration plot.

A holding potential of 0.46 V vs Ag/AgCl was chosen for chronoamperometry based on the linear region in the cyclic voltammogram seen in fig. 4.11. This method was used as a result of shifting anodic peak. A calibration plot was then obtained over a linear range. At intervals of 1 minute, under constant stirring, 2 mM additions of creatinine were made to the electrochemical cell containing 1M KOH. Based on the average current of the time interval of each addition, a calibration plot was made (fig. 4.11B). The calibration plot shows a linear response between 4-20 mM creatinine of R^2 = 0.996 with a sensitivity of 0.02 µA/mM. The systematic noise is due to action of the stirring bar, but has been averaged out for the purpose of the calibration plot.

Further repeats of the 2-20 mM creatinine additions (chronoamperometry at a fixed potential of 0.46 V vs Ag/AgCl) were done in 1 M KOH to analyse the reproducibility of the sensor response (fig. 4.12).
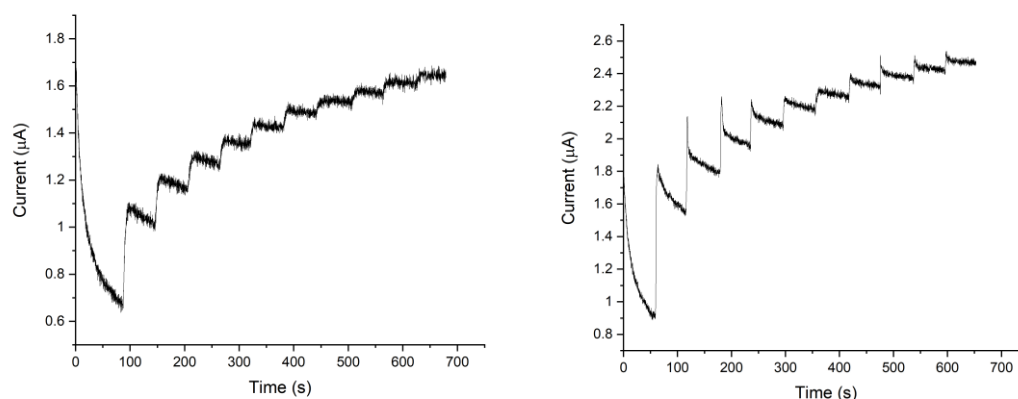
Figure 4.12: Chronoamperometry at 0.46 V vs Ag/AgCl with 2 mM standard additions of creatinine under constant stirring in 1M KOH.

It was seen that the repeat chronoamperometry response was not linear and plateaued at creatinine concentrations higher than 20 mM (fig. 4.12). This inconsistent response was frustrating as it could not be improved. Many attempts were made to use different fixed potentials and to adjust the manner in which additions were made. We also noted that the current response at the fixed potential was quite variable, giving a different range.

4.3.4.1.2 Studies using 0.1M KOH

Creatinine additions in the range 2-20 mM were made in 0.1M KOH in the electrochemical cell at a scan rate of 50 mV/s cycling between 0.3 to 0.62 V vs Ag/AgCl. Selecting a potential of 0.50 V vs Ag/AgCl from the CV (linear region), chronoamperometry was performed with 2 mM additions. The fixed potential for chronoamperometry chosen included 0.49 V, 0.50 V and 0.51 V vs Ag/AgCl, all of which gave no stepwise response showing inconsistency and low sensitivity (not shown). The chronoamperometric response fixed at 0 .50 V vs Ag/AgCl is shown below in fig. 4.14. It can be seen that there were no distinct steps (showing low sensitivity for creatinine) and additional noise which might be due to the stirring effects. The CV shows that the anodic peak current decreases as the concentration of creatinine increases (fig. 4.13).
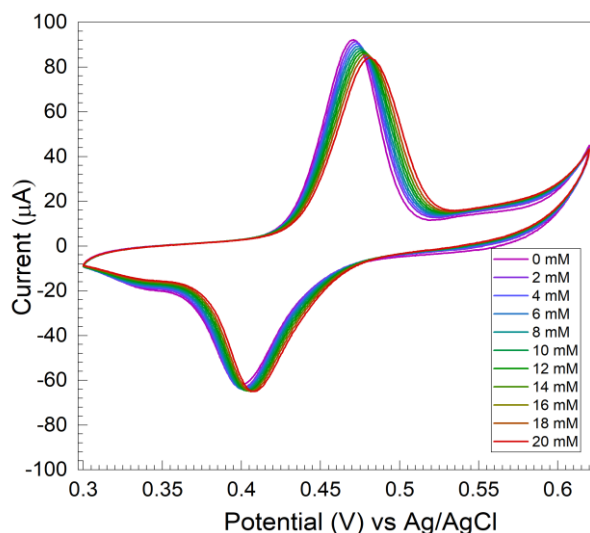
Figure 4.13: 0-20 mM additions of creatinine to 0.1M KOH solution at a scan rate of 50 mV/s cycling between 0.3 and 0.62V vs Ag/AgCl.
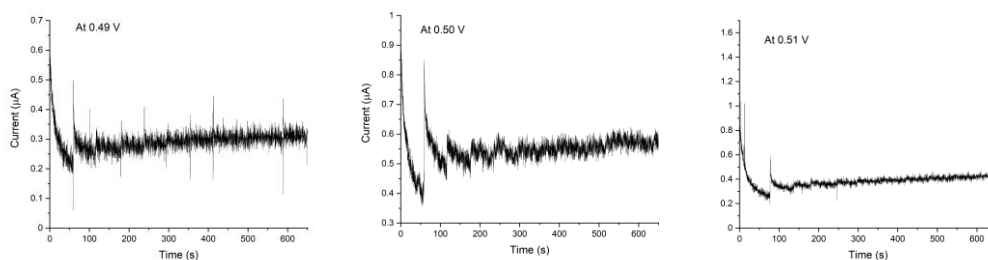
Figure 4.14: Chronoamperometry with 2 mM standard additions of creatinine under constant stirring in 0.1M KOH.

Various repeat studies were performed in 0.1 M KOH. The system showed low sensitivity and no stepwise response to creatinine was observed (fig. 4.14).

4.3.4.1.3 Studies using 0.01M KOH

2 mM creatinine additions were made in the range 2-20 mM in 0.01M KOH solution in the electrochemical cell to obtain CVs as shown in fig. 12. A similar mechanism is observed in the CV in a Ni-GCE system with 0.01 M KOH. As the creatinine concentration increases, the anodic peak current decreases (fig. 4.15).

From this CV, a fixed potential of 0.74 V vs Ag/AgCl was chosen for chronoamperometry analysis. Similar to the results obtained for 0.1 M KOH, the sensitivity of the response was low as no distinct steps at each concentration were observed (fig. 4.16).
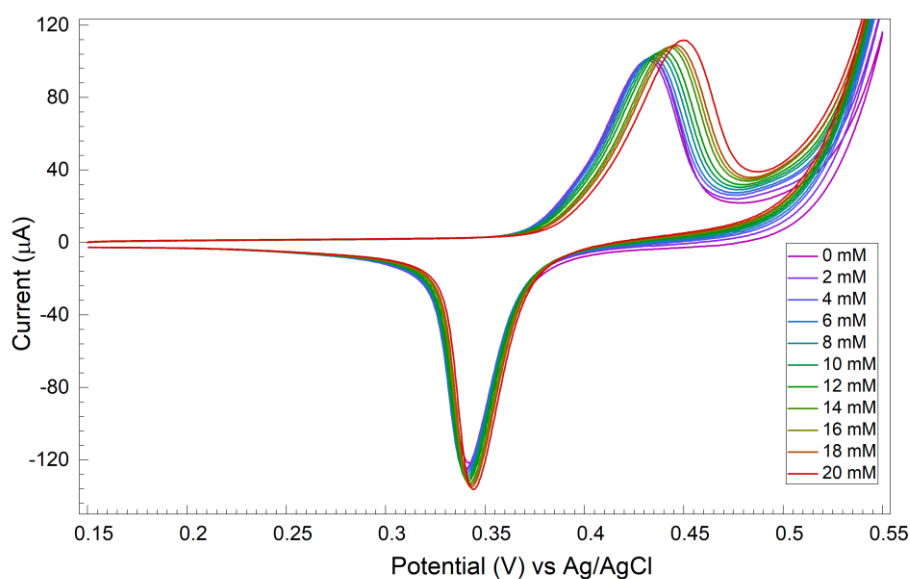
111
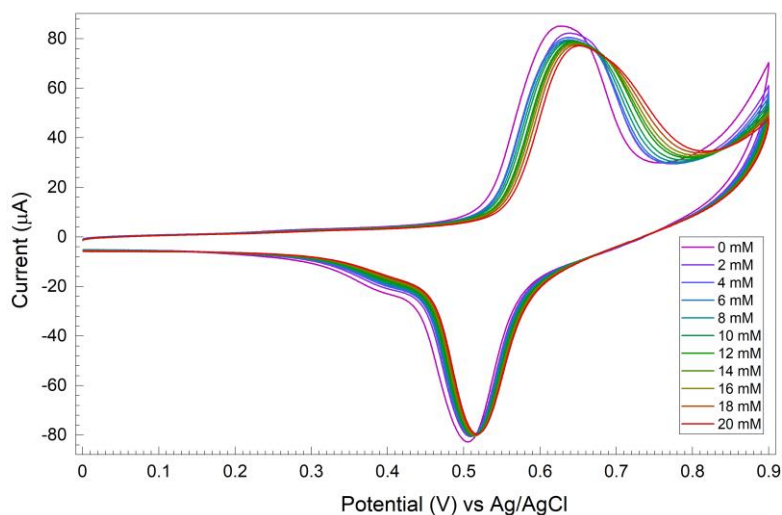
Figure 4.15: 2-20 mM additions of creatinine to 0.01M KOH solution at a scan rate of 50 mV/s cycling between 0 and 0.9V vs Ag/AgCl.
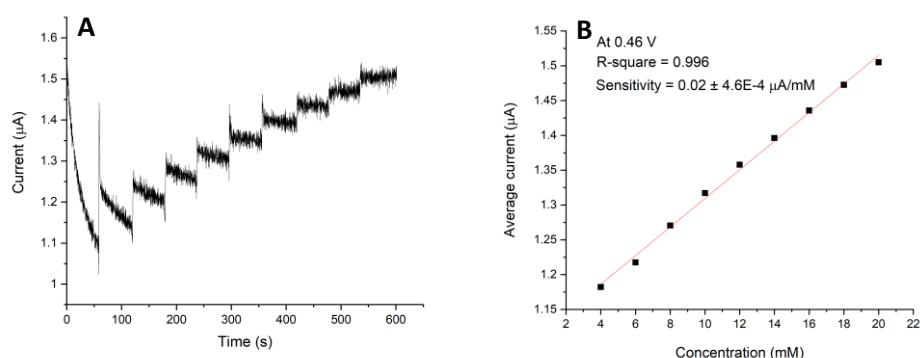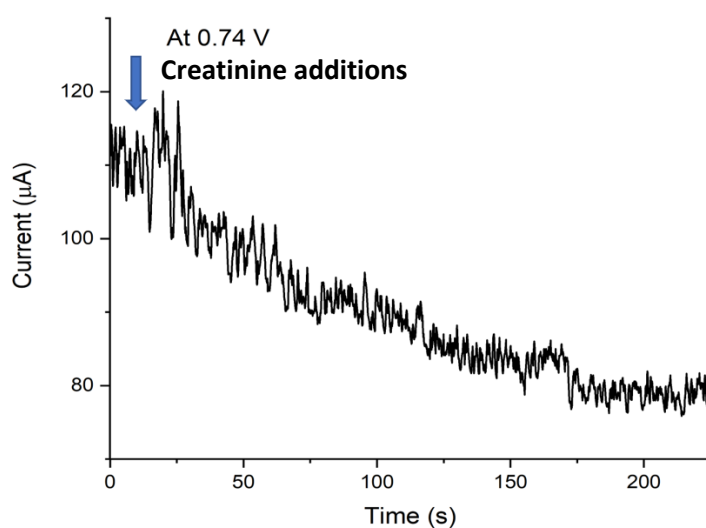

Figure 4.16: Chronoamperometry at 0.74 V vs Ag/AgCl with 2 mM standard additions of creatinine under constant stirring in 0.01M KOH

In conclusion, it can be seen that electrochemical experiments performed in 1 M KOH solution show maximum sensitivity of 0.02 µA/mM (calculated from calibration graph based on step response) relative to 0.1 M and 0.01 M KOH. It can also be understood that as the concentration of hydroxide ion decreases, the peak current decreases with creatinine additions as less NiOOH is present on the surface of GCE to oxidise creatinine. However, an opposite trend is seen with 1M KOH where the peak current increases due to sufficient NiOOH available for oxidation of creatinine.

4.3.5 Effect of Nickel electrodeposition time

Changing the electrodeposition time has a significant effect on the morphology of the composite material on the surface of GCE. Studies have shown that in order to enhance the electroactivity of the catalysts (like nickel acting as an electrocatalyst), small or nano-sized particles can be deposited on the surface of substrates like carbon or graphite [40]. The current density has been observed to be significantly high in case of dispersed Ni on electrode substrates like graphite due to large surface area [4]. In contrast, various studies have also shown that smooth nickel surface inhibits the electro-oxidation reaction due to adsorption of oxygen from the solution and is therefore not an efficient catalyst [4, 46]. In order to study the influence of the Ni-NPs on the GCE, deposition parameters like deposition time was varied to see the effect on the response current [23]. Previous study on Ni NPs has shown that 50s and 150s gave maximum response values. Hence, based on this, the electrodeposition time was varied from 30s to 240s and the sensitivity towards creatinine was compared. It has also been observed that a deposition time of 300s or more resulted in a thick nickel film on GCE[18].

The electrocatalytic activity towards creatinine oxidation of NiNPs-GCE was investigated at different electrodeposition times with CV study (fig. 4.17). According to the CVs, the anodic current at 10 mM creatinine addition varies significantly at Ni-GCEs electrodeposited at times between 30-240s. The anodic current response increases significantly up to 120s deposition times and then decreases at 240s. This could be due to the larger surface area of the Ni-NPs (at 120s) in comparison to the nickel film based GCE formed when the electrodeposition times are 240s and possibly higher. This effect of electrodeposition time has also been observed in another study [42]. In order to have higher sensor sensitivity, 120s was chosen as the optimised time for nickel deposition for further studies.
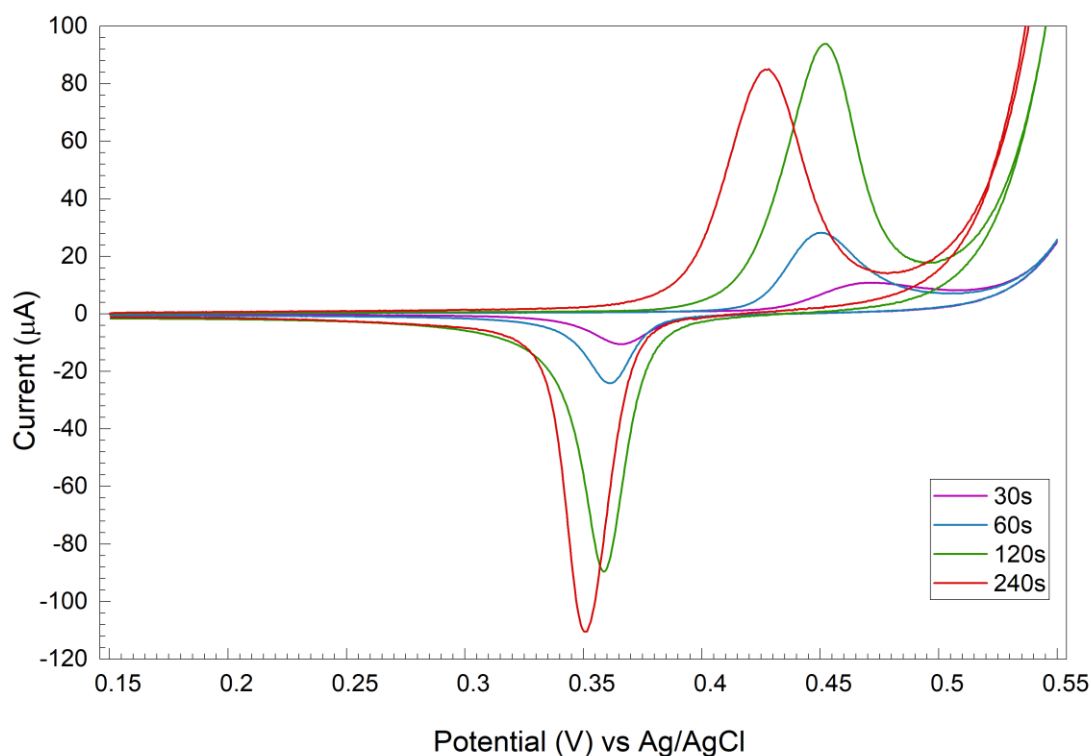
Figure 4.17: CV study of different nickel electrodeposition times with 10 mM creatinine in 1 M KOH solution.

Following electrodeposition at increasing times (30 s, 60 s & 120 s) of Ni on GCE, the electrode was cycled in 1 M KOH for 200 cycles at 0.2 V/s in order to fully develop the beta phase of the $Ni(OH)_2$ layer. The electrodes were then dried under nitrogen and imaged using a scanning electron microscope (SEM). Fig. 4.18 (with Ni nanoparticles) shows the SEM of the Ni-GCE. It was observed that the GCE surface was fully covered with Ni nanoparticles of the size 24-35 nm at all three deposition times. It appears the Ni nanoparticles deposited randomly on the surface of the GCE. Fig. 4.18A (30 s electrodeposition time) shows a partial coverage of the electrode. The mass of nickel on GCE at the three electrodeposition times (based on Faraday's law[47]) was 37.43 $\mu g/cm^2$, 43.00 $\mu g/cm^2$ and 110.71 $\mu g/cm^2$ for 30 s, 60 s and 120 s electrodeposition, respectively calculated based on chronoamperometry data. This coverage increases with the deposition time, showing 120 s (fig. 4.18C) giving the maximum uniform coverage of the surface with densely packed but distinct together Ni-NPs, providing a large surface area to the electrode. It has been mentioned in a previous study that this uniform structure may enhance electron transfer and better electrocatalytic activity of nickel [41].
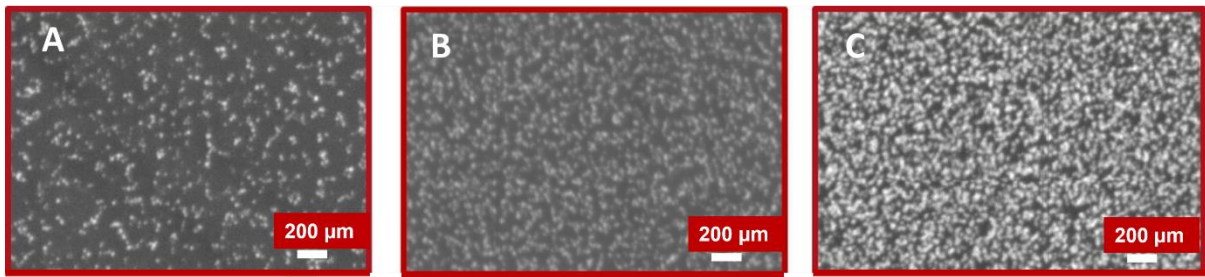
Figure 4.18: SEM images of Ni-GCE (x 50, 000) at electrodeposition times of A) 30s B) 60s C) 120s.

4.3.6 Ni-GCE ferro-/ferricyanide redox coupled system

4.3.6.1 Nickel based glassy carbon electrode system

In *Chapter 3* on a bare GCE creatinine sensor system, the novel response of creatinine in the presence of alkaline ferricyanide was discussed. The ferricyanide is said to oxidise the creatinine to methyl guanidine and creatol, other small organic molecules. As such, we sought to explore the oxidising potential of a nickel-based GCE in an alkaline ferri/ferrocyanide system, to see if the combination of electrocatalytic oxidants could enhance the sensor performance. While NiOOH was not especially responsive to creatinine, it may be responsive to its oxidation products.

Figure 4.19 shows the response of the Ni-GCE to 2 mM creatinine additions in the presence of 1 mM ferrocyanide and 0.1 M KCl in 0.1 M KOH. The equivalent figure without KCl is given in the appendix, and shows a similar but slightly diminished response. Two redox couple responses in this system are observed: ferri/ferrocyanide redox response of creatinine at ca. 0.32 V and the $Ni(OH)_2$/NiOOH redox response at higher potentials. The CVs showed a linear peak height response, giving the plot in Fig. 4.19. This was 20 fold more sensitive to creatinine than in the absence of ferrocyanide, with a sensitivity and LOD of 4.5 µA/mM and 0.65 mM analysed at 0.52 V vs Ag/AgCl. The system without KCl in alkaline ferricyanide (fig. 4.20) gave slightly lower sensitivity (3 µA/mM) and a higher LOD (1.03 mM).
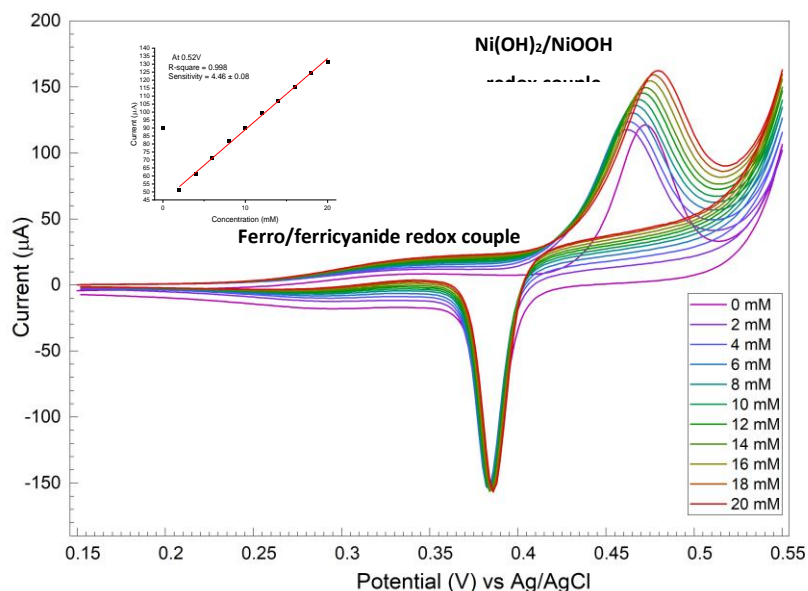
Figure 4.19: Ni-GCE based alkaline ferricyanide system in 0.1 M KCl for creatinine detection.
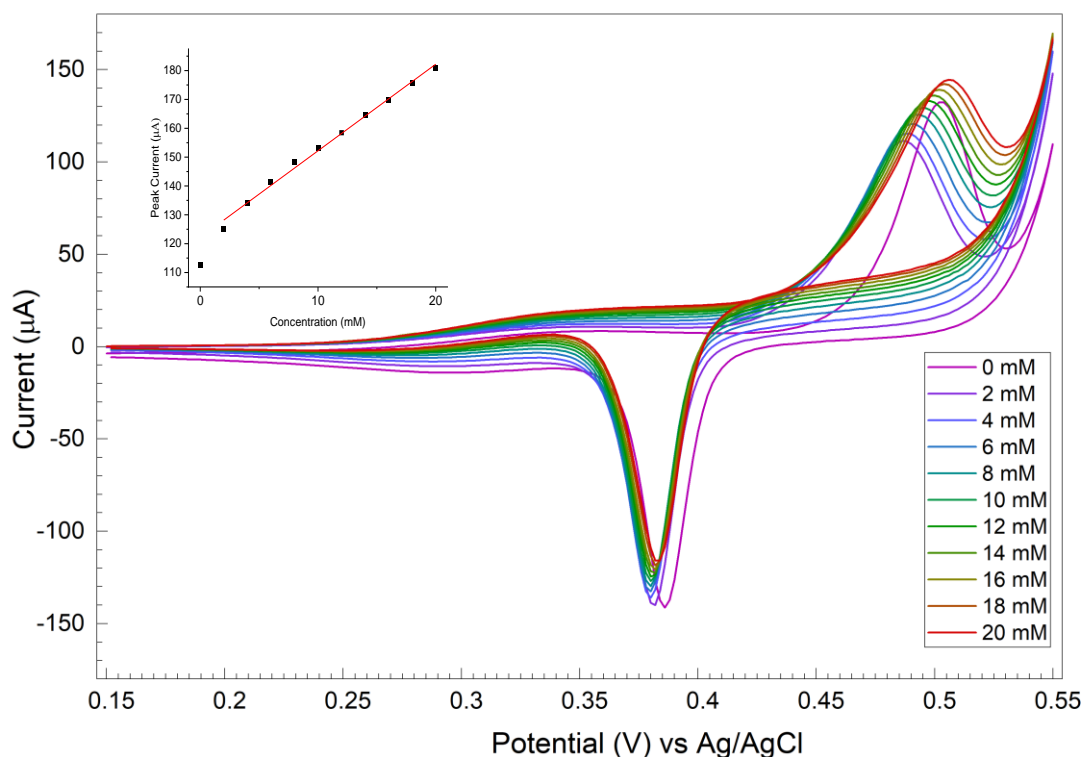
Figure 4.20: Nickel-GCE based alkaline ferricyanide study for creatinine detection.

As found from NMR studies in *Chapter 3*, Section 3.4, the reaction products of creatinine oxidation by ferricyanide in alkali conditions are found to be methylguanidine and creatol. It is possible these are formed in the first instance by ferrocyanide oxidising to ferricyanide. Then, in the vicinity of the electrode, react and oxidise on the surface of the Ni-GCE. Ni oxide electrodes were investigated by Fleichsmann and others in the 1970s for amine oxidation. Creatol an alcohol derivative of creatinine, is also likely electroactive on nickel, due to the alcohol group[48]. The oxidation of first stage oxidation products gives rise to an increasing anodic current response with increasing concentrations of creatinine on the surface Ni-GCE, meaning the creatinine oxidation product is catalytically active on NiOOH, which irreversibly oxidises the first product. This system was first tested with a nickel electrodeposited GCE in alkaline ferricyanide and the initial results showed a significant linear response in terms of peak current (fig. 4.20).

Attempts were made to reproduce this work at a later date, but as shown in Figure 4.21, the electrodeposition of nickel on the surface of GCE was inconsistent according to the procedures followed before. This is evident from the study of the blank solution in 10 ml of 1 M KOH (which was

used later for conditioning CV cycles), as varying peak currents are observed for different repeats performed (fig. 4.21), despite identical deposition procedures being used. This makes it clear that the extent of deposition of nickel on GCE each time is varying significantly. As the electrodeposition was done on different GCEs each time, the growth of nickel nanoparticles may be of different morphology as a result of its growth on each electrode.

As previously mentioned, it was understood that the ferrocyanide reaction at lower potentials give rise to creatol and methylguanidine (creatinine oxidation products with ferro/ferricyanide KOH system), which then potentially further oxidises on the surface of Ni-GCE giving rise to increasing peak anodic currents.
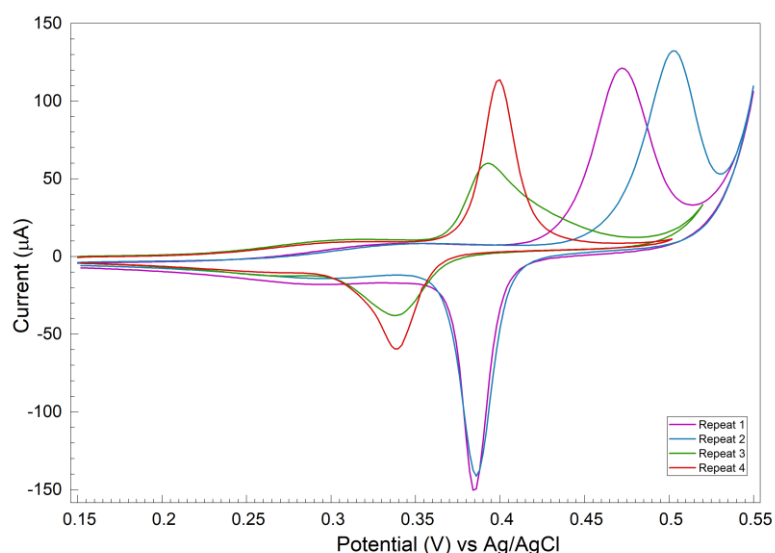
Figure 4.21: Inconsistent responses for blank using Ni-GCE in alkaline ferrocyanide solution analysed using CV study on different Ni-GCEs with a fresh setup each time..

As the deposition of nickel onto GCE was proving so inconsistent, regardless of the preparation of the electrode, an alternative nickel platform was sought to study the response of creatinine with and without ferrocyanide.

4.3.6.2 Nickel foam-based electrode system

It has been previously studied that nickel foam is the best electrode to replace GCE, overcoming traditional modification process[49]. The active material load on the surface of the WE increases as a result of three-dimensional structure of the nickel foam[50]. Due to the increased active sites on the surface of WE, the sensitivity and the current output (mA range) from the sensor can be significantly enhanced. Additionally, to overcome the limitations of GCE modification processes as seen previously with inconsistent Ni deposition procedures, Ni foam study has been performed.

4.3.6.2.1 Morphology analysis

An electrode of commercial nickel foam was fabricated in house. It was housed in a PTFE platinum electrode holder with 10 x 15 mm platinum sheet (fig. 4.22). 1 cm^2 of the nickel foam was immersed in the cell solution for the electrochemical study (fig. 4.22A).
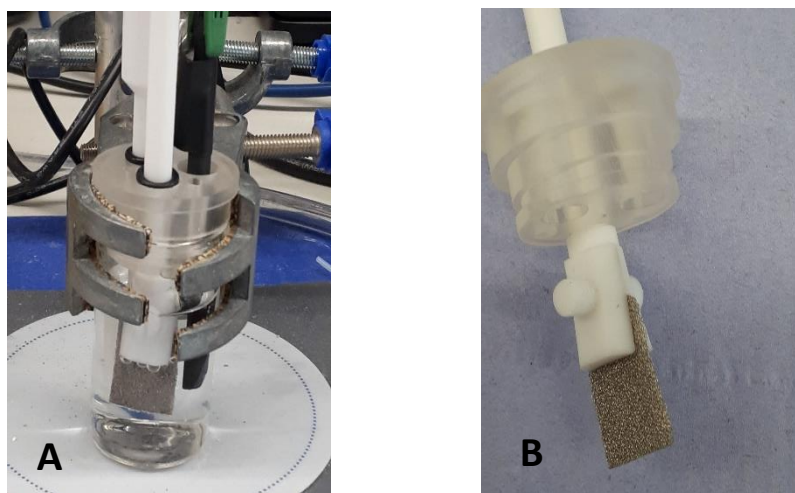
Figure 4.22: Nickel foam housed in a PTFE electrode holder.

SEM images of the nickel foam in Figure 4.23 clearly show the significantly high surface area (fig. 4.23A) with pore sizes approximately 100-120 µm. This high surface area in this structure of Ni foam can significantly enhance the current response and the sensitivities obtained for creatinine detection, potentially improving the sensing platform. The morphology of the foam is studied to observe the high surface area in the structure of the nickel foam.
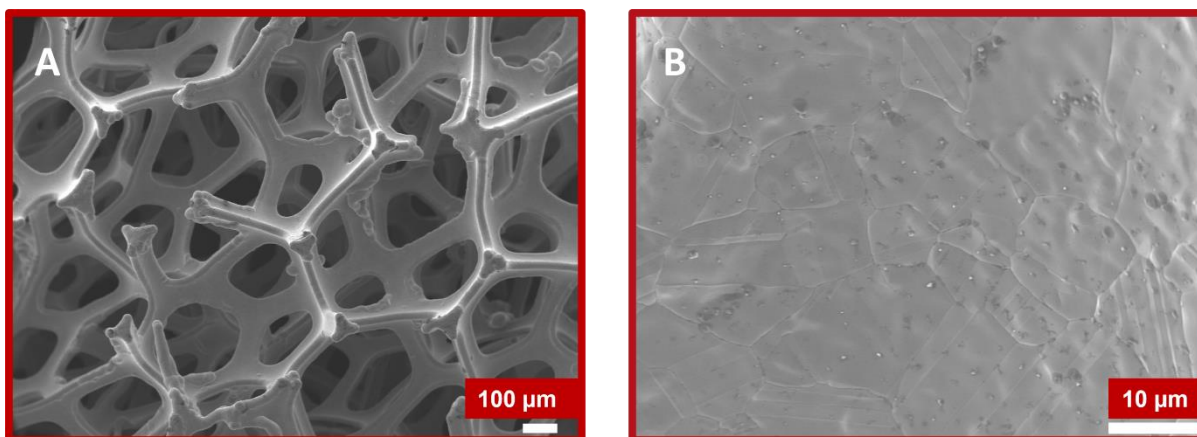
Figure 4.23: SEM images of Ni foam A) x70 B) x2000.

In future work, the surface of Ni foam after conditioning cycles in 1 M KOH can also be analysed to understand further the behaviour of the foam post conditioning and its behaviour with alkaline solutions.

4.3.6.2.2 Electrochemical detection of creatinine

A high surface area sensing system was investigated with nickel foam immersed in 1 mM ferrocyanide and 1 M KOH for creatinine detection. This would mean the limitation of inconsistency in electrodeposition of nickel would be eliminated and a more sensitive and consistent response towards creatinine could potentially be observed. To prepare the Ni(OH)$_2$ layer on the nickel foam, 200 conditioning cycles (200) in 1 M KOH were initially performed akin to the Ni-GCE (fig. 4.24). This would allow the Ni(OH)$_2$ layers on the surface of the electrode to "settle", to obtain accurate calibration data for creatinine detection where an increase in current is as a result of creatinine oxidation only and not enrichment of the nickel hydroxide layer. It was observed that sufficient settling of Ni(OH)$_2$ layers was obtained at the end of the conditioning (CV scan 200) .
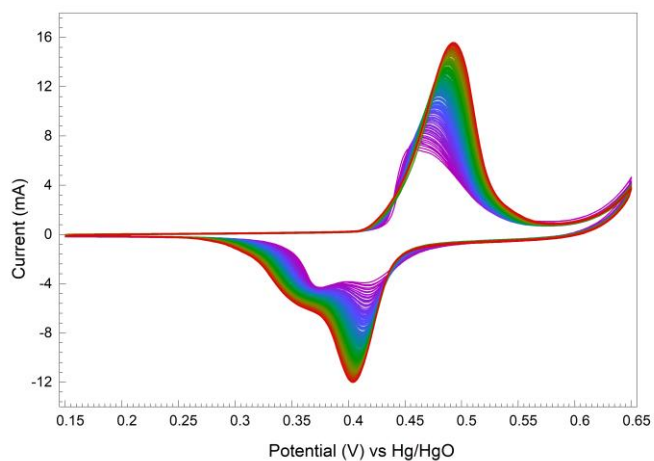
Figure 4.24: Conditioning cycles with nickel foam electrode in 1 M KOH
at a scan rate of 50 mV/s.

A high creatinine concentration range (2-8 mM) was first investigated with the nickel foam electrode. A linear and highly sensitive current response was observed with respect to peak current and current was analysed at a fixed potential of 0.55 V vs Hg/HgO (fig. 4.25 and 4.26). Nickel foam was not tested in absence of ferrocyanide, as a result of having understood from previous Ni-GCE studies that no ferri/ferrocyanide redox peak will be observed and the creatinine oxidation products will not be generated at the Ni electrode.
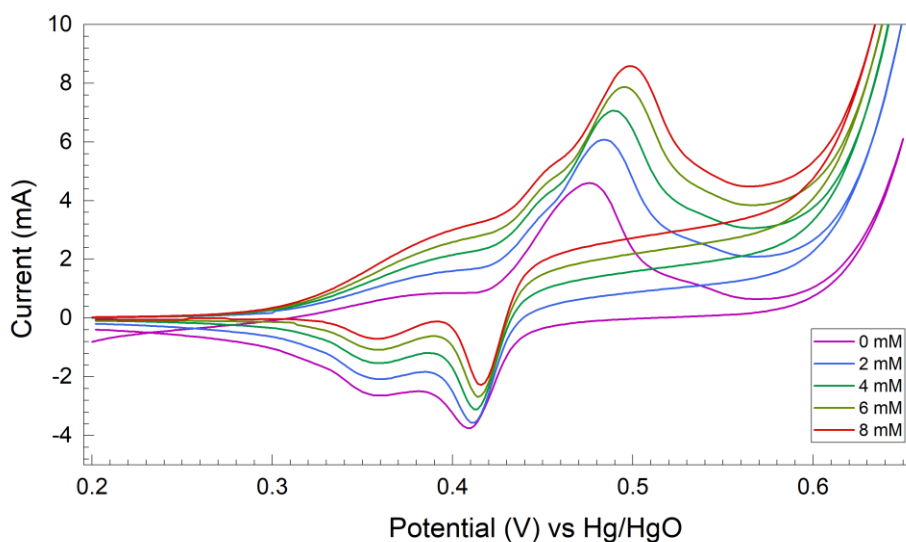
Figure 4.25: CV study to analyse response of creatinine additions (2-8 mM) on nickel foam 1 electrode in alkaline ferrocyanide solution at a scan rate of 10 mV/s.
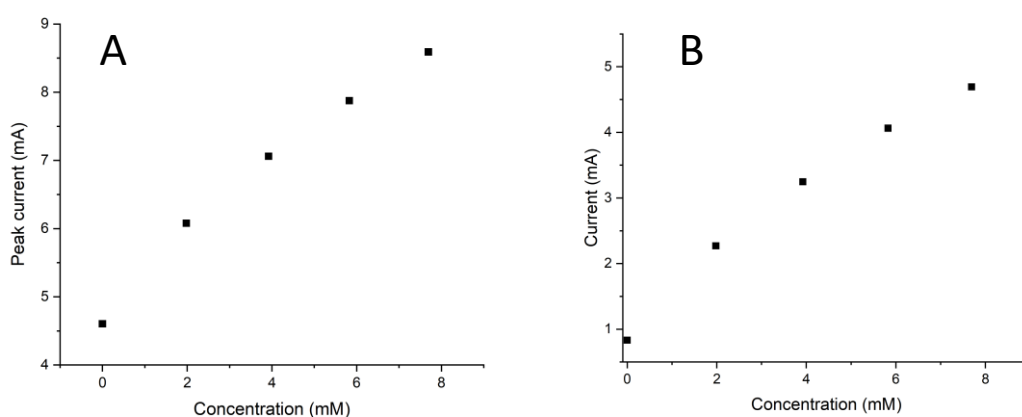
Figure 4.26: A) Peak current vs concentration calibration graph with 2-8 mM creatinine additions to nickel foam after volume correction B) Current vs concentration calibration graph analysed at a fixed potential of 0.55 V vs Hg/HgO with 2-8 mM creatinine additions to nickel foam after volume correction.

A LOD of 710.8 µM with 0.44 ± 0.02 mA/mM sensitivity was obtained from peak current (fig. 4.26A) and LOD of 705.7 µM with 0.43 ± 0.03 mA/mM sensitivity was obtained from the current response at 0.55 V vs Hg/HgO (fig. 4.26B). The system was further investigated at the clinically relevant range of 4.4 – 13.3 mM (urine creatinine outside this range may indicate kidney conditions as reported[43]) in 10 ml 1 M KOH and 1 mM ferrocyanide corresponding to a range of 0.2-2.4 mM on dilution in 10 ml solution (fig. 4.28). It is to be noted that the calibration data has been analysed after volume correction due to additions of 100 µl of stock solution of creatinine (from 200 mM stock) each time added .
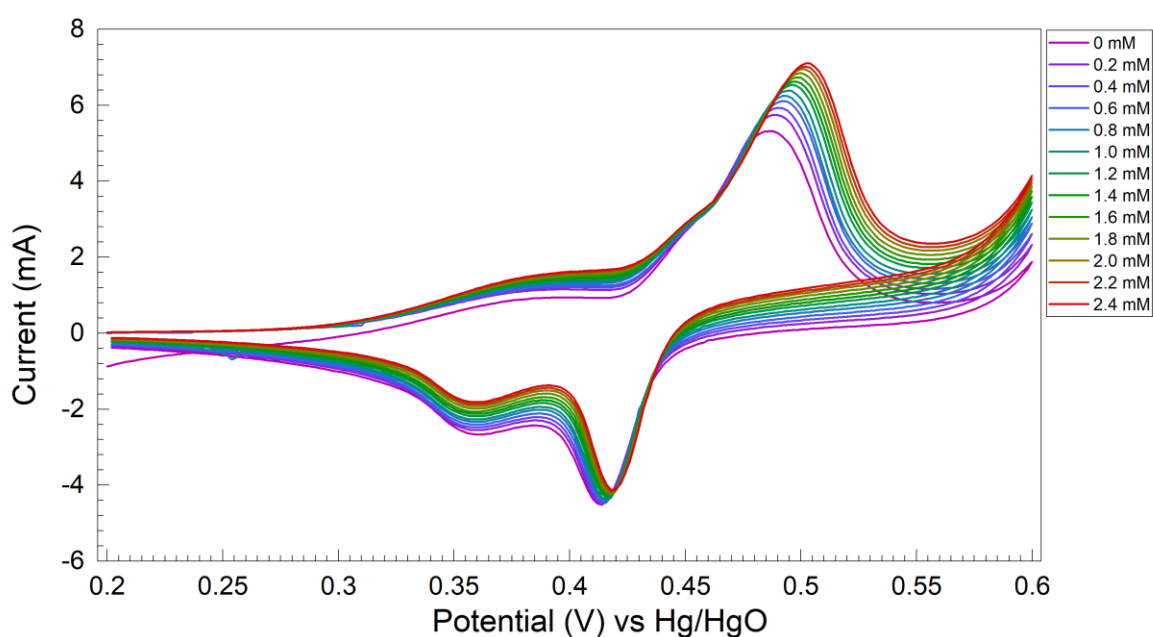
Figure 4.28: Electrochemical study with Ni foam 1 on creatinine additions in the range 0.2-2.4 mM in 10 ml 1 M KOH and 1 mM ferrocyanide.
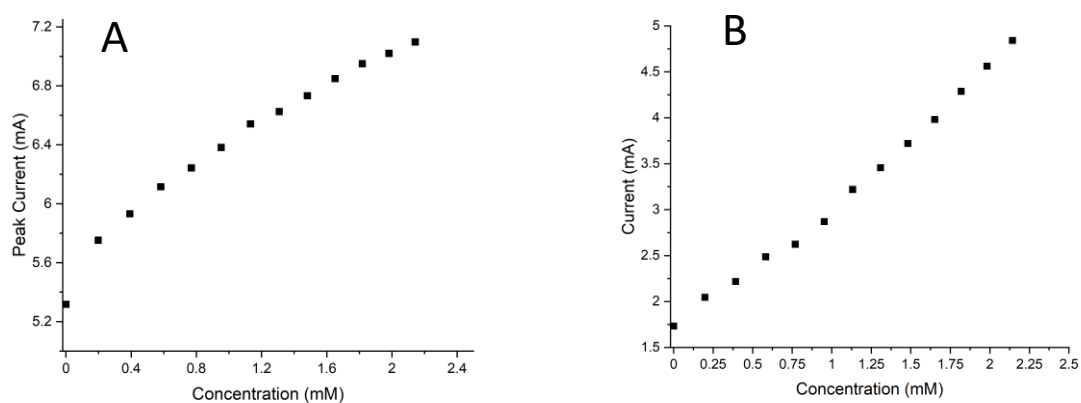
Figure 4.27: A) Peak current vs concentration calibration graph with 0.2-2.4 mM creatinine additions to nickel foam after volume correction B) Current vs concentration calibration graph analysed at a fixed potential of 0.52 V vs Hg/HgO with 0.2-2.4 mM creatinine additions

As expected, a lower LOD of 0.13 mM with sensitivity 0.69 ± 0.02 mA/mM was obtained from fig. 4.27A and LOD of 0.11 mM with sensitivity 1.46 ± 0.04 mA/mM was obtained from fig. 4.27B, in comparison to that at higher creatinine concentrations between 2-8 mM.

This study was repeated with a new piece of nickel foam (nickel foam 2) that was conditioned initially using the same procedure as above and then creatinine additions were made in 1 M KOH and 1 mM ferrocyanide solution. A comparison of conditioning CV study was made between nickel foam 1 and 2 at cycle 200 (fig. 4.30). It was clear that repeatability in results could not be obtained.
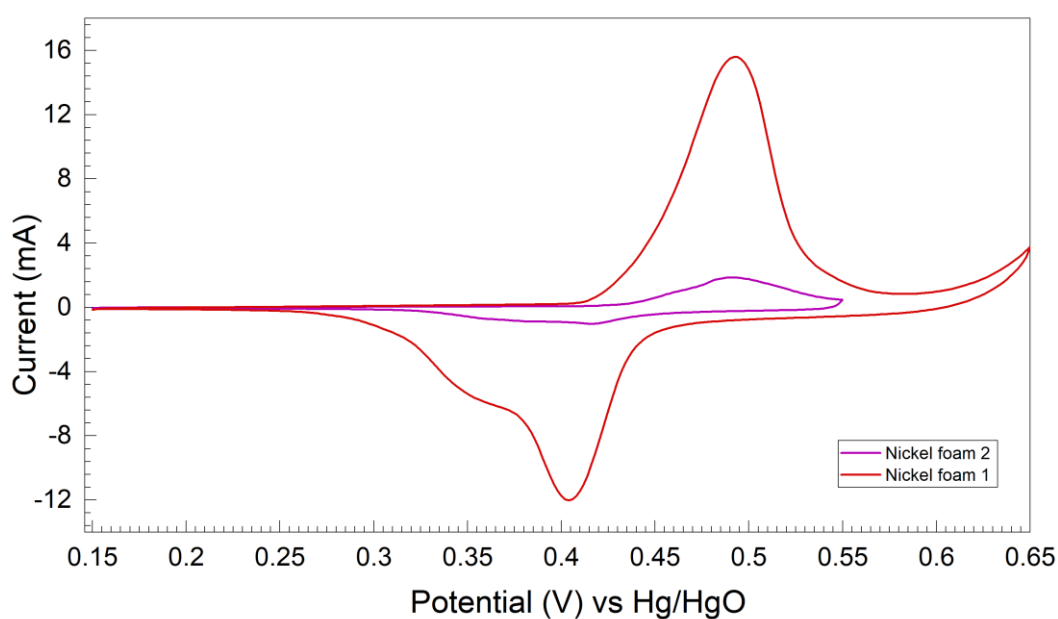
Figure 4.29: Comparison of 200th CV scan for conditioning of Ni foams 1 and 2 in 1 M KOH at a scan rate of 10 mV/s.

Although, further studies with creatinine additions on nickel foam 2 showed linearity in results with creatinine concentrations between 1-9 mM at a scan rate of 50 mV/s (fig. 4.31), meaning that further optimisation of this system in terms of repeatability could allow use of this electrode for creatinine detection at higher concentration ranges. It is to be noted that with nickel foam 2, a higher scan rate of 50 mV/s was used for creatinine detection as 10 mV/s (used in case for nickel foam 1) gave significantly low current response (fig. 4.29).
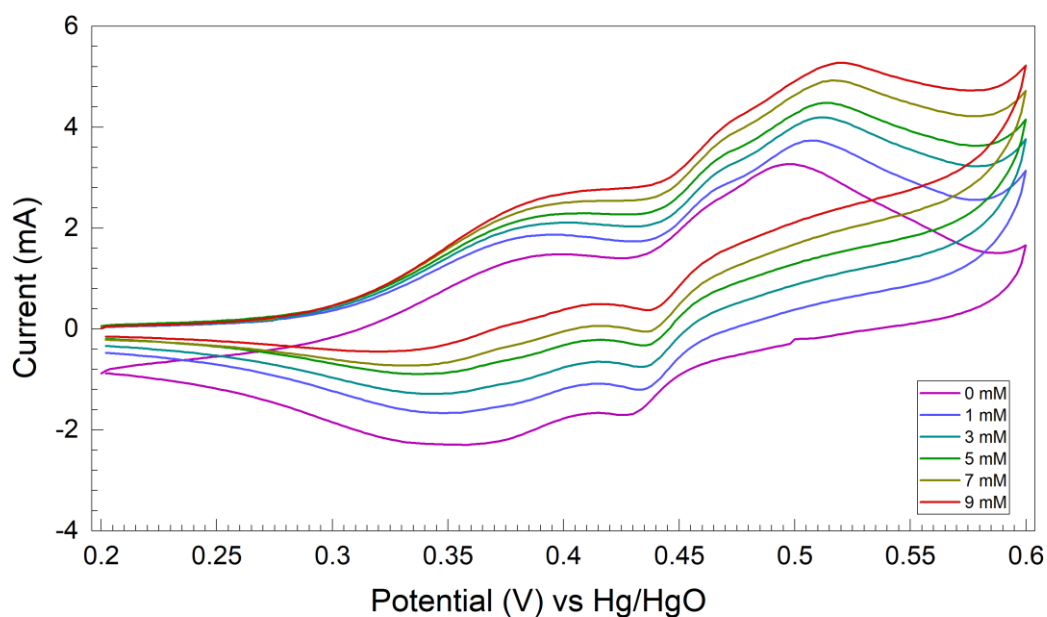
Figure 4.31: Ni foam 2 study with creatinine additions in the range 1-9 mM in 1 M KOH and 1 mM ferrocyanide at a scan rate 50 mV/s.
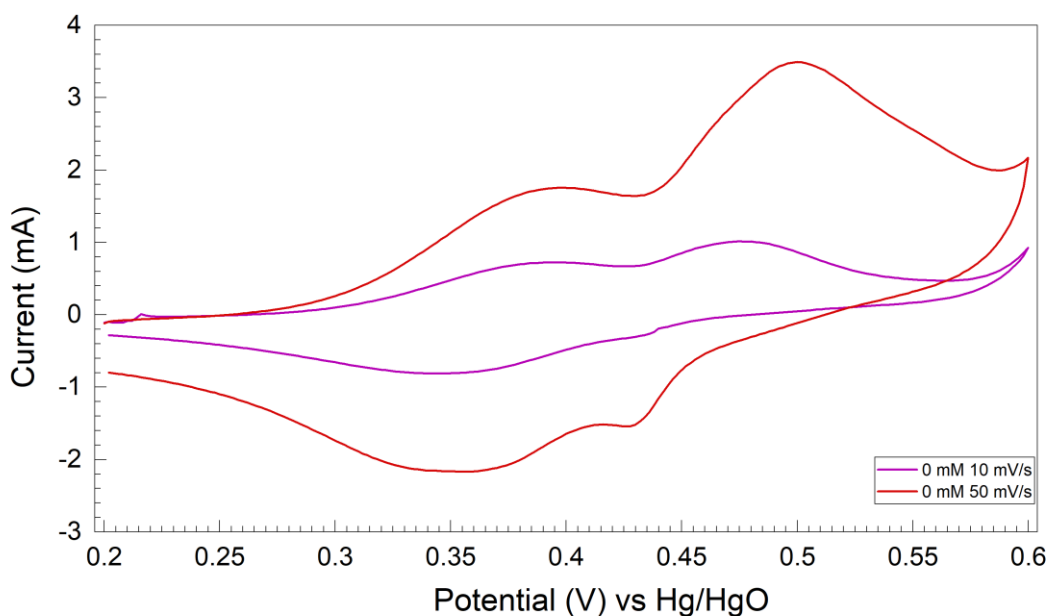
Figure 4.30: Comparison of scan rate 10 mV/s and 50 mV/s with nickel foam 2 in 1 M KOH and 1 mM ferrocyanide solution without creatinine addition.

A further study was done (fig. 4.32) with nickel foam 2 to observe the redox response at lower creatinine concentration range 0.2-1 mM with 0.2 mM creatinine additions was done to obtain response in the relevant clinical range of 4.4-13.3 mM (clinical creatinine range in urine) when diluted in cell with 10 ml 1 M KOH and 1 mM ferrocyanide.
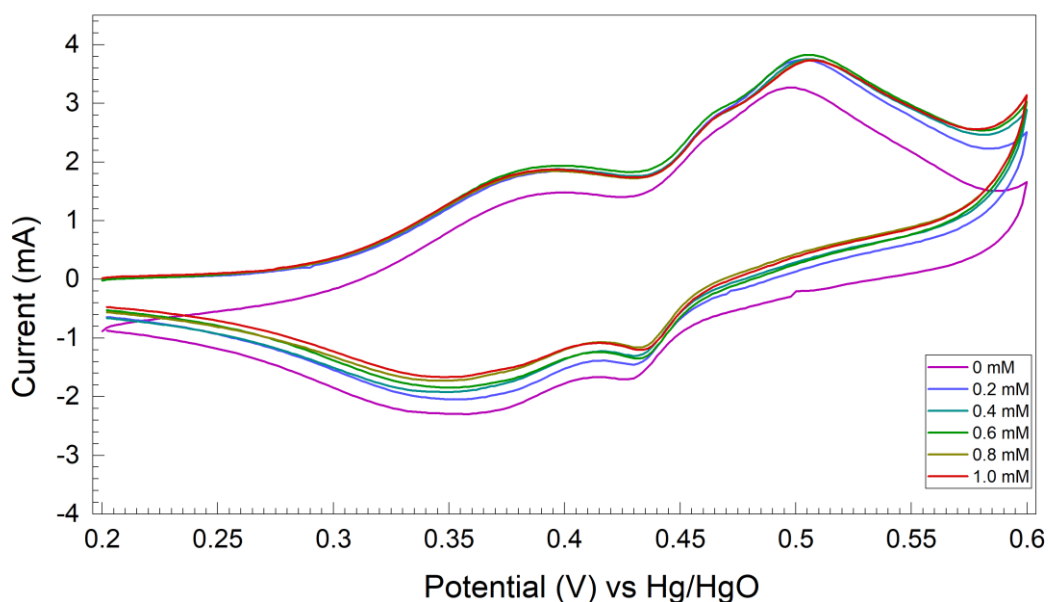
Figure 4.32: CV electrochemical study with 0.2 mM creatinine additions in the range of 0.2-1 mM at a scan rate of 50 mV/s in 1 M KOH and 1 mM ferrocyanide.

There was not a consistent linear response towards creatinine oxidation with the ferri/ferrocyanide redox response. Although there is an increase in current at the 0.2 mM creatinine addition in the cell, at higher concentrations there is no linear response (fig. 4.32).

Although, there was inconsistency between different Ni foams, a pre-treatment and cleaning procedure before conditioning in 1 M KOH could be done to achieve repeatability in results ensuring there is no changes in the surface of each Ni foam used. It was later realised that this procedure may generate the required consistent results.

4.3.7 Interference studies with urea

Avoidance of interfering urea in creatinine detection (for analysis in real samples including urine) remains a challenge. Urea is oxidised catalytically at nickel electrodes and this has been reported in various studies previously [51-55]. In this work, the effect on urea was investigated on the previously

developed Ni-GCE sensor system to understand the extent of interference. 2-20 mM additions of urea were made in 1 M KOH solution with Ni-GCE as the working electrode (fig. 4.33).
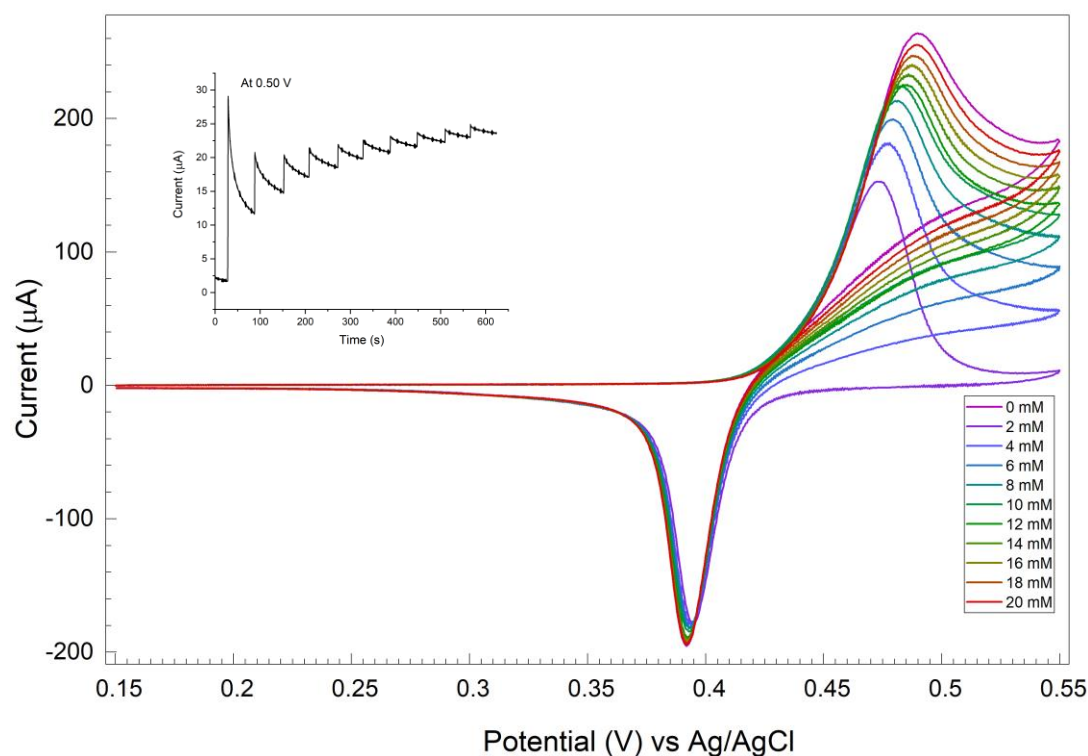
Figure 4.33: 0-20 mM additions of urea to 1M KOH solution at a scan rate of 50 mV/s cycling between 0.15 to 0.55 V vs Ag/AgCl.

It is clear that urea oxidises on the Ni-GCE from the increase in anodic peak current with increasing urea concentration (fig. 4.33). The response far outweighs that of creatinine, meaning that the interference in a real urine sample would be too great. Urea is present in urine at concentrations 50 fold more than that in blood – daily excretion of 342 mmol in 490 to 2690 ml urine [56]. Carpenter & Stuve have studied simultaneous oxidation of urea and creatinine at nickel foam electrodes. Creatinine formed a stable complex with the nickel electrode in comparison to urea causing site blocking due to adsorption. Although as a result, the overall current response decreased [57].

The activity of nickel towards urea is not unexpected. The active centre of urease contains nickel(II) ions, acting as cofactors for enzymes that oxidise urea [58]. Should the nickel based creatinine sensor be further developed, it would be necessary to eliminate the urea response. Further studies could look

at the introduction of membrane-based working electrode systems to prevent entry of urea to the Ni-GCE based on charge or size exclusion. However this was not in the scope of this work.

4.4 Conclusions and future work

In summary, nickel-based electrodes (Ni-GCE and Ni foams) were investigated for electrocatalytic creatinine detection. Initially, creatinine sensing was done using a nickel modified glassy carbon electrode (Ni-GCE) in 1 M KOH and there was not a significant current response as a result of creatinine oxidation where sensitivity of 0.02 µA/mM was obtained. A 200 fold higher current response and sensitivity (4 µA/mM) was observed in alkaline ferrocyanide solutions (in 1 M KOH and 1 mM ferrocyanide) where it was assumed that the oxidation products from the oxidation of creatinine with ferricyanide (methylguanidine and creatol) subsequently reacted with NiOOH that forms on the surface on nickel.

Unfortunately, there was variation in electrodeposition of nickel NPs on the surface of GCE giving inconsistent nickel modification, which affected the repeatability of studies with creatinine and ferricyanide. A commercial nickel foam electrode was then evaluated, to try to attain more consistent response. This gave much higher sensitivities (0.44 mA/mM and 1.46 mA/mM) due to its significantly higher surface area, however it too was not giving reproducible results when using different nickel foam samples. The Ni foam system may benefit from further optimisation of the preparation techniques for pre-treatment and cleaning to allow generation of same surface of Ni on each nickel foam to allow high repeatability in terms of creatinine oxidation.

Finally, the Ni-GCE was used to consider the response of urea, as it was anticipated to have a strong oxidation on nickel. A high current response to typical physiological concentrations of urea in urine meant the Ni-GCE would not be suited to urine samples for creatinine analysis. For blood sample, a much lower detection limit and higher sensitivity would be required. Techniques could be developed to eliminate or reduce the extent of urea interference potentially through use of membrane systems that prevent entry of urea onto the WE of the sensor.

4.5 References

1. M. Fleischmann, K. Korinek and D. Pletcher, *Journal of Electroanalytical Chemistry and Interfacial Electrochemistry*, 1971, **31**, 39-49.

2. Y. G. Lee and T. C. Chou, *Electroanalysis: An International Journal Devoted to Fundamental and Practical Aspects of Electroanalysis*, 2003, **15**, 1589-1597.

3. A. Safavi, N. Maleki and E. Farjami, *Biosensors and Bioelectronics*, 2009, **24**, 1655-1660.

4. M. A. Rahim, R. A. Hameed and M. Khalil, *Journal of power sources*, 2004, **134**, 160-169.

5. B. S. Hui and C. O. Huber, *Analytica chimica acta*, 1991, **243**, 279-285.

6. I. G. Casella, T. R. Cataldi, A. M. Salvi and E. Desimoni, *Analytical Chemistry*, 1993, **65**, 3143-3150.

7. R. Barnard, C. Randell and F. Tye, *Journal of Applied Electrochemistry*, 1980, **10**, 109-125.

8. Y. Zhang, X. Xiao, Y. Sun, Y. Shi, H. Dai, P. Ni, J. Hu, Z. Li, Y. Song and L. Wang, *Electroanalysis*, 2013, **25**, 959-966.

9. X. Gao, W. Feng, Z. Zhu, Z. Wu, S. Li, S. Kan, X. Qiu, A. Guo, W. Chen and K. Yin, *Advanced Materials Interfaces*, 2021, **8**, 2002133.

10. S. Marini, N. Ben Mansour, M. Hjiri, R. Dhahri, L. El Mir, C. Espro, A. Bonavita, S. Galvagno, G. Neri and S. G. Leonardi, *Electroanalysis*, 2018, **30**, 727-733.

11. L.-M. Lu, L. Zhang, F.-L. Qu, H.-X. Lu, X.-B. Zhang, Z.-S. Wu, S.-Y. Huan, Q.-A. Wang, G.-L. Shen and R.-Q. Yu, *Biosensors and Bioelectronics*, 2009, **25**, 218-223.

12. A. Hayat, S. K. B. Mane, N. Shaishta, J. Khan, A. Hayat, G. Keyum, I. Uddin, F. Raziq, M. Khan and G. Manjunatha, *Journal of The Electrochemical Society*, 2019, **166**, B1602.

13. L.-P. Jia and H.-S. Wang, *Sensors and Actuators B: Chemical*, 2013, **177**, 1035-1042.

14. L. Shabnam, S. N. Faisal, A. K. Roy and V. G. Gomes, *ChemElectroChem*, 2018, **5**, 3799-3808.

15. K. E. Toghill, L. Xiao, N. R. Stradiotto and R. G. Compton, *Electroanalysis: An International Journal Devoted to Fundamental and Practical Aspects of Electroanalysis*, 2010, **22**, 491-500.

16. X. Wen, J. Xi, M. Long, L. Tan, J. Wang, P. Yan, L. Zhong, Y. Liu and A. Tang, *Journal of Electroanalytical Chemistry*, 2017, **805**, 68-74.

17. E. O. Nachaki, P. M. Ndangili, N. M. Naumih and E. Masika, *ChemistrySelect*, 2018, **3**, 384-392.

18. D. Trivedi, J. Crosse, J. Tanti, A. J. Cass and K. E. Toghill, *Sensors and Actuators B: Chemical*, 2018, **270**, 298-303.

19. M. A. Ehsan and A. Rehman, *Analytical Methods*, 2020, **12**, 4028-4036.

20. K. Carpenter and E. M. Stuve, *Journal of Applied Electrochemistry*, 2021, **51**, 945-957.

21. K. Rikitake, I. OKA, M. ANDO, T. YOSHIMOTO and D. TSURU, *The Journal of Biochemistry*, 1979, **86**, 1109-1117.

22. N. R. Stradiotto, K. E. Toghill, L. Xiao, A. Moshar and R. G. Compton, *Electroanalysis: An International Journal Devoted to Fundamental and Practical Aspects of Electroanalysis*, 2009, **21**, 2627-2633.

23. M. Li, X. Bo, Z. Mu, Y. Zhang and L. Guo, *Sensors and Actuators B: Chemical*, 2014, **192**, 261-268.

24. C. M. Brett, O. Brett and A. Electrochemistry, 1993.

25. D. Pletcher and F. C. Walsh, *Industrial electrochemistry*, Springer Science & Business Media, 2012.

26. M. Giovanni, A. Ambrosi and M. Pumera, *Chemistry–An Asian Journal*, 2012, **7**, 702-706.

27. D. Giovanelli, N. S. Lawrence, L. Jiang, T. G. Jones and R. G. Compton, *Sensors and Actuators B: Chemical*, 2003, **88**, 320-328.

28. Y.-C. Weng and T.-C. Chou, *Journal of The Electrochemical Society*, 2006, **153**, H127.

29. M. Jafarian, F. Forouzandeh, I. Danaee, F. Gobal and M. Mahjani, *Journal of Solid State Electrochemistry*, 2009, **13**, 1171-1179.

30. W. Visscher and E. Barendrecht, *Journal of electroanalytical chemistry and interfacial electrochemistry*, 1983, **154**, 69-80.

31. P. Oliva, J. Leonardi, J. Laurent, C. Delmas, J. Braconnier, M. Figlarz, F. Fievet and A. De Guibert, *Journal of Power sources*, 1982, **8**, 229-255.

32. K. E. Toghill, L. Xiao, M. A. Phillips and R. G. Compton, *Sensors and actuators B: Chemical*, 2010, **147**, 642-652.

33. J. Desilvestro, D. A. Corrigan and M. J. Weaver, *Journal of The Electrochemical Society*, 1988, **135**, 885.

34. D. MacArthur, *Journal of The Electrochemical Society*, 1970, **117**, 422.

35. D. S. Hall, D. J. Lockwood, C. Bock and B. R. MacDougall, *Proceedings of the Royal Society A: Mathematical, Physical and Engineering Sciences*, 2015, **471**, 20140792.

36. A. El-Shafei, *Journal of Electroanalytical Chemistry*, 1999, **471**, 89-95.

37. G. Briggs and P. Snodin, *Electrochimica Acta*, 1982, **27**, 565-572.

38. F. Hahn, B. Beden, M. Croissant and C. Lamy, *Electrochimica acta*, 1986, **31**, 335-342.

39. R. Barnard, C. Randell and F. Tye, *Journal of Applied Electrochemistry*, 1980, **10**, 109-125.

40. Q. Yi, W. Huang, W. Yu, L. Li and X. Liu, *Electroanalysis: An International Journal Devoted to Fundamental and Practical Aspects of Electroanalysis*, 2008, **20**, 2016-2022.

41. H. Guo, Z. Huang, Y. Zheng and S. Weng, *Int. J. Electrochem. Sci*, 2015, **10**, 10703-10712.

42. L. Luo, F. Li, L. Zhu, Y. Ding, Z. Zhang, D. Deng and B. Lu, *Colloids and Surfaces B: Biointerfaces*, 2013, **102**, 307-311.

43. M. L. Bishop, *Clinical Chemistry: Principles, Techniques, and Correlations, Enhanced Edition: Principles, Techniques, and Correlations*, Jones & Bartlett Learning, 2020.

44. D. T. Sawyer, A. Sobkowiak and J. L. Roberts, *Electrochemistry for chemists*, Wiley, 1995.

45. Y. Wang, D. Zhang, W. Peng, L. Liu and M. Li, *Electrochimica Acta*, 2011, **56**, 5754-5758.

46. S. Maximovitch and G. Bronoel, *Electrochimica Acta*, 1981, **26**, 1331-1338.

47. C. G. Zoski, *Handbook of electrochemistry*, Elsevier, 2006.

48. K. Nakamura and K. Ienaga, *Experientia*, 1990, **46**, 470-472.

49. H. Shu, S. Peng, T. Lai, X. Cui, J. Ren, T. Chen, X. Xiao and Y. Wang, *Journal of Electroanalytical Chemistry*, 2022, **919**, 116524.

50. H. J. Jo, A. Shit, H. S. Jhon and S. Y. Park, *Journal of Industrial and Engineering Chemistry*, 2020, **89**, 485-493.

51. N. S. Nguyen, G. Das and H. H. Yoon, *Biosensors and Bioelectronics*, 2016, **77**, 372-377.

52. C. Bao, Q. Niu, Z.-A. Chen, X. Cao, H. Wang and W. Lu, *RSC advances*, 2019, **9**, 29474-29481.

53. T. S. K. Naik, S. Saravanan, K. S. Saravana, U. Pratiush and P. C. Ramamurthy, *Materials Chemistry and Physics*, 2020, **245**, 122798.

54. W. Yan, D. Wang and G. G. Botte, *Electrochimica Acta*, 2012, **61**, 25-30.

55. M. Vidotti, M. Silva, R. Salvador, S. C. de Torresi and L. Dall'Antonia, *Electrochimica Acta*, 2008, **53**, 4030-4034.

56. L. Liu, H. Mo, S. Wei and D. Raftery, *Analyst*, 2012, **137**, 595-600.

57. K. Carpenter and E. M. Stuve, *Journal of Applied Electrochemistry*, 2021, **51**, 945-957.

58. A. Kozitsina, Z. V. Shalygina, S. Dedeneva, G. Rusinov, S. Tolshchina, E. Verbitskiy and K. Z. Brainina, *Russian Chemical Bulletin*, 2009, **58**, 1119-1125.

Chapter 5 - Screen printed electrode (SPE) based Creatinine Sensing

5.1 Introduction

With hospitals coming under intense pressure recently, it is even more important to detect analytes in bodily fluids in a point-of-care (POC) setting. There is a significant need to develop portable, low-cost sensing methods that give quick results, and at the same time are reliable in terms of quantitative and qualitative measurements. Detection of glucose in blood is a widely used POC platform that uses screen-printed electrodes, using small portable electronics (e.g., potentiostat in case of electrochemistry). POC testing with screen-printed electrodes can replace various conventional sensing methods. The idea is to have a quick POC creatinine test at hospitals and general practitioner (GP) surgeries to screen for kidney conditions in particular early stages of kidney disease. The sensor must be able to detect both healthy and unhealthy ranges of creatinine (normal reported range of creatinine in urine is between 4.4-13.3 mM[2]) in samples with high enough selectivity and sensitivity.

In this chapter, the aim was to translate the chemistries developed in *Chapters 3* & *4* to a low cost and simple miniaturised sensor for creatinine detection using screen printed carbon electrodes (SPCEs). Bare and modified SPCEs are used in an alkaline ferrocyanide solution to detect creatinine (fig. 5.1). This setup has not been previously investigated for creatinine sensing. Furthermore, Nafion (Nf) modified SPCEs are also used to see the effect on interference with ascorbic acid (AA) and uric acid (UA). There exists interference in most sensing setups and the aim is to minimise their effects on creatinine detection. The setup was also used with ferrocyanide hydrogels/KOH for single on-spot measurements in artificial urine samples. The bare SPE setup was tested with artificial urine samples as part of the standard addition study.
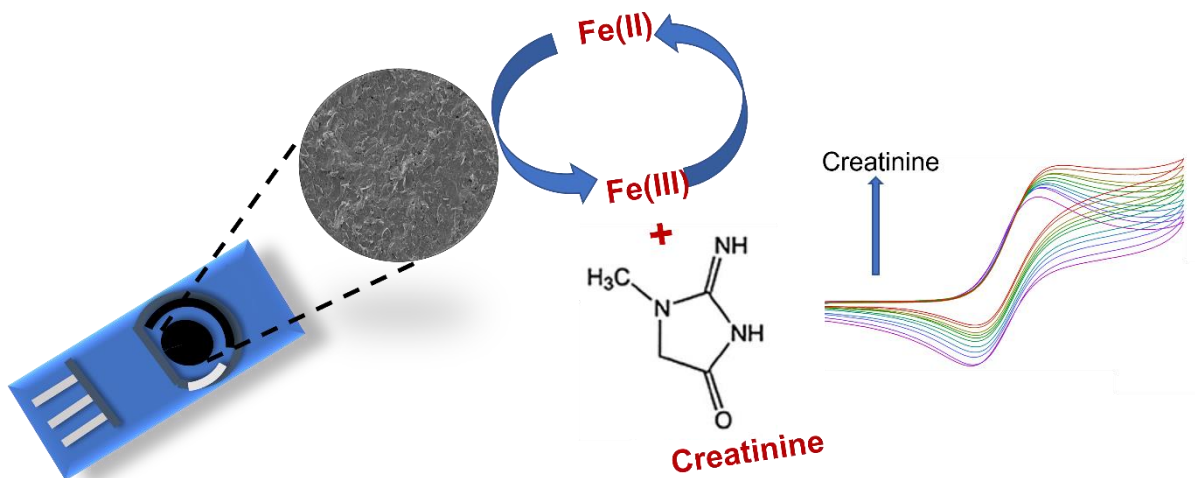
Figure 5.1: Electrochemical sensing of creatinine using a SPE system.

It has become more important to develop disposable low-cost miniaturised point-of-care systems for decentralised on-spot measurements in clinical settings to decreased hospitalization times, reducing contamination as samples are less travelled, decreasing hospital expenses and bills and the load on medical care [3-5]. Use of POCT technology also means a way of individual self-monitoring[6] and support patients at earlier stages in disease development before chronic symptoms develop by earlier identification. SPCEs have high stability, are compact, low cost, precise, sensitive, rapid and have high reproducibility which adds to its benefits for miniaturisation and use in point-of-care (POC) settings [4]. The aim is to achieve low unit prices at high manufacturing volumes using the SPCE technology [7]. Use of SPCEs has allowed a commercialisation route from 'lab to market'. This technology has been investigated for developing disposable sensors for detection of different analytes including glucose (for monitoring diabetes which is a billion dollar per annum global market [8]) due to its low cost and high reproducibility [9-15]. These have also been previously used for detection of uric acid[16, 17] and dopamine[18, 19] . SPCEs are produced with conducting pastes (carbon, Ag/AgCl, etc) on a substrate. Carbon paste electrodes, are low cost and have minimal background current which adds to its advantages for use in a SPCE setup [7]. Immobilisation of a bioreagent layer can also be done on the surface of the SPCEs for biosensing applications [20].

Nafion (Nf) is a perfluorinated polymer that has received increasing attention in the area of electrochemical sensing due to its interference minimising properties from ascorbic acid (AA) and uric acid(UA). The negatively charged Nf membrane prevents/minimises entry of AA and UA (which are

also negatively charged) to the surface of the working electrode, thus minimising the extent of interference in real samples like blood or urine. Nf based creatinine detection has been previously performed in a study where carbon nanotubes based SPCEs were prepared with Nafion (5 wt%) by drop casting method [21]. The performance of SPEs can be further increased in terms of sensitivity, stability and selectivity through use of nanomaterials that can introduce large amounts of defect sites, reducing the amount of polymeric binder on the surface of SPEs. Carbon black (CB) is one such low cost nanomaterial compound, characterised by a high number of defect sites [22].

SPCEs have been previously used for detection of creatinine in a number of studies [23-29]. Chen et al. developed ferrocenemethanol-based SPCEs using enzyme inks [23], which gives high selectivity but adds to high costs of enzymes and stability problems. Ashakirin et al. performed creatinine detection with copper based molecularly imprinted polymers (MIPs) on SPCEs [27]. A SPCE based enzymatic amperometric creatinine biosensor was designed by Dasgupta et al. based on complexing 1-methylhydantoin (enzymatic product with creatinine) to cobalt to produce the redox signal. The complex generates a signal that is proportional to the concentration of creatinine [28]. Kumar et al. investigates iron binding property of creatinine in designing a non-enzymatic sensor on disposable carbon printed electrodes for analysis in clinical urine samples [30]. An enzymeless pre-anodized SPE sensor was also developed by Chen at al. but required various treatment procedures including addition of chloride ions (to allow reaction of active methylene group on creatinine with the surface functional groups on the pre-anodised SPE) and pre-concentration [31]. Previous studies on using SPEs for creatinine detection either involve complex procedures involving use of MIPs or high cost due to use of enzymes. Some studies although use non-enzymatic procedures and may have advantages in terms of low cost.

To advance the work in previous chapters the development of the creatinine sensing method into a POC format with a miniaturised electrochemical cell (in the form of SPEs) was explored. Here, we present a simple and low cost SPCE creatinine detection platform (using alkaline ferrocyanide) with minimised interference towards interferents of ascorbic acid (AA) and uric acid (UA) by use of CB/Nf membranes. As a proof-of-concept, the system was also tested for one-spot analysis with ferrocyanide hydrogels, though this requires considerable further optimisation in terms of reproducibility of drop cast procedures. The SPEs were characterised using voltammetry and microscopy. To the best of our knowledge, there is no such report of a non-enzymatic system for creatinine analysis.

5.2 Experimental

5.2.1 Chemicals

Potassium hydroxide (Fisher Scientific), potassium ferricyanide (99+%), potassium ferrocyanide trihydrate, 99+%, for analysis (Acros Organics), creatinine anhydrous, ≥98%, Poly(vinyl alcohol) Mw 89,000-98,000, 99+% hydrolyzed (Sigma-Aldrich), potassium chloride (Sigma-Aldrich), sodium chloride (Fisher Scientific), urea, 99.0-100.5% (Sigma-Aldrich), Bovine Serum Albumin, lyophilized powder, ≥96% (Sigma-Aldrich), sodium phosphate monobasic, ≥99% (Sigma-Aldrich) was purchased and used without further purification. L(+)-Ascorbic acid, 99% (Acros Organics), Glucose (Sigma-Aldrich) and uric acid, 99% (Thermo Scientific) were purchased. Nafion (Nf), 5% w/w in water and 1-propanol was purchased from Alfa Aesar. Carbon black was purchased from Sigma Aldrich.

5.2.2 Materials and methods

SPEs used in this study were commercially manufactured. Carbon ink (WE) based SPEs with Ag/AgCl RE and carbon based CE (purchased from Flex Medical Solutions) were used for part of the study and were used with in-house made SPE connector. Carbon paste (WE and CE) with Ag/AgCl RE (purchased from Metrohm DropSens) based SPEs were also used for part of the study and used with Metrohm SPE connector.

5.2.3 Quantification calculations and analysis

The 3σ and 10σ methods were used to calculate the limit of detection (LOD) and limit of quantification (LOQ) respectively (Equation 5.1 and 5.2) from calibration plot[32].

LOD = 3 x error of y-intercept/gradient of the line   (Equation 5.1)

LOQ = 10 x error of y-intercept/gradient of the line   (Equation 5.2)

5.2.4 Errors in analytical measurements

% Recovery = *Detected concentration/spiked concentration x 100 (ref [33])*   (Equation 5.3)

% Error = *(Measured value – actual value)/actual value x 100*   (Equation 5.4)

5.2.4 Morphology analysis

Bare SPCE, Nf/SPCE, and CB/Nf/SPCE were analysed by SEM using JEOL JSM-7800F SEM microscope. The conditions for surface analysis were 5 kV acceleration voltage, WD 10 mm and magnification of x 500 and x 5000.

5.2.5 Artificial urine sample analysis with bare SPEs

Standard addition method was used to evaluate the accuracy of the sensor response towards creatinine present in artificial urine (AU) solutions. Tests were performed with 2 mM, 10 mM, 17 mM and 25 mM creatinine (CR) in AU solutions. Blank CV was taken at the potentials -0.2 to 0.5 V (vs Ag/AgCl) with 50 mV/s scan rate and a step potential of 2 mV in 10 ml 1 M KOH and 1 mM ferrocyanide. Following this, 1 ml from creatinine in AU solution (with respective creatinine concentrations as mentioned) was added and CV was recorded with same settings. Then, three known additions of 0.4 mM creatinine were made to the 11 ml solution from 200 mM creatinine stock solution (adding 22 μl each time). CV was again taken with same settings. Total of three repeats (n=3) were performed for each concentration. Standard addition analysis was done to evaluate the accuracy of the sensing platform.

5.2.6 Preparation of Nf/SPEs

Nf/SPCEs were prepared by drop casting 10 μl of 2 wt% Nf solution on the carbon paste WE (of Metrohm DropSens SPCEs) and left to dry to form a thin film on the SPCEs. Interference tests using AA and UA were then performed to analyse the effect of Nf membrane on eliminating or minimising the interferences.

5.2.6.1 Interference study

Interference study with ascorbic acid (AA), uric acid (UA) and glucose (Glu) were performed with and without creatinine, aiming to minimise the extent of interference in the creatinine sensing system. The potential window analysed was between 0 to 1.1 V vs Ag/AgCl with a step potential of 0.002 V and a scan rate of 50 mV/s. First CV scan was analysed for all the studies.

5.2.7 Preparation of CB/Nf/SPEs

An optimised procedure for Nf/CB ink preparation was followed from that obtained in *Chapter 2,* where a 2 wt% Nf solution with 10 mg CB was prepared. The ink was sonicated for 20 mins. 10 μl of the ink was drop cast on SPEs (Metrohm DropSens) and left to dry.

5.2.7.1 Interference study

Interference study with AA, UA and Glu were performed with and without creatinine. The potential window analysed was between -0.2 to 0.4 V vs Ag/AgCl with a step potential of 2 mV and a scan rate of 10 mV/s.

5.2.8 Preparation of PVA hydrogel/KOH-ferrocyanide film SPEs

A novel procedure was followed. PVA was dissolved in deionised water (10 % w/v) at 100°C for 2h to obtain a homogeneous solution. SPEs were immersed in 1 mM ferrocyanide solution in DI water for 20 mins and left to dry at room temperature. 60 μl of PVA gel was drop cast on the SPEs and left to

dry, after which SPEs were immersed in 1M KOH for 20 mins. CV studies were performed once the SPEs were dry.

5.2.9 Preparation of ferrocyanide/KOH/PVA hydrogel SPEs

5 w/v% PVA solution was prepared (which has pH range between 5 to 6.5) to prepare ferrocyanide hydrogels. Part of the procedure was followed by a study by Russo et al. [34]. PVA hydrogels were synthesised with 5 mM ferrocyanide incorporated into the 5 w/v% PVA gel. 5 mM ferrocyanide solution in DI water was prepared and heated to 85°C, after which PVA was added sequentially to form a 5 w/v% gel solution. 60 µl of the PVA/ferrocyanide gel was drop cast on the SPEs. The SPEs were then placed in freezer at -20°C for 24h, and thawed before use for physically cross-linking the gel to form hydrogel. A freeze-thawing technique was used for this process.

5.2.10 Electrochemical study with SPEs

The SPEs (from Flex Medical Solutions and Metrohm DropSens) were connected to the SPE connector (fig. 5.2) and connected to the Ivium EmSTAT 3+ potentiostat which was used in conjunction with the software (PSTrace). The electrochemical study was analysed using techniques including cyclic voltammetry (CV).
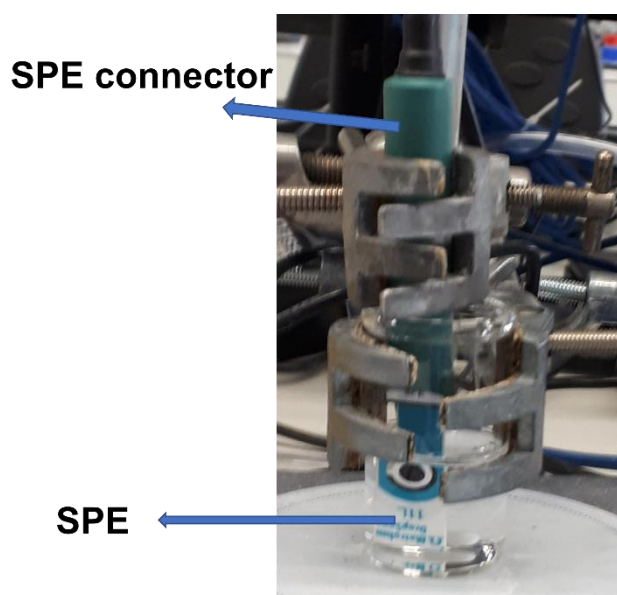
Figure 5.2: A photograph to show the Metrohm DropSens SPE electrochemical system as used in the laboratory.

5.3 Results and Discussion

5.3.1 Morphology analysis

The morphology of bare, Nf and CB-Nf electrodes was analysed using SEM. The presence of Nf and CB/Nf was confirmed through the SEM analysis. Irregularly shaped randomly orientated micrometric flakes of graphite are seen in case of bare SPE (fig. 5.3A). A clear film of Nafion is present on the surface of Nafion/SPE (fig. 5.3B). Fig. 5.3C and 5.3D show a uniform rough surface with high surface area carbon black.
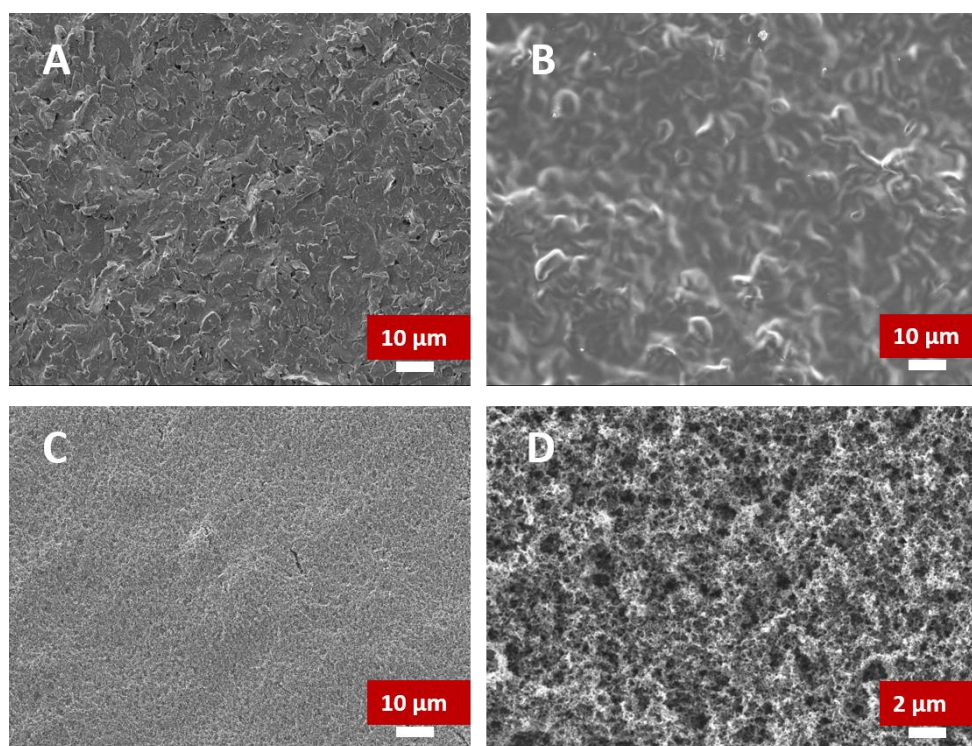
Figure 5.3: SEM images of A) Bare SPE (x 500) B) Nafion-SPE (x 500) C) Carbon black/Nafion/SPE (x 500) D) Carbon black/Nafion/SPE (x 5000).

This high surface area allows to increase the conductivity and enhancing the electron kinetics at the electrode surface.

The experimental evidence from SEM analysis shows the good dispersion of CB-Nf ink prepared, giving results of uniform CB-Nf film on the surface of drop coated SPE (fig. 5.3C and 5.3D). CB agglomerates can be observed on the surface of CB/Nf/SPE, with high surface area. It has been previously observed that CB primary particles spontaneously form nanostructured aggregates, as a result forming characteristic porous structures [35]. Varied particle sizes are seen on the surface of CB/Nf/SPE.

5.3.2 Creatinine electrochemical study on bare SPE system

This study (with three repeats) was carried out in an electrochemical cell setup where the SPE connected to the SPE connector was immersed in a 10 ml solution of 1 M KOH and 1 mM ferrocyanide (fig. 5.2). It is evident from fig. 5.4, that a EC' electrocatalytic mechanism exists on the SPCE system (same as that seen with bare GCE system in *Chapter 3*), where the electrochemical step (ferrocyanide converts to ferricyanide) is followed by the chemical step of creatinine oxidation, giving rise to increasing anodic currents at 0.50 V as the concentration of creatinine increases. The calibration plot inset of Figure 5.4 shows average linearity of $R^2 = 0.99$, yet there was considerable variability between measurements as seen in the error bars. These correspond to the same SPE in replicated analysis.

For creatinine additions ranging 2 – 20 mM the LOD was calculated using the average measurement using the 3σ method[32] was found to be 0.20 mM, and LOQ was calculated based on 10σ method[32] to be 0.68 mM. The sensitivity of the sensor was calculated to 0.30 ± 0.01 µA/mM. It could be understood that 4.4-13.3 mM is the normal level of creatinine in urine reported[2] and this sensor can measure 0.68 mM (using CV technique) as the lowest concentration showing the applicability of this system in real settings. Additionally, as accepted in industry the LOD for a sensor must be at least 10 times lower than the lower reference linear range, which in this case is acceptable to have LOD of 0.20 mM as compared to detecting the lower creatinine concentration of 4.4 mM. It is also to be noted that the normal clinical ranges of creatinine is reported to different values in many literature reports[2, 36, 37] as it can vary based on different factors including dehydration, etc. Therefore, considering the range 4.4-13.3 mM as normal creatinine levels in urine, we also analysed the sensor at higher concentration ranges for spiking studies (e.g., 25 mM creatinine in artificial urine). Despite, this difference in concentration ranges, when the creatinine measured concentration is combined with albumin (calculating ACR ratio), it would be a robust clinical index for early screening of kidney conditions *(more detail in Chapter 6 on future work)*.

The absolute error in the calibration graph (calculated based on taking average of highest and lowest values in the three measurements), shows high variability which could be due to the fact that these repeat measurements were done on the same SPE. It could be possible that products of creatinine oxidation may be adsorbed to the SPE surface, causing a change in current response at each concentration as seen in the calibration graph. Although, the linearity in the response clearly shows this system can be further optimised on different SPEs further giving lower values in errors.
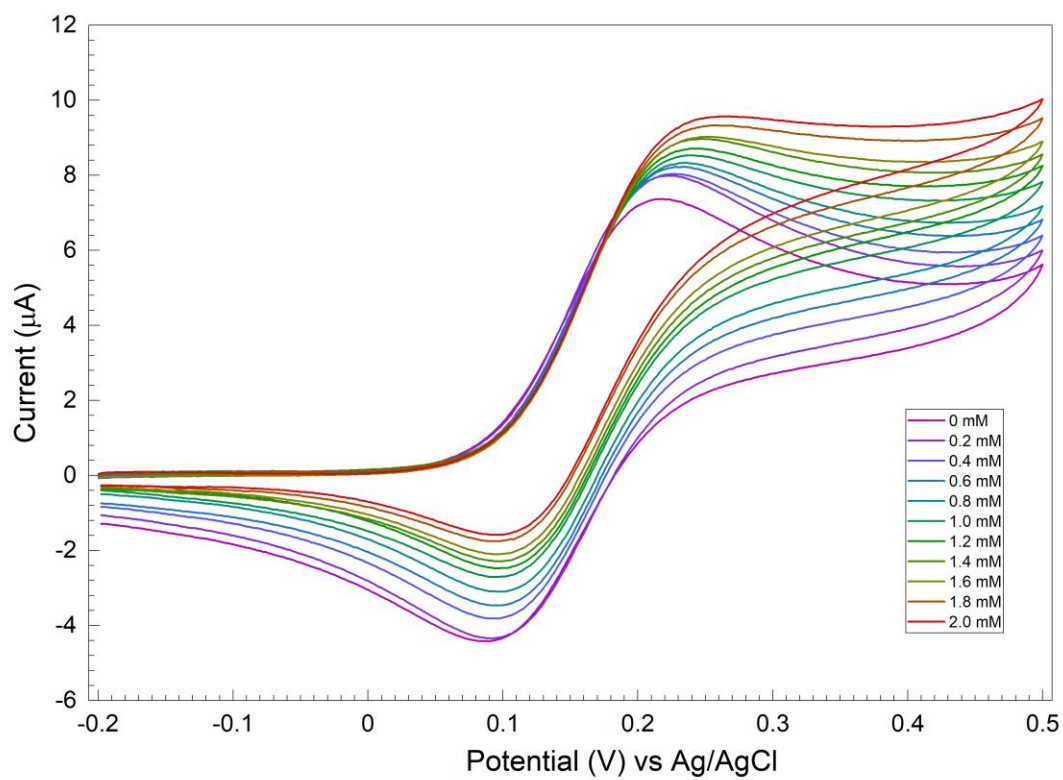
Figure 5.4: CV study of creatinine additions to bare SPCE in 1 M KOH and 1 mM ferrocyanide at 0.50 V vs Ag/AgCl. Calibration data shows LOD of 0.20 mM and a sensitivity of 0.30 ± 0.01 μA/mM for n=3.
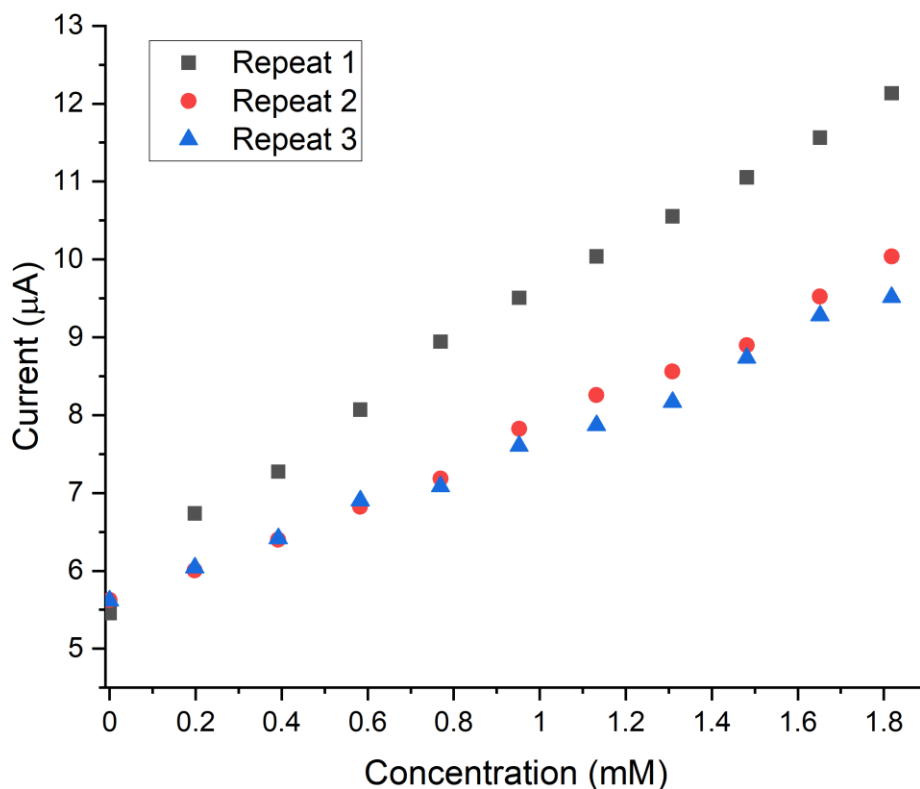
Figure 5.5: Current response as a function of concentration for 3 repeats performed on same bare SPE.

Fig. 5.4 and 5.5 show the results for 0.2 mM additions of creatinine. Repeats 2 and 3 in fig. 5.5 were conducted consecutively on the same, rinsed SPCE in fresh solution. It is noted that the first set has a higher current response than the subsequent sets. In set 1 the data showed a greater sensitivity of 25.3 μA mM^{-1} cm^{-2} but the linearity of R^2 = 0.984 gave an LOD of 150.7 μM and the LOQ was 502.4 μM. In the repeated sets, the sensitivity dropped slightly to 16.4 μA mM^{-1} cm^{-2} but with improved linearity with R^2 of 0.997 the LOD improved to 60 μM.

A number of previous studies have used SPE based creatinine detection in particular with copper based electrodes. Some of the non-enzymatic studies done on SPE based creatinine sensing are summarised below (table 5.1). It is to be noted that the creatinine study mentioned using SPE electrodes in urine have a much lower detection range for e.g., 10 – 2000 μM[38], where before sensor detection a dilution procedure must be required to detect creatinine in the above range as the clinical relevant range is between 4.4 – 13.3 mM[2]. This work however, could be further developed into a low-

cost sensor system for one spot analysis without requiring any pre-treatment (dilution) procedures before measurement.

Table 5.1: Summary of previous studies of creatinine detection with SPEs in different samples.

Modification of electrode	Detection range	LOD	Sample	Reference
Pre-treated SPCE/CuNPs	10 – 160 µM	0.1 µM	Artificial saliva	26
Paper-based SPCE (CuO/IL/rGO)	10 – 2000 µM	0.22 µM	Urine	38
CuNPs/SPCE	6-378 µM	0.0746 µM	Serum	39
Nafion/polyacrylic gel Cu(II)/Cu_2O/SPCE	1 – 2000 µM	0.3 µM	Saliva	40
Bare SPCE	2 – 18 mM	0.2 mM	Artificial urine	This work

5.3.2.1 Sensor analysis with artificial urine

To further evaluate the accuracy of detecting creatinine in artificial urine at lower and higher levels of the clinical reference range (4.4 – 13.3 mM), we performed standard addition study with three repeats (n=3) at each concentration. The accuracy of the analysis technique was checked using artificial urine (AU) solutions with different concentrations of creatinine (2 mM, 10 mM, 17 mM and 25 mM creatinine in AU). It is to be noted that the normal range of creatinine in urine is between 4.4-13.3 mM[2]. Creatinine levels in urine out of this range may indicate kidney conditions in particular chronic kidney disease (CKD), therefore the sensor was tested at these creatinine concentrations in AU (table 5.2). . The results for a 10 mM "unknown" addition from creatinine solution in artificial urine are presented in Figure 5.6. The results are also summarised in Table 5.2.
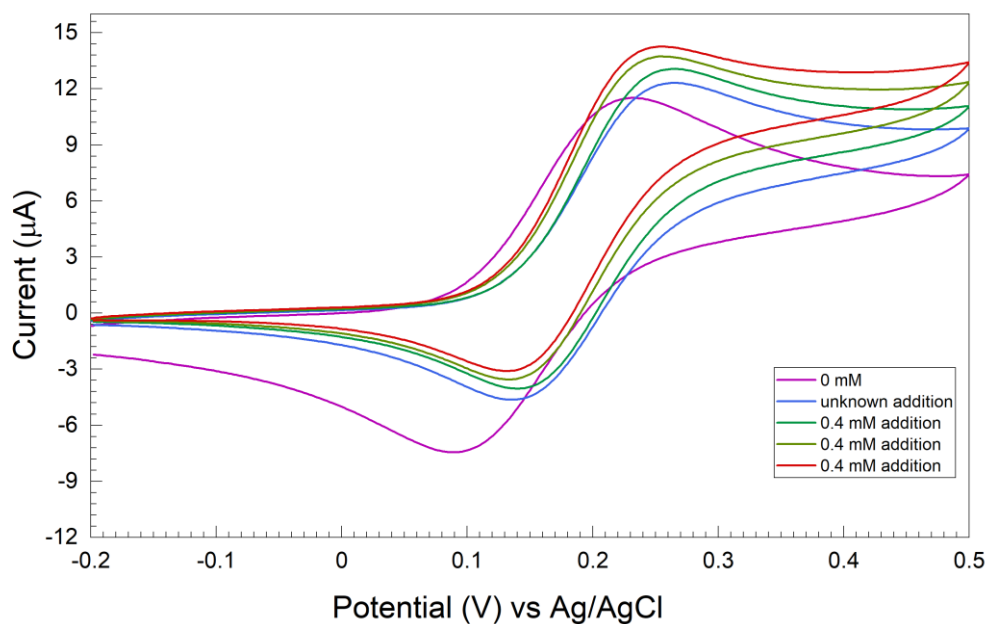
Figure 5.6: CV for 10 mM unknown addition from creatinine solution in artificial urine (with three known 0.4 mM creatinine additions from 200 mM stock).

Table 5.2: Recovery studies with creatinine at different concentrations using the bare SPE system in electrochemical cell (n=3).

At 0.5 V vs Ag/AgCl				
1 ml added from stock to 10 ml 1 M KOH + 1 mM ferrocyanide				
CR stock in AU (mM)	Spiking (mM)	Detected (mM)	Error %	Recovery %
2	0.18	0.04 ± 0.02	75.8	22.2
10	0.91	0.51 ± 0.09	43.9	56.0
17	1.55	0.77 ± 0.12	50.2	49.7
25	2.27	1.36 ± 0.23	40.16	59.9

This work shows significantly low recovery (22.2 %) at lower concentrations of 2 mM creatinine in artificial urine. The trend shows that there is maximum error of 75.8% at lower creatinine concentrations in artificial urine (2 mM CR in AU), which means the sensor is not very sensitive and selective at lower concentrations. The error % is lower and recovery % is higher at higher concentrations in comparison (at 10 mM, 17 mM and 25 mM). Literature studies on creatinine detection with SPEs show recovery % varying between 84.9% and 101.15% as summarised in table 5.3.

Table 5.3: Literature summary of recovery studies performed on real samples with SPEs for creatinine detection.

Modification of SPE	Sample	Recovery %	Reference
(CuO/IL/ERGO/SPCE) (copper oxide and ionic liquid composite-rGO/SPCE	Serum	98% to 101.15%	38
PVA gel-Cu(II) PEDOT:PSS/cuprous oxide nanoparticles	Sweat	92.1%	41
Cuprous nanoparticles encapsulated by polyacrylic acid (PAA) gel-Cu(II)	Urine	84.9%	40
Copper	Serum	95.6% and 98%	39

The highest recovery found in our creatinine bare SPE study as part of this project was 59.9%, which is significantly much lower than seen in other studies in literature. Using nanomaterials including copper, would significantly enhance the response current and sensitivity and selectivity of the sensor, giving much higher recoveries. Additionally, studies have also used PVA and PAA gel-based sensors to form a matrix with the metal nanoparticles, such that the catalytic activity is maintained. We studied this (*discussed later in this chapter*), where PVA hydrogel was used to form a matrix with ferrocyanide and KOH, such that the sensor can be effectively used for a test without pre-treatment of the sample. Therefore, further optimisation of the system is required to achieve higher recoveries and lower errors. This could be done through SPE modification with high conductivity materials including carbon black (CB) or reduced graphene oxide (rGO), which may enhance the current response and improve sensitivity. The literature in Table 5.3 also shows gels and liquids have been successfully employed. The mechanism of these hydrogels such as PVA are not clear, but they may serve to improve the SPE performance in the alkaline ferrocyanide system as well. This is explored later in section 5.3.7.

5.3.2.2 Interference analysis with bare SPEs

Interference with ascorbic acid (AA), uric acid (UA) and glucose were analysed using cyclic voltammetry (CV) on the bare SPE (fig. 5.7). It was evident that there was a significant interference from UA and AA (seen as oxidation at approximately 0 V vs Ag/AgCl) on bare SPE in 1 mM ferrocyanide and 1 M KOH solution.

It is also evident that glucose does not interfere with this creatinine sensing system at 0.5 V vs Ag/AgCl and was not further analysed. Further work to reduce this interference with AA and UA, a Nafion film with carbon black (Nf/CB/SPE) system was investigated to allow an enhanced redox response (due to high conductivity of CB) and at the same time suppress interference (due to Nf film that prevents entry of AA and UA to the surface of the SPE causing less extent of oxidation and interference in the system).
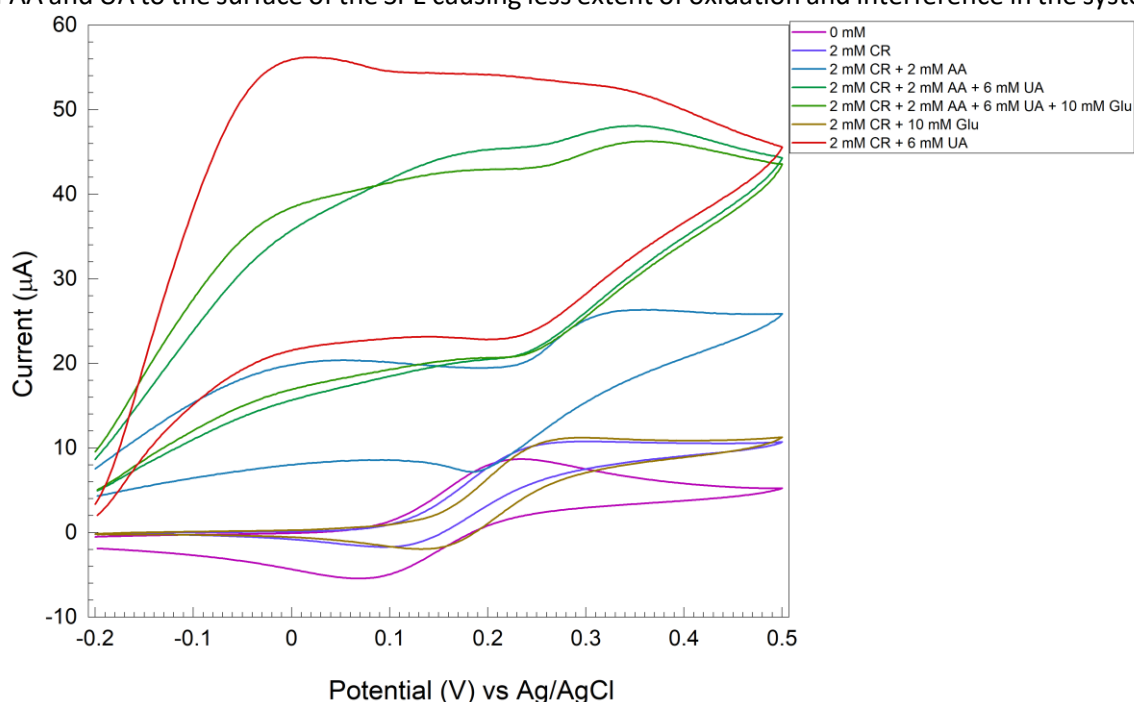
Figure 5.7: Interference analysis with AA, UA and glucose on bare SPE system.

These are discussed in the following sections.

5.3.3 Nafion modified SPEs

Nafion (Nf) was investigated to reduce the extent of interference of AA and UA as it has been seen to have a similar behaviour on GCE sensor platform *(Chapter 3).* Nafion based creatinine sensors have been previously developed enzymatically [42, 43] and non-enzymatically [44, 45]. In *Chapter 3*, a 2 wt% Nf solution was considered as the optimised concentration for creatinine detection and was therefore used in this study with SPEs. A study was performed to optimise the scan rate which should be used for the electrochemical study on creatinine detection using the Nf/SPCE. It was necessary to choose

an optimised scan rate that favours redox response and resident time at the electrode surface. The slower the scan rate, the more time for ferrocyanide to move through the Nf film onto the surface of the SPE where it is oxidised. However, if the scan rate is too low, it will cause mass transport limitations and a larger diffusion layer develops and the observed currents will be much lower affecting the sensitivity of the sensor. Two scan rates, 5 and 50 mV/s, were tested in 1 mM ferrocyanide in 1 M KOH. Disappointingly, there was no clear redox couple for the ferrocyanide at either of the scan rates, A slight oxidation was observed from around 0.6 V/ Ag/AgCl for both scan rates (fig. 5.8). Therefore, 50 mV/s scan rate was chosen for further evaluation of electrochemical response to creatinine. This scan rate study was done on the same SPE.

This CVs in Figure 5.8 clearly shows the high resistance caused at the surface of the SPE due to the Nf film. This has also been reported previously in another study, where Nf film causes decrease in currents due to higher resistance, hindering the electronic exchange at the surface of the electrode[46]. Nevertheless, it was hoped that despite no reversible redox coupe for the ferrocyanide being seen, that the oxidation at ca. 0.6 V would be enhanced by the presence of creatinine.
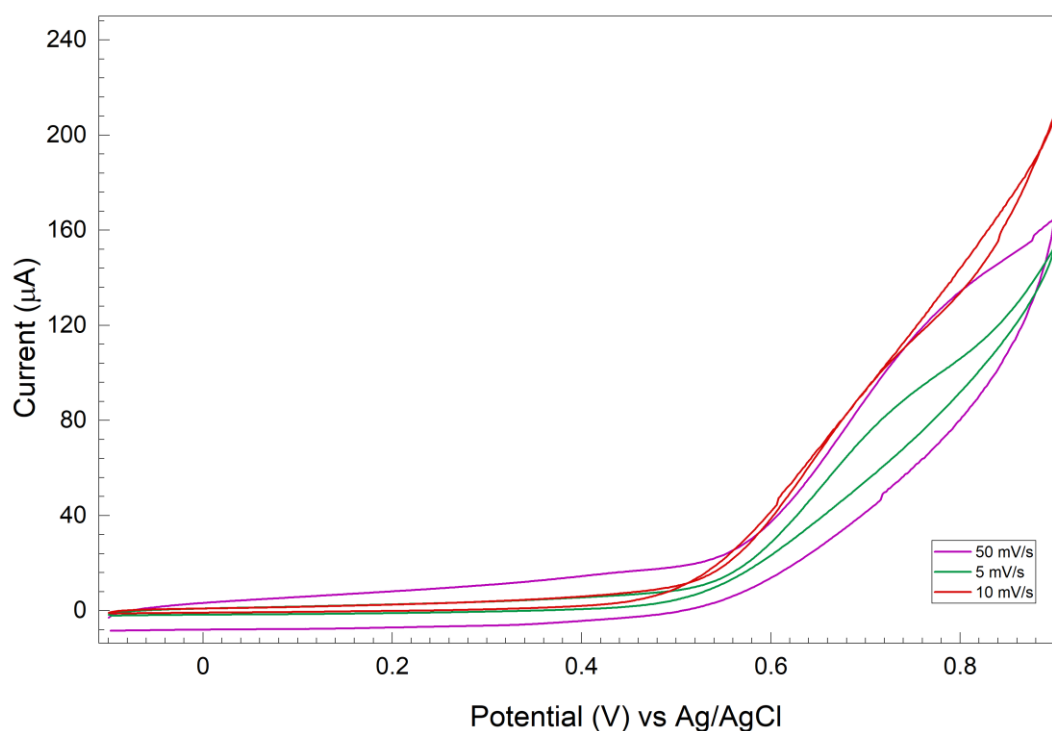

Figure 5.8: CV study on a Nafion modified SPCE in 1 mM ferrocyanide and 1 M KOH solution at different scan rates.

5.3.3.1 Electrochemical detection of creatinine and interferences

Creatinine additions (2-6 mM) were performed on Nf/SPCE and analysed using cyclic voltammetry (CV) (fig. 5.9). Although there was a current increase at 0.9 V (vs Ag/AgCl) with addition of 2 mM creatinine to 1 M KOH and 1 mM ferrocyanide solution, no linear current response was observed on further creatinine additions. Furthermore, no redox response was observed meaning the Nf film was highly resistive towards electron transfer processes as mentioned before. Therefore, it was decided that a conductivity modifier would be necessary to decrease the resistivity of the film (section 5.3.4)

An interference study with ascorbic acid (AA), uric acid (UA) and glucose (Glu) was performed to understand if Nf prevents AA, UA and Glu from entering the Nf film and eliminates the high extent of interference due to oxidation at the surface of the SPE (seen at 0 V vs Ag/AgCl) which has seen to occur otherwise in case of bare SPE system (inset to fig. 5.9 – *more detail in bare SPE section*).

It can be observed from fig. 5.9 that oxidation of AA and UA that is present at -0.1 V vs Ag/AgCl and at higher potentials is not seen in CVs with Nf SPE, clearly showing that Nf film prevents oxidation of interferents at lower potentials. At a potential of 0.9 V vs Ag/AgCl seen in CV with Nf SPE, the interferents cause a decrease in current signal from when only creatinine was added in 1 M KOH and 1 mM ferrocyanide solution. There is a 23 % decrease in the current as a result of interferences and the current only in presence of creatinine observed at 0.9 V vs Ag/AgCl. It is also to be noted that glucose does not interfere with the redox system as observed in the case of the bare SPE system and in fig. 5.10 (inset), and was not further explored in terms of interference studies.
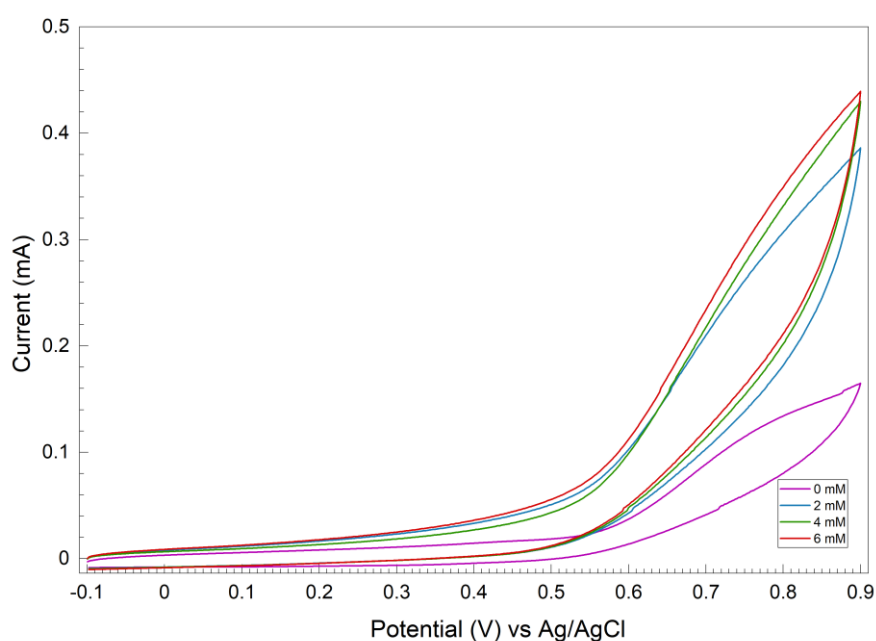
Figure 5.9: CV study with creatinine additions to Nf/SPE in alkaline ferrocyanide at 50 mV/s scan rate.
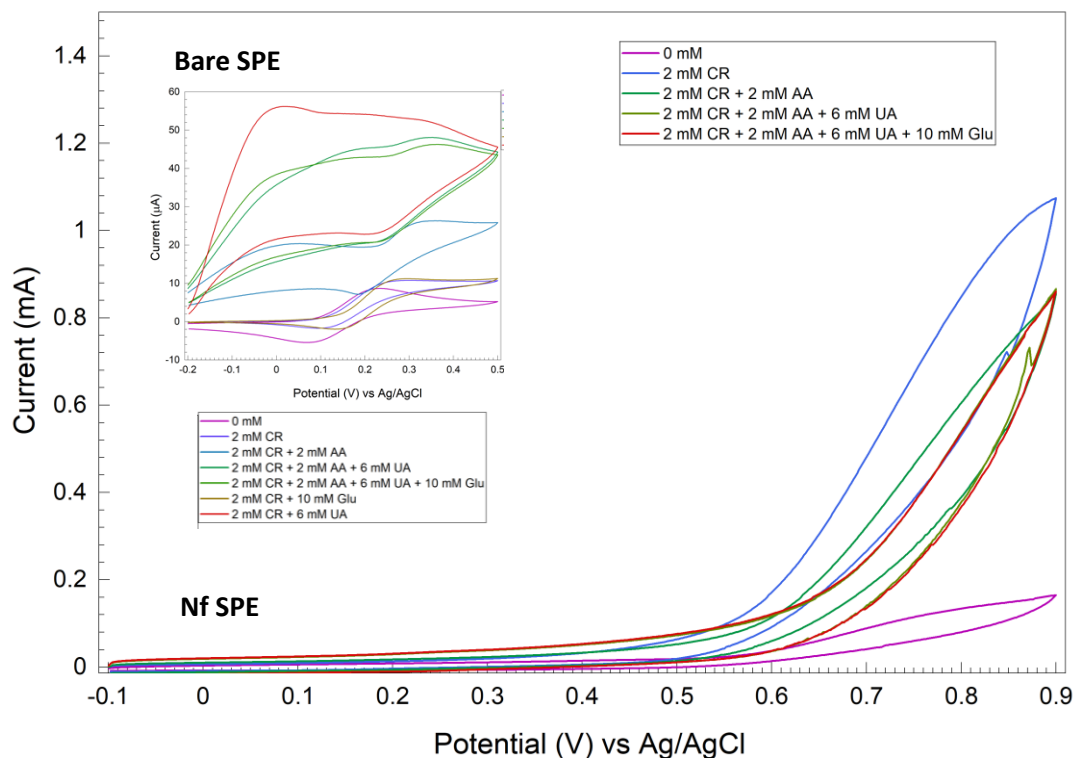
Figure 5.10: Interference analysis with UA, AA and Glu on Nf SPE in 1 mM ferrocyanide and 1 M KOH (Inset to figure: interference analysis comparison with bare SPE)

5.3.4 CB/Nafion modified SPEs

Carbon black (CB) based SPEs have been previously reported for electrochemical sensing applications [22, 47], due to their significantly enhanced electrochemical behaviour as a result of a large number of defect sites reported on SPEs. The peak-to-peak separation has been observed to decrease, with increase in anodic and cathodic peak currents, showing higher electron transfer rates [48]. Additionally, the low cost of CB makes it suitable for development of low cost SPE based disposable sensors for creatinine detection. This work for the first time presents use of CB/Nafion SPEs for creatinine detection.

A stable dispersion of CB/Nf (2 wt% nafion with 10 mg CB as *optimised in Chapter 3 with bare GCE system*) was obtained by sonicating the solution for 20 mins, to have a homogenous, stable ink-like suspension. SEM technique as mentioned, was used to confirm the presence of uniform film of CB/Nf on the surface of SPEs.

5.3.4.1 Blank studies in 1 mM ferrocyanide and 1 M KOH

A CV scan of the CB/Nf/SPCE in 1 mM ferrocyanide at a scan rate of 50 mV/s showed no ferri/ferrocyanide redox response (fig. 5.12). In repeat studies, beyond 0.5 V vs Ag/AgCl, similar to the range showed in Figures 5.12 and 5.13, water oxidation was seen in the CV. It was hypothesised that no ferri/ferrocyanide redox response could be seen due to insufficient time for ferrocyanide and KOH to pass through the CB/Nf film to the surface of the SPE for oxidation or reduction at higher scan rates. Therefore, a lower scan rate (10 mV/s) was tried, as shown in Figure 5.13. Here, the redox couple was observed, a possible result of exhaustive electrolysis of ferri/ferrocyanide at thin film conditions on the surface of SPEs[49], although the peaks were less defined in comparison to that on a bare SPCE due to the well-known insulating behaviour of the Nafion film [50] (fig.5.13).
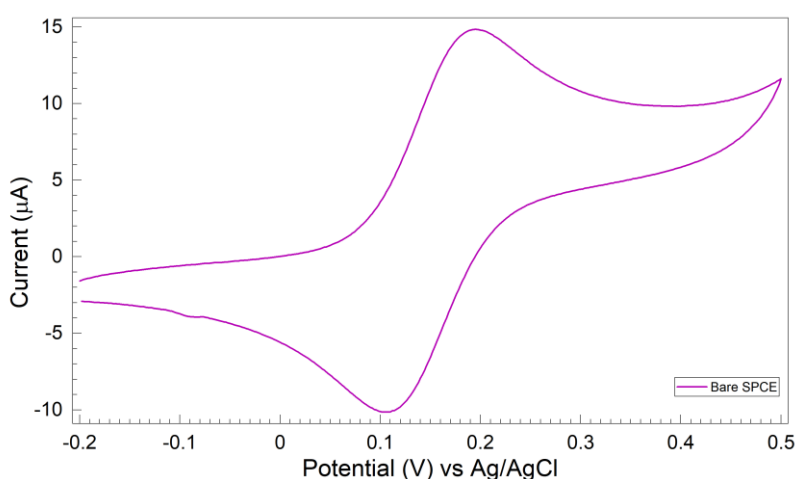

Figure 5.11: CV performed on a bare SPCE at 50 mV/s in 1 mM ferrocyanide and 1 M KOH (blank) without creatinine.
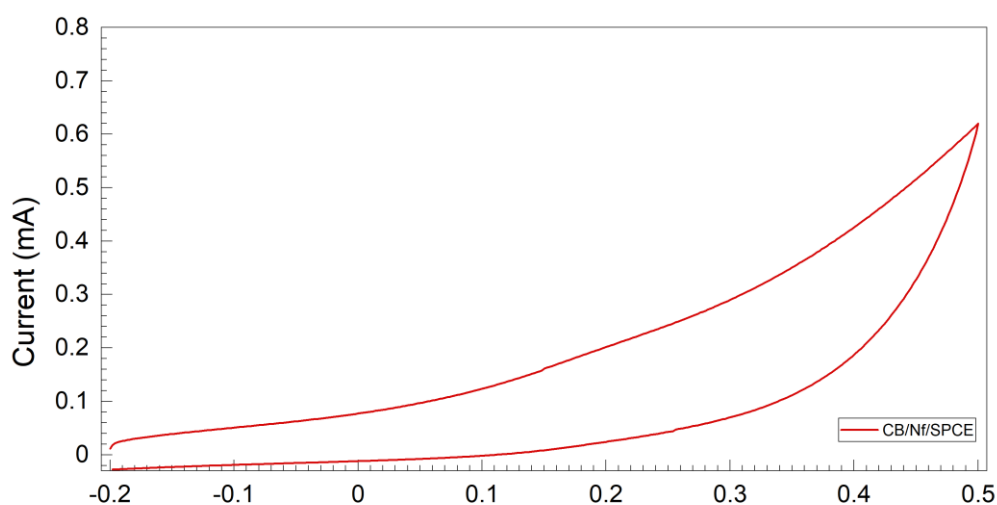
Figure 5.12: CV performed on a CB/Nf/SPCE at 50 mV/s in 1 mM ferrocyanide and 1 M KOH (blank) without creatinine.
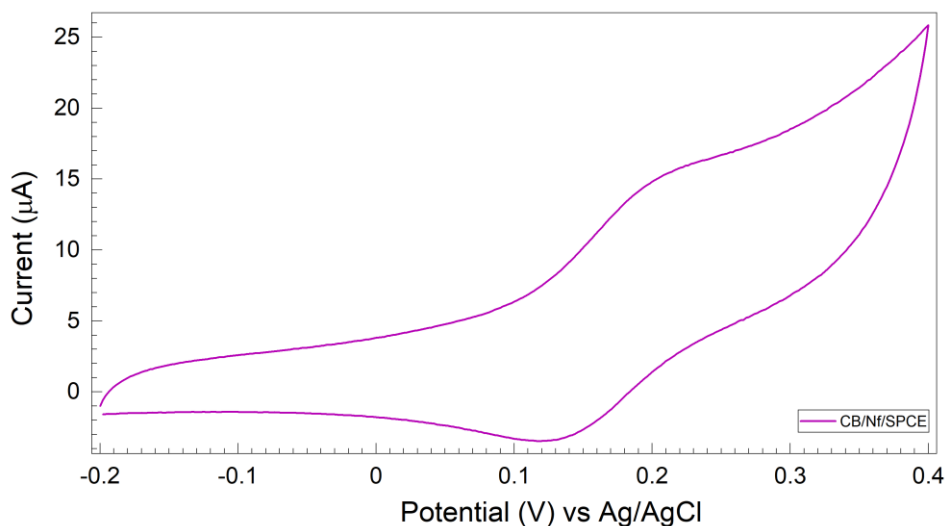
Figure 5.13: CV performed on a CB/Nf/SPCE at 10 mV/s in 1 mM ferrocyanide and 1 M KOH (blank) without creatinine.

Slower scan rates were therefore used in subsequent studies in the presence of creatinine.

5.3.4.2 Electrochemical detection of creatinine

CV studies at a scan rate of 10 mV/s, were applied for electrochemical detection of creatinine initially in the range of 0-8 mM creatinine in 1 M KOH and 1 mM ferrocyanide solution.

An initial CV study (fig. 5.14) shows a linear increase in oxidation current at 0.4 V vs Ag/AgCl with creatinine additions in the range 2-8 mM with the CB/Nf/SPCE. While there is a positive increase in current response with increasing additions of creatinine, the CV shows there is not a linear increase. Further repeat experiments (n=3) were done to obtain ae calibration curve and to estimate the LOD and LOQ by considering the region below the upper limit of linearity in case the calibration plot is in the form of a curve. Figure 5.15 shows one of the three repeats undertaken with the same CB/Nf/SPE for 2 mM additions from 0 – 20 mM creatinine.
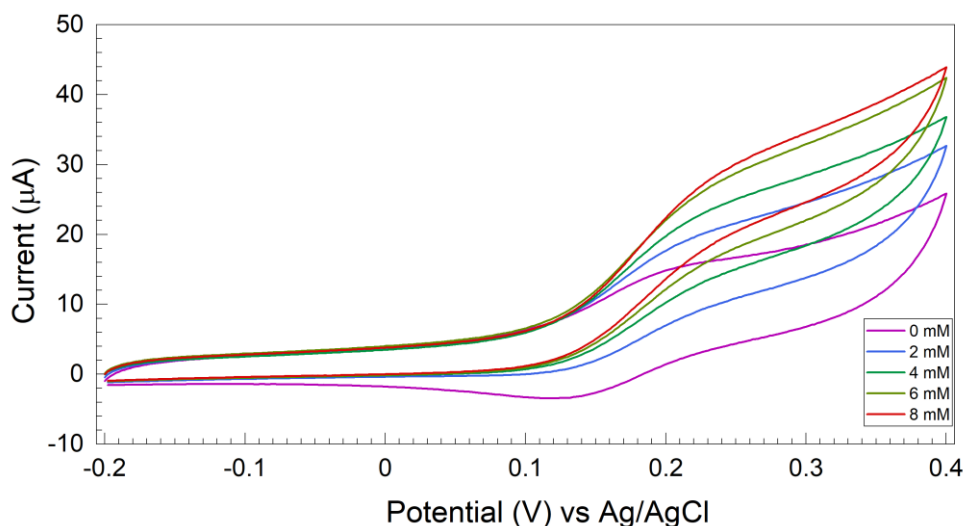
Figure 5.14: Electrochemical detection of creatinine in the range 0-8 mM on CB/Nf/SPCE with a scan rate of 10 mV/s.

Volume correction was performed (considering the adjusted volume and the total moles) on this CV analysis as a result of making 100 µl creatinine additions to cell at each 2 mM concentration increase. The volume additions affected significantly at higher concentrations.

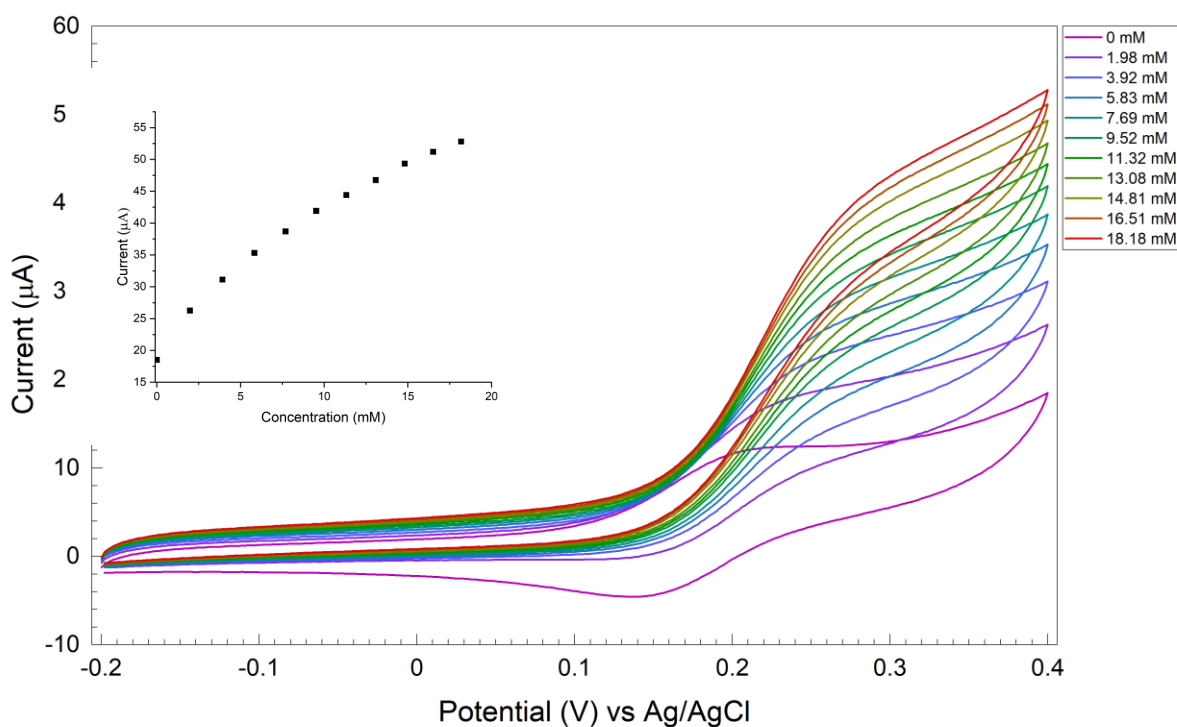*Figure 5.15: Electrochemical detection of creatinine in the range 0-20 mM on CB/Nf/SPCE with a scan rate of 10 mV/s (n=3).*

A similar EC′ redox mechanism (as seen with bare SPEs) is observed with creatinine additions to CB/Nf/SPEs (fig. 5.15). First the ferrocyanide converts to ferricyanide electrochemically (in the forward scan) as the potential is scanned positively. As the ferricyanide forms, it reacts with creatinine

oxidising it (causing increasing anodic currents) and redox conversion of remaining ferricyanide back to ferrocyanide occurs in the reverse scan. As a result of some ferricyanide is consumed for the creatinine oxidation, the cathodic current occurring due to conversion of ferricyanide to ferrocyanide decreases.
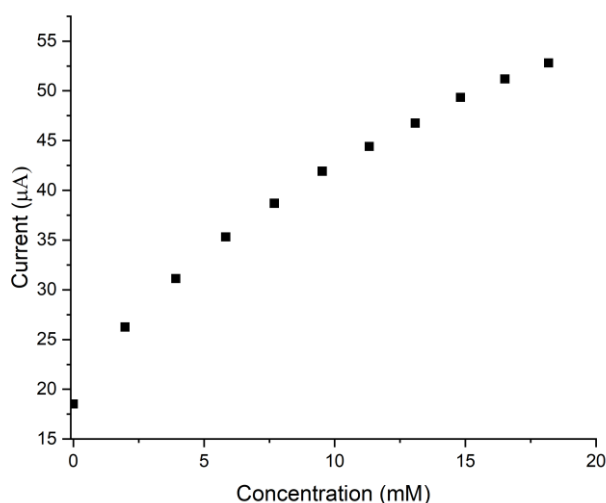
Figure 5.16: Calibration graph for creatinine detection with CB/Nf SPE analysed from CV at 0.4 V vs Ag/AgCl.

Figure 5.15 shows the calibration data for the CVs in Fig. 5.14, for the current response at 0.4 V vs Ag/AgCl. A curved calibration graph is observed in this case. A non-linear increase in current as the creatinine concentration increases is observed despite volume correction. This curving data set is believed to be a result of the CB/Nf film that limits the rate of diffusion of creatinine and ferrocyanide molecules to the electrode surface, when the creatinine concentration is high. Despite a non-linear response, the LOD and LOQ could be determined as 1.09 mM and 3.63 mM, respectively based on the first four data points in the calibration graph (fig. 5.15). Further optimisation of the film thickness, the scan rate, and CB quantity could overcome the challenges observed here.

The data could be repeated in two studies on the same electrode, but the response for the third calibration could not be obtained because of change in the surface of the SPE. Qualitatively, the SPE looked different due to repeated calibrations. The repeatability in CV response could not be obtained on different CB/Nf/SPEs either. This is a significant problem in the production of a sensing platform where consistency is key to a successful product. Fig. 5.17 shows the CB/Nf modified SPE.

Figure 5.17: CB/Nf modified SPEs before use in electrochemical study.

5.3.4.3 Interference study with CB/Nf/SPEs

An interference study with AA and UA was performed on a CB/Nf/SPE to check the extent of interference that occurs on bare SPEs at lower potentials in presence of alkaline ferrocyanide. In comparison to interference seen with bare SPEs (Fig 5.18), the oxidation current response at -0.1 V vs Ag/AgCl is significantly lowered, evident from Fig. 5.18. While it is difficult to compare the data directly, due to different scan rates and the presence of ferrocyanide in Figure 5.18, it is evident that the AA and UA do not give rise to a large oxidation response at 0 V. The baseline of the current response is shifted relative to the blank and CR only data sets, but it is a background offset that could be accounted for in a further developed sensing system. Overall, the CB/Nf on the surface of SPE significantly reduces the extent of interference from UA and AA.
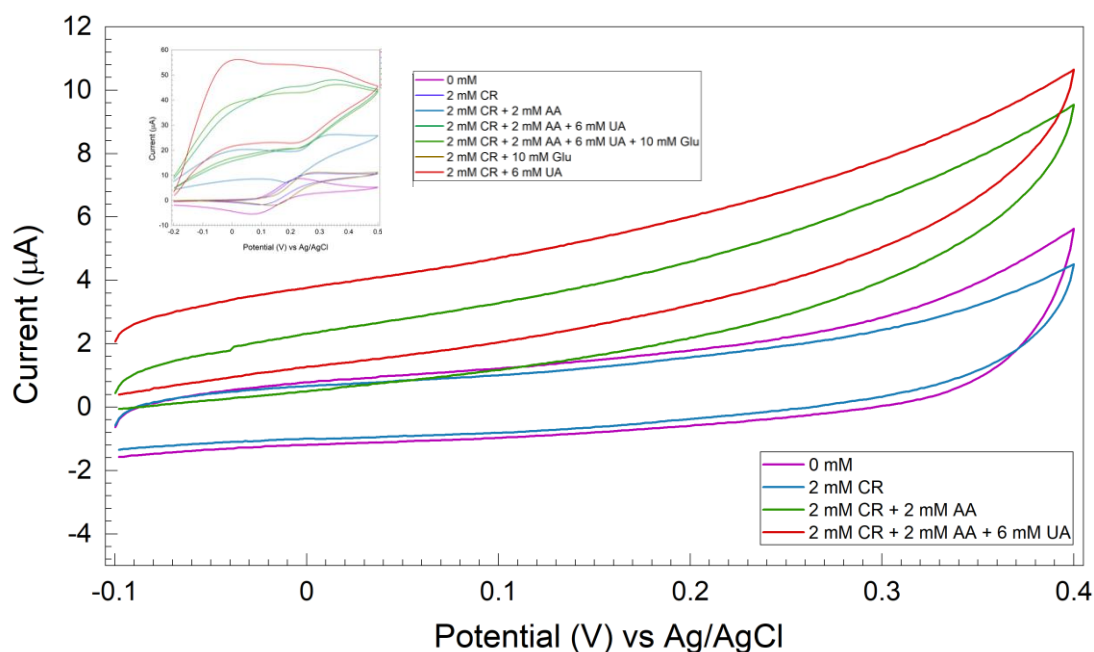

Figure 5.18: Interference study with AA and UA using CB/Nf/SPE (inset – bare SPE interference study for comparison).

5.3.5 Electrochemical performance of PVA gel/KOH-ferrocyanide film SPEs

Due to the resistivity and diffusion limitations perceived of the CB/Nf based SCPEs, the idea to investigate SPE creatinine systems for one-spot analysis using bound ferrocyanide and hydroxide was developed. A novel procedure with the aim to have ferrocyanide-KOH film on the surface of SPEs was followed. Two brands of SPEs were studied in this section, one from Flex Medical Solutions and the Metrohm DropSens SPEs already discussed in previous sections.

Hydrogels consist of 3D network of polymers (fig. 5.19) that swell and can retain water without dissolving[51]. Hydrogels can be categorised into physical or chemical gels[52]. PVA improves the mechanical stability of the hydrogel significantly[52]. The idea is to hold the ferrocyanide and KOH in a polymer matrix that is stable for the electrochemical study. In this section of the initial study, PVA gel was drop cast on the surface of SPEs, after immersing in 1 mM ferrocyanide. After the gel was dry, the SPEs were then immersed in 1 M KOH solution. CV studies were then performed.
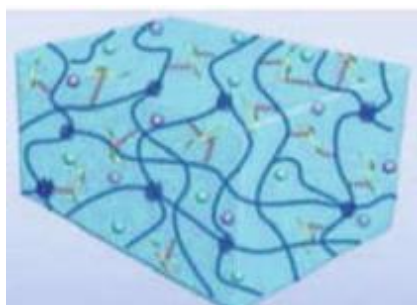
Figure 5.19: Schematic of a typical hydrogel[1].

No ferri/ferrocyanide redox response was observed on addition of 60 µl of 20 mM creatinine (CR) solution in DI water as a spot test on the surface of SPE (fig. 5.20 and 5.21). Repeat with a second SPE (D2) showed no redox peak beyond 0.5 V vs Ag/AgCl, but showing a result in water oxidation instead. A possible explanation to the conclusion was the fact that there was no ferrocyanide or KOH present in the PVA gel layer as a result of dispersion of ferrocyanide or KOH from the SPE surface back into the 1 M KOH solution. It also suggests that the PVA gel was not physically cross-linked, not allowing retention of the film, as a result of drop casting PVA gel on SPE surface according to the procedure followed.

Figure 5.20: SPE setup for spot test on ferrocyanide-KOH film SPE D1.
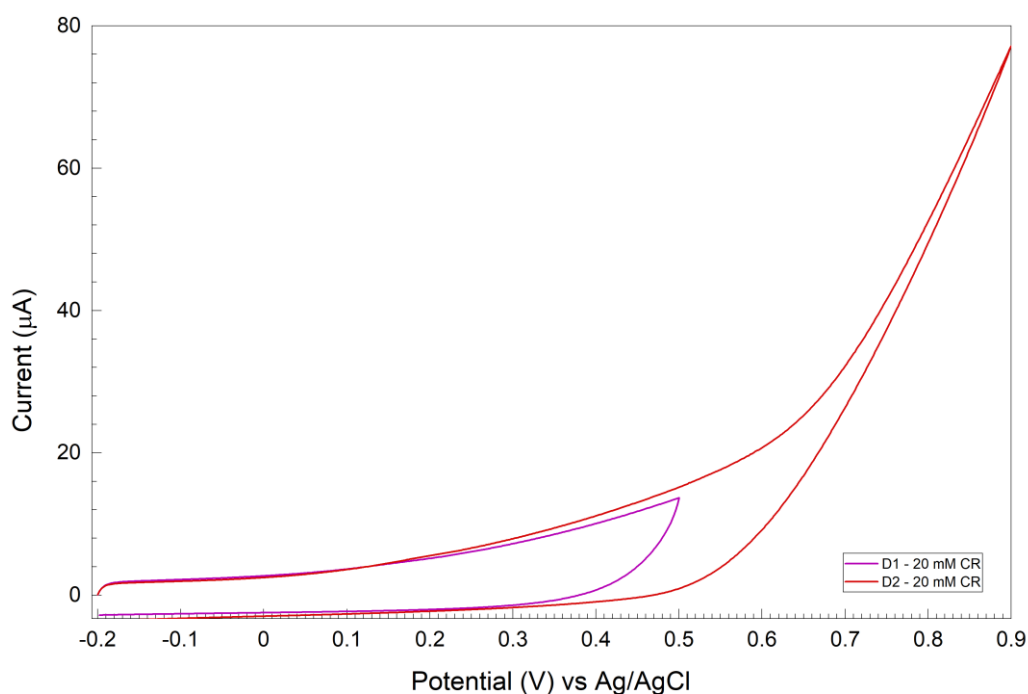
Figure 5.21: Electrochemical CV study with 2 mM creatinine addition on prepared ferrocyanide-KOH film SPEs at a scan rate of 50 mV/s with a step potential of 2 mV.

Further studies then investigated a way to optimise a way in producing a PVA hydrogel (with the immersion method in 1 mM ferrocyanide and 1 M KOH solution) that would have the capability to have polymeric chains that could form a 3D network capable of forming a network of ferrocyanide and KOH in the form of a film on the surface of the SPEs.

5.3.6 PVA hydrogel/ferrocyanide-KOH film based SPEs

Hydrogels are hydrophilic 3D polymeric structures that have large water content [53]. A polyvinylalcohol (PVA) gel was prepared by the physical cross-linking method of cyclic freeze-thaw method to "hold"

the ferrocyanide-KOH on the surface of the SPEs. The idea of using a ferrocyanide hydrogel was followed from a study by Russo et al. [34]. To the best of our knowledge, there is no study that combines designing of PVA based ferrocyanide hydrogels. Further part of the study performed followed a freeze-thaw procedure of producing PVA hydrogel on the surface of SPE from[54] , where after drop casting a 10 % w/v PVA gel on SPEs, the electrodes were placed in freezer at -20°C for 24h. The SPEs were then immersed in 1 mM ferrocyanide and 1 M KOH solution for 20 mins with the aim to form a thin film on the surface. The free-thaw method is a physical cross-linking method that has two steps in the hydrogel formation – the freezing and the thawing stages. Freezing controls the ice crystallisation process and thawing allows formation of ordered polymeric 3D structures [53]. The idea is to have a considerably high swelling ratio such that ferrocyanide-KOH films can be retained on the SPE surface in the polymeric matrix.

Electrochemical CV study performed with addition of 2 mM creatinine, showed the ferri/ferrocyanide redox response although the response was not reversible with less defined oxidation and reduction peaks (fig. 5.22).
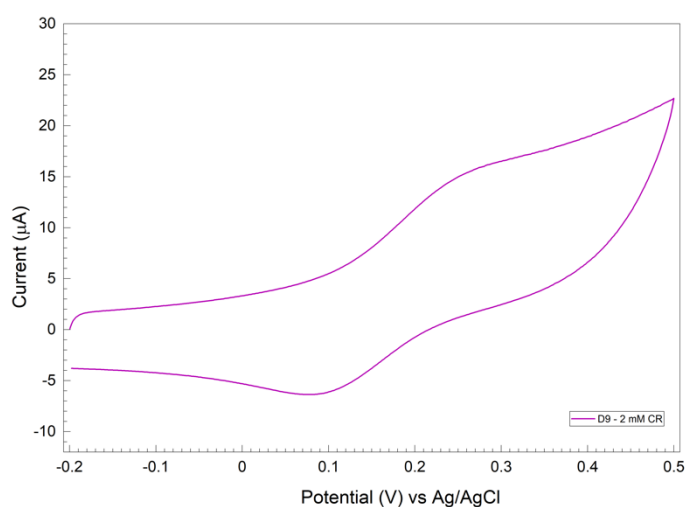
Figure 5.22: Electrochemical CV study on PVA hydrogel ferrocyanide-KOH film based SPEs with 2 mM creatinine addition at a scan rate of 50 mV/s.

Although, from fig. 5.22 it could be concluded that PVA hydrogel comprised part of the ferrocyanide-KOH film which can be observed as a ferri/ferrocyanide redox response in the CV. The next part of the procedure involved production of PVA ferrocyanide hydrogels with the aim to achieve a better ferri/ferrocyanide redox response (in terms of well defined oxidation and reduction peaks) by a more

efficient technique to form a network of ferrocyanide in a hydrogel matrix. Part of the procedure was followed from the study by Russo et al. [34].

5.3.7 PVA/ferrocyanide hydrogel/KOH SPEs

Initial study using PVA ferrocyanide hydrogels involved immersion in 1 M KOH for 10 mins (to form an alkaline film) after freeze-thawing method was used in forming the PVA-ferrocyanide hydrogel (not shown). The results confirmed no ferri/ferrocyanide redox response, possibly due to dispersion of ferrocyanide from the hydrogel into the 1M KOH solution during the immersion process, leaving no/low concentration of ferrocyanide in the PVA hydrogel resulting in no redox response. This allowed investigation into alternative ways of placing 1 M KOH on the surface of the SPEs by drop casting technique (for 24h) followed by production of the PVA-ferrocyanide hydrogels.

An initial blank (without creatinine) experiment was performed to check if the PVA-ferrocyanide hydrogel (with presence of KOH film) gave a reversible or quasi-reversible redox response to ferri/ferrocyanide, which would be ideal to proceed into for further experiments (fig. 5.23). A peak-to peak separation of 70 mV was obtained, showing well-defined quasi-reversible redox behaviour of the electrochemical system meaning electron transfer kinetics is not significantly sluggish in this case.
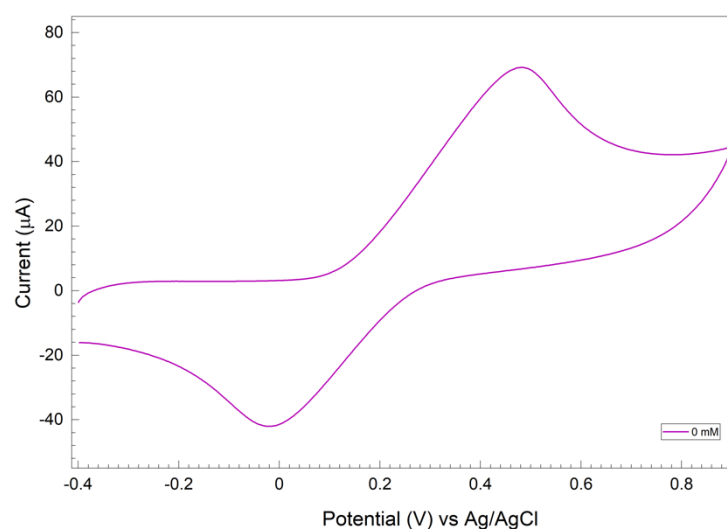
Figure 5.23: Electrochemical response at 50 mV/s obtained from PVA-
ferrocyanide/KOH hydrogels at 0 mM creatinine (blank).

Further CV test with creatinine addition was performed on PVA/ferrocyanide hydrogel SPEs prepared with drop casting 1M KOH (for 24h) to monitor the oxidation current, which increased with an addition of 2 mM creatinine (fig. 5.24). An increase in oxidation current at 0.9 V vs Ag/AgCl could be monitored, to generate a calibration graph of creatinine concentration vs oxidation current.
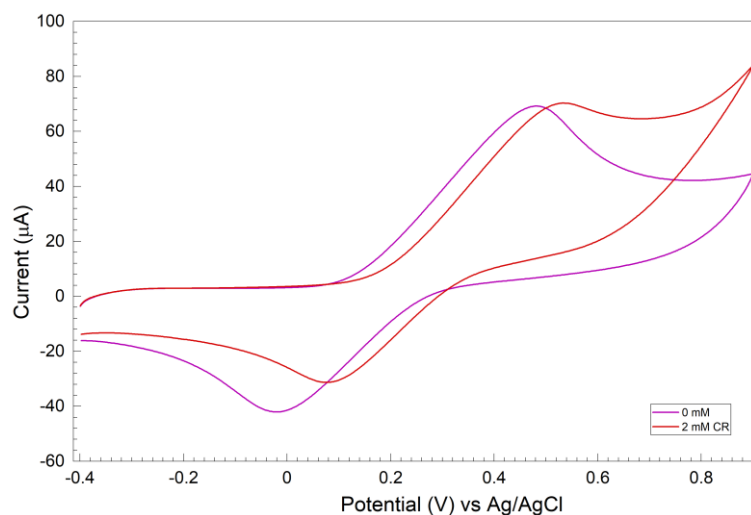
Figure 5.24: Electrochemical response from PVA-ferrocyanide-KOH hydrogel with 2 mM creatinine (CR) addition at 50 mV/s scan rate.

5.3.7.1 Electrochemical detection of creatinine

A CV test with 2 mM creatinine in DI water (fig. 5.25), 2 mM creatinine in artificial urine (AU) (fig. 5.27) and 20 mM creatinine in DI water (fig. 5.26) was tested on SPEs (Flex Medical Solutions) to see the effect on reproducibility. It is evident that there is significant variability in responses of peak oxidation currents meaning that the drop casting technique or the method of preparation of hydrogels is leading to variability and difference in hydrogel networks obtained on the surface of SPEs. Drop casting technique has been reported as limited in production of uniformly modified surfaces and therefore results in less reproducibility[55]. This could result in different localised concentrations of ferrocyanide and KOH on the surface of SPEs, then causing a varied response in oxidation current on addition of creatinine in DI water or AU. This can be minimised in future work by using an automated drop casting setup, to reduce the extent of variability or by printing ferrocyanide hydrogels on the surface of SPEs *(discussed in Chapter 6 on future work)*
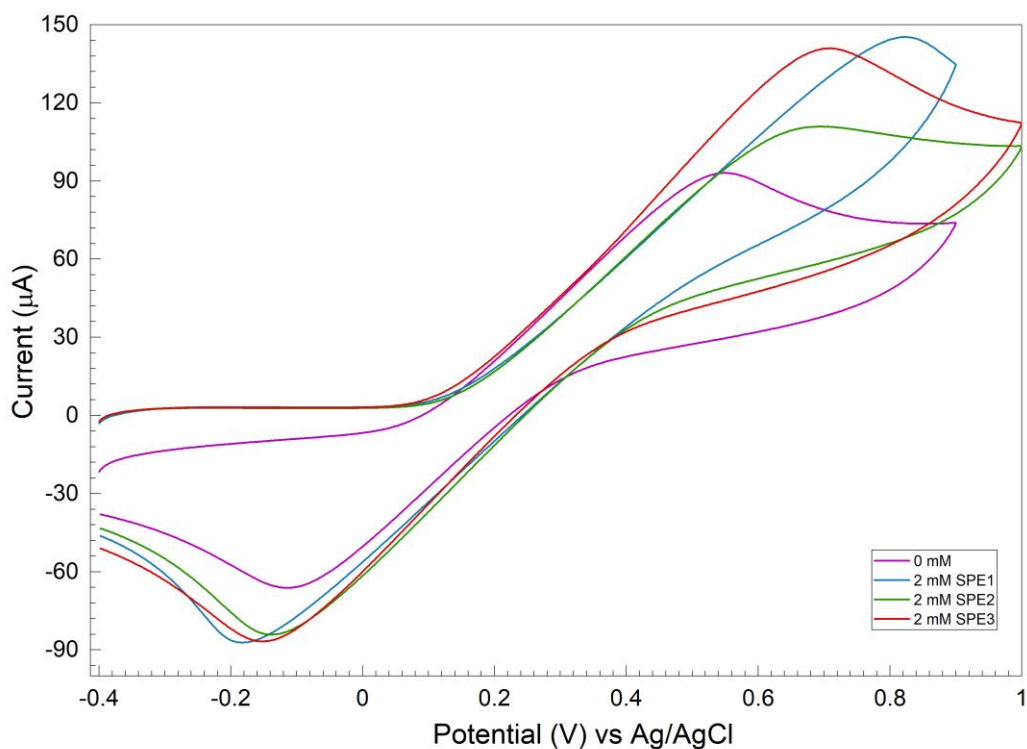
Figure 5.25: Repeatability CV study at 2 mM creatinine addition on different SPEs (Flex Medical Solutions).

It is evident that there exists different electron transfer kinetics along with different mass transport mechanism on each SPE (fig. 5.25), as a result giving variability in the oxidation currents. This is observed also in fig. 5.26 and 5.27. All processes exist showing quasi-reversible kinetics as the peak separation is greater than 59 mV (with n=1). It could also be possible as the hydrogels have been physically cross-linked by the freeze-thaw method, the PVA hydrogels may not form a fixed layer on the surface of the SPE, where a chemically cross-linked hydrogel could overcome this disadvantage and allow more consistent results (*more detail in Chapter 6 – Conclusions and future work*).
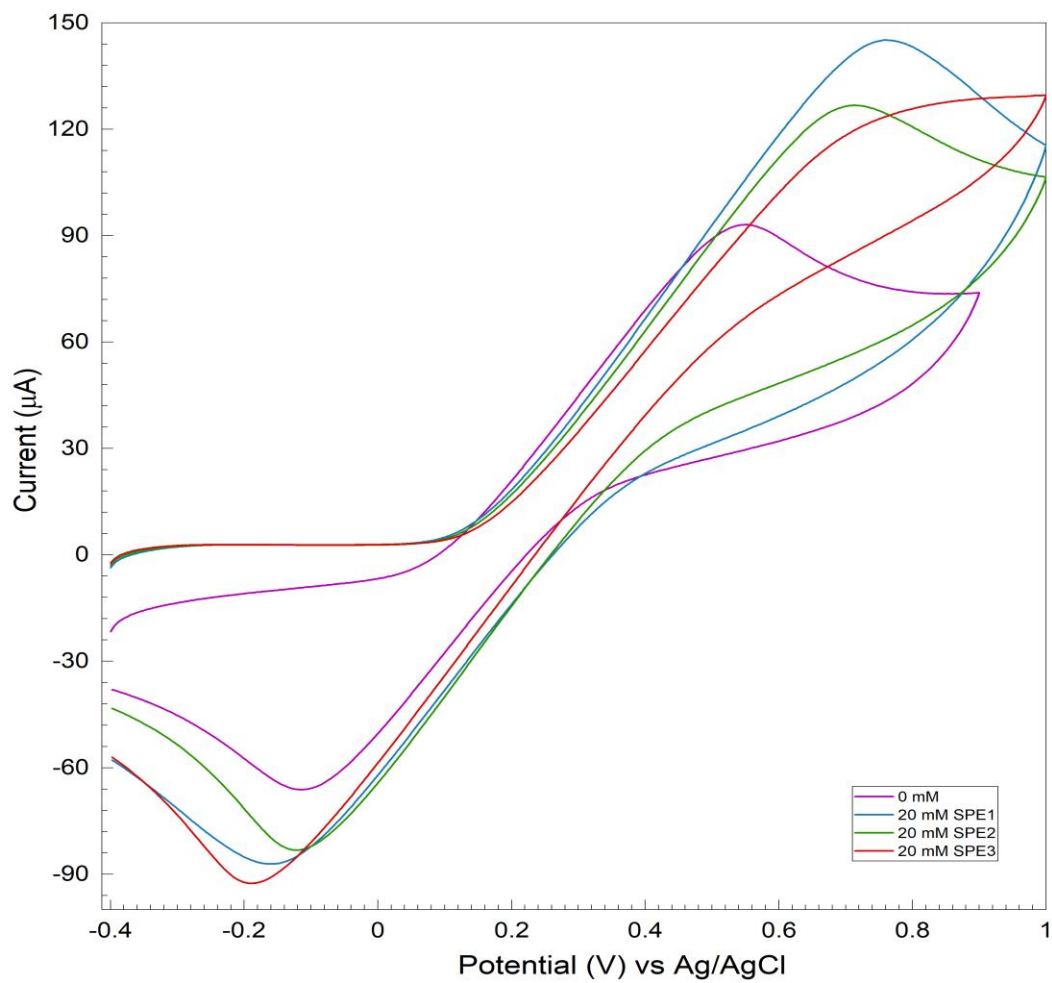
Figure 5.26: Repeatability CV study at 20 mM creatinine addition on different SPEs (Flex Medical Solutions).
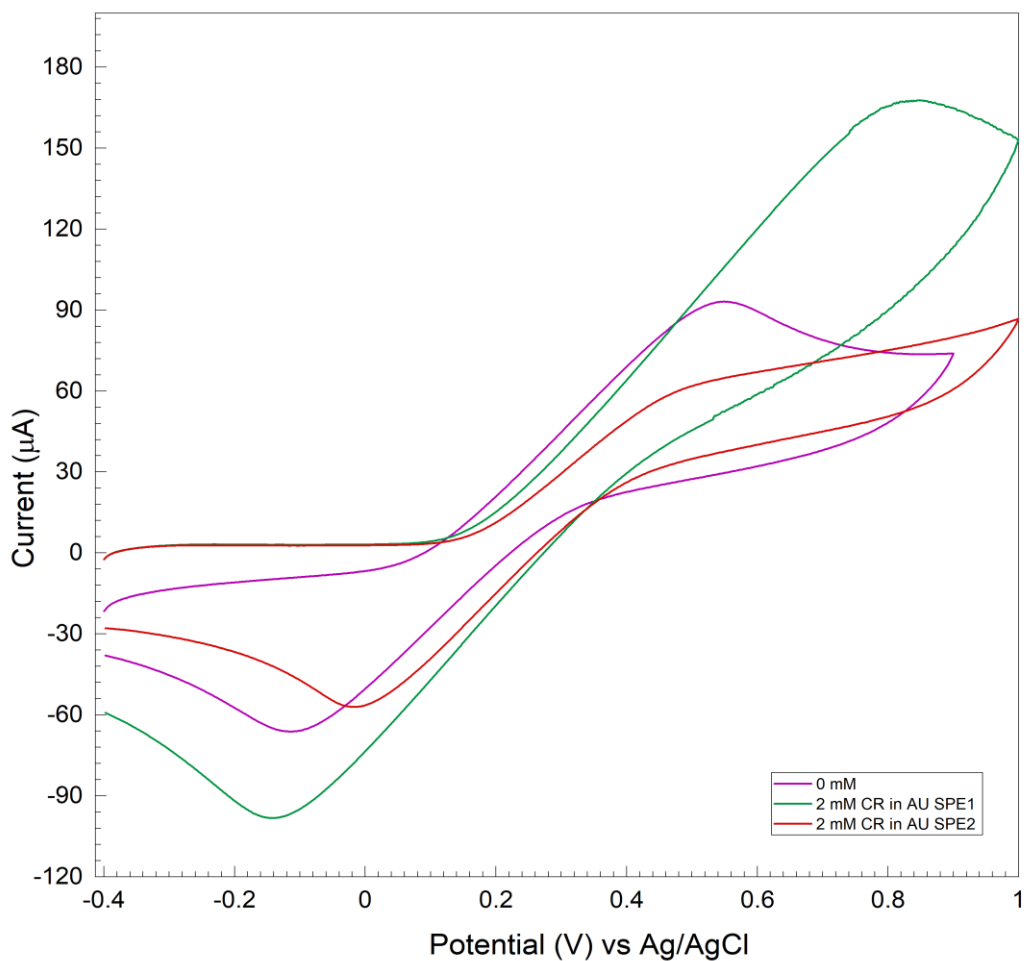
Figure 5.27: Repeatability CV study at 2 mM creatinine (in artificial urine) addition on different SPEs (Flex Medical Solutions).

Repeat studies with ferrocyanide/KOH hydrogels were also performed at a later stage with SPEs purchased from Metrohm DropSens. Similar results on variability in data (on different SPEs) with creatinine additions (for blank and 4 mM) were observed (fig. 5.28 and 5.29), However the quality in redox response was markedly improved.

159
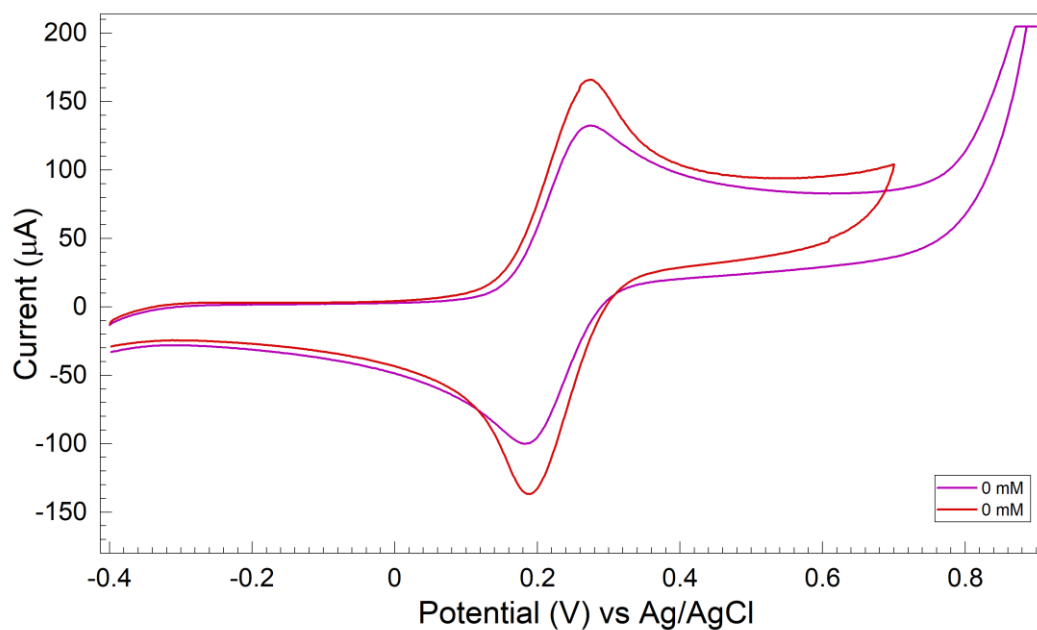
Figure 5.29: Blank study with PVA/ferrocyanide/KOH hydrogels on different Metrohm SPEs.
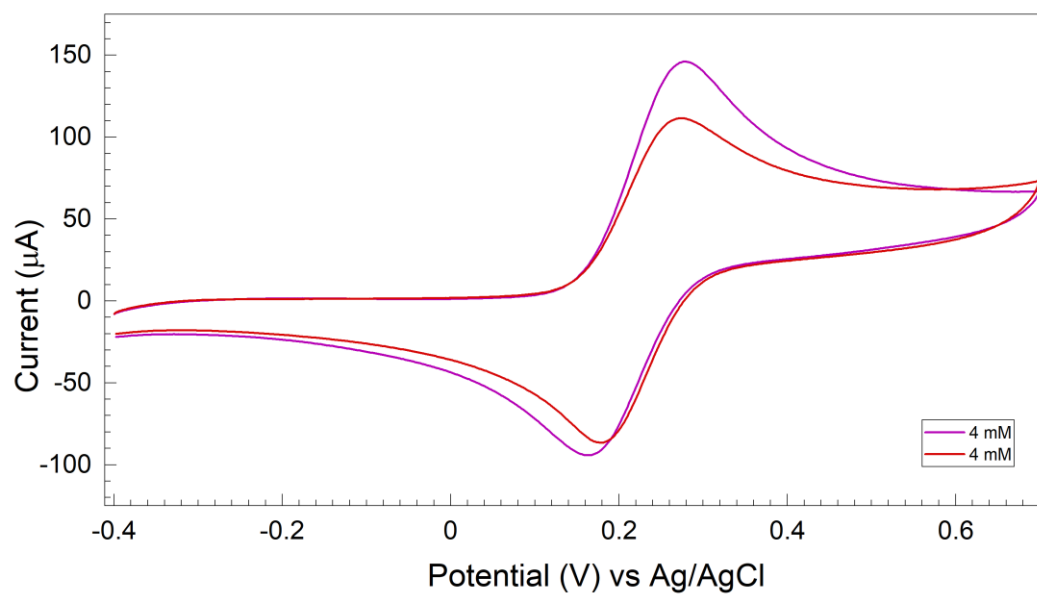
Figure 5.28: 4 mM creatinine additions study with PVA/ferrocyanide/KOH hydrogels on different Metrohm SPEs.

As a result of significant variability in results, interference study was not carried out for these SPEs.

5.3.8 Voltammetric performance comparison of SPEs

CV comparison in a blank solution of 1 mM ferrocyanide and 1 M KOH was made between carbon ink SPEs (Flex Medical Solutions) and carbon paste SPEs (Metrohm DropSens) using the ferro/ferricyanide redox system with 1 mM ferrocyanide in 1 M KOH. The peak separations were compared and analysed to check the reversibility from the CV study. Flex Medical Solutions SPEs resulted in lower reversibility in this alkaline the ferro/ferricyanide redox system. This may be also due to the nature of the conducting paths and carbon composition at the WE in the SPE specifically as studied before [56].
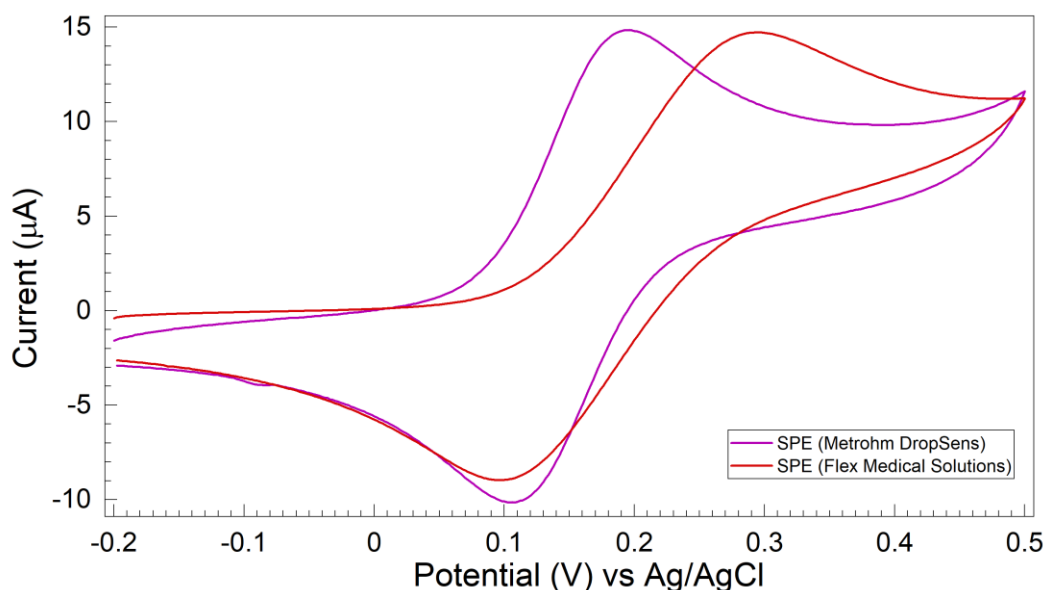
*Figure 5.30: CV study on bare carbon ink SPCEs (Flex Medical Solutions) and bare carbon paste SPCEs (Metrohm DropSens) in a blank solution of 1 mM ferrocyanide and 1 M KOH at a scan rate of 50 mV/s.*

Metrohm DropSens SPE gave more quasi-reversible behaviour with peak to peak separation of 100 mV (fig. 5.30), whereas this was 200 mV with the Flex Medical Solutions SPEs in this particular redox system.

It has been observed and reviewed previously that carbon ink SPEs may have higher resistivities than other conductive inks [56]. The charge transfer properties must be suited to the end-application. In this study, it was concluded that the carbon ink SPEs (Flex Medical Solutions) suffered charge transfer problems for our application in particular.

Further to this evaluation, SPEs (Metrohm DropSens) were used for further studies for development of creatinine sensing system.

5.4 Conclusions and future work

Current POC devices are expensive and with low reproducibility. This non-invasive, highly analytically reliable (able to detect healthy and unhealthy levels of creatinine) low cost method could add to overall reduction in costs in the healthcare systems. With some fine tuning this method can be optimised and introduced as a more robust POC device (than existing devices) with portable electronics at hospitals and GP surgeries. Although, creatinine could be detected at the bare SPE, the high extent of interference with UA and AA requires use of membrane systems like Nafion that can prevent entry of these interferents on the surface of the WE. Therefore, nafion/CB systems (that show reduction in interference with AA and UA in presence of creatinine) need to be further optimised to provide consistent results with creatinine detection. The SPE systems described in this chapter show that creatinine can be detected effectively using these electrochemical techniques.

The CB concentration in the ink (10 mg/ml) chosen was based on the results from the GCE study in *Chapter 3.* Although, an optimisation study could be useful where CB based nafion SPCEs can be optimised in terms of different CB dispersion concentration in particular for SPE setup. This could significantly affect the sensitivity of the sensor as a result of varying peak currents. Additionally, CB could be printed on SPE surface, followed by drop casting with nafion to get repeatable and consistent results. Future work needs to be performed to get consistent data output from ferrocyanide hydrogel-based SPE. The problem with reproducibility can be eliminated by printing alkaline ferrocyanide hydrogels on the SPE surface. Moreover, pre-treatment of bare SPEs could also enhance the sensor output and sensitivity, which could be performed as part of future work.

5.5 References

1. M. Wang, J. Bai, K. Shao, W. Tang, X. Zhao, D. Lin, S. Huang, C. Chen, Z. Ding and J. Ye, *International Journal of Polymer Science*, 2021, **2021**, 1-16.

2. M. L. Bishop, *Clinical Chemistry: Principles, Techniques, and Correlations, Enhanced Edition: Principles, Techniques, and Correlations*, Jones & Bartlett Learning, 2020.

3. J. Wang, *Biosensors and Bioelectronics*, 2006, **21**, 1887-1892.

4. A. G.-M. Ferrari, S. J. Rowley-Neale and C. E. Banks, *Talanta Open*, 2021, **3**, 100032.

5. C. E. Banks and E. P. Randviir, *Bioanalysis*, 2014, **6**, 109-111.

6. J. P. Metters, R. O. Kadara and C. E. Banks, *Analyst*, 2011, **136**, 1067-1076.

7. S. Manjushree and P. S. Adarakatti, *Recent Developments in Green Electrochemical Sensors: Design, Performance, and Applications*, 2023, 1-21.

8. K. C. Honeychurch and J. P. Hart, *TrAC Trends in Analytical Chemistry*, 2003, **22**, 456-469.

9. M. F. Bergamini, A. L. Santos, N. R. Stradiotto and M. V. B. Zanoni, *Journal of pharmaceutical and biomedical analysis*, 2007, **43**, 315-319.

10. M. F. M. Noh and I. E. Tothill, *Analytical and bioanalytical chemistry*, 2006, **386**, 2095-2106.

11. C. Parat, S. Betelu, L. Authier and M. Potin-Gautier, *Analytica chimica acta*, 2006, **573**, 14-19.

12. D. Ji, L. Liu, S. Li, C. Chen, Y. Lu, J. Wu and Q. Liu, *Biosensors and Bioelectronics*, 2017, **98**, 449-456.

13. W. McCormick and D. McCrudden, *Journal of Electroanalytical Chemistry*, 2020, **860**, 113912.

14. V. Gubala, L. F. Harris, A. J. Ricco, M. X. Tan and D. E. Williams, *Analytical chemistry*, 2012, **84**, 487-515.

15. T. Dayakar, K. Venkateswara Rao, J. Park, P. Krishna, P. Swaroopa and Y. Ji, *Journal of Materials Science: Materials in Electronics*, 2019, **30**, 9725-9734.

16. F. S. da Cruz, F. de Souza Paula, D. L. Franco, W. T. P. dos Santos and L. F. Ferreira, *Journal of Electroanalytical Chemistry*, 2017, **806**, 172-179.

17. W. Shi, J. Li, J. Wu, Q. Wei, C. Chen, N. Bao, C. Yu and H. Gu, *Analytical and Bioanalytical Chemistry*, 2020, **412**, 7275-7283.

18. X. Shen, F. Ju, G. Li and L. Ma, *Sensors*, 2020, **20**, 2781.

19. S. Ku, S. Palanisamy and S.-M. Chen, *Journal of colloid and interface science*, 2013, **411**, 182-186.

20. G. Cui, S. J. Kim, S. H. Choi, H. Nam, G. S. Cha and K.-J. Paeng, *Analytical chemistry*, 2000, **72**, 1925-1929.

21. D.-S. Ciou, P.-H. Wu, Y.-C. Huang, M.-C. Yang, S.-Y. Lee and C.-Y. Lin, *Sensors and Actuators B: Chemical*, 2020, **314**, 128034.

22. F. Arduini, A. Amine, C. Majorani, F. Di Giorgio, D. De Felicis, F. Cataldo, D. Moscone and G. Palleschi, *Electrochemistry communications*, 2010, **12**, 346-350.

23. P. Chen, Y. Peng, M. He, X.-C. Yan, Y. Zhang and Y.-N. Liu, *Int. J. Electrochem. Sci*, 2013, **8**, 8931-8939.

24. M. A. A. Khushaini, N. H. Azeman, A. G. Ismail, C.-H. Teh, M. M. Salleh, A. A. A. Bakar, T. H. T. A. Aziz and A. R. M. Zain, *Scientific reports*, 2021, **11**, 23519.

25. K. Income, N. Ratnarathorn, N. Khamchaiyo, C. Srisuvo, L. Ruckthong and W. Dungchai, *International Journal of Analytical Chemistry*, 2019, **2019**.

26. A. Domínguez-Aragón, A. S. Conejo-Dávila, E. A. Zaragoza-Contreras and R. B. Dominguez, *Chemosensors*, 2023, **11**, 102.

27. S. N. Ashakirin, M. H. M. Zaid, M. A. S. M. Haniff, A. Masood and M. M. R. Wee, *Measurement*, 2023, 112502.

28. P. Dasgupta, V. Kumar, P. R. Krishnaswamy and N. Bhat, *ACS omega*, 2020, **5**, 22459-22464.

29. M. A. A. Khushaini, N. H. Azeman, C.-H. Teh, R. Daik, A. G. Ismail, B. Y. Majlis, M. M. Salleh, W. A. H. W. M. Adnan, T. H. T. A. Aziz and A. A. A. Bakar, *IEEE Sensors Journal*, 2022, **22**, 9268-9275.

30. V. Kumar, S. Hebbar, R. Kalam, S. Panwar, S. Prasad, S. Srikanta, P. Krishnaswamy and N. Bhat, *IEEE Sensors Journal*, 2017, **18**, 830-836.

31. J.-C. Chen, A. Kumar, H.-H. Chung, S.-H. Chien, M.-C. Kuo and J.-M. Zen, *Sensors and Actuators B: Chemical*, 2006, **115**, 473-480.

32. C. Brett and A. M. O. Brett, *Electroanalysis*, Oxford University Press, 1998.

33. P. Wilson, S. Sorto and A. K. Apawu, *Chemistry-Methods*, 2022, **2**, e202100049.

34. M. Russo, H. Warren, G. M. Spinks, D. R. MacFarlane and J. M. Pringle, *Australian Journal of Chemistry*, 2018, **72**, 112-121.

35. Z. Li, J. Zhang and S. Chen, *Express Polymer Letters*, 2008, **2**, 695-704.

36. R. R. Kumar, M. O. Shaikh and C.-H. Chuang, *Analytica Chimica Acta*, 2021, **1183**, 338748.

37. C. L. Gonzalez-Gallardo, N. Arjona, L. Álvarez-Contreras and M. Guerra-Balcázar, *RSC advances*, 2022, **12**, 30785-30802.

38. S. Boobphahom, N. Ruecha, N. Rodthongkum, O. Chailapakul and V. T. Remcho, *Analytica Chimica Acta*, 2019, **1083**, 110-118.

39. J. Raveendran, P. Resmi, T. Ramachandran, B. G. Nair and T. S. Babu, *Sensors and Actuators B: Chemical*, 2017, **243**, 589-595.

40. S. Kalasin, P. Sangnuang, P. Khownarumit, I. M. Tang and W. Surareungchai, *ACS Biomaterials Science & Engineering*, 2020, **6**, 1247-1258.

41. S. Kalasin, P. Sangnuang and W. Surareungchai, *ACS Biomaterials Science & Engineering*, 2020, **7**, 322-334.

42. C.-Y. Yang, K.-C. Lin, S.-M. Chen, Y.-S. Hou and D.-H. Zhao, *International journal of electrochemical science*, 2015, **10**, 3738-3745.

43. J.-S. Do, Y.-H. Chang and M.-L. Tsai, *Materials chemistry and physics*, 2018, **219**, 1-12.

44. S. Kalasin, P. Sangnuang, P. Khownarumit, I. M. Tang and W. Surareungchai, *ACS Biomaterials Science & Engineering*, 2020, **6**, 5895-5910.

45. M. J. Pedrozo-Penafiel, T. Lopes, L. M. Gutierrez-Beleno, M. E. M. Da Costa, D. G. Larrude and R. Q. Aucelio, *Journal of Electroanalytical Chemistry*, 2020, **878**, 114561.

46. X. Kang, Z. Mai, X. Zou, P. Cai and J. Mo, *Analytical biochemistry*, 2007, **363**, 143-150.

47. D. Talarico, F. Arduini, A. Constantino, M. Del Carlo, D. Compagnone, D. Moscone and G. Palleschi, *Electrochemistry Communications*, 2015, **60**, 78-82.

48. F. Arduini, F. Di Nardo, A. Amine, L. Micheli, G. Palleschi and D. Moscone, *Electroanalysis*, 2012, **24**, 743-751.

49. S. Hernandez-Aldave, A. Tarat, J. D. McGettrick and P. Bertoncello, *Nanomaterials*, 2019, **9**, 221.

50. Y. Chen, Q. Zhong, G. Li, T. Tian, J. Tan and M. Pan, *Ionics*, 2018, **24**, 3905-3914.

51. E. M. Ahmed, *Journal of advanced research*, 2015, **6**, 105-121.

52. M. A. Darabi, A. Khosrozadeh, Y. Wang, N. Ashammakhi, H. Alem, A. Erdem, Q. Chang, K. Xu, Y. Liu and G. Luo, *Advanced Science*, 2020, **7**, 1902740.

53. W. X. Waresindo, H. R. Luthfianti, A. Priyanto, D. A. Hapidin, D. Edikresnha, A. H. Aimon, T. Suciati and K. Khairurrijal, *Materials Research Express*, 2023.

54. T. N. T. Tran, H.-J. Chung and D. G. Ivey, *Electrochimica Acta*, 2019, **327**, 135021.

55. A. K. S. Kumar, Y. Zhang, D. Li and R. G. Compton, *Electrochemistry Communications*, 2020, **121**, 106867.

56. A. Morrin, A. J. Killard and M. R. Smyth, *Analytical letters*, 2003, **36**, 2021-2039.

Chapter 2 – Conclusions and future work

6.1 Introduction

Recently, there is an urgent need to develop sensor systems that give early diagnostic response towards various clinical conditions including chronic kidney disease (CKD) and which can be used effectively for clinical monitoring applications. The idea is to have a major focus on disease prevention along with disease diagnosis. Many kidney conditions are asymptomatic and urine dipsticks are currently used for repeated testing and screening [1]. Detection based on 24 h urine collection is often unreliable and rarely used in clinical practice today. Participating in the ICURe Discovery program and gaining understanding from conversations with clinicians, we understood that a spot urine albumin to creatinine ratio (ACR) urine test is a robust clinical index to screen and evaluate clinical conditions with the kidneys. ACR > 2.5 or 3.5 mg/mmol may indicate kidney conditions and a further evaluation and investigation would be required to be done by the nephrologists who may further evaluate the condition with a serum eGFR test[1].

This project has focused on development on sensor platforms for creatinine detection, which can be effectively optimised further into development of a potential POCT device (CreaSense) (with albumin detection) that can be used at either GP clinics or even at homes by patients (fig. 6.1). CreaSense can potentially be used for screening applications at clinics or hospitals and would add to advantages including time and cost savings in terms of processing and transport of samples to labs. This would greatly have an effect on economics and add to clinical benefits.
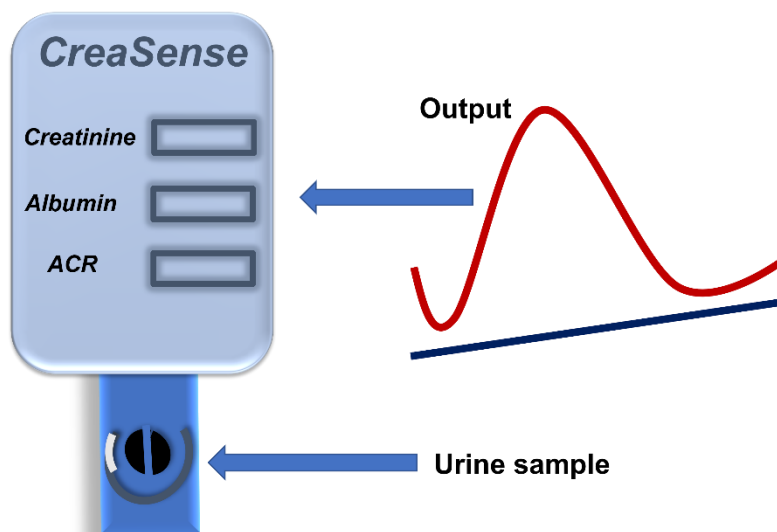

Figure 2.1: CreaSense POCT device measuring creatinine and albumin concentrations.

This chapter concludes the work done on designing creatinine sensing platforms as part of the PhD project. Future work following on from this project is discussed in detail along with the information from the ICURe Discovery program.

6.2 Conclusions

The aim has been to develop creatinine sensing platforms that can detect kidney disease at earlier stages, especially for patients at high risk (e.g., patients with diabetes can develop complications including diabetic nephropathy which can lead to end stage renal disease).

Chapter 3 describes a novel, simple, low-cost method to detect creatinine non-enzymatically using a bare GCE system in alkaline ferrocyanide. This technique was further translated into a miniaturised SPE platform in *Chapter 5*. Various interferences with ascorbic acid (AA), uric acid (UA), urea and glucose (Glu) have been investigated. AA and UA were the major interferents and glucose was non-interfering. With SPE systems, further optimisation with Nafion based systems (negatively charged membrane) is required. These interferences from negatively charged AA and UA can be eliminated effectively, not only applicable to the sensors systems in Chapter 3 and 5 (on bare carbon electrode sensing with alkaline ferrocyanide) but may also be applicable to nickel systems in Chapter 4, if urea interference can additionally be eliminated through size exclusion membrane techniques (as urea reacts at nickel electrodes).

Overall, the PhD project has focused on detection and miniaturisation of the creatinine sensing technology using the SPE sensor systems. Through the participation in ICURe Discovery program and from conversations with clinicians, it was understood that a sensor device that can simultaneously measure creatinine and albumin concentrations (giving ACR – albumin to creatinine ratio), would be a robust screening device for patients at high risk of CKD or at early stages of CKD.

6.3 Future work

Future work could involve development of further electrode materials, electrochemical techniques, pre-treatment of electrodes and hydrogel-based sensing for creatinine detection. Particular focus on albumin detection techniques will be part of the next postdoc project.

Bimetallic nanomaterials could be used for creatinine (and albumin) detection, where the sensitivity could be significantly enhanced as a result of better kinetics and charge transfer. The concept is to have more number of active sites, for increasing velocity of the electrochemical reaction. To our knowledge, the only bimetallic sensor reported for creatinine was based on CuAg nanoparticles [2]. Different bimetallic systems for creatinine detection can be investigated further.

The majority of project involved use of electrochemical techniques of cyclic voltammetry and chronoamperometry. Although CV is a simple and reproducible technique, the capacitive current (at the electrode-solution interface) limits the linear range and the LOD to much higher values. Therefore, employing more sensitive voltammetric techniques for e.g., differential pulse voltammetry (DPV) or square wave voltammetry (SWV) could be used in further studies. Further design into setting these techniques effectively in a POC device would be required.

Further work in Chapter 5 (on SPE based sensors) can be done using the pre-treatment technique. SPCE pre-treatment activates the working surface in terms of surface oxygen functionalities on the electrode surface and these electrodes have new edge exposures in the carbon microstructure. This can increase sensitivity and specificity towards target analytes [3, 4]. An applied overpotential of 2 V vs Ag/AgCl in PBS or NaOH can allow pre-anodization to occur on the surface of the SPEs. A study on pretreated-SPCEs has been performed by Prasad et al. for multi-analyte detection where three distinguishable signals are observed for detection of ascorbic acid, uric acid and dopamine [5]. Moreover, SPCEs can also be modified with metal nanoparticles for sensing applications aiming to have faster electron transfer [6]. Choudhry and Banks have performed a study on electrolytically fabricating nickel microrods on screen printed electrodes for oxidation of alcohols [4]. Therefore, nickel based SPEs can also be investigated for creatinine detection.

The repeatability of hydrogel-based sensor performance may be achieved using the technique of printing hydrogels on the surface of SPEs. Ferrocyanide/PVA/KOH based hydrogels could be printed as part of future work.

6.3.1 ICURe Discovery program

Detection of only urine creatinine is not a robust technique to screen CKD as a 24h urine test would be required which increases the risk of inaccuracies and also increases the turnaround time of results. Albuminuria (a condition where albumin is present in urine) is the most frequently used marker of kidney damage in primary care practices today [7]. Over 50% of CKD cases can be missed if albuminuria is ignored [8].

Furthermore, through market testing of the idea (in the ICURe Discovery program), it was understood that a creatinine urine-based sensor when combined with detection of albumin/creatinine ratio, would allow more accurate one-spot analysis tests instead of 24h tests if only urine creatinine was measured. This would greatly increase the accuracy of the screening tests in patients with early signs of kidney disease in the primary care settings (GP surgeries). The current dipstick urine tests, which also give a ratio of albumin/creatinine can only detect kidney conditions accurately when the disease enters into critical stages in case of emergencies. Therefore, there exists a significant gap in detecting kidney conditions at early stages in routine clinical analysis in primary care. The wider applicability of this potential device would be in primary care settings with the aim to prevent the disease or delay the progression of the early stages of the kidney disease using medicines.

This project could further be extended in terms of detecting albumin/creatinine ratio and towards the device development. This section explains the steps towards the feasibility of the research idea and its commercialisation potential.

6.3.1.1 Market Discovery insights

Market testing of the idea was done through conversations with clinicians (GPs, cardiologists and nephrologists) and members of the academic health science network (AHSN). It was understood that it is significantly critical to detect creatinine and screen CKD at early stages as it is asymptomatic. There exists a significant gap in screening patients with early kidney disease as dipsticks remain less accurate to detect low concentrations of albumin in urine. According to the QOF database (2022), only 29 % CKD patients were screened with urine test. ACR test is preferred as a more accurate test by GPs than dipstick urine test. A urine spot test would add to the accuracy and also convenience to patients and the clinicians. The applicability of a POCT device that measures ACR would not only be beneficial at GP clinics, but also at pharmacies and for patients having diabetic reviews. The nephrologists

(secondary care clinical settings) consider measuring creatinine in blood as a more robust biomarker if the disease has progressed to later stages. The aim is to allow early detection at primary care settings (GP clinics, pharmacies or diabetic reviews) and prevent disease progression with medicines. The low cost and simple ACR POCT device can also be considered for use in emerging markets where there is a need of better access to primary care.

Considering the market testing process, we understood that the idea of detecting creatinine and albumin is feasible in the market. Further product optimisation and refinement is needed to further develop this idea. A clear value proposition is demonstrated in various markets. The next steps to this project would include research in the area of developing a low cost and simple albumin sensor (part of the next postdoc project), followed by participation in ICURe Explore program which would involve further market testing and conversations with clinicians and manufacturers.

6.4 References

1. I. Wilkinson, I. B. Wilkinson, T. Raine, K. Wiles, A. Goodhart, C. Hall and H. O'Neill, *Oxford handbook of clinical medicine*, Oxford university press, 2017.

2. M. García-Barajas, A. Trejo-Domínguez, J. Ledesma-García, L. Arriaga, L. Á. Contreras, J. Galindo-de-la-Rosa, N. Arjona and M. Guerra-Balcázar, 2019.

3. A. Domínguez-Aragón, A. S. Conejo-Dávila, E. A. Zaragoza-Contreras and R. B. Dominguez, *Chemosensors*, 2023, **11**, 102.

4. N. A. Choudhry and C. E. Banks, *Analytical Methods*, 2011, **3**, 74-77.

5. K. S. Prasad, G. Muthuraman and J.-M. Zen, *Electrochemistry Communications*, 2008, **10**, 559-563.

6. J. P. Metters, R. O. Kadara and C. E. Banks, *Analyst*, 2011, **136**, 1067-1076.

7. J. I. Park, H. Baek, B. R. Kim and H. H. Jung, *PloS one*, 2017, **12**, e0171106.

8. K. T. Mills, Y. Xu, W. Zhang, J. D. Bundy, C.-S. Chen, T. N. Kelly, J. Chen and J. He, *Kidney international*, 2015, **88**, 950-957.
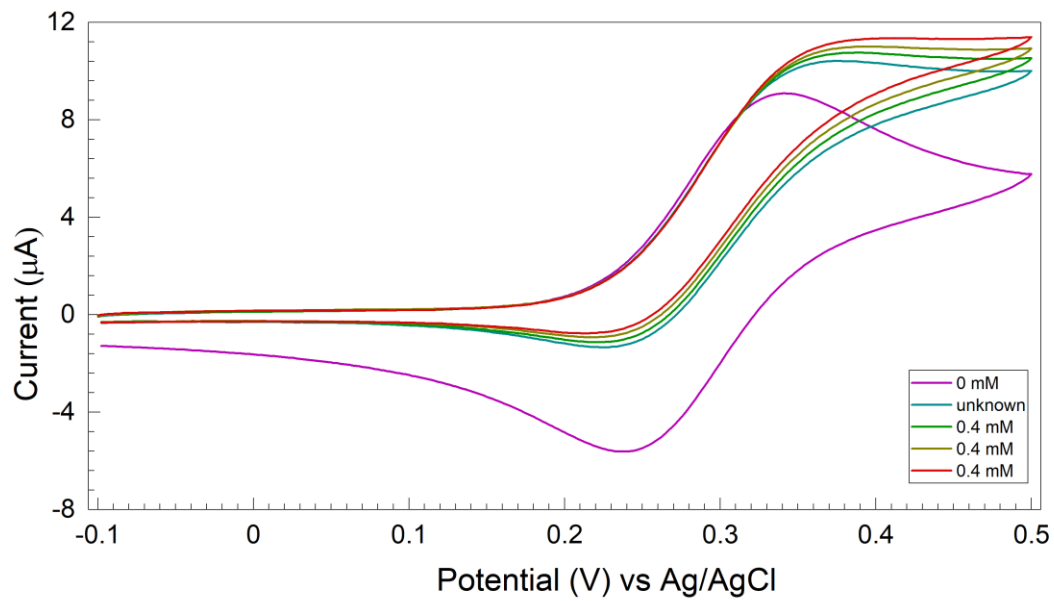
Appendix A

A.1 Standard addition study with ''unknown'' creatinine additions

A.1.1 10 mM CR in water unknown addition
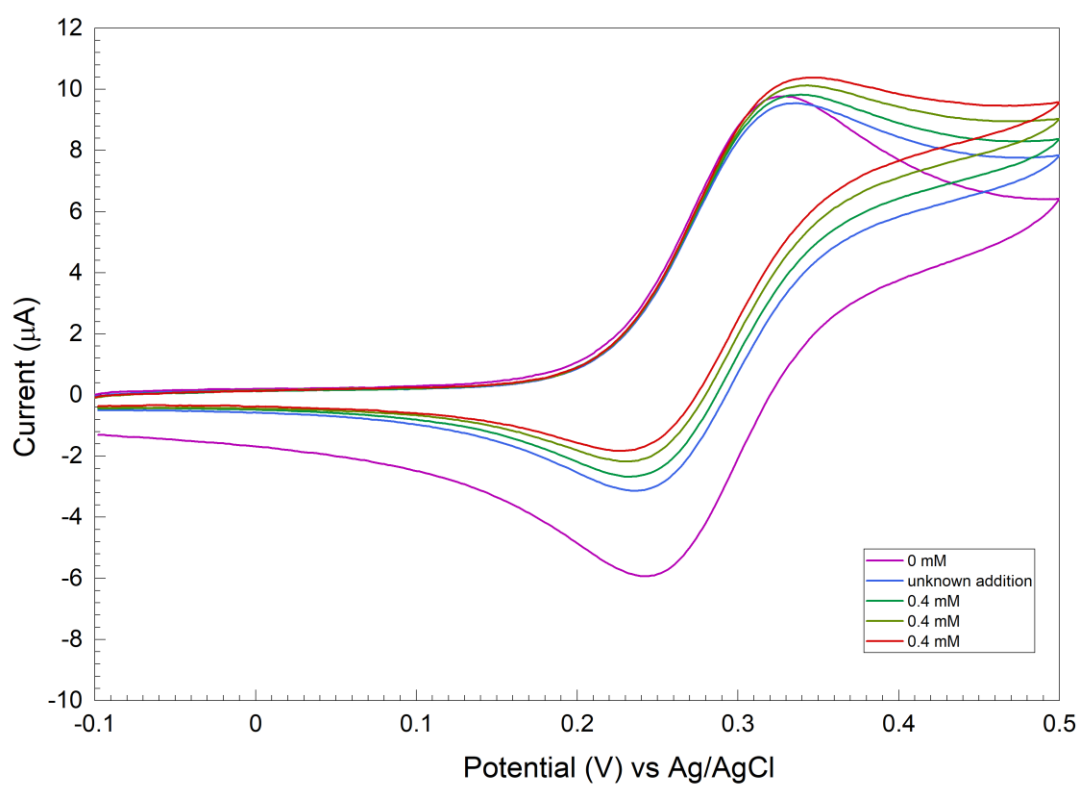
A.1: Standard addition study with a 10 mM CR in water unknown addition followed by three known 0.4 mM CR additions from 200 mM CR stock in water.
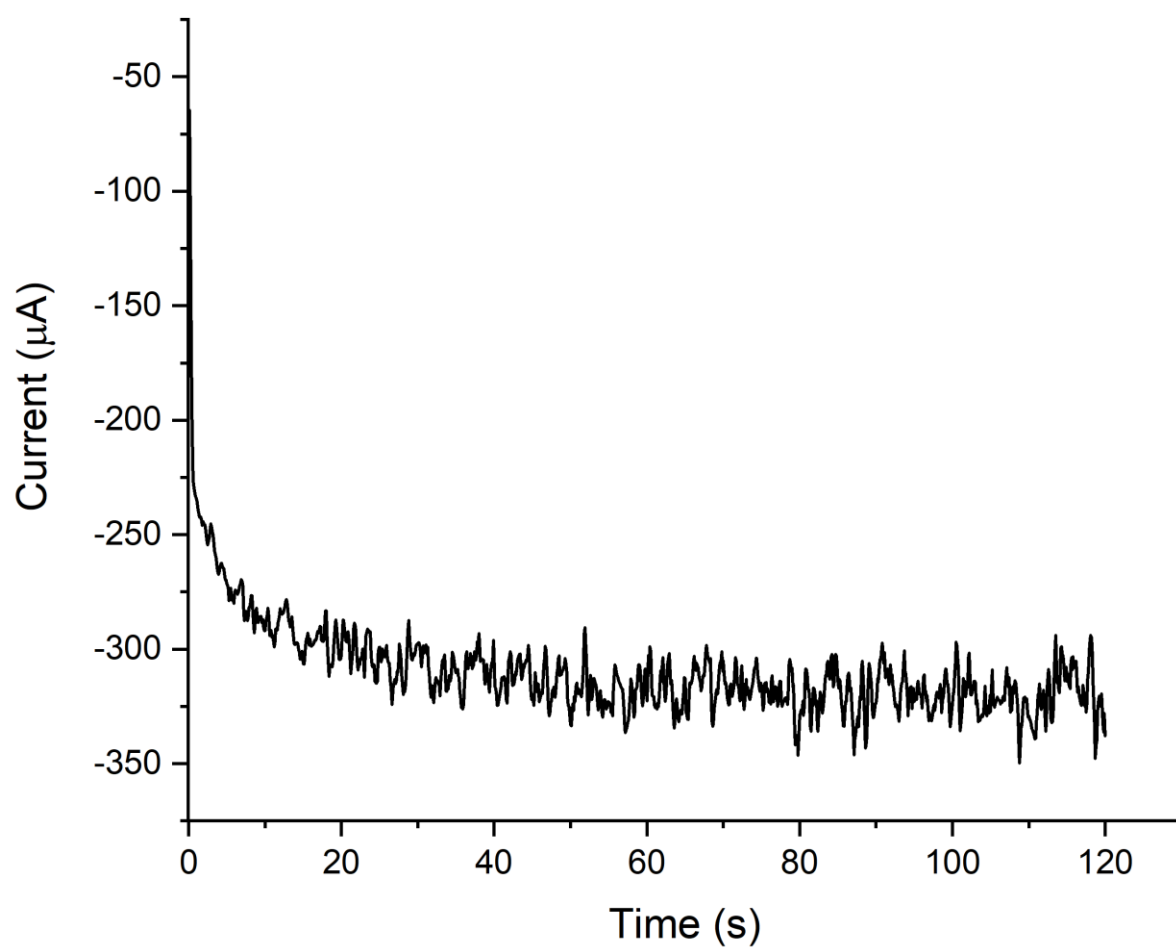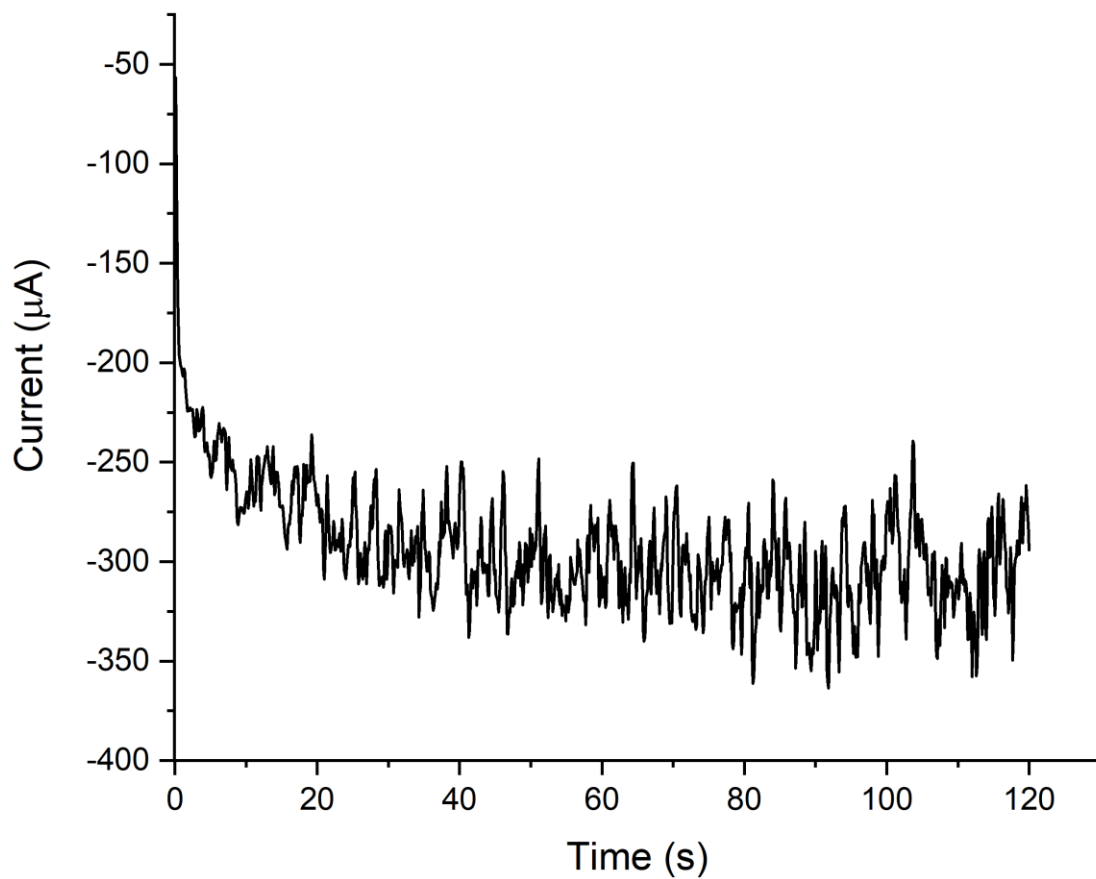
A.2: Standard addition study with a 25 mM CR in water unknown addition followed by three known 0.4 mM CR additions from 200 mM CR stock in water.
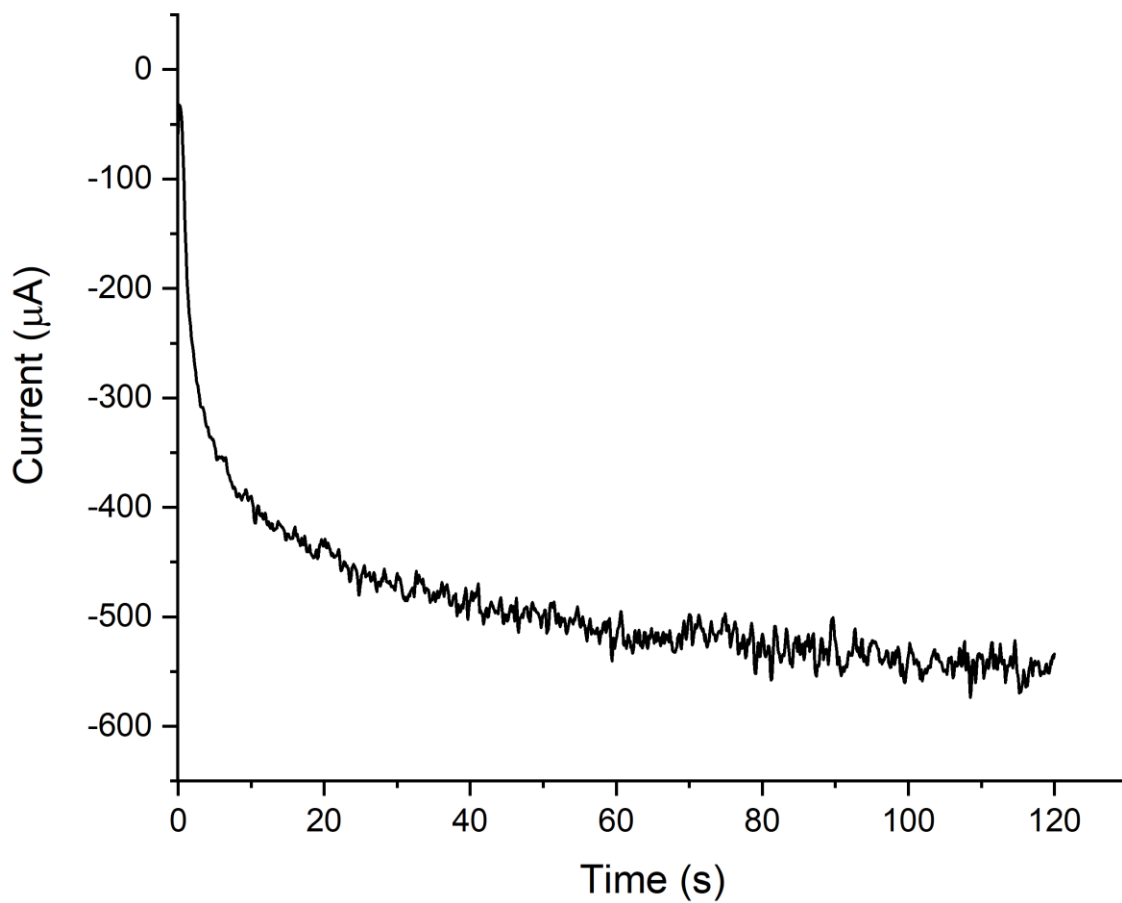
Appendix B

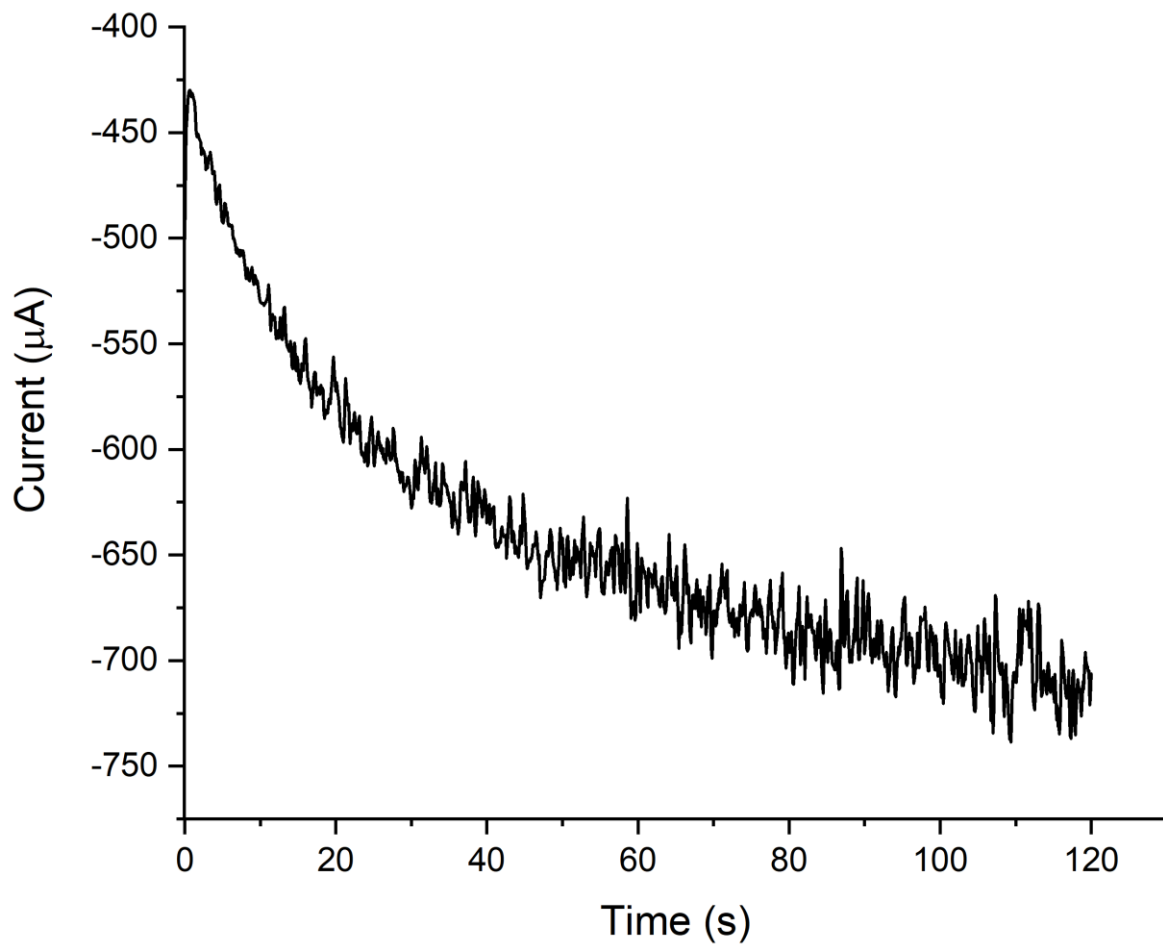## B.1 Chronoamperometry data for Nickel electrodeposition on same GCE at 120s

B.1: Chronoamperometry data at -1.3 V vs Ag/AgCl at 120s for repeat 1.

B.2: Chronoamperometry data at -1.3 V vs Ag/AgCl at 120s for repeat 2.

B.3: Chronoamperometry data at -1.3 V vs Ag/AgCl at 120s for repeat 3.

B.4: Chronoamperometry data at -1.3 V vs Ag/AgCl at 120s for repeat 4.